Astro-Archaeology in the Triangulum Galaxy

ASTRO-ARCHAEOLOGY IN THE TRIANGULUM GALAXY: STUDYING GALAXY FORMATION AND EVOLUTION WITH THE GLOBULAR CLUSTERS AND STELLAR HALO IN M33

By

ROBERT COCKCROFT , M.Sci., M.Sc.

A Thesis
Submitted to the School of Graduate Studies
in Partial Fulfillment of the Requirements
for the Degree of

Doctor of Philosophy

McMaster University

DOCTOR OF PHILOSOPHY (2012) McMaster University
(Physics and Astronomy) Hamilton, Ontario

TITLE: Astro-Archaeology in the Triangulum Galaxy: Studying Galaxy Formation and Evolution with the Globular Clusters and Stellar Halo in M33

AUTHOR: Robert Cockcroft, M.Sci. (University College London), M.Sc. (McMaster University)

SUPERVISOR: Professor William E. Harris

NUMBER OF PAGES: xxi, 231

Abstract

The currently-favoured cosmological paradigm, ΛCDM, predicts that galaxies are built up from smaller galaxies in a bottom-up process known as hierarchical merging. ΛCDM is extremely successful for large-scale structures, but is less so for the detailed features of individual galaxies. We can study these features - the galaxies' foundations and the remnants of the smaller components that built them - only in the closest galaxies in which we can resolve individual stars. In this thesis, we use data from the Canada-France-Hawaii Telescope (CFHT)/MegaCam as part of the Pan-Andromeda Archaeological Survey (PAndAS) to observe M33 (the Triangulum Galaxy) and the detailed features of its old stellar population. The study of these details is vital for our understanding of galaxy formation and evolution.

We search for two types of components within the old stellar population: globular star clusters and the faint, diffuse stellar halo. We find only one new unambiguous outer halo star cluster, in addition to the five previously known in the M33 outer halo (10 kpc $\lesssim r \lesssim$ 50 kpc). A further 2440 cluster *candidates* are identified, which we analyse using two different types of simulated clusters. We are able to describe the type of clusters that are likely to remain hidden from our searches.

Our study of a population of red giant branch (RGB) stars far from the M33 disk reveals a low-luminosity, centrally concentrated component which we interpret as the discovery of M33's halo. It is everywhere in our data fainter than $\mu_V \sim 33$ mag arcsec^{-2}, with scale length $r_{exp} \sim 20$ kpc, an overall luminosity not more than a few percent of the total luminosity of M33, and is possibly also not azimuthally symmetric.

For M33 to have so few outer halo clusters compared to M31 and to have such a low-luminosity halo, with the possible asymmetry that we see, suggests tidal stripping of M33's halo components by M31 - a view that is also favoured by the morphology of the disk substructure and recent modelling.

To Mum and Dad

Co-Authorship

Chapters 2 and 4 are original papers written by myself, Robert Cockcroft, and have been re-formatted to conform to the specifications of the McMaster thesis style. Chapter 2 was published in *The Astrophysical Journal*, with reference Cockcroft, R.; Harris, W. E.; Ferguson, A. M. N.; Huxor, A.; Ibata, R.; Irwin, M. J.; McConnachie, A. W.; Woodley, K. A.; Chapman, S. C.; Lewis G. F.; and, Puzia, T. H., Volume 730, Issue 2, pages 112-123, Bib. Code: 2011ApJ...730..112C, DOI: 10.1088/0004-637X/730/2/112. Chapter 4 was submitted to *The Monthly Notices of the Royal Astronomical Society* on 22^{nd} May 2012, and now contains the revised manuscript, submitted in response to the referee's comments on 28^{th} August 2012. The listed authors are Cockcroft, R.; McConnachie, A. W.; Harris, W. E.; Ibata, R.; Irwin, M. J.; Ferguson, A. M. N.; Fardal, M. A.; Babul, A.; Chapman, S. C.; Lewis, G. F.; Martin, N. F.; and, Puzia, T. H.

Authorship guidelines for papers that use data from the Pan-Andromeda Archaeological Survey (PAndAS), as the above papers do, suggest that after the main researchers (in this case, R. Cockcroft, W. E. Harris and A. McConnachie), R. Ibata and M. J. Irwin are listed for their contribution to the program proposal and subsequent data reduction, in addition to other group members who have made contributions the paper (which can include suggestions to improve paper drafts, but does not guarantee co-authorship).

Chapters 1 (the introduction), 3 and 5 (the summary) are also my original work, with the exception of the Chapter 1's figures. I have obtained permission to use these figures in my thesis from the authors. Chapter 3 is a paper in preparation, and will have co-authors Harris, W. E.; Ibata, R.; Irwin, M. J.; Barmby, P.; Leigh, N.; Umbreit, S.; Sills, A.; Glebbeek, E.; Woodley, K. A.; and, Fabbro, S.

I grant an irrevocable, non-exclusive license to McMaster University and to Library and Archives Canada to reproduce this material as part of this thesis.

Acknowledgements

Throughout my studies in astronomy, I have received much mentorship, guidance and support - most especially from my supervisor, Dr Bill Harris, to whom I am sincerely grateful. I have had the privilege to work with Bill over the past six years, and admire the way he not only navigates deftly through the research projects in an efficient yet relaxed manner, but can also instill confidence and composure in me.

I am also deeply indebted to Drs Pauline Barmby, Laura Parker and Alison Sills, my supervisory committee members, who have greatly contributed throughout the years with fresh perspectives, ideas and encouragement.

My research has allowed me to meet many other motivational people, and I would like to thank Drs Alan McConnachie, Annette Ferguson, Avon Huxor, Mike Irwin, Nathan Leigh, Kristin Woodley and everyone on the PAndAS and CFHT teams.

The outreach projects that I have undertaken at McMaster University constantly remind me of the reasons why I enjoy studying astronomy. It has been my pleasure to share my passion for outreach with my friends, colleagues and role models, Drs Sarah Symons, Doug Welch, Ralph Pudritz, and Mike Reid, and Caroline Burgess - inspirations, all of them.

Important for any department to work effectively is a strong team of support staff, and we are very fortunate to have one here in the Department of Physics and Astronomy. Mara Esposto, Cheryl Johnston, Rosemary McNiece, Liz Penney and Tina Stewart: thank you so much for enabling my various jobs to run so smoothly and also making them much more enjoyable and fun in the process.

Finally, many heart-felt thanks to my family and friends: to my parents, my brother and sister and their families, my grandparents, my partner and his family, and all of my friends at University College London and McMaster University who have joined me at various stages along my path in astronomy.

Mum and Dad, thank you especially to you, for always being there, and for walking that fine line between giving me your honest opinions while constantly supporting whatever decision I make. Cal, you grew up being my little sister, but I think of you in many ways as a big sister now for the strength and sensibility you show. I look forward to seeing you and Pippa more in the near future. Andrew, it's always a pleasure to see you and your beautiful family. I'd be happy to be half as successful as you are by the time I'm your age.

And to Ken: I know you hate roller coasters, but thank you more than you know for joining me on this one. I could not have done it without you. Our future together is going to be exciting, and I'm very much looking forward to it!

"God does not play dice with the universe; [S]He plays an ineffable game of [her/]his own devising, which might be compared, from the perspective of any of the other players, to being involved in an obscure and complex version of poker in a pitch dark room, with blank cards, for infinite stakes, with a dealer who won't tell you the rules, and who smiles all the time."

Neil Gaiman (b. 1960), and
Terry Pratchett (b. 1948)

"Why should we demand that the universe make itself clear to us? Why should we care?... It is something about understanding the totality of existence, the essential defining reality of things, the entire universe and [our] place in it. It is a groping among stars for final answers, a wandering the infinitesimal for the infinitely general, a deeper and deeper pilgrimage into the unknown."

Julian Jaynes (1920-1997)

"The final mystery is oneself. When one has weighed the sun in the balances, and measured the steps of the moon, and mapped out the seven heavens star by star, there still remains oneself. Who can calculate the orbit of [her/]his own soul?"

Oscar Wilde (1854-1900)

"There are many windows through which we can look out into the world, searching for meaning... Most of us, when we ponder on the meaning of our existence, peer through but one of these windows onto the world. And even that one is often misted over by the breath of our finite humanity. We clear a tiny peephole and stare through. No wonder we are confused by the tiny fraction of a whole that we see. It is, after all, trying to comprehend the panorama of the desert or the sea through a rolled-up newspaper."

Jane Goodall (b. 1934)

Table of Contents

List of Figures

List of Tables

List of Acronyms

ACS	Advanced Camera for Surveys
AGB	Asymptotic giant branch
BCG	Brightest cluster galaxy
CADC	Canadian Astronomy Data Centre
CASU	Cambridge Astronomical Survey Unit
CCD	Charge-coupled device
cE	Compact elliptical galaxy
CFHT	Canada-France-Hawaii Telescope
CMB	Cosmic microwave background
CMD	Colour-magnitude diagram
COBE	Cosmic Microwave Background Explorer
dE	Dwarf elliptical galaxy
DGTO	Dwarf galaxy transition object
DM	Dark matter
DoS	Disk of satellites
DR	Data release
dSph	Dwarf spheroidal galaxy
E	Elliptical galaxy
EC	Extended cluster
ESC	Extended star cluster
ESO	European Southern Observatory
FWHM	Full-width half-maximum
GC	Globular cluster
GCS	Globular cluster system
gE	Giant elliptical galaxy
HB	Horizontal branch
HST	Hubble Space Telescope
IMF	Initial mass function
INT	Isaac Newton Telescope
IR	Infrared
IPAC	Infrared Processing and Analysis Center
IRAF	Image Reduction and Analysis Facility

KS	Kolmogorov-Smirnov
ΛCDM	Lambda-Cold Dark Matter
LG	Local Group
LMC	Large Magellanic Cloud
LSS	Large-scale structure
MC	Monte Carlo
MCs	Magellanic Clouds
MDF	Metallicity distribution function
MP	Metal poor
MR	Metal rich
MSTO	Main sequence turn-off
MW	Milky Way
NASA	(US) National Aeronautics and Space Administration
NED	NASA/IPAC Extragalactic Database
NGC	New General Catalogue
NOAO	(US) National Optical Astronomy Observatory
NRC	(Canadian) National Research Council
NSERC	(Canadian) Natural Sciences and Engineering Research Council
OH	Outer Halo
PAndAS	Pan-Andromeda Archaeological Survey
Pan-STARRS	Panoramic Survey Telescope and Rapid Response System
PFUEI	Prime Focus Universal Extragalactic Instrument
PoS	Plane of satellites
PSF	Point-spread function
RBC	Revised Bologna Catalogue
RGB	Red giant branch
SDSS	Sloan Digital Sky Survey
SE	Source Extractor
SGB	Sub-giant branch
SM07	Sarajedini and Mancone (2007)
SMBH	Supermassive black hole
SMC	Small Magellanic Cloud
S/N	Signal-to-noise
SP	Structural parameter
TRGB	Tip of the red giant branch
UCD	Ultra-compact dwarf galaxy
UCO	Ultra-compact object
UFD	Ultra-faint dwarf galaxy
UKIRT	United Kingdom Infrared Telescope
UV	Ultra-violet
VPOS	Vast polar structure
WD	White dwarf

WFCAM	Wide field camera
WFPC	Wide-field planetary camera
WMAP	Wilkinson Microwave Anisotropy Probe
WIYN	University of Wisconsin-Madison, Indiana University, Yale University and NOAO Observatory
YMC	Young massive cluster

Chapter 1

Introduction

"We are probably nearing the limit of all we can know about astronomy."

SIMON NEWCOMB (1835-1909)

"Cosmologists are always wrong, but never in doubt."

LEV LANDAU (1908-1968)

Far from Simon Newcomb's famous sentiments, there are a great number of questions that astronomers still pose - although obviously our knowledge has continued to advance since the 19th century. Below is a non-exhaustive list from Wesson (2001) of some of the most pressing problems facing astronomy and physics, and although this list was composed over a decade ago the majority of the problems still remain unanswered:

1. Supersymmetry and Vacuum Fields
2. The Electromagnetic Zero-Point Field
3. The Cosmological Constant Problem

4. The Hierarchy Problem
5. Grand Unification
6. Quantum Gravity
7. Neutrinos
8. The Identity of Dark Matter
9. The Microwave Background Horizon Problem
10. Particle Properties and Causality
11. Fundamental Constants
12. Was There a Big Bang?
13. The Topology of Space
14. The Dimensionality of the World
15. Machs Principle
16. Negative Mass
17. The Origin of Galaxies and Other Structure
18. The Origin of the Spins of Galaxies
19. The Angular Momentum/Mass Relation
20. Life and the Fermi-Hart Paradox

The primary purpose of this thesis is to further understand the 17th point above: the origins of galaxies, both their formation and evolution. As Wesson points out, however, subjects in astrophysics overlap with one another, so that these problems often cannot be treated in an isolated manner and that advances in one field can also lead to progress in others.

In this first chapter, we therefore thoroughly set the context of our work by broadly reviewing the related fields. We begin with a brief summary of the current cosmological paradigm, and then describe the different types of galaxies found in the Universe, the components that make up those galaxies, and the Local Group (the galaxies within $r \sim 3$ Mpc from our Galaxy, a relatively nearby part of the Universe). We then focus on the relevant galactic components that we scrutinize in later chapters, and end by introducing the studies undertaken in this thesis on one of our nearest neighbouring galaxies: the Triangulum Galaxy (M33).

1.1 The Lambda Cold Dark Matter Paradigm

Referred to as "the standard model", the Lambda Cold Dark Matter (ΛCMD) cosmological paradigm attempts to explain - for the most part, successfully - not only our earliest observations of the Universe but also the grand scheme of structure (e.g., galaxies, clusters and filaments) and its expansion throughout the entire Universe. It can also describe primordial nucleosynthesis, explaining the general abundances of isotopes of hydrogen, helium and other light elements, and the *acceleration* of the Universe's expansion. There is obviously a huge amount of literature on this subject, and we only provide the briefest overview here.

The relatively recent advances in precision cosmology, especially those due to the Wilkinson Microwave Anisotropy Probe (WMAP; Bennett et al. 2003), have allowed many key parameters to be measured with unprecedented accuracy. For example, combining measurements of the cosmic microwave background (CMB; Penzias & Wilson 1965; Larson et al. 2011), baryonic acoustic oscillations (e.g., Peebles & Yu 1970; Eisenstein et al. 1998; Percival et al. 2010) and the Hubble constant (e.g., Riess et al. 2009; Komatsu et al. 2011), leads to results in estimates for the age of the Universe, $\tau = 13.75 \pm 0.11$ Gyr, and its composition (Jarosik et al., 2011). The abundances of each component are usually described relative to the so-called "critical density", ρ_c, of the Universe. This is the density which was thought to control whether or not the Universe would eventually contract or expand forever (however, see the effects of dark energy below). Rees (2001) calculates that the critical density is comparable to just 5 atoms per cubic metre, which is closer to a true vacuum than any artificial vacuum that we can produce on Earth. The density parameter, $\Omega_{component}$, is defined as the ratio of the component's density, $\rho_{component}$, to the critical density, ρ_c. The sum of all the density parameters has a present day value of $\Omega_0 \sim 1$ (Jarosik et al., 2011). There are presently three main constituents: baryonic matter density, $\Omega_b = 0.045 \pm 0.002$, cold dark matter density, $\Omega_c = 0.227 \pm 0.014$, and dark energy density, $\Omega_\Lambda = 0.728^{+0.015}_{-0.016}$ (Jarosik et al., 2011). WMAP estimates will likely be refined by the Planck space telescope, launched in 2009 and with first major analyses expected later this year (2012).

The smallest constituent of the Universe, the baryonic component, is the only part which is directly observable (e.g., stars, planets, gas and cosmic dust), and is what we study in this thesis. We still do not know what constitutes the dark components although we clearly see evidence for their existence. Dark matter appears to interact gravitationally with the baryonic matter but not through electromagnetic forces. Oort (1932) and Zwicky (1933) were the first to see evidence for this material - in the orbital velocities of stars in our Galaxy, the Milky Way (MW), and galaxies in clusters, respectively - and it was Zwicky who coined the term dark matter (DM). We can further infer its existence through, for example, galactic rotation curves (e.g., Rubin & Ford 1970), the Tully-Fisher relation (Tully & Fisher, 1977), velocity dispersions within galaxies (e.g., Faber & Jackson 1976) and gravitational lensing of galaxy clusters (e.g., Brainerd et al. 1996). The effects of dark energy are seen through the measurements of supernova Type Ia standard candles, which show that the Universe's expansion is increasing at an accelerated rate (e.g., Riess et al. 1998; Perlmutter et al. 1999).

Galaxies are composed mostly of DM (as high even as possibly $\lesssim 90\%$, as DM becomes more dominant with fainter galaxies, e.g., as shown in Figure

9 of Mateo 1998) with some baryonic matter, and galaxies make the present Universe quite "lumpy". Our deepest observations suggest that galaxies have already formed at very early times in the Universe ($z \sim$8-8.5, or $\sim$600 million years after recombination; Bouwens et al. 2010). However, the Big Bang's remnant radiation, the CMB, reveals that the early Universe was incredibly smooth with temperature fluctuations of only 10^{-5} (Jarosik et al., 2011). The ΛCDM paradigm predicts that these temperature fluctuations trace the earliest density variations, which then act as the seeds for the large scale structure that we see in the present Universe. But how exactly do galaxies grow (and grow so quickly) from these cosmic seeds? There are broadly two methods that can be used to answer this question: either study different galaxies at various redshifts throughout the Universe and see how they change over a cosmological timescale, or observe the closest galaxies (i.e., the galaxies in which we can resolve individual stars) in as much detail as possible to understand each and every component, how they interact and how they could have arisen. In this thesis, I use the latter method (much like archaeology).

There are two classic proposals about how galaxies form: they fragment from the very largest structures in a top-down fashion (or "monolithic collapse"; Eggen et al. 1962) or they form bottom up through multiple mergers of smaller components (or "hierarchical merging"; Searle & Zinn 1978). The latter scenario is favoured by the majority of galaxy formation models and simulations, and is consistent with ΛCDM.

Apart from the two obvious problems regarding the unknowns of dark matter and dark energy, there are other concerns with the ΛCDM paradigm, the most prominent of which we mention briefly here. The cusp-core problem highlights that ΛCDM predicts galaxy centres which are much more peaked, or cusped, than the observed flatter profiles, which are cored, because the models are non-dissipative (e.g., de Blok 2010 and references therein). ΛCDM also has "a missing satellite problem", as it predicts an overabundance of small companion galaxies, known as dwarf satellite galaxies, which are not observed (e.g., Kauffmann et al. 1993; Klypin et al. 1999; Moore et al. 1999; Springel et al. 2008; Diemand et al. 2008). A further problem is the difference in composition (primarily metallicity) between the surviving dwarf satellites and the stellar halo, which is thought to have been built up from disrupted dwarfs (Helmi et al., 2006). Various solutions to these problems are proposed but it is unclear which is correct. However, recent discoveries of ultra-faint dwarfs, (extended) clusters at large galactocentric radii, and advances in the capabilities of new surveys that probe the environments of galaxies have prompted renewed interest in this topic. We further discuss these advances in Section 1.4, to set the context and motivate the research in this thesis.

1.2 Galaxy Types and Their Components

Edwin Hubble famously sequenced galaxies based on their observed morphologies (Hubble, 1926), and produced what we now call the Hubble Tuning Fork. A modern version of this diagram is shown in Figure 1.1. These diagrams are composed mainly of three types of galaxies: ellipticals, spirals and lenticulars (or S0s, which have an intermediate morphology between ellipticals and spirals). Galaxies that do not fit into the three categories are called irregular galaxies. As Hubble thought this sequence of galaxies occurred as an evolutionary progression, he named ellipticals and spirals as early- and late-type galaxies, respectively - a naming convention that we continue to use today in a somewhat confusing manner as we know it no longer applies. Spirals may form ellipticals upon merging, and in some cases a disk may then reform (e.g., Springel & Hernquist 2005; Wang et al. 2012b).

We are mainly concerned with late-types in this thesis, so we begin by describing their general properties further here. These spirals (see Figure 1.2) are so called because of the spiral arm features (e.g., Romero-Gómez et al. 2007; Bertin & Amorisco 2010) that can be seen in their rotating disk of stars, gas and dust (e.g., Block et al. 2007; Wada et al. 2011). They can be further subdivided into barred (SB) or unbarred (S) galaxies, depending on whether or not a bar is seen extending from the central regions of the galaxies and from which the spiral arms begin (e.g., Cabrera-Lavers et al. 2008; Nair & Abraham 2010; van den Bergh 2011). Lower case letters appear after the S(B) designation, such that S(B)a spirals have numerous, tightly wound arms but S(B)c galaxies have less, and looser arms (Hubble, 1926). van den Bergh (1960a,b) also added "luminosity classes" within each of these categories, with Roman numeral labels from I to V with decreasing luminosity. Sandage (2005) notes that although these classes were originally based on the regularity or order of the spiral arm structure in each galaxy, this was later shown to correspond to the galaxies' luminosities - with a four-magnitude range between classes I and V.

Ongoing star formation occurs within the arms (e.g., Elmegreen 2011), and as such contain many hot, young stars making the arms more visible than the rest of the disk (e.g., Grosbøl & Dottori 2012). The disk can also be decomposed into different components: the bar, the "thin disk", which contains relatively young stars, and the "thick disk", which - as the name implies - is spatially more extended above and below the thin disk, is more diffuse and contains older stars (e.g., Haywood 2008; Sánchez-Janssen et al. 2010). Late-types usually, but not always, have a bulge of stars at the centre of the disk, and independent of the disk (e.g., Böker et al. 2002; Walcher et al. 2005; Oohama et al. 2009). The bulge may be "classical", i.e., similar to elliptical galaxies in that they contain older, redder stars, or may have been built through secular evolution, i.e., forming from disk processes (Combes, 2009). All of these components are embedded in a faint sphere of stars, called a stellar halo (e.g., Kinman et al. 2012; Greene et al. 2012), which itself is enveloped in a dark matter halo (e.g., Navarro et al. 1997; Merritt et al. 2006). Sprinkled throughout are star clusters, which are compact groups of $\lesssim 10^6$ stars; some associated more with the disk, while others have properties similar to the halo (e.g., Zinn 1985; Kissler-Patig et al. 1997). We later discuss stellar halos and star clusters in much more detail in Sections 1.4.5 and 1.4.4, respectively.

Early-type galaxies have a huge range in size and luminosity. Brightest cluster galaxies (BCGs) are the largest examples, and some of these (called cD's) have vast, extended outer halos. gE's generally have a larger body and more extensive outer halo than normal ellipticals. The closest examples are the gE's Maffei 1 at 3.0 $\pm$ 0.3 Mpc, (Fingerhut et al., 2003), and NGC 5128 at 3.8 $\pm$ 0.1 Mpc (Harris et al., 2010). cD galaxies are found at the heart of galaxy clusters, and have elliptical-like nuclei but much more extended envelopes (e.g., Morgan 1958; Matthews et al. 1964; Carrasco et al. 2010). The nearest example of a cD galaxy is M87 (16.4 $\pm$ 0.5 Mpc; Bird et al. 2010). The closest intermediate-luminosity, "normal" ellipticals can be found in the Leo (10 Mpc), Virgo (16 Mpc) and Fornax (19 Mpc) galaxy clusters (Harris et al., 2007a). As even the closest cD's, giant and "normal" elliptical galaxies are relatively far away and outside of the Local Group, we do not discuss these further here.

However, there are estimated to be over 100 of the ellipticals' smaller siblings in the Local Group, and they can be split into four classes (McConnachie, 2012). Compact ellipticals (cE's) have luminosity ranges similar to normal E's (-23 $\lesssim M_B \lesssim$ -15) but have a reduced spatial extent (1-10 kpc; e.g., Chilingarian et al. 2009; Kormendy et al. 2009; Huxor et al. 2011b). Dwarf ellipticals (dE's) are similar in spatial scale to cE's but are fainter (-18 $\lesssim M_B \lesssim$ -13; e.g., Michielsen et al. 2008; Aguerri & González-García 2009). Dwarf spheroidals (dSph's) were, until relatively recently, the faintest satellite galaxies known (-15 $\lesssim M_B \lesssim$ -8), and as a result the only examples known are those found in our Galaxy (e.g., Tolstoy et al. 2009) and M31 (e.g., Tollerud et al. 2012). Now, however, even fainter dwarf galaxies, the "ultra-faint dwarfs" (or UFDs, discussed more below) have been discovered within the last decade. Figure 1.3 shows the distribution of these various galaxy classes in both magnitude-surface brightness and magnitude-half-light radius spaces. We explore the differences between the different categories in the following sections.

1.3 The Local Group

The Local Group (LG) provides us with the best opportunity to study old stellar populations because the galaxies within it are close enough that we can easily resolve their individual stars. In this thesis, we focus in particular on M33 - a galaxy that is quite different to all of its nearby neighbours - and its oldest stellar components (both the stellar halo and the old globular clusters).

The LG is dominated by two galaxies: the MW and the Andromeda galaxies. Although they are approximately equal in size (e.g., Watkins et al. 2010; McMillan 2011), they bring with them quite different galactic retinues.

There are broadly two types of dwarf galaxies in the MW: brighter "classical" dwarf spheroidals (e.g., see the earliest discovery by Shapley 1938), and the ultra-faint dwarfs (UFDs; e.g., Brown et al. 2012) that have been discovered in the past few years thanks in part to the the Sloan Digital Sky Survey (SDSS; e.g., Abazajian et al. 2003; Aihara et al. 2011). The MW has two dwarf irregular galaxies (the Large and Small Magellanic Clouds; LMC and SMC, respectively). The discovery of Pisces II (Belokurov et al., 2010) brings the total number of MW dwarf galaxies to 27. This sample is expected to be incomplete, not least because below Galactic latitudes of $b < 30$ degrees the Galactic disk obscures our view (McConnachie, 2012).

Our Galaxy also hosts over 157 globular clusters (GCs; Harris 1996, December 2010 version). GCs are spherical collections of up to 10^6 gravitationally-bound, approximately coeval stars (although some show clear signs of multiple stellar populations, as we discuss further in Section 1.4.3). Section 1.4.4 further describes globular clusters, and properties of globular cluster systems (GCSs). Appendix A also contains details on the catalogues of GCSs of the Local Group galaxies.

How typical is the MW for having this collection of satellite objects compared to other galaxies with similar luminosities? If it is atypical, could this explain some of the discrepancies between ΛCDM and observations? Observations (e.g., Liu et al. 2011; Tollerud et al. 2011) and numerical simulations (Boylan-Kolchin et al., 2010; Busha et al., 2011) suggest that to have two satellites the size of the MCs is somewhat atypical, but will occur 5-25% of the time. This estimate increases if just one MC-analog is required. Tollerud et al.

(2011) also show that the LMC is atypically bluer than LMC-analogs, giving further support that it may be undergoing a triggered star formation period as it tidally interacts with the MW. Strigari & Wechsler (2012) show that by limiting the study to dwarf galaxies *brighter* than Sagittarius (the third brightest MW dwarf, after the LMC and SMC), the MW has a statistically similar number of classical dwarf spheroidals to MW-analogs.

In comparison, M31 has 29 dwarfs so far discovered (see Richardson et al. 2011; Slater et al. 2011; Bell et al. 2011, and also Figure 1.4), and there is evidence for a group of AGB stars near the north-east edge of the disk suggestive of an additional dwarf (Davidge, 2012). The radial distribution of dwarfs around M31 shows no decline out to the radii so far probed (e.g., $\sim$150 kpc by PAndAS; Richardson et al. 2011), so it is likely there are more dwarfs to be found at large projected radii. In size-luminosity space, the dwarf galaxy satellites of MW and M31 have no statistically differing distributions (Brasseur et al., 2011). M31 has only one dwarf irregular galaxy (IC10), but also has one compact elliptical (M32), three dwarf ellipticals (NGCs 147, 185 and 205), a transition dwarf (LGS3), a low-mass spiral (M33), and $\sim$3 times as many GCs as the MW (Revised Bologna Catalogue, version 4, December 2009; Galleti et al. 2004 - see Appendix A for details).

M31 GCs differ from MW GCs not just in number; M31 has more relatively bright clusters at large radii, and some of these are quite diffuse (e.g., Mackey et al. 2007; Huxor et al. 2011a). MW GCs at large radii are only moderately extended, but very faint (i.e., the Palomar clusters) with the exception of NGC 2419, which may be a remnant core of tidally stripped dwarf galaxy. Note that these faint clusters are still brighter than some of the UFDs. In general, the GCs' radii appear to increase with galactocentric distance (see

Figure 1.5). However, Tanvir et al. (2012) point out that selection effects could prevent us from seeing such clusters nearby because their diffuse nature would make them difficult to detect. There may also be a physical selection effect if such clusters are not able to survive tidal disruption when they are closer to the centre of the Galaxy.

Apart from the properties just mentioned (number, luminosity, spatial extent, and spatial distribution), other GC properties that are commonly measured and compared are their metallicities (i.e., the heavy-element abundances), ellipticities and orbits.

M33 is the third most massive and a unique member in the LG, and is the primary focus of this thesis. As such, we discuss this galaxy in context throughout this work (in particular, see Sections 2.1 and 4.2.4 for introductory material), but we briefly highlight here a number of features here not discussed elsewhere. Martin et al. (2009) suggest that And XXII may be a satellite of M33 ($\sim$40 kpc away) rather than M31 ($\sim$200 kpc away), a claim supported by systemic velocity measurements from spectroscopic information (Tollerud et al., 2012), and of interest because this would make And XXII the first known satellite of a satellite. M33 has a smaller number of GCs ($\sim$18 that have ages $> 10^{10}$ years) compared to its larger neighbours, and has 428 confirmed star clusters (both old GCs *and* young clusters; see Appendix A for details of the M33 GCS).

We note that the distance to M33 has historically been uncertain, with estimates ranging between 730 ± 168 kpc (Brunthaler et al., 2005) to 964 ± 54 kpc (Bonanos et al., 2006). In Chapter 2 we use 870 kpc, consistent with Huxor et al. (2009) and Sarajedini & Mancone (2007). In Section 3.2.1 we use 784 kpc, as used by Barmby et al. (2009). In Section 3.2.2 and throughout Chapter

4, we use 809 kpc, consistent with McConnachie et al. (2004). The latest PAndAS estimate is 820^{+20}_{-19} kpc (Conn et al., 2012). The different distances we use arise because we were being consistent with the preceding papers in individual projects. However, if we were to interchangeably use these different distances, this would only affect the structural parameter results in Chapter 3 - and then, only to a degree smaller than the differences we measure by using different models to measure the structural parameters.

1.4 Halos and Their Contents

We primarily study stellar halos and GCs in this thesis. However, these objects are necessarily linked to dwarf satellite galaxies. We further explore the reasons why in more detail below in Sections 1.4.2 and 1.4.3, but we briefly summarize both their importance and connection to halos and clusters here.

Some objects that we currently classify as GCs may be the remnant cores of dwarfs (and if so, it is likely that they contributed to the stellar halo when they were tidally disrupted). We also note that subgroups such as clusters and dwarfs were more cleanly classified in the past, but relatively recent work has revealed that there is considerable overlap between these different subgroups and that classifications are becoming increasingly difficult (e.g., Brodie et al. 2011, Hwang et al. 2011, and McConnachie 2012).

For example, it has been common to plot magnitude versus half-light radius[1] for these objects (i.e., to consider M_V-r_h space). This parameter space in particular was chosen because the quantities are easily measurable and characterize the whole galaxy. Earlier versions also showed distinct groups of

[1]We note that the half-light radius, r_h or $r_{1/2}$, is also known as the effective radius, r_e

objects and correlations between different groups, implying that there were clear physical origins for each. However, now the picture is more ambiguous - and a recent example is shown in Figure 1.6 (discussed in more detail in Section 1.4.3).

The increase in ambiguity among the various subgroups, especially as seen on the M_V-r_h diagrams, has arisen because of the greater sensitivity of today's instruments that allow us to uncover steadily fainter objects. The discoveries of both the UFDs and ongoing events such as the discovery of the Sagittarius dwarf galaxy (Ibata et al., 1994) and its disruption (Ibata et al., 2001), have seen a resurgence of interest in dwarfs and their role interacting with and shaping the structure of their parent galaxies. As building blocks in the hierarchical merging process, it is essential to further understand them and their place within the ΛCDM paradigm. As Aguerri & González-García (2009) point out, however, we are still uncertain of their origin; do they collapse as a smaller version of regular elliptical galaxies, are they stripped galaxies, or are they tidal debris?

We begin by exploring the current literature on halo components, first with dwarf galaxies and then move on to discuss GCs and stellar halos.

1.4.1 Dwarf Satellite Galaxies

As mentioned previously, one of the problems with the ΛCDM paradigm is that it predicts one if not two orders of magnitude more satellite galaxies compared to the numbers that we currently observe (e.g., Kauffmann et al. 1993; Klypin et al. 1999; Moore et al. 1999; Springel et al. 2008; Diemand et al. 2008). Various solutions have been proposed such as the suppressed formation of these small galaxies via a photoionizing background - possibly the reionization radiation - or by supernova-driven winds (e.g., Benson et al. 2002; Okamoto et al. 2008).

The missing *massive* satellites problem (Boylan-Kolchin et al., 2011; Parry et al., 2012) could be solved by making the mass of the MW, M_{MW}, smaller by a factor of 2-3 than current estimates (Wang et al., 2012a; Vera-Ciro et al., 2012). A lighter MW may not have a high enough rotation speed ($\gtrsim$ 220 km s^{-1}) although other data allows the M_{MW} to be smaller (Wang et al., 2012a). Vera-Ciro et al. (2012) also point out that this lowers the probability of the MW hosting the Magellanic Clouds (MCs).

It is also possible that at least the bright dwarfs are not remnants of primordial mergers (Metz & Kroupa, 2007). If the bright dwarfs were primordial satellites, we would expect them to be as old as the population of halo field stars - but they do not appear to be from spectroscopic studies of stellar metallicity (e.g., Helmi et al. 2006; Tolstoy et al. 2009) and RR Lyrae pulsation properties (e.g., Dall'Ora et al. 2003; Bersier & Wood 2002).

What might the primordial satellite galaxies instead be? Metz & Kroupa (2007) suggest that they could be ultra-faint dwarfs (UFDs), and if so they could also potentially answer the missing satellite problem (at least at fainter magnitudes). Only a handful of UFDs have been discovered so far, but this is partly because of the limitations of the SDSS, the data which enabled the discovery of the majority of UFDs. The SDSS is only capable of reaching magnitudes of $r \sim 22.5$ or effective distances of tens of kpc (Munoz et al., 2012) and has so far covered 14000 square degrees (only $\sim 35\%$ of the total sky with the 8th Data Release[2]). Therefore, deeper (e.g., Subaru/HyperSuprimeCam)

[2]http://www.sdss3.org/dr8/

and faster (e.g., Pan-STARRS, SkyMapper, the Dark Energy Survey and the Large Synoptic Survey Telescope) surveys are expected to reveal tens to hundreds more UFDs (Koposov et al., 2008; Tollerud et al., 2008). The ages of stars within the UFDs are also consistent with them being the primordial subpopulation of dwarfs (see, e.g., Frebel et al. 2010; Moretti et al. 2009; Dall'Ora et al. 2012).

In suggesting the brighter dwarfs are not primordial merger remnants, Metz & Kroupa (2007) propose that they were instead created by tidal forces of subsequent mergers and are therefore tidal dwarf galaxies. That tidal forces might be at work in galaxies is not a new idea (e.g., Zwicky 1956). Observations have shown that tidal dwarf galaxies can form through interactions of their larger parent galaxies (e.g., the Antennae Galaxies; Mirabel et al. 1992).

Further clues to the dwarfs' past may come from their spatial distribution. Bailin et al. (2008) show that, in general, elliptical and red spiral galaxies host satellites that are preferentially located towards their major axes, whereas blue spirals have an isotropic distribution. That the MW satellites had an isotropic distribution was observed decades ago (e.g., the "Magellanic Plane" proposed by Lynden-Bell 1976), and makes the MW atypical because its dwarfs appear to be more on a plane. These observations have recently been revisited in light of the growing number of MW satellites. The "disk-of-satellites" (DoS) is inclined to the classical stellar disk by $\sim$88 degrees (Metz et al., 2007), and appears to be rotationally supported (Metz et al., 2008). We note that some authors prefer the term "plane-of-satellites" (PoS) so that the rotational support is not inferred (e.g., Keller et al. 2012). We adopt this terminology to leave open the ambiguity of the origin of the anisotropic distribution of the dwarfs.

The latest work by the Kroupa group on the PoS is by Pawlowski et al. (2012) who combine the results of the MW dwarf satellites, young halo GCs and the streams of stars and gas (which approximately trace out the orbit of their progenitor; e.g., Odenkirchen et al. 2003). Pawlowski et al. suggest the MW is surrounded by a vast polar structure (VPOS) which extends between 10-250 kpc, making it even greater in spatial extent that the PoS, and is aligned such that the MW appears to be an ancient remnant polar-ring galaxy (e.g., Whitmore et al. 1990). The probability of finding 7 of the 14 analysed streams in alignment is only 0.3% if assuming an isotropic distribution. They claim that individual infalling galaxies do not align to form a disk structure. However, Keller et al. (2012) find that when they similarly consider young halo GCs at $>$10 kpc, they also find a plane of objects (24$\pm$4 kpc thick and inclined 8$\pm$5 degrees to MW disk's polar axis) but unlike Pawlowski et al. (2012) they say that their findings are consistent with accretion from large-scale structure (LSS) filaments, and that the young halo GCs are tracers of the disrupted dwarf galaxies that created the stellar halo. For $<$10 kpc, and for the old halo (OH; $\sim$13 Gyr) GCs the distributions are isotropic.

Pawlowski et al. (2012) suggest that the VPOS implies that the MW either had a major merger or a "fly-by" merger, possibly with M31 or the LMC. However, in the case of an MW-M31 interaction, it is difficult to resolve this idea with proper motion measurements (Sohn et al., 2012) and N-body and semi-analytic simulations (van der Marel et al., 2012) that imply the MW and M31 have yet to have had their first pass with one another. If such an encounter did occur with either M31 or the LMC, should they not also show anisotropy?

The idea of a PoS around M31 was only proposed relatively recently (see "A Polar Great Circle of Satellites?" in Grebel et al. 1999). Metz et al. (2007) show that subsets of the M31 dwarfs could be in a disk (inclined 59 degrees to M31 disk), but with no apparent relation between the MW and M31 PoS's as they are inclined $\sim$55 degrees to one another. Incorporating some of the newly-discovered UFDs, Metz et al. (2009a) find that they lie on the same PoS. The M31 PoS is oriented edge-on from the MW's perspective - with a common N-S direction to the MW, as expected from a tidal interaction. The whole collection of M31 dwarf satellites has not yet been analysed with regards to the PoS, although Richardson et al. (2011) do mention that 24 out of the 34 satellites lie on the M31's side closest to the MW.

Just as it has been suggested that the MW and some of its dwarfs have been formed through a major merger, a similar argument has been put forward for M31 - most recently by Fardal et al. (2008) and Hammer et al. (2010). Hammer et al. apply Occam's razor to say that many of M31's features can be explained by a major merger $\sim$5-8 Gyr ago, and they show this through simulations which successfully explain many but not all of M31's features. M31 halo substructures have similar metallicities (Ferguson et al 2005), and Hammer et al. say that this is unlikely if they are due to multiple different minor mergers. They also note that it would no longer be necessary to identify all the different remnant progenitors. As deeper data sets become available, it is becoming harder to justify that these progenitors exist.

How has M33 affected the satellite system of M31? It could have disturbed the M31 dwarfs, in a similar manner to M32 if M32 was previously large enough (e.g., Bekki et al. 2001). Davidge et al. (2012) claim that there was a "high" probability that M31 and M33 had a close encounter with one another in the relatively recent past, and summarize the timings of such an event based on different evidence: (1) the star formation history suggests such an event occurred >0.5 Gyr ago (Davidge & Puzia, 2011); (2) the position and velocity of M31 places it at 1-3 Gyrs (Putman et al., 2009); (3) Bekki (2008) suggests 4-8 Gyr using the HI bridge between M31 and M33 (Braun & Thilker, 2004); (4) the simulation in McConnachie et al. (2009) suggests several Gyrs; and, (5) an encounter would trigger star formation in M31's disk (McConnachie et al., 2009; Davidge & Puzia, 2011), and Saglia et al. (2010) measure M31's disk stars' age to be 4-8 Gyr, consistent with this picture.

Given that there is evidence that both the MW and M31 have a PoS, we discuss these findings and their implications for both galaxies together here. Metz et al. (2007, 2009b) argue that the host disks and satellite disks of both galaxies are inclined to the supergalactic plane (de Vaucouleurs, 1953), and therefore unlikely to be funnelled down through it. However, Libeskind et al. (2009) find that MW-analogs with at least 11 satellites are found to have a PoS 30% of the time. Kroupa et al. (2010) claim that this is a selection effect: the host-satellite groups occur only 1.4% of the time in simulations by Libeskind et al. so only 0.4% (or 30% of 1.4%) of MW-analog galaxies would have a PoS similar to the MW. Libeskind et al. (2011) and Lovell et al. (2011) show in simulations that the PoS can be reproduced if satellites are accreted along large-scale structure (LSS) filaments. Keller et al. (2012) suggest that we see this as both the PoS of both the MW and M31 broadly align with the Virgo and Fornax galaxy clusters. Keller et al. (2012) point out that MCs are on the PoS, but question whether or not they should be included in the analysis with the other dwarf galaxies in light of the results from Besla et al. (2010) which show that the MCs may be on their first infall to the MW. However Keller et al. say that if they were to be on their first infall, this information would support the idea of LSS filamentary accretion. Pawlowski et al. (2012) also note that the LMC stream has a normal close to the PoS normal (∼20 degrees).

Based on existing evidence, we conclude that it seems more plausible that M31 has undergone a major merger rather than the MW. However, that M31 may have done so does not, we believe, then mean that the ΛCDM paradigm fails to explain the build up and evolution of the Local Group. Deeper data may reveal the existence of more ultra-faint dwarfs (UFDs) and therefore further provide hints at reconciling current failures of ΛCDM on the small scales.

1.4.2 Dwarf Satellite Galaxies' Globular Clusters

If dwarf satellite galaxies have been accreted onto the host galaxy, they might be expected to bring with them their own entourage of GCs that they possessed before the merger. Indeed, there is evidence for dwarfs that have GCs associated with them.

Since the discovery of the MW's Sagittarius dwarf spheroidal galaxy (Ibata et al., 1994), there are a number of GCs that have been suggested to belong to it, but only four are considered true members (M54, Arp 2, Terzan 7 and 8; Da Costa & Armandroff 1995) with many others as former members. Salinas et al. (2012) look at two bound GCs of Sagittarius (Arp 2 and Terzan 8), and two that have been stripped from it (NGC 5634 and Palomar 12). The bound GCs have large core radii and low concentrations compared to those that have been stripped. Blue straggler analysis in the bound GCs suggest that they have not yet relaxed, with Terzan 8 less relaxed than Arp 2 (Salinas et al., 2012). These bound GCs are also similar to the extended star clusters because of their low concentrations and large half-light radii ($\sim$ 15 pc). Salinas et al. (2012) further suggest that Terzan 8 is similar to ω Cen, NGC 2419 and Palomar 14 (e.g., Ferraro et al. 2006, Dalessandro et al. 2008 and Beccari et al. 2011, respectively) in that it is not relaxed.

Other dwarfs with their own GCs include Fornax (e.g., Cole et al. 2012) and Canis Major (e.g., Forbes et al. 2004). Fornax is unique amongst the previous examples as it is the only undisrupted dwarf to have bound GCs. Dwarfs outside of the LG have also been seen to have their own GCS (e.g., Miller et al. 1998).

1.4.3 Globular Clusters as Remnants of Dwarf Satellite Galaxies

If we again take a look at an example of the M_V-r_h space, it is apparent that the boundaries between GCs, dwarfs and other objects are not so clear. Figure 1.6 is from Hwang et al. (2011; their Figure 7). The plot includes many different types of objects from various sources: GCs (MW, LMC, NGC 5128, and the central Fornax cluster galaxy, NGC 1399), ESCs (M31, M33, and the barred irregular LG galaxy, NGC 6822), "faint fuzzies" (NGC 5195, a dwarf of the Whirlpool Galaxy, NGC 5194; in the region indicated by the extra axes), ultra-compact dwarfs (UCDs; Fornax cluster; see next paragraph), dwarf galaxy transition objects (DGTOs; Virgo cluster), dwarf galaxies (MW, M31), and UFDs (MW). The dashed line represents the van den Bergh & Mackey (2004) limit ($\log(R_h) = 0.2M_V + 2.6$), below which are "typical" GCs. Anything above this line is considered an outlier in some way, and is less likely to have formed via the same evolutionary path as the objects below the line. Obvious outliers are labelled (i.e., ωCen and NGC 2419), as well as the NGC 6822 ESCs in Hwang et al.'s study (C1-C4), and two previously discovered clusters by the *Hubble Space Telescope* (HST; H7 and H8). Hwang et al. (2011) also highlight the "avoidance zone", the very faint box defined by -9.4 $\lesssim M_V \lesssim$ -8.0 and 10 $\lesssim R_h \lesssim$ 60 pc.

In discussing Figure 1.6, a new stellar system has been introduced - UCDs - so we briefly digress to describe these objects. Occupying a similar location in M_V-r_h space to DGTOs, their origin is still somewhat of a mystery. Objects of this type were first revealed over a decade ago. Hilker et al. (1999) discovered two compact stellar objects that had surface brightnesses similar to GCs but luminosities like dEs, in the Fornax Spectroscopic Survey (FSS, Ferguson 1989). Drinkwater et al. (2000) found an extra three compact stellar objects and revisited the two from Hilker et al., to show that all five had magnitudes between the brightest MW GC (ωCen; Harris 1996, December 2010 version) and compact dwarf galaxies. They suggested that they could be star clusters or M32-analogues. Mieske et al. (2002) asked if they are distinct population or if they are a smooth extension of an already-known population. They spectroscopically observed a collection of "ultra-compact objects" (UCO's), including twelve of the brightest GCs (4 previously known objects: 2 from Hilker et al., 2 from the NGC 1399 GC study in Kissler-Patig et al. 1999). Their deeper study allowed them to show that the magnitudes of all their objects suggested a smooth transition between GCs and UCOs for all but one UCO. This one exception was found to have a relatively high metallicity of Fe/H $\sim$ -0.5. Mieske et al. continued with a smaller subsample composed of UCO's in pre-existing wide-field images of the Fornax cluster, for which they were able to obtain radial velocities, and found that the subsample's distribution was consistent with that of the GCS. Similarly, the spatial distribution was similar between the UCOs and GCs. Hilker (2011) summarizes the latest findings concerning UCDs: there are >150 candidates from a combined sample in the Fornax, Hydra I, Centaurus and Virgo galaxy clusters, and he suggests that this sample is heterogeneous. The blue, metal-poor (MP) UCDs appear as an extension of the blue, MP GCs, whereas the red, metal-rich (MR) UCDs extend to higher luminosities. Hilker suggests that the latter group may therefore be massive star cluster complexes in merger or starburst galaxies. Chiboucas et al. (2011) have also found 27 and 14 high- and low-confidence UCD candidates, respectively, in the Coma Cluster.

To continue exploring the apparent overlap with GCs and other stellar systems, it appears that some objects that we currently define as GCs were the nuclei of dE's in earlier times of their evolution. Majewski et al. (2012) highlight several objects that can be seen at various stages of this transformation, starting with the least transformed objects: (1) the cluster M54 still appears to be within its parent galaxy, the Sagittarius dwarf; (2) CL 77 (Annibali et al., 2012), also known as B15 (Strader et al., 2012), has evidence of tidal tails, is elliptical ($\epsilon \sim 0.24$; Annibali et al. 2011), and is located in the starburst irregular NGC 4449, a galaxy just outside of the LG (3.82 ± 0.18 Mpc); (3) Palomar 14 (Sollima et al., 2011) has no galaxy or streams, but possible short tails; and (4) ωCen and G1 have no parent galaxy, streams or tails.

If ω Cen and G1 do not show any signs of the transformation process, but rather appear to have completed it, what other clues do we have that they were at one time dE nuclei? Both objects are amongst the largest clusters, they have multiple stellar populations (e.g., Bellini et al. 2010), a chemical abundance spread (e.g., Johnson & Pilachowski 2010), they are both flattened (e.g., Pancino et al. 2000; Meylan et al. 2001), and they have larger-than-normal velocity dispersions for GCs, and thus larger M/L ratios (e.g., Sollima et al. 2009). G1 may also have a central black hole (Gebhardt et al., 2002), and a stream of stars close by (Ferguson et al., 2002). ωCen has a retrograde orbit (Dinescu et al., 1999), and tidal debris (Majewski et al., 2012).

Various other clusters also show evidence for multiple stellar populations (e.g., Kacharov & Koch 2012), but perhaps the most interesting is NGC 1851 as it appears to have a *bimodal* population (e.g., Salaris et al. 2008) such that Carretta et al. (2010, 2011) suggest it is a merged system of two clusters.

Other clusters may also be remnants of dE nuclei, for example because of their large size (e.g., the MW's NGC 2419, van den Bergh & Mackey 2004; or M31's 037-B327, Ma et al. 2006) or because they appear to be in the process of dissolution (e.g., Pal 5, Rockosi et al. 2002; Odenkirchen et al. 2003; or NGC 5466, Belokurov et al. 2006). UmaII is also an interesting case; when it was first identified it was unclear whether it was a GC or a dwarf (Grillmair, 2006), although it was later classified as a UFD (Zucker et al., 2006). Further observations have revealed that it is elongated and extended (e.g., Muñoz et al. 2010), and possibly in the process of breaking up. It was originally thought to be progenitor of the Orphan Stream (Fellhauer et al., 2007), but this does not appear to be the case now (Muñoz et al., 2010; Newberg et al., 2010).

Various other objects remain somewhat controversial as to their nature. One such example is the newly-discovered ultra-faint (M_V=-0.4±0.9) object in Ursa Minor - which could be a cluster or a dwarf satellite galaxy (Munoz et al., 2012). These authors favour the former, although either way it is one of the faintest objects in each category. As a GC, it would compete with Segue 3 to be the faintest (M_V=0.0±0.8; Fadely et al. 2011). In two final examples, Gilmore et al. (2007) argue that dwarfs Segue 1 and Coma Berenices should be considered large GCs, but Simon & Geha (2007) and Geha et al. (2009) say that spectroscopic information suggests that these objects have DM and are therefore dwarfs.

1.4.4 Globular Clusters

Globular clusters are the remnants of galaxy formation, having been accreted or created during merger and accretion processes, and they provide a snapshot of galactic conditions at the time of their formation. GCs subsequent redistribution can give hints of their host's evolutionary history, through their spatial structure and kinematics. They are *generally* luminous and compact objects that can be used as tracers of material otherwise too faint to see, such as halos or substructure, to estimate the shape of their host (e.g., Shapley 1918a,b), or used as a distance indicator (e.g., Rejkuba 2012). How many GCs would we expect a particular galaxy to have? The GC population size varies with the size of the host galaxy and is described by the specific frequency, S_N (Harris & van den Bergh, 1981),

$$S_N \equiv N_{GC} 10^{0.4(M_V+15)} \tag{1.1}$$

where N_{GC} is the number of GCs in a particular system, and M_V is the visual absolute magnitude of the host galaxy. Converting the host galaxy luminosities in Section 4.2 to magnitudes, and also using the number of clusters for the MW, M31 and M33 in Section 1.3, we find the specific frequencies for these galaxies are $S_N = 0.6$, 1.4 and 1.4, respectively. Typical S_N values for spirals galaxies are $S_N \lesssim 1$ (e.g., Georgiev et al. 2010), although there is considerable scatter, so these values for the LG spirals are not unexpected. The absolute number of GCs in any one system ranges from a handful (e.g., Sagittarius dwarf galaxy, Da Costa & Armandroff 1995), through several hundred (e.g., the MW, Harris 1996, December 2010 version; and M31, Revised Bologna Catalogue, version 4, December 2009, Galleti et al. 2004), to several thousands or even tens of thousands (e.g., M87, Strader et al. 2011b).

As we have already seen, it is *not* always possible to cleanly define the various objects within galaxies. Even within the subgroup of star clusters, luminosities and sizes come in a wide range (see Figure 1.6). A fairly recent discovery has been the clusters which have a more extended nature (extended star clusters, "ECs" or "ESCs", also known as "faint fuzzies"). Hwang (2011) summarizes the recent research on these objects, and comments that they appear to be seen in various types of galaxies: the MW (van den Bergh & Mackey, 2004), M31 (Huxor et al., 2005, 2011a), SB0s (e.g., Brodie & Larsen 2002; Hwang & Lee 2006; Hwang et al. 2011), and NGC 6822 (dIrr; Hwang et al. 2005, 2011). The origin(s) of ECs remains a puzzle, but several theories have been advanced (Hwang, 2011). ECs may be: tidally stripped dwarf galaxy cores (as may already apply to GCs in general); two or more merged clusters; a natural stochastic variation in clusters (i.e., the natural range of clusters includes ECs); or, a result of GC evolution (Gieles et al., 2011). Hwang et al. (2011) comment that their M_V-r_h plot shows an apparent break between ECs and the brighter UCDs/DGTOs (similar to the one seen in Figure 1.6) so that they speculate perhaps the brighter group are due to the former two ideas (i.e., stripped cores or merged clusters), while the fainter objects are due to the latter two. Brüns et al. (2011) also show with numerical simulations that ECs can form in tidal tails of interacting galaxies. Their distribution may also further our understanding. The M31 ECs appear to be associated with stellar streams (Collins et al., 2009; Huxor et al., 2011a). The ECs in NGC 5195 and M51 show an elongated spatial distribution (Hwang & Lee, 2006, 2008), which is different from those in NGC 1023 that are generally in the disk (Larsen & Brodie, 2000).

What about the spatial distribution of GCs in general? The radial distributions of GCSs are usually described either with a power law,

$$\Sigma_{GCS} \propto r^{-\alpha}, \tag{1.2}$$

or by a Sersic profile,

$$\Sigma_{GCS} \propto exp\left[\left(\frac{r}{r_e}\right)^{\frac{1}{n}} - 1\right]. \tag{1.3}$$

where the de Vaucouleurs profile is a specific example of the Sersic profile with $n = 4$. The power law is used over a restricted radial range (to the extent of the most distant GC), it over-predicts the innermost distribution (i.e., the GCS core flattens, e.g., Harris 1991), and the index has a range of 1 (massive gEs) $\lesssim \alpha \lesssim$ 2.5 (smallest Es; Brodie & Strader 2006). $\alpha \approx 2$ for both the Galactic GCS (Harris, 2001) and the M31 GCS (Racine, 1991). The de Vaucouleurs profile has a typical range for the scale radius of $10 \lesssim r_e \lesssim 50$ h^{-1} kpc. In most, but not all (e.g., M87 and M49 in Virgo; Harris 1986) cases the GCS extends to larger radii than the galaxy's halo. Harris (1986) suggests that larger galaxies' GCSs are more dependent on the initial conditions of their host galaxies, whereas smaller galaxies' GCSs are dominated more by subsequent processes that their host galaxies undergo.

The shape of GCSs is generally spheroidal. For the MW, Bica et al. (2006) find that the metal-rich (MR) GCs show an oblate spheroidal distribution, whereas the metal-poor (MP) GCs are in almost a perfect spheroid. Perrett et al. (2002) studied the M31 GCS; the MR GCs are spatially concentrated, but do not show any flattening similar to the MW MR GCs, whereas the distribution for the M31 MP GCs is not clear (it *may* have halo and thick-disk components).

It is also interesting to look at the most isolated GCs and ask why they are so distant from their host galaxy. In the MW, the most distant clusters are as follows (with Galactocentric distances from Harris 1996, 2010 edition): NGC 2419 (89.9 kpc); Pal 3 (95.7 kpc); Eridanus (95.0 kpc); Pal 4 (111.2 kpc); and, AM-1 (124.6 kpc). The most isolated cluster known up until recently was MGC1 in M31 at a projected distance of 117 kpc (or deprojected, 220 ± 20 kpc; Mackey et al. 2010). For comparison, some of the most distant *dwarf satellite galaxies* are Leo I (Held et al., 2010) at 256 kpc from the MW, and And XXVIII (Slater et al., 2011) in M31 at 365^{+17}_{-1} kpc from M31. "GC-2" in the M81 group, has replaced MGC1 as the most distant cluster, as it is located 406 ± 97 kpc behind M81 along line of sight (Jang et al. 2012; M81 is at 3.63 ± 0.14 Mpc, Durrell et al. 2010). Jang et al. also point out that GC-2 is travelling away from M81 at 200 km s^{-1}. They suggest it may have either been ejected during interactions with the group's larger galaxies, formed in isolation, or it could be a dwarf galaxy remnant - but such definitive conclusions will require further data.

Not all clusters appear by themselves. The LMC is particularly noteworthy in this regard as it has 473 candidate binary star clusters / triple star clusters / associations (Dieball et al. 2002; 10% of all clusters in LMC), but it is not the only galaxy with such clusters as the MW (NGC 869/NGC 884, e.g., Currie et al. 2010), M31 (Holland et al., 1995), the SMC (Hatzidimitriou & Bhatia, 1990) and NGC 5128 (Minniti et al., 2004) also all have binary clusters. Mucciarelli et al. (2012) acknowledge that some of these binaries are simply line-of-sight occurrences, but due to their sheer number some of them must be genuine bound clusters. They may have been born independently and later become bound, or they could have been born from the same progenitor cloud. One true bound pair is known in the LMC: NGCs 2136 and 2137. Mucciarelli et al. (2012) say that they will either finally merge or the smaller of the two will become completely disrupted by the larger. As they have such similar chemical compositions, if they merged the product would appear as a single cluster with a large ellipticity, as is observed in some LMC GCs (e.g., Mucciarelli et al. 2007).

There are several interesting features that clusters show when considering a galaxies' entire population of clusters (i.e., the GCS). The well-known $M_{SMBH} - \sigma_{bulge}$ relation (e.g., Ferrarese & Merritt 2000, Magorrian 2000), between the mass of the supermassive black hole (M_{SMBH}) and the velocity dispersion of the stars in the bulge (σ_{bulge}), can be extended to both M$_{SMBH}$-$\#_{GCs}$ (Harris & Harris, 2011) and M$_{SMBH}$-σ_{GCs} (Sadoun & Colin, 2012) relations. If M33 has a supermassive black hole, its mass is estimated to be M$_{SMBH}$ $\sim 10^6$ $M_\odot$ using data on the σ_{GCs} from Schommer et al. (1991) and Chandar et al. (2002). However, they note that results from other types of measurements are not converging so a more accurate estimate will require further data.

The vast majority of GCSs show bimodality on a colour-magnitude diagram. There is an age-metallicity degeneracy when looking at the GCS colours, but spectroscopic measurements are less affected by this degeneracy and the bimodality is still present (e.g., Strader et al. 2007, Beasley et al. 2008). Some GCS data can also be fit using trimodal distributions (e.g., Blom et al. 2012). These different subpopulations suggest different phases of star formation in the galaxies' past. It is thought that the blue (MP) clusters formed early in the host galaxy, and red (MR) clusters formed later (Forbes et al., 1997) or through mergers (Ashman & Zepf, 1992), while the opposite has also been suggested, i.e., that red clusters formed with host galaxy, and blue clusters are accreted from lower-metallicity dwarf galaxies (Côté et al., 1998).

Marín-Franch et al. (2009) observe 64 MW GCs as part of the ACS Survey of MW GCs. These GCs have a Galactocentric range between 1.2 kpc and 21.4 kpc. Marín-Franch et al. show that the MW GCs have two subsets: one that is older ($\sim$13 Gyr) and more metal poor with the opposite for the second subset. The latter is mostly associated with Sagittarius and Canis Major dwarf galaxies, which prompted Forbes & Bridges (2010) to suggest that one-quarter of the MW GCs have been accreted. It is then inferred that 6-8 satellites were accreted, and these satellites brought with them their GCs (Mackey & Gilmore, 2004; Forbes & Bridges, 2010).

The environment is obviously important for a galaxy's formation and evolution, i.e., whether a galaxy is isolated (e.g., Cho et al. 2012), or is part of a group or cluster (e.g., Côté et al. 2004; Jordán et al. 2007; Carter et al. 2008). Cho et al. (2012) note that bimodality becomes less pronounced in less luminous galaxies, as the red subpopulation dwindles to leave only the bluer clusters.

Some MW GCs also have streams, e.g. Pal 5 (Odenkirchen et al., 2001) and NGC 5466 (Grillmair & Johnson, 2006; Belokurov et al., 2006), implying that they might also contribute to the halo in a similar manner to dwarf galaxies.

In this section, we have briefly summarized some of the properties of GCs, not only in the MW but in the Local Group and further afield. They are clearly important stellar systems, of interest in themselves but also for the clues that they provide for galaxy formation and evolution.

1.4.5 Stellar Halos

Rather than studying relatively compact stellar systems, such as dwarf galaxies and globular clusters, it is possible instead to look at the entire faint and diffuse stellar halo composed of isolated field stars in which the host galaxy resides.

Unlike GCs, which tend to be bimodal in colour, field stars are usually unimodal on the metal-rich side (Harris & Harris, 2002; Peng et al., 2008). The metal-rich GCs and stellar halos have similar chemical and spatial properties (e.g., Helmi 2008; Martell et al. 2011).

The MP halo is thought to have been built from accretion events - both the direct contribution from merging galaxies that are subsequently disrupted, and also from excited stars within the host galaxy (Searle & Zinn, 1978; Ibata et al., 1994; Bullock & Johnston, 2005; Zolotov et al., 2009; Carollo et al., 2010). Martell & Grebel (2010) suggest $\lesssim 50\%$ of stars formed in GCs.

In Section 4.1, we discuss recent literature on the halos of the most massive members of the Local Group and briefly summarize studies of halos beyond the Local Group. Here, we expand on both the MW halo and on the study of halos beyond the Local Group.

1.4.5.1 The Milky Way Halo

From within the Galaxy we are in a unique position to be able to measure the 6D phase-space (location and velocity) and chemical abundances of many individual stars (Carollo et al., 2012). There is a growing amount of literature that the MW halo has at least two components (e.g., Carollo et al. 2007 and references therein). Carollo et al. (2007) use SDSS data to observe over 2x10^4 stars with distances out to 20 kpc from the Sun, and velocities for half of the sample out to 4 kpc. They also find evidence for inner and outer halo components from several different measurements, and estimate that the inner halo dominates out to 10-15 kpc from the Galactic Centre, and the outer halo becomes more prominent at a distance beyond 15-20 kpc. The two components have different iron abundances ($[\mathrm{Fe/H}]_{inner} \sim -1.6$; $[\mathrm{Fe/H}]_{outer} \sim -2.2$) and density profiles (the axial ratios of the inner and outer halos are estimated to be $\sim$ 0.6 and $\sim$ 0.9-1.0, respectively). Miceli et al. (2008) present observations of RR Lyrae stars, and find two distinct populations (Oosterhoff types I and II) with different profiles: $\rho \sim R^{-2.26\pm0.07}$ and $\rho \sim R^{-2.88\pm0.11}$. Carollo et al. (2012) find that the Galactocentric rotational velocities and its dispersion are $v_{\phi,inner} = 7 \pm 4$ km s^{-1} and $\sigma_{V_\phi,inner} = 93 \pm 35$ km s^{-1}, and $v_{\phi,outer} = -80 \pm 13$ km s^{-1} and $\sigma_{V_\phi,outer} = 138 \pm 58$ km s^{-1}.

Carollo et al. (2007) discuss what the different properties of the two-component halo imply about the progenitors in each case. The inner halo, they suggest, would have been built with relatively few but relatively massive progenitors that merged dissipationally, while less massive but more numerous progenitors would have created the outer halo through dissipationless mergers and tidal disruptions. The composition of an outer halo composed in such a way appears to match current observations (e.g., Roederer 2009; Nissen & Schuster 2010; Schlaufman et al. 2011; Carollo et al. 2012). Courteau et al. (2011) photometrically analyse M31's halo and find that it can be described by 2D and 3D power-law profiles with indices of $\sim -2.5 \pm 0.2$ and -3.5, both similar to the MW's, and it dominates beyond $\gtrsim 9$ kpc.

1.4.5.2 Halos Beyond the Local Group

As we will discuss further in Section 4.1, detections of halos around galaxies outside of the Local Group are very difficult. Here, we provide further details of these studies, beginning with searches for halos around single late-type galaxies.

One of the problems plaguing distant halo detections is demonstrated by NGC 5907. Earlier observations (e.g., Sackett et al. 1994a) led to conclusions of a halo-like structure, but were revealed to be obscured detections of concentric arcs and loops from a low-mass accreting satellite (Shang et al., 1998). Similarly, a diffuse extended component around NGC 4244 is observed up to ~15 kpc above the thin disk and reaches a surface brightness detection limit of $\mu_R \approx 31$ mag arcsec $^{-2}$ (Buehler et al., 2007; de Jong et al., 2007; Seth et al., 2007). However, Buehler et al. note that this feature is asymmetric, suggesting that it is more likely due to a relatively recent accretion event rather than a true halo.

It may be that deeper observations that reach fainter surface brightness magnitude limits will reveal an underlying halo component in addition to the brighter substructure components seen in the above examples, exactly as we see in the Local Group. This also seems to be the case in the Milky Way analogue galaxy, NGC 891, where observations reveal a stellar halo (Tikhonov

& Galazutdinova, 2005; Mouhcine et al., 2007; Rejkuba et al., 2009) with a broad range of colour values suggesting a broad stellar metallicity distribution function (mean [Fe/H]≈ -0.9) and old, metal-poor stars. In their ~90 kpc x 90 kpc observations Mouhcine et al. (2010b) also detect both a giant stream, which is measured out to ~50 kpc at its greatest extent, and a "cocoon-like" envelope around the bulge and disk of the galaxy extending 15 kpc and 40 kpc, along the minor and major axes, respectively.

Possibly the furthest hint of a galactic stellar halo comes from a distant edge-on disk galaxy located in the *Hubble Ultra-Deep Field* image (Zibetti & Ferguson, 2004). Colour and structure of emission at $\mu_{V,i,z} \approx$ 29-30 mag arcsec^{-2} (or $\mu_{g,r,i} \approx$ 28-29 mag arcsec^{-2} in the rest-frame equivalents) above the disk are similar to those found in SDSS stacked images of local disk galaxies, which are discussed below.

In other examples, the picture is more confusing as components that may be halos are indistinguishable from extensions of the thick disk or bulge (Dalcanton & Bernstein, 2002; de Jong et al., 2008; Barker et al., 2009, 2012).

Several studies look at large collections of galaxies and stack their images, rather than look at individual galaxies. Zibetti et al. (2004) analyze 1047 edge-on galaxies from the Sloan Digital Sky Survey (SDSS) Large-Scale Structure Sample 10 (LSS10; Blanton et al. 2003). By stacking the re-scaled images, Zibetti et al. are able to reach $\mu_r \approx 31$ mag arcsec^{-2}, and find that the resulting extended stellar component can be described by a 2D $\Sigma \approx r^{-2}$ law (or a 3D $\rho \approx r^{-3}$ law), and is possibly redder than the known reddest stellar populations (the authors caution that this colour difference is not observed throughout all colour bands, and that there are large uncertainties). This result is at least consistent with the idea that all galaxies have stellar halos, and that these halos are old and surprisingly metal enriched. However, Zackrisson et al. (2011) and Zackrisson & Micheva (2011) highlight a discrepancy between nearby studies that resolve individual stars in the stellar halo, versus surface photometry of more distant galaxies which appear to have much redder colours. They outline observational requirements to help resolve this issue, but advances are likely to require a time-intensive ground-based study on the next-generation space telescope. Another problem is the claim that instrumental scattered galaxy light is responsible for much - but not all - of the detected signal of halos in edge-on galaxies (de Jong, 2008). However, even after de Jong subtracts the scattered contribution, a halo is still apparent and is well fit using a Sersic profile.

Other work on combined images includes that by Bergvall et al. (2010) who stack 1510 nearly edge-on galaxies from SDSS Data Release 5 (DR5), reaching $\mu_r \approx 31$ mag arcsec^{-2}. Even after accounting for light scattering effects, a red excess is still seen. The authors suggest dust extinction and a bottom-heavy IMF could explain this excess. Tal & van Dokkum (2011) stack over 42500 SDSS DR7 images of luminous red galaxies, extending out to 400 kpc around the centre of the stacked galaxies and reaching $\mu_r \approx 30$ mag arcsec^{-2}; the observed stellar halos (≤ 100 kpc) are best fit with a Sersic profile. Beyond 100 kpc, the authors suggest that the observed excess light could be due to intragroup or intracluster light, or perhaps a change in the light profile of the galaxy itself.

Halos have also been observed around other types of galaxies, not just late-type edge-on galaxies. Weil et al. (1997) see a faint diffuse asymmetrical structure around the Virgo Cluster's central elliptical galaxy, M87, out to 100 kpc, which they claim is from an accreted spheroidal galaxy. Studies of planetary nebulae (Doherty et al., 2009) and globular clusters (Romanowsky et al., 2011) support this idea. Nearby starburst galaxies are also seen to have faint stellar envelopes (Bailin et al., 2011; Ryś et al., 2011a). Harris et al. (2007b) observed the Leo elliptical NGC 3379 and saw a metal-poor halo. In the giant elliptical NGC 5128 (Centaurus A), large-scale substructure is seen out to $\gtrsim$ 20 kpc (Malin et al., 1983; Peng et al., 2002). The metallicity and age distribution for the NGC 5128 halo stars at a projected galactocentric distance $R \sim 40$ kpc have been explicitly derived by Rejkuba et al. (2011), from a deep HST/ACS dataset - unique for any giant elliptical. They find that about 80% of the stellar population there is classically old at $t = 12$ Gyr with a very broad range in metallicity ($0.0001 \leq Z \leq 0.04$).

1.5 Introduction to the Following Chapters

We have seen, in the preceding sections, that old halo components are vital to help our understanding of the conditions in which galaxies first form and also how they subsequently evolve. Within the Local Group, most attention has been directed towards the two most massive members, the MW and M31. The halo of the third most massive member, M33, has had relatively little scrutiny. The aim of this thesis is observe M33's halo with an unprecedented combination of depth and coverage, which allows us to search for outer halo globular clusters (Chapters 2 and 3), and also for a stellar halo (Chapter 4).

The observations within this thesis come from the Pan-Andromeda Archaeological Survey (PAndAS; P.I.: A. McConnachie; McConnachie et al. 2009), which is an international collaboration composed of ∼40 researchers mainly in Canada, the UK, France, the US, Australia and Germany. We use the Canada-France-Hawaii Telescope (CFHT) with the large ($\sim$one square degree) field-of-view instrument, MegaCam, in observing semesters between 2008 and 2012. PAndAS is an extension of the Isaac Newton Telescope/Wide-Field Camera survey (Ferguson et al., 2007) and a previous CFHT survey (Ibata et al., 2007). Further details of the observations are given in Sections 2.2 and 4.3.

Chapter 2 begins with the search for globular clusters, and results in a catalogue of objects that have various degrees of confidence as to whether or not they are a cluster candidate (or are instead only a background galaxy or foreground star). Chapter 3 extends the analysis for cluster candidates by using simulated clusters and also further measurements of the clusters and cluster candidates. In Chapter 4, rather than search for clusters of stars we instead search for individual red-giant branch candidate stars that compose the stellar halo. We finish, in Chapter 5, by summarizing our conclusions and discussing future work.

Bibliography

Abazajian, K., Adelman-McCarthy, J. K., et al. 2003, AJ, 126, 2081

Abe, F., Bond, I. A., et al. 1999, AJ, 118, 261

Aguerri, J. A. L. and González-García, A. C. 2009, A&A, 494, 891

Aihara, H., Allende Prieto, C., et al. 2011, ApJS, 193, 29

Annibali, F., Tosi, M., Aloisi, A., and van der Marel, R. P. 2011, AJ, 142, 129

Annibali, F., Tosi, M., Aloisi, A., van der Marel, R. P., and Martinez-Delgado, D. 2012, ApJ, 745, L1

Ashman, K. M. and Zepf, S. E. 1992, ApJ, 384, 50

Bailin, J., Bell, E. F., Chappell, S. N., Radburn-Smith, D. J., and de Jong, R. S. 2011, ApJ, 736, 24

Bailin, J., Power, C., Norberg, P., Zaritsky, D., and Gibson, B. K. 2008, MNRAS, 390, 1133

Barker, M. K., Ferguson, A. M. N., Irwin, M., Arimoto, N., and Jablonka, P. 2009, AJ, 138, 1469

Barker, M. K., Ferguson, A. M. N., Irwin, M. J., Arimoto, N., and Jablonka, P. 2012, MNRAS, 419, 1489

Barmby, P., McLaughlin, D. E., Harris, W. E., Harris, G. L. H., and Forbes, D. A. 2007, AJ, 133, 2764

Barmby, P., Perina, S., et al. 2009, AJ, 138, 1667

Barnaby, D. and Thronson, Jr., H. A. 1992, AJ, 103, 41

Beasley, M. A., Bridges, T., et al. 2008, MNRAS, 386, 1443

Beccari, G., Sollima, A., et al. 2011, ApJ, 737, L3

Bekki, K. 2008, MNRAS, 390, L24

Bekki, K., Couch, W. J., Drinkwater, M. J., and Gregg, M. D. 2001, ApJ, 557, L39

Bell, E. F., Slater, C. T., and Martin, N. F. 2011, ApJ, 742, L15

Bellini, A., Bedin, L. R., Piotto, G., Milone, A. P., Marino, A. F., and Villanova, S. 2010, AJ, 140, 631

Belokurov, V., Evans, N. W., Irwin, M. J., Hewett, P. C., and Wilkinson, M. I. 2006, ApJ, 637, L29

Belokurov, V., Walker, M. G., et al. 2010, ApJ, 712, L103

Belokurov, V., —. 2009, MNRAS, 397, 1748

Bennett, C. L., Halpern, M., et al. 2003, ApJS, 148, 1

Benson, A. J., Frenk, C. S., Lacey, C. G., Baugh, C. M., and Cole, S. 2002, MNRAS, 333, 177

Bergvall, N., Zackrisson, E., and Caldwell, B. 2010, MNRAS, 405, 2697

Bersier, D. and Wood, P. R. 2002, AJ, 123, 840

Bertin, G. and Amorisco, N. C. 2010, A&A, 512, A17

Besla, G., Kallivayalil, N., Hernquist, L., van der Marel, R. P., Cox, T. J., and Kereš, D. 2010, ApJ, 721, L97

Bica, E., Bonatto, C., Barbuy, B., and Ortolani, S. 2006, A&A, 450, 105

Bird, S., Harris, W. E., Blakeslee, J. P., and Flynn, C. 2010, A&A, 524, A71

Bland-Hawthorn, J., Vlajić, M., Freeman, K. C., and Draine, B. T. 2005, ApJ, 629, 239

Blanton, M. R., Hogg, D. W., et al. 2003, ApJ, 592, 819

Block, D. L., Combes, F., et al. 2007, A&A, 471, 467

Blom, C., Spitler, L. R., and Forbes, D. A. 2012, MNRAS, 420, 37

Böker, T., Laine, S., et al. 2002, AJ, 123, 1389

Bonanos, A. Z., Stanek, K. Z., et al. 2006, ApJ, 652, 313

Bouwens, R. J., Illingworth, G. D., et al. 2010, ApJ, 709, L133

Boylan-Kolchin, M., Bullock, J. S., and Kaplinghat, M. 2011, MNRAS, 415, L40

Boylan-Kolchin, M., Springel, V., White, S. D. M., and Jenkins, A. 2010, MNRAS, 406, 896

Brainerd, T. G., Blandford, R. D., and Smail, I. 1996, ApJ, 466, 623

Brasseur, C. M., Martin, N. F., Macciò, A. V., Rix, H.-W., and Kang, X. 2011, ApJ, 743, 179

Braun, R. and Thilker, D. A. 2004, A&A, 417, 421

Brodie, J. P. and Larsen, S. S. 2002, AJ, 124, 1410

Brodie, J. P., Romanowsky, A. J., Strader, J., and Forbes, D. A. 2011, AJ, 142, 199

Brodie, J. P. and Strader, J. 2006, ARA&A, 44, 193

Brown, T. M., Tumlinson, J., et al. 2012, ApJ, 753, L21

Brüns, R. C., Kroupa, P., Fellhauer, M., Metz, M., and Assmann, P. 2011, A&A, 529, A138

Brunthaler, A., Reid, M. J., Falcke, H., Greenhill, L. J., and Henkel, C. 2005, Science, 307, 1440

Buehler, S., Ferguson, A. M. N., Irwin, M. J., Arimoto, N., and Jablonka, P. 2007, in IAU Symposium, Vol. 241, IAU Symposium, ed. A. Vazdekis & R. F. Peletier, 321–322

Bullock, J. S. and Johnston, K. V. 2005, ApJ, 635, 931

Busha, M. T., Wechsler, R. H., Behroozi, P. S., Gerke, B. F., Klypin, A. A., and Primack, J. R. 2011, ApJ, 743, 117

Cabrera-Lavers, A., González-Fernández, C., Garzón, F., Hammersley, P. L., and López-Corredoira, M. 2008, A&A, 491, 781

Carollo, D., Beers, T. C., et al. 2012, ApJ, 744, 195

Carollo, D., —. 2010, ApJ, 712, 692

Carollo, D., —. 2007, Nature, 450, 1020

Carrasco, E. R., Gomez, P. L., et al. 2010, ApJ, 715, L160

Carretta, E., Gratton, R. G., et al. 2010, ApJ, 722, L1

Carretta, E., Lucatello, S., Gratton, R. G., Bragaglia, A., and D'Orazi, V. 2011, A&A, 533, A69

Carter, D., Goudfrooij, P., et al. 2008, ApJS, 176, 424

Chandar, R., Bianchi, L., Ford, H. C., and Sarajedini, A. 2002, ApJ, 564, 712

Chiboucas, K., Tully, R. B., et al. 2011, ApJ, 737, 86

Chilingarian, I., Cayatte, V., et al. 2009, Science, 326, 1379

Cho, J., Sharples, R. M., et al. 2012, MNRAS, 422, 3591

Cohen, J. G. and Blakeslee, J. P. 1998, AJ, 115, 2356

Cole, D. R., Dehnen, W., Read, J. I., and Wilkinson, M. I. 2012, ArXiv e-prints

Collins, M. L. M., Chapman, S. C., et al. 2009, MNRAS, 396, 1619

Collins, M. L. M., —. 2010, MNRAS, 407, 2411

Combes, F. 2009, in Astronomical Society of the Pacific Conference Series, Vol. 419, Galaxy Evolution: Emerging Insights and Future Challenges, ed. S. Jogee, I. Marinova, L. Hao, & G. A. Blanc, 31

Conn, A. R., Ibata, R. A., Lewis, G. F., Parker, Q. A., and Zucker, D. B. 2012, ApJ, in prep

Côté, P., Blakeslee, J. P., et al. 2004, ApJS, 153, 223

Côté, P., Marzke, R. O., and West, M. J. 1998, ApJ, 501, 554

Courteau, S., Widrow, L. M., et al. 2011, ApJ, 739, 20

Currie, T., Hernandez, J., et al. 2010, ApJS, 186, 191

Da Costa, G. S. and Armandroff, T. E. 1995, AJ, 109, 2533

Dalcanton, J. J. and Bernstein, R. A. 2002, AJ, 124, 1328

Dalessandro, E., Lanzoni, B., Ferraro, F. R., Vespe, F., Bellazzini, M., and Rood, R. T. 2008, ApJ, 681, 311

Dall'Ora, M., Kinemuchi, K., et al. 2012, ArXiv e-prints

Dall'Ora, M., Ripepi, V., et al. 2003, AJ, 126, 197

Davidge, T. J. 2012, ApJ, 749, L7

Davidge, T. J., McConnachie, A. W., et al. 2012, ApJ, 751, 74

Davidge, T. J. and Puzia, T. H. 2011, ApJ, 738, 144

de Blok, W. J. G. 2010, Advances in Astronomy, 2010 de Jong, J. T. A., Martin, N. F., Rix, H.-W., Smith, K. W., Jin, S., and Macciò, A. V. 2010, ApJ, 710, 1664

de Jong, R. S. 2008, MNRAS, 388, 1521

de Jong, R. S., Radburn-Smith, D. J., and Sick, J. N. 2008, in Astronomical Society of the Pacific Conference Series, Vol. 396, Formation and Evolution of Galaxy Disks, ed. J. G. Funes & E. M. Corsini, 187

de Jong, R. S., Seth, A. C., et al. 2007, ApJ, 667, L49

De Propris, R., Phillipps, S., et al. 2005, ApJ, 623, L105

de Vaucouleurs, G. 1953, AJ, 58, 30

Dieball, A., Müller, H., and Grebel, E. K. 2002, A&A, 391, 547

Diemand, J., Kuhlen, M., et al. 2008, Nature, 454, 735

Dinescu, D. I., van Altena, W. F., Girard, T. M., and López, C. E. 1999, AJ, 117, 277

Doherty, M., Arnaboldi, M., et al. 2009, A&A, 502, 771

Drinkwater, M. J., Jones, J. B., Gregg, M. D., and Phillipps, S. 2000, Publications Astronomical Society of Australia, 17, 227

Durrell, P. R., Sarajedini, A., and Chandar, R. 2010, ApJ, 718, 1118

Eggen, O. J., Lynden-Bell, D., and Sandage, A. R. 1962, ApJ, 136, 748

Eisenstein, D. J., Hu, W., and Tegmark, M. 1998, ApJ, 504, L57

Elmegreen, B. G. 2011, in EAS Publications Series, Vol. 51, EAS Publications Series, ed. C. Charbonnel & T. Montmerle, 19–30

Faber, S. M. and Jackson, R. E. 1976, ApJ, 204, 668

Fadely, R., Willman, B., et al. 2011, AJ, 142, 88

Fardal, M. A., Babul, A., Guhathakurta, P., Gilbert, K. M., and Dodge, C. 2008, ApJ, 682, L33

Fellhauer, M., Evans, N. W., et al. 2007, MNRAS, 375, 1171

Ferguson, A., Irwin, M., Chapman, S., Ibata, R., Lewis, G., and Tanvir, N. 2007, Resolving the Stellar Outskirts of M31 and M33 (Island Universes: Berlin: Springer), 239

Ferguson, A. M. N., Irwin, M. J., Ibata, R. A., Lewis, G. F., and Tanvir, N. R. 2002, AJ, 124, 1452

Ferguson, H. C. 1989, AJ, 98, 367

Ferrarese, L. and Merritt, D. 2000, ApJ, 539, L9

Ferraro, F. R., Sollima, A., Rood, R. T., Origlia, L., Pancino, E., and Bellazzini, M. 2006, ApJ, 638, 433

Fingerhut, R. L., McCall, M. L., et al. 2003, ApJ, 587, 672

Forbes, D. A. and Bridges, T. 2010, MNRAS, 404, 1203

Forbes, D. A., Brodie, J. P., and Grillmair, C. J. 1997, AJ, 113, 1652

Forbes, D. A., Strader, J., and Brodie, J. P. 2004, AJ, 127, 3394

Fraternali, F., Oosterloo, T., and Sancisi, R. 2004, A&A, 424, 485

Frebel, A., Simon, J. D., Geha, M., and Willman, B. 2010, ApJ, 708, 560

Galleti, S., Federici, L., Bellazzini, M., Fusi Pecci, F., and Macrina, S. 2004, A&A, 416, 917

Gebhardt, K., Rich, R. M., and Ho, L. C. 2002, ApJ, 578, L41

Geha, M., Willman, B., et al. 2009, ApJ, 692, 1464

Georgiev, I. Y., Puzia, T. H., Goudfrooij, P., and Hilker, M. 2010, MNRAS, 406, 1967

Gieles, M., Heggie, D. C., and Zhao, H. 2011, MNRAS, 413, 2509

Gilmore, G., Wilkinson, M. I., et al. 2007, ApJ, 663, 948

Gómez, M., Geisler, D., Harris, W. E., Richtler, T., Harris, G. L. H., and Woodley, K. A. 2006, A&A, 447, 877

Grebel, E. K., Kolatt, T., and Brandner, W. 1999, in IAU Symposium, Vol. 192, The Stellar Content of Local Group Galaxies, ed. P. Whitelock & R. Cannon, 447

Greene, J. E., Murphy, J. D., Comerford, J. M., Gebhardt, K., and Adams, J. J. 2012, ApJ, 750, 32

Grillmair, C. J. 2006, ApJ, 645, L37

Grillmair, C. J. and Johnson, R. 2006, ApJ, 639, L17

Grosbøl, P. and Dottori, H. 2012, A&A, 542, A39

Haşegan, M., Jordán, A., et al. 2005, ApJ, 627, 203

Hammer, F., Yang, Y. B., Wang, J. L., Puech, M., Flores, H., and Fouquet, S. 2010, ApJ, 725, 542

Harris, G. L. H. 2010, PASA, 27, 475

Harris, G. L. H. and Harris, W. E. 2011, MNRAS, 410, 2347

Harris, G. L. H., Rejkuba, M., and Harris, W. E. 2010, PASA, 27, 457

Harris, W. E. 1986, AJ, 91, 822

—. 1991, ARA&A, 29, 543

—. 1996, AJ, 112, 1487

Harris, W. E. 2001, in Saas-Fee Advanced Course 28: Star Clusters, ed. L. Labhardt & B. Binggeli, 223

Harris, W. E. and Harris, G. L. H. 2002, AJ, 123, 3108

Harris, W. E., Harris, G. L. H., Layden, A. C., and Stetson, P. B. 2007a, AJ, 134, 43

Harris, W. E., Harris, G. L. H., Layden, A. C., and Wehner, E. M. H. 2007b, ApJ, 666, 903

Harris, W. E. and van den Bergh, S. 1981, AJ, 86, 1627

Hatzidimitriou, D. and Bhatia, R. K. 1990, A&A, 230, 11

Haywood, M. 2008, MNRAS, 388, 1175

Heesen, V., Krause, M., Beck, R., and Dettmar, R.-J. 2009, A&A, 506, 1123

Held, E. V., Gullieuszik, M., Rizzi, L., Girardi, L., Marigo, P., and Saviane, I. 2010, MNRAS, 404, 1475

Helmi, A. 2008, A&A Rev., 15, 145

Helmi, A., Irwin, M. J., et al. 2006, ApJ, 651, L121

Hilker, M. 2011, in EAS Publications Series, Vol. 48, EAS Publications Series, ed. M. Koleva, P. Prugniel, & I. Vauglin, 219–224

Hilker, M., Infante, L., Vieira, G., Kissler-Patig, M., and Richtler, T. 1999, A&AS, 134, 75

Holland, S., Fahlman, G. G., and Richer, H. B. 1995, AJ, 109, 2061

Hubble, E. P. 1926, ApJ, 64, 321

Hunter, D. A., van Woerden, H., and Gallagher, J. S. 1999, AJ, 118, 2184

Huxor, A., Ferguson, A. M. N., et al. 2009, ApJ, 698, L77

Huxor, A. P., —. 2011a, MNRAS, 414, 770

Huxor, A. P., Phillipps, S., Price, J., and Harniman, R. 2011b, in EAS Publications Series, Vol. 48, EAS Publications Series, ed. M. Koleva, P. Prugniel, & I. Vauglin, 257–258

Huxor, A. P., Tanvir, N. R., et al. 2005, MNRAS, 360, 1007

Hwang, N. 2011, in Stellar Clusters and Associations: A RIA Workshop on Gaia, 357–359

Hwang, N. and Lee, M. G. 2006, ApJ, 638, L79

—. 2008, AJ, 135, 1567

Hwang, N., Lee, M. G., et al. 2011, ApJ, 738, 58

Hwang, N., Lee, M. G., et al. 2005, in IAU Colloq. 198: Near-fields cosmology with dwarf elliptical galaxies, ed. H. Jerjen & B. Binggeli, 257–258

Ibata, R., Irwin, M., Lewis, G. F., and Stolte, A. 2001, ApJ, 547, L133

Ibata, R., Martin, N. F., et al. 2007, ApJ, 671, 1591

Ibata, R. A., Gilmore, G., and Irwin, M. J. 1994, Nature, 370, 194

Irwin, J. A. and Madden, S. C. 2006, A&A, 445, 123

Irwin, M. and Hatzidimitriou, D. 1995, MNRAS, 277, 1354

Irwin, M. J., Ferguson, A. M. N., Huxor, A. P., Tanvir, N. R., Ibata, R. A., and Lewis, G. F. 2008, ApJ, 676, L17

Jablonka, P., Tafelmeyer, M., Courbin, F., and Ferguson, A. M. N. 2010, A&A, 513, A78

James, P. A. and Casali, M. M. 1998, MNRAS, 301, 280

Jang, I. S., Lim, S., Park, H. S., and Lee, M. G. 2012, ApJ, 751, L19

Jarosik, N., Bennett, C. L., et al. 2011, ApJS, 192, 14

Johnson, C. I. and Pilachowski, C. A. 2010, ApJ, 722, 1373

Jordán, A., Blakeslee, J. P., et al. 2007, ApJS, 169, 213

Kacharov, N. and Koch, A. 2012, ArXiv e-prints

Kalirai, J. S., Beaton, R. L., et al. 2010, ApJ, 711, 671

Kauffmann, G., White, S. D. M., and Guiderdoni, B. 1993, MNRAS, 264, 201

Keller, S. C., Mackey, D., and Da Costa, G. S. 2012, ApJ, 744, 57

Kinman, T. D., Cacciari, C., Bragaglia, A., Smart, R., and Spagna, A. 2012, MNRAS, 422, 2116

Kissler-Patig, M., Grillmair, C. J., Meylan, G., Brodie, J. P., Minniti, D., and Goudfrooij, P. 1999, AJ, 117, 1206

Kissler-Patig, M., Richtler, T., Storm, J., and della Valle, M. 1997, A&A, 327, 503

Klypin, A., Kravtsov, A. V., Valenzuela, O., and Prada, F. 1999, ApJ, 522, 82

Komatsu, E., Smith, K. M., et al. 2011, ApJS, 192, 18

Koposov, S., Belokurov, V., et al. 2008, ApJ, 686, 279

Kormendy, J., Fisher, D. B., Cornell, M. E., and Bender, R. 2009, ApJS, 182, 216

Kregel, M. and van der Kruit, P. C. 2005, MNRAS, 358, 481

Kroupa, P., Famaey, B., et al. 2010, A&A, 523, A32

Larsen, S. S. and Brodie, J. P. 2000, AJ, 120, 2938

Larson, D., Dunkley, J., et al. 2011, ApJS, 192, 16

Laustsen, S. and West, R. M. 1980, Journal of Astrophysics and Astronomy, 1, 177

Lequeux, J., Combes, F., Dantel-Fort, M., Cuillandre, J.-C., Fort, B., and Mellier, Y. 1998, A&A, 334, L9

Libeskind, N. I., Frenk, C. S., Cole, S., Jenkins, A., and Helly, J. C. 2009, MNRAS, 399, 550

Libeskind, N. I., Knebe, A., Hoffman, Y., Gottlöber, S., Yepes, G., and Steinmetz, M. 2011, MNRAS, 411, 1525

Liu, L., Gerke, B. F., Wechsler, R. H., Behroozi, P. S., and Busha, M. T. 2011, ApJ, 733, 62

Lovell, M. R., Eke, V. R., Frenk, C. S., and Jenkins, A. 2011, MNRAS, 413, 3013

Lynden-Bell, D. 1976, MNRAS, 174, 695

Ma, J., van den Bergh, S., et al. 2006, ApJ, 636, L93

Mackey, A. D., Ferguson, A. M. N., et al. 2010, MNRAS, 401, 533

Mackey, A. D. and Gilmore, G. F. 2004, MNRAS, 355, 504

Mackey, A. D., Huxor, A., et al. 2007, ApJ, 655, L85

Magorrian, S. J. 2000, in Astronomical Society of the Pacific Conference Series, Vol. 197, Dynamics of Galaxies: from the Early Universe to the Present, ed. F. Combes, G. A. Mamon, & V. Charmandaris, 205

Majewski, S. R., Beaton, R. L., et al. 2007, ApJ, 670, L9

Majewski, S. R., Nidever, D. L., et al. 2012, ApJ, 747, L37

Malin, D. F., Quinn, P. J., and Graham, J. A. 1983, ApJ, 272, L5

Marín-Franch, A., Aparicio, A., et al. 2009, ApJ, 694, 1498

Martell, S. L. and Grebel, E. K. 2010, A&A, 519, A14

Martell, S. L., Smolinski, J. P., Beers, T. C., and Grebel, E. K. 2011, A&A, 534, A136

Martin, N. F., de Jong, J. T. A., and Rix, H.-W. 2008, ApJ, 684, 1075

Martin, N. F., Ibata, R. A., et al. 2006, MNRAS, 371, 1983

Martin, N. F., McConnachie, A. W., et al. 2009, ApJ, 705, 758

Martínez-Delgado, D., Peñarrubia, J., Gabany, R. J., Trujillo, I., Majewski, S. R., and Pohlen, M. 2008, ApJ, 689, 184

Martini, P. and Ho, L. C. 2004, ApJ, 610, 233

Mateo, M. L. 1998, ARA&A, 36, 435

Matthews, T. A., Morgan, W. W., and Schmidt, M. 1964, ApJ, 140, 35

McConnachie, A. W. 2012, ArXiv e-prints

McConnachie, A. W., Huxor, A., et al. 2008, ApJ, 688, 1009

McConnachie, A. W. and Irwin, M. J. 2006, MNRAS, 365, 1263

McConnachie, A. W., Irwin, M. J., Ferguson, A. M. N., Ibata, R. A., Lewis, G. F., and Tanvir, N. 2004, MNRAS, 350, 243

McConnachie, A. W., Irwin, M. J., et al. 2009, Nature, 461, 66

McLaughlin, D. E. and van der Marel, R. P. 2005, ApJS, 161, 304

McMillan, P. J. 2011, MNRAS, 414, 2446

Merritt, D., Graham, A. W., Moore, B., Diemand, J., and Terzić, B. 2006, AJ, 132, 2685

Metz, M. and Kroupa, P. 2007, MNRAS, 376, 387

Metz, M., Kroupa, P., and Jerjen, H. 2007, MNRAS, 374, 1125

—. 2009a, MNRAS, 394, 2223

Metz, M., Kroupa, P., and Libeskind, N. I. 2008, ApJ, 680, 287

Metz, M., Kroupa, P., Theis, C., Hensler, G., and Jerjen, H. 2009b, ApJ, 697, 269

Meylan, G., Sarajedini, A., Jablonka, P., Djorgovski, S. G., Bridges, T., and Rich, R. M. 2001, AJ, 122, 830

Miceli, A., Rest, A., et al. 2008, ApJ, 678, 865

Michielsen, D., Boselli, A., et al. 2008, MNRAS, 385, 1374

Mieske, S., Hilker, M., and Infante, L. 2002, A&A, 383, 823

Miller, B. W., Lotz, J. M., Ferguson, H. C., Stiavelli, M., and Whitmore, B. C. 1998, ApJ, 508, L133

Minniti, D., Rejkuba, M., Funes, J. G., and Kennicutt, Jr., R. C. 2004, ApJ, 612, 215

Mirabel, I. F., Dottori, H., and Lutz, D. 1992, A&A, 256, L19

Moore, B., Ghigna, S., et al. 1999, ApJ, 524, L19

Moretti, M. I., Dall'Ora, M., et al. 2009, ApJ, 699, L125

Morgan, W. W. 1958, PASP, 70, 364

Mouhcine, M., Harris, W. E., Ibata, R., and Rejkuba, M. 2010a, MNRAS, 404, 1157

Mouhcine, M., Ibata, R., and Rejkuba, M. 2010b, ApJ, 714, L12

—. 2011, MNRAS, 415, 993

Mouhcine, M., Rejkuba, M., and Ibata, R. 2007, MNRAS, 381, 873

Muñoz, R. R., Geha, M., and Willman, B. 2010, AJ, 140, 138

Mucciarelli, A., Ferraro, F. R., Origlia, L., and Fusi Pecci, F. 2007, AJ, 133, 2053

Mucciarelli, A., Origlia, L., Ferraro, F. R., Bellazzini, M., and Lanzoni, B. 2012, ApJ, 746, L19

Munoz, R. R., Geha, M., et al. 2012, ArXiv e-prints

Nair, P. B. and Abraham, R. G. 2010, ApJ, 714, L260

Navarro, J. F., Frenk, C. S., and White, S. D. M. 1997, ApJ, 490, 493

Newberg, H. J., Willett, B. A., Yanny, B., and Xu, Y. 2010, ApJ, 711, 32

Nissen, P. E. and Schuster, W. J. 2010, A&A, 511, L10

Odenkirchen, M., Grebel, E. K., et al. 2003, AJ, 126, 2385

Odenkirchen, M., —. 2001, ApJ, 548, L165

Okamoto, T., Gao, L., and Theuns, T. 2008, MNRAS, 390, 920

Oohama, N., Okamura, S., Fukugita, M., Yasuda, N., and Nakamura, O. 2009, ApJ, 705, 245

Oort, J. H. 1932, Bull. Astron. Inst. Netherlands, 6, 249

Pancino, E., Ferraro, F. R., Bellazzini, M., Piotto, G., and Zoccali, M. 2000, ApJ, 534, L83

Parry, O. H., Eke, V. R., Frenk, C. S., and Okamoto, T. 2012, MNRAS, 419, 3304

Pawlowski, M. S., Pflamm-Altenburg, J., and Kroupa, P. 2012, MNRAS, 2990

Peebles, P. J. E. and Yu, J. T. 1970, ApJ, 162, 815

Peng, E. W., Ford, H. C., Freeman, K. C., and White, R. L. 2002, AJ, 124, 3144

Peng, E. W., Jordán, A., et al. 2008, ApJ, 681, 197

Penzias, A. A. and Wilson, R. W. 1965, ApJ, 142, 419

Percival, W. J., Reid, B. A., et al. 2010, MNRAS, 401, 2148

Perlmutter, S., Aldering, G., et al. 1999, ApJ, 517, 565

Perrett, K. M., Bridges, T. J., et al. 2002, AJ, 123, 2490

Pohlen, M., Balcells, M., Lütticke, R., and Dettmar, R.-J. 2004, A&A, 422, 465

Putman, M. E., Peek, J. E. G., et al. 2009, ApJ, 703, 1486

Racine, R. 1991, AJ, 101, 865

Rees, M. 2001, Basic Books, "Just Six Numbers: The Deep Forces that Shape the Universe"

Rejkuba, M. 2012, Ap&SS, 25

Rejkuba, M., Harris, W. E., Greggio, L., and Harris, G. L. H. 2011, A&A, 526, A123

Rejkuba, M., Mouhcine, M., and Ibata, R. 2009, MNRAS, 396, 1231

Richardson, J. C., Irwin, M. J., et al. 2011, ApJ, 732, 76

Richtler, T., Dirsch, B., Larsen, S., Hilker, M., and Infante, L. 2005, A&A, 439, 533

Riess, A. G., Filippenko, A. V., et al. 1998, AJ, 116, 1009

Riess, A. G., Macri, L., et al. 2009, ApJ, 699, 539

Rockosi, C. M., Odenkirchen, M., et al. 2002, AJ, 124, 349

Roederer, I. U. 2009, AJ, 137, 272

Romanowsky, A. J., Strader, J., et al. 2011, ArXiv e-prints

Romero-Gómez, M., Athanassoula, E., Masdemont, J. J., and García-Gómez, C. 2007, A&A, 472, 63

Rubin, V. C. and Ford, Jr., W. K. 1970, ApJ, 159, 379

Rudy, R. J., Woodward, C. E., Hodge, T., Fairfield, S. W., and Harker, D. E. 1997, Nature, 387, 159

Ryś, A., Grocholski, A. J., van der Marel, R. P., Aloisi, A., and Annibali, F. 2011a, A&A, 530, A23

—. 2011b, A&A, 530, A23

Sackett, P. D., Morrisoni, H. L., Harding, P., and Boroson, T. A. 1994a, Nature, 370, 441

Sackett, P. D., Rix, H.-W., Jarvis, B. J., and Freeman, K. C. 1994b, ApJ, 436, 629

Sadoun, R. and Colin, J. 2012, ArXiv e-prints

Saglia, R. P., Fabricius, M., et al. 2010, A&A, 509, A61

Salaris, M., Cassisi, S., and Pietrinferni, A. 2008, ApJ, 678, L25

Salinas, R., Jílková, L., Carraro, G., Catelan, M., and Amigo, P. 2012, MNRAS, 421, 960

Sánchez-Janssen, R., Méndez-Abreu, J., and Aguerri, J. A. L. 2010, MNRAS, 406, L65

Sandage, A. 2005, ARA&A, 43, 581

Sarajedini, A. and Mancone, C. L. 2007, AJ, 134, 447

Schlaufman, K. C., Rockosi, C. M., Lee, Y. S., Beers, T. C., and Allende Prieto, C. 2011, ApJ, 734, 49

Schommer, R. A., Christian, C. A., Caldwell, N., Bothun, G. D., and Huchra, J. 1991, AJ, 101, 873

Searle, L. and Zinn, R. 1978, ApJ, 225, 357

Seth, A., de Jong, R., Dalcanton, J., and GHOSTS Team. 2007, in IAU Symposium, Vol. 241, IAU Symposium, ed. A. Vazdekis & R. F. Peletier, 523–524

Shang, Z., Zheng, Z., et al. 1998, ApJ, 504, L23

Shapley, H. 1918a, PASP, 30, 42

—. 1918b, Proceedings of the National Academy of Science, 4, 224

—. 1938, Nature, 142, 715

Simon, J. D. and Geha, M. 2007, ApJ, 670, 313

Slater, C. T., Bell, E. F., and Martin, N. F. 2011, ApJ, 742, L14

Sohn, S. T., Anderson, J., and van der Marel, R. P. 2012, ApJ, 753, 7

Sollima, A., Bellazzini, M., et al. 2009, MNRAS, 396, 2183

Sollima, A., Martínez-Delgado, D., Valls-Gabaud, D., and Peñarrubia, J. 2011, ApJ, 726, 47

Springel, V. and Hernquist, L. 2005, ApJ, 622, L9

Springel, V., White, S. D. M., et al. 2008, Nature, 456, 73

Stil, J. M. and Israel, F. P. 2002, A&A, 392, 473

Stonkutė, R., Vansevičius, V., et al. 2008, AJ, 135, 1482

Strader, J., Beasley, M. A., and Brodie, J. P. 2007, AJ, 133, 2015

Strader, J., Caldwell, N., and Seth, A. C. 2011a, AJ, 142, 8

Strader, J., Romanowsky, A. J., et al. 2011b, ApJS, 197, 33

Strader, J., Seth, A. C., and Caldwell, N. 2012, AJ, 143, 52

Strigari, L. E. and Wechsler, R. H. 2012, ApJ, 749, 75

Tal, T. and van Dokkum, P. G. 2011, ApJ, 731, 89

Tanvir, N. R., Mackey, A. D., et al. 2012, MNRAS, 422, 162

Tikhonov, N. A. and Galazutdinova, O. A. 2005, Astrophysics, 48, 221

Tollerud, E. J., Beaton, R. L., et al. 2012, ApJ, 752, 45

Tollerud, E. J., Boylan-Kolchin, M., Barton, E. J., Bullock, J. S., and Trinh, C. Q. 2011, ApJ, 738, 102

Tollerud, E. J., Bullock, J. S., Strigari, L. E., and Willman, B. 2008, ApJ, 688, 277

Tolstoy, E., Hill, V., and Tosi, M. 2009, ARA&A, 47, 371

Tully, R. B. and Fisher, J. R. 1977, A&A, 54, 661

van den Bergh, S. 1960a, ApJ, 131, 558

—. 1960b, ApJ, 131, 215

—. 1996, AJ, 112, 2634

—. 2011, AJ, 141, 188

van den Bergh, S. and Mackey, A. D. 2004, MNRAS, 354, 713

van der Marel, R. P., Besla, G., Cox, T. J., Sohn, S. T., and Anderson, J. 2012, ApJ, 753, 9

Vera-Ciro, C. A., Helmi, A., Starkenburg, E., and Breddels, M. A. 2012, ArXiv e-prints

Vlajić, M., Bland-Hawthorn, J., and Freeman, K. C. 2009, ApJ, 697, 361

Wada, K., Baba, J., and Saitoh, T. R. 2011, ApJ, 735, 1

Walcher, C. J., van der Marel, R. P., et al. 2005, ApJ, 618, 237

Wang, J., Frenk, C. S., Navarro, J. F., and Gao, L. 2012a, ArXiv e-prints

Wang, J., Hammer, F., Athanassoula, E., Puech, M., Yang, Y., and Flores, H. 2012b, A&A, 538, A121

Watkins, L. L., Evans, N. W., and An, J. H. 2010, MNRAS, 406, 264

Weil, M. L., Bland-Hawthorn, J., and Malin, D. F. 1997, ApJ, 490, 664

Wesson, P. S. 2001, Space Sci. Rev., 98, 329

Whitmore, B. C., Lucas, R. A., McElroy, D. B., Steiman-Cameron, T. Y., Sackett, P. D., and Olling, R. P. 1990, AJ, 100, 1489

Wyder, T. K., Hodge, P. W., and Zucker, D. B. 2000, PASP, 112, 1162

Zackrisson, E., de Jong, R. S., and Micheva, G. 2011, ArXiv e-prints

Zackrisson, E. and Micheva, G. 2011, ArXiv e-prints

Zepf, S. E., Liu, M. C., Marleau, F. R., Sackett, P. D., and Graham, J. R. 2000, AJ, 119, 1701

Zheng, Z., Shang, Z., et al. 1999, AJ, 117, 2757

Zibetti, S. and Ferguson, A. M. N. 2004, MNRAS, 352, L6

Zibetti, S., White, S. D. M., and Brinkmann, J. 2004, MNRAS, 347, 556

Zinn, R. 1985, ApJ, 293, 424

Zolotov, A., Willman, B., et al. 2009, ApJ, 702, 1058

Zucker, D. B., Belokurov, V., et al. 2006, ApJ, 650, L41

Zwicky, F. 1933, Helvetica Physica Acta, 6, 110

—. 1956, Ergebnisse der exakten Naturwissenschaften, 29, 344

Table 1.1: Summary of (tentative) halo detections beyond the Local Group. Classifications and distances are from the NASA Extragalactic Database, and references for the inclinations and halo follow in Table 1.2. The inclination angle is defined such that $i = 90°$ is an edge-on galaxy and $i = 0°$ is face-on.

Name or number of objects	Classification	Inclination (degrees)	Distance (Mpc)[1]
	Individual late-type galaxy studies		
NGC 253	SAB(s)c sb[2]	78	3.8±0.3
NGC 300	SA(s)d	42	1.6±0.1
NGC 891	SA(s)b	89.8±0.5	10.1±0.7
NGC 1569	IBm sb[2]	63	1.2±0.2
NGC 4449	IBm sb[2]	45	3.5±0.3
NGC 2403	SAB(s)cd	60	3.7±0.3
NGC 3957	SA0	88±1	19.0±1.4
NGC 4144	SAB(s)cd	84	4.3±0.3
NGC 4244	SA(s)cd	∼90	3.5±0.3
NGC 4650	SB(s)0	85	36.8±2.6
IC 5249	SBd	89	30.7±2.2
NGC 5907	SA(s)c	87	11.6±0.8
HUDF galaxy[3]		edge-on	(z=0.32)
	Studies of multiple galaxies		
14	late-type	8 edge-on	-
47	late-type	edge-on	-
1047	(stacked)	edge-on	-
1510	(stacked)	edge-on	-
42000	luminous red (stacked)	-	-
	Individual early-type galaxy studies		
M87	cD pec	-	16.5±1.2

Continued on next page

Table 1.1 – continued from previous page

Name or number of objects	Classification	Inclination (degrees)	Distance (Mpc)[1]
NGC 3379	E1	-	10.4±0.7
NGC 5128	E2 (Harris, 2010)	-	3.8±0.1 (Harris et al., 2010)

1. Local Group distances from N.E.D.
2. Starburst galaxy.
3. Located at ($\alpha = 3^h32^m39^s$, $\delta = -27^d47'29''$).

Table 1.2: Sources for the inclination angle and possible halo detections in Table 1.1.

Name or number of objects	Inclination source	Halo reference(s)
	Individual late-type galaxy studies	
NGC 253	Heesen et al. (2009)	Bailin et al. (2011)
NGC 300	Vlajić et al. (2009)	Bland-Hawthorn et al. (2005)
NGC 891	Kregel & van der Kruit (2005)	Tikhonov & Galazutdinova (2005), Mouhcine et al. (2007), Rejkuba et al. (2009)
NGC 1569	Stil & Israel (2002)	Ryś et al. (2011b)
NGC 4449	Hunter et al. (1999)	Ryś et al. (2011b)
NGC 2403	Fraternali et al. (2004)	Barker et al. (2012)
NGC 3957	Pohlen et al. (2004)	Jablonka et al. (2010)
NGC 4144	Tikhonov & Galazutdinova (2005)	Tikhonov & Galazutdinova (2005)
NGC 4244	Tikhonov & Galazutdinova (2005)	Tikhonov & Galazutdinova (2005), Buehler et al. (2007), de Jong et al. (2007),

Continued on next page

Table 1.2 – continued from previous page

Name or number of objects	Inclination source	Halo reference(s)
		Seth et al. (2007)
NGC 4650	Laustsen & West (1980)	Sackett et al. (1994b)
IC 5249	Abe et al. (1999)	Abe et al. (1999)
NGC 5907	Barnaby & Thronson (1992)	Sackett et al. (1994a),
		Rudy et al. (1997),
		James & Casali (1998),
		Lequeux et al. (1998),
		Zheng et al. (1999),
		Zepf et al. (2000),
		Irwin & Madden (2006),
		Martínez-Delgado et al. (2008)
HUDF galaxy	Zibetti & Ferguson (2004)	Zibetti & Ferguson (2004)
	Studies of multiple galaxies	
14	-	de Jong et al. (2008)
47	-	Dalcanton & Bernstein (2002)
1047	-	Zibetti et al. (2004)
1510	-	Bergvall et al. (2010)
42000	-	Tal & van Dokkum (2011)
	Individual early-type galaxy studies	
M87	-	Weil et al. (1997)
NGC 3379	-	Harris et al. (2007b)
NGC 5128	(Harris, 2010)	Mouhcine et al. (2011)

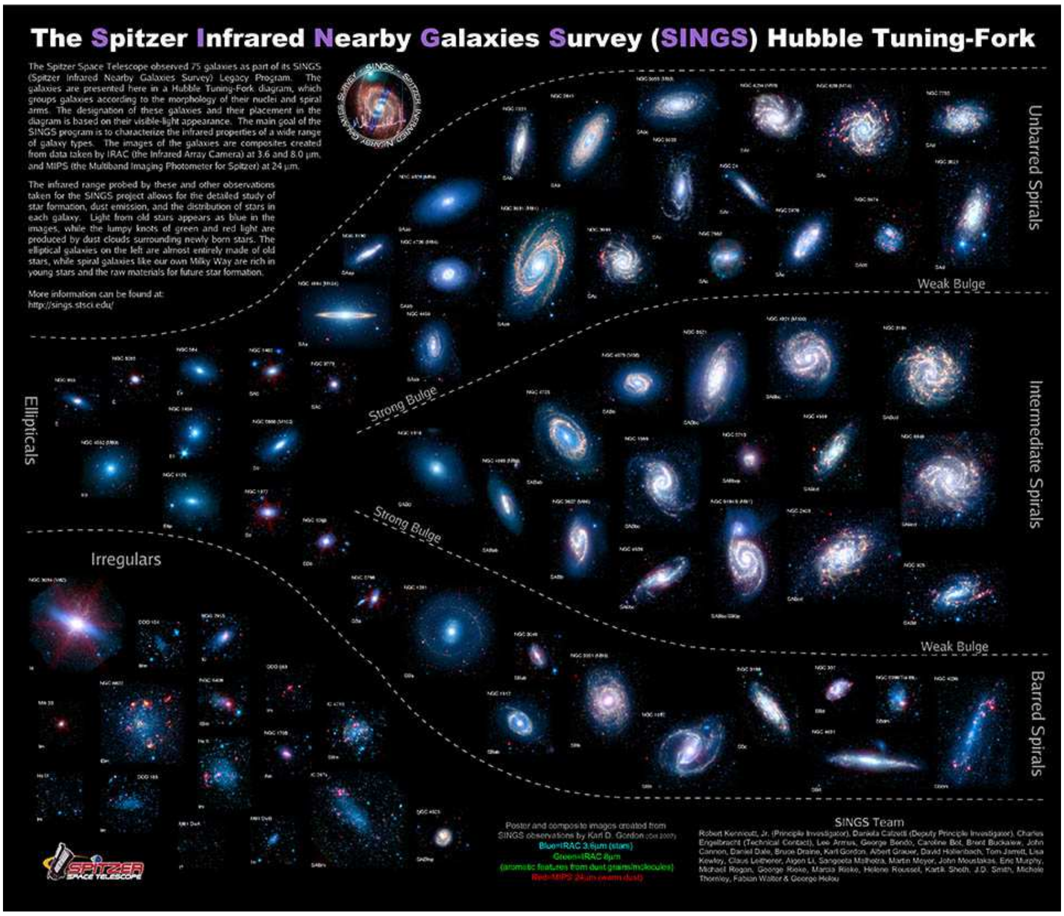

Figure 1.1: A modern version of Hubble's tuning fork, compiled using infrared data from the Spitzer Space Telescope. Credit: NASA/JPL-Caltech/K. Gordon (STScI) and the SINGS Team (2007).

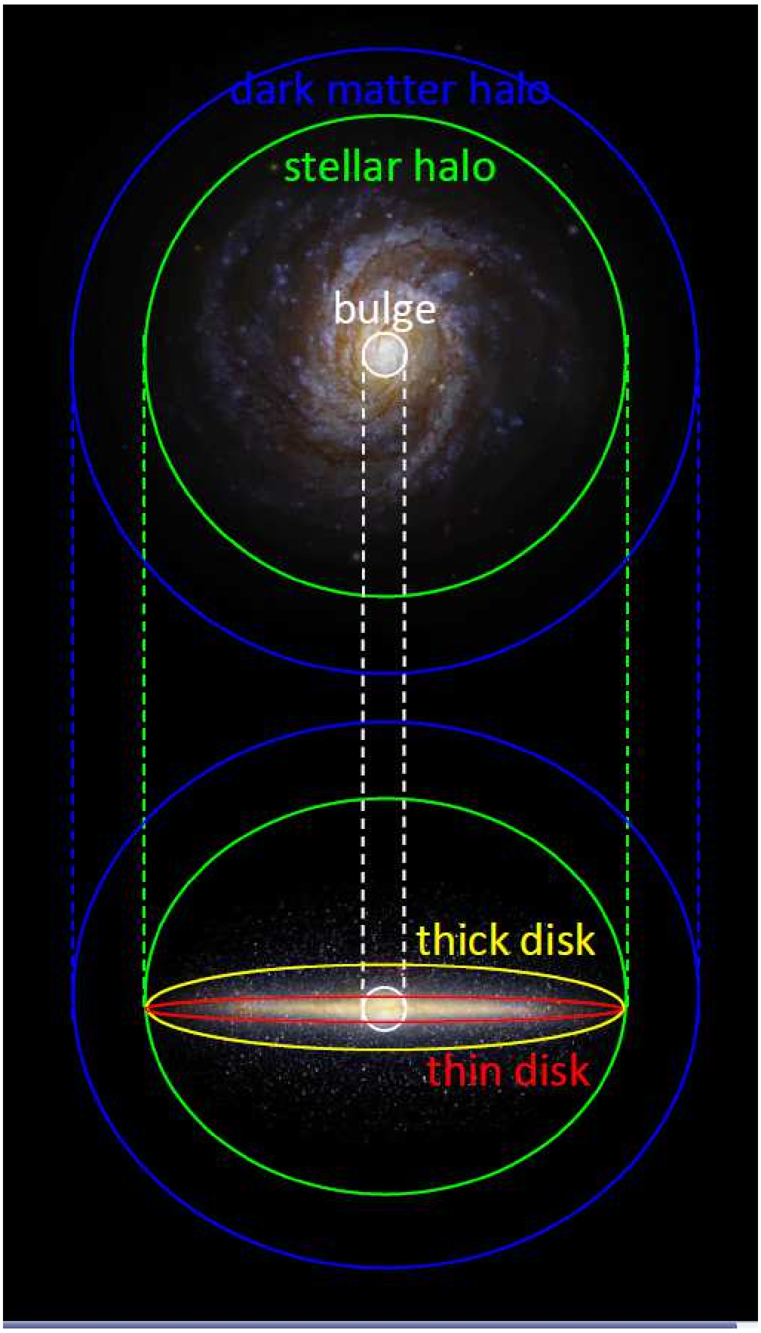

Figure 1.2: The major components of a spiral galaxy. The top and bottom background images are M100 (R. Gendler et al., ESO/IDA/Danish 1.5m) and the MW (N. Wright, NASA/COBE), respectively. Adapted from a figure by D. E. Gary (New Jersey Institute of Technology).

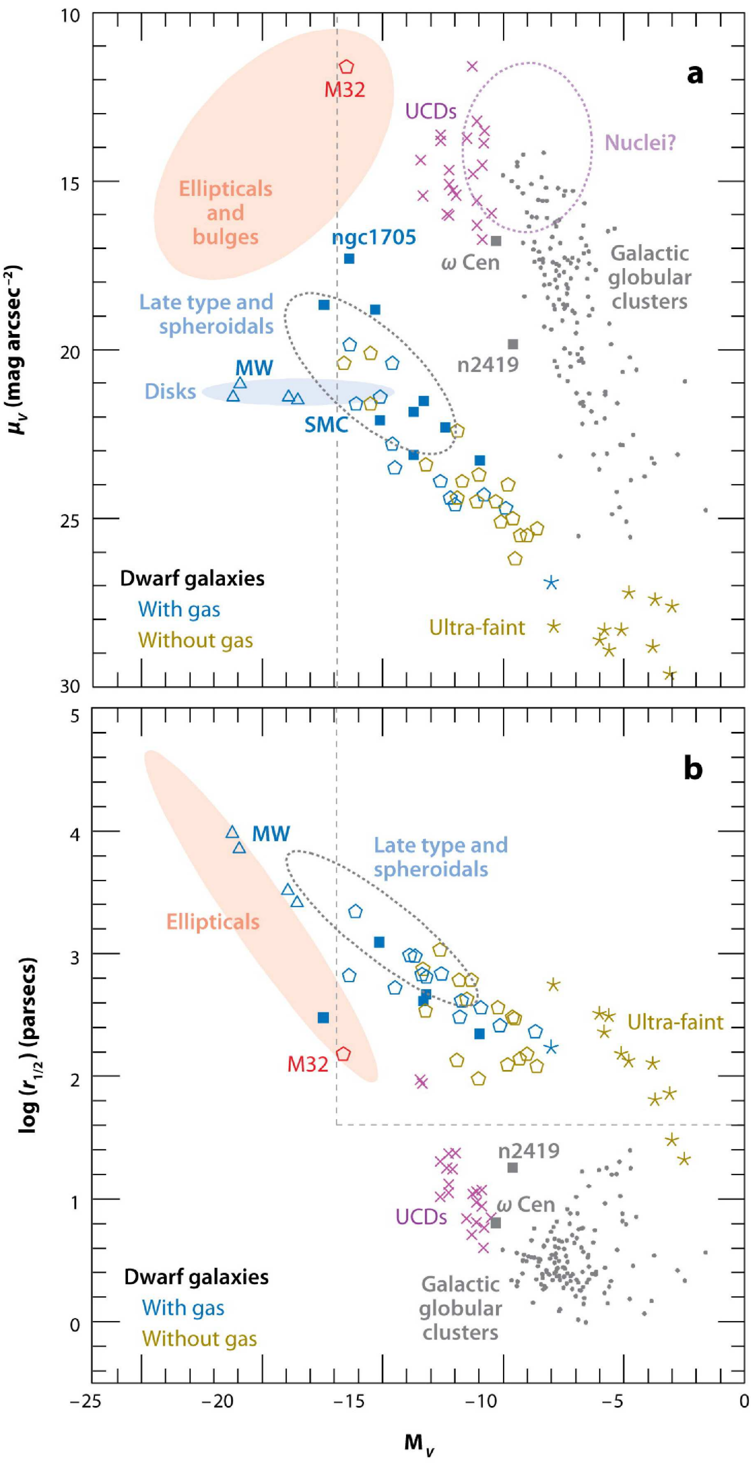

Figure 1.3: Tolstoy et al. (2009)'s Figure 1: The top and bottom plots show the distribution of various galaxy classes in both magnitude-surface brightness and magnitude-half-light radius spaces, respectively.

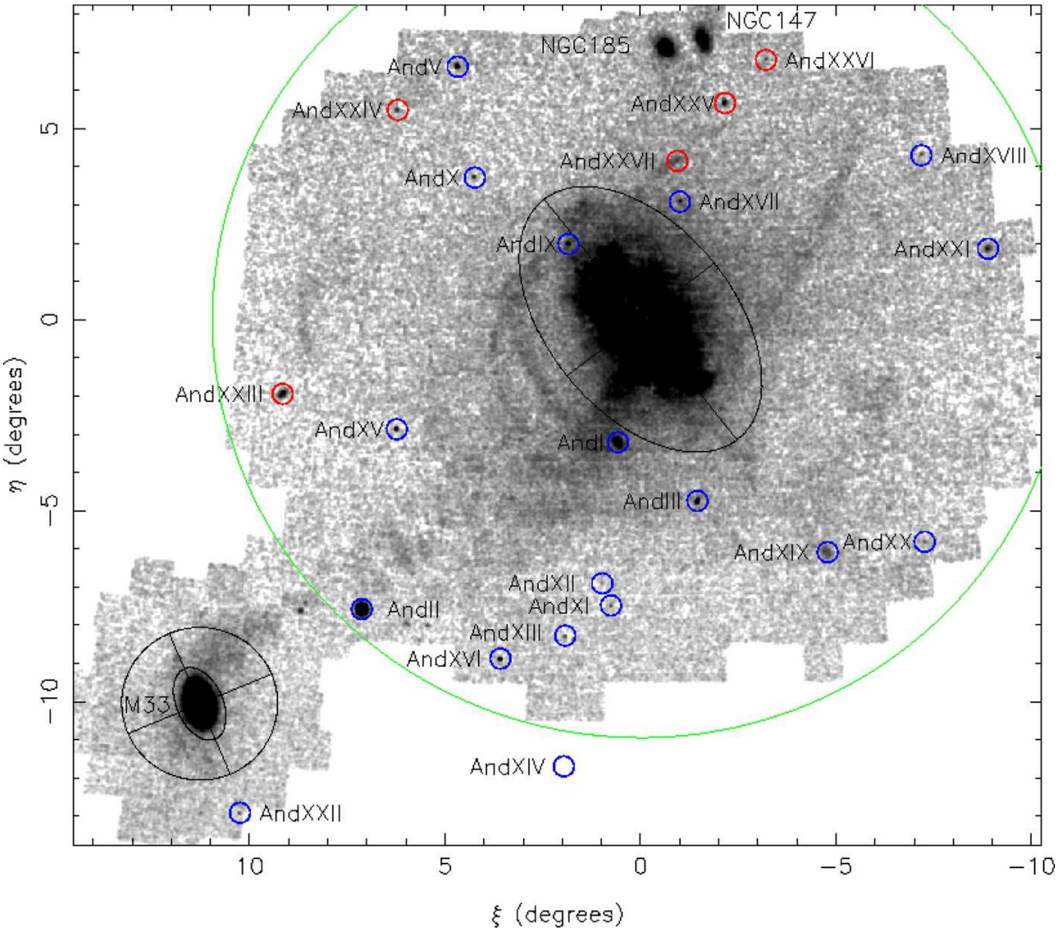

Figure 1.4: Richardson et al. (2011)'s Figure 1: Surface density map of candidate RGB stars (defined by colour and magnitude) surrounding M31 (centre) and M33 (bottom left). Some contamination from foreground stars and background galaxies expected. Previously known M31 dwarf spheroidals are shown in blue, with the 5 new dwarfs discovered by Richardson et al. shown in red.

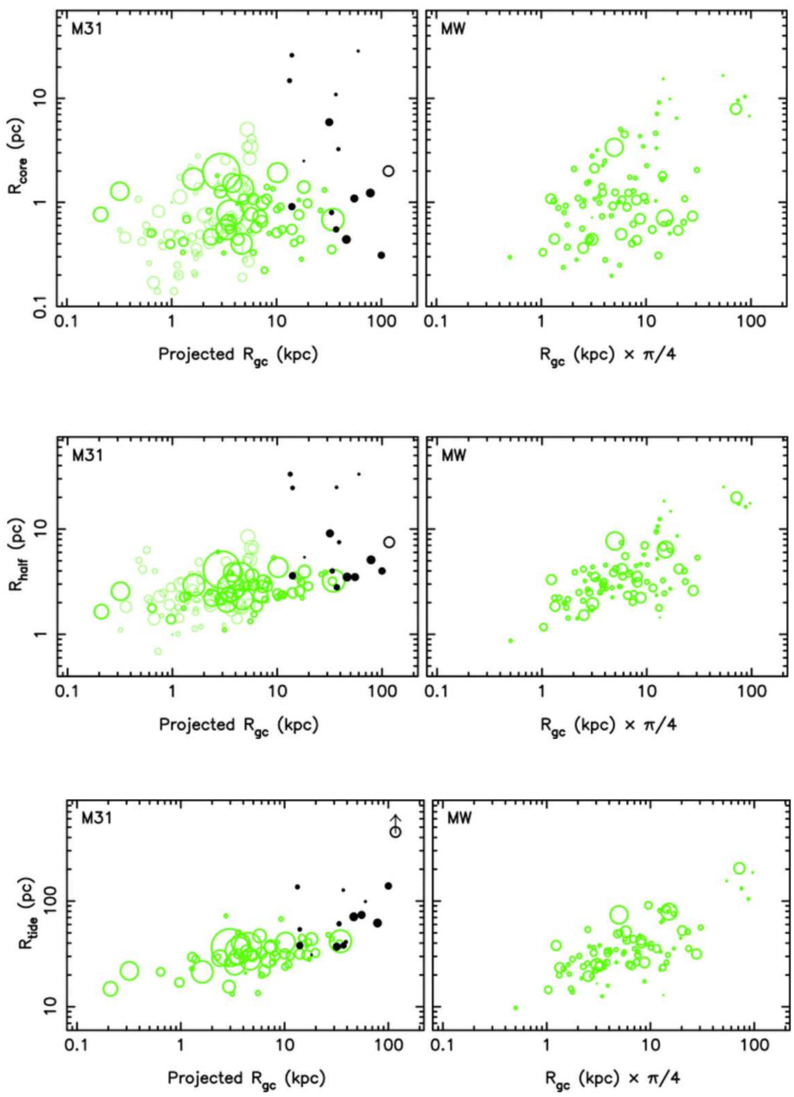

Figure 1.5: Tanvir et al. (2012)'s Figures 15, 16 and 17: King core model (top), half-light radius (middle) and tidal radius (bottom) plotted against projected galactocentric radius for M31 GCs (left) and MW GCs (right). Each circle's area is proportional to the cluster's luminosity that it represents. The various different circles in the left-hand panels are from the following sources: solid, black (Tanvir et al., 2012), open, black (MGC1; Mackey et al. 2010), green, open (darker; Barmby et al. 2007) and (lighter; Strader et al. 2011a). For the Strader et al. points in the top-left panel, r_0 is plotted and not r_c. Strader et al. did not provide tidal radii, so these points are omitted from the bottom-left panel. The data in the right-hand panels is from McLaughlin & van der Marel (2005), with the 3D Galactocentric radius corrected to show a projected radius so that it is comparable to the M31 data.

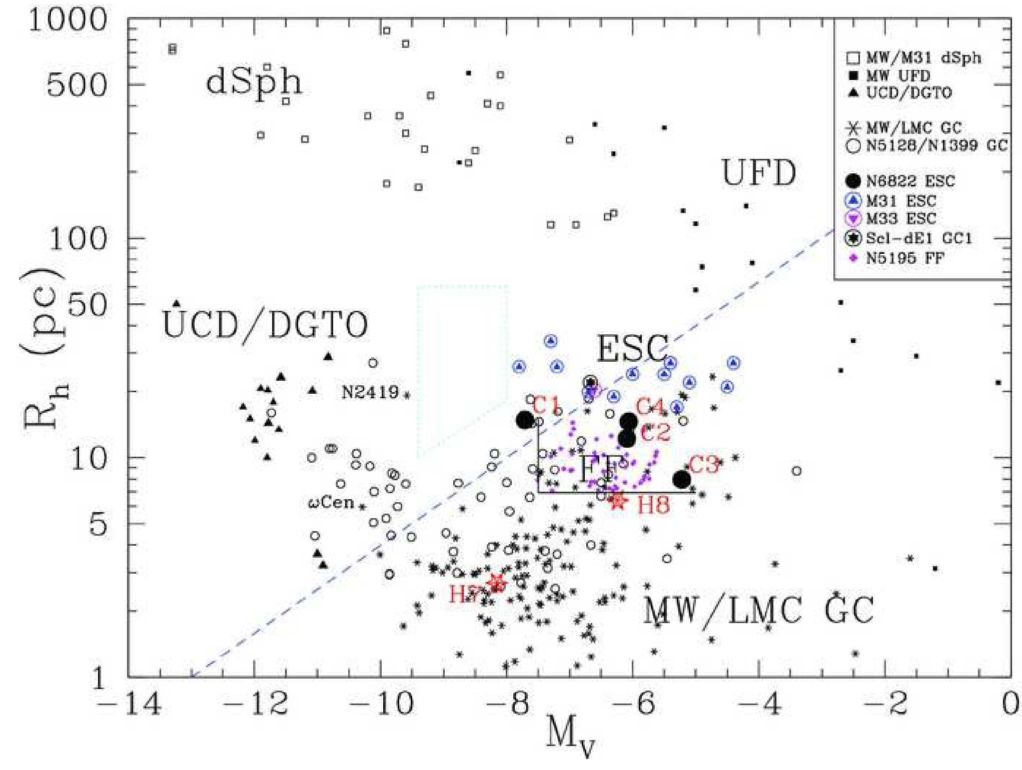

Figure 1.6: Hwang et al. (2011)'s Figure 7: Half-light radii against magnitudes for various stellar systems: GCs from the MW and LMC (van den Bergh, 1996; van den Bergh & Mackey, 2004), NGC 5128 (Martini & Ho, 2004; Gómez et al., 2006; Mouhcine et al., 2010a), and NGC 1399 (Richtler et al., 2005); extended clusters from M31 (Huxor et al., 2005, 2011a), M33 (Stonkutė et al., 2008), and NGC 6822 (C1-C4; Hwang et al. 2011); dwarf galaxies in the MW (Irwin & Hatzidimitriou, 1995; Kalirai et al., 2010) and M31 (McConnachie & Irwin, 2006; Martin et al., 2006, 2009; Ibata et al., 2007; Majewski et al., 2007; Irwin et al., 2008; McConnachie et al., 2008; Collins et al., 2010; Kalirai et al., 2010); NGC 1399 ultra-compact dwarf galaxies (Mieske et al., 2002; De Propris et al., 2005) and dwarf galaxy transition objects (Haşegan et al., 2005); MW UFDs (Martin et al., 2008; Belokurov et al., 2009, 2010; de Jong et al., 2010); "faint fuzzy" clusters in NGC 5195 (Hwang et al., 2005), as indicated by the L-shape; and NGC 6822 Hubble clusters H7 and H8 (Cohen & Blakeslee, 1998; Wyder et al., 2000). The dashed line is the locus $\log(R_h)=0.2M_V+2.6$ defined by van den Bergh & Mackey (2004) as the upper limit for typical GCs on the R_h-M_V plane. The faint box defined by -9.4$\lesssim M_V \lesssim$-8.0 and 10$\lesssim R_h \lesssim$60 pc, is the unoccupied region or "avoidance zone" (see Sections 1.4.4 and 1.4.3).

Chapter 2

The M33 Globular Cluster System with PAndAS Data: the Last Outer Halo Cluster?

Robert Cockcroft, William E. Harris, Annette M. N. Ferguson, Avon Huxor, Rodrigo Ibata, Mike J. Irwin, Alan W. McConnachie, Kristin A. Woodley, Scott C. Chapman, Geraint F. Lewis and Thomas H. Puzia

The Astrophysical Journal, Volume 730, Issue 2, pages 112-123,

Bib. Code: 2011ApJ...730..112C, DOI: 10.1088/0004-637X/730/2/112

"The important thing is not to stop questioning. Curiosity has its own reason for existing. One cannot help but be in awe when he contemplates the mysteries of eternity, of life, of the marvelous structure of reality. It is enough if one tries merely to comprehend a little of this mystery every day."

ALBERT EINSTEIN (1879-1955)

2.1 Introduction and Background

Globular cluster systems (GCSs) are important tracers of galaxy formation and evolution. For example, the substructure within a galactic halo reveals its merger history, and globular clusters (GCs) can be used as one tracer of such substructure (e.g., Lynden-Bell & Lynden-Bell 1995). In this paper, we look at the Triangulum Galaxy (M33) which is the third most massive galaxy within our Local Group although it is much less well-studied than the Milky Way (MW), the Magellanic Clouds or Andromeda (M31).

In addition to the well-known stream from the disrupting Sagittarius dwarf galaxy, other evidence for substructure within the Milky Way includes the Monoceros ring, the Orphan stream, and other more subtle over-densities (e.g., Ibata et al. 1995; Newberg et al. 2002; Belokurov et al. 2006, 2007). M31's substructure is being revealed in more and more detail with large-scale structures of very low surface brightness, including several arcs, shells and streams (Ferguson et al., 2002; Ibata et al., 2005, 2007; Kalirai et al., 2006; Richardson et al., 2008; McConnachie et al., 2009).

Subdivisions within the MW GCS have been observed (e.g., Searle & Zinn 1978; Mackey & Gilmore 2004) with evidence that at least some are the result of accretions of dwarf satellite galaxies (Bellazzini et al., 2003; Mackey & Gilmore, 2004; Forbes et al., 2004). Certain clusters still appear to be associated with their accreted satellites: most prominently, clusters associated with Sagittarius (e.g., Layden & Sarajedini 2000; Newberg et al. 2003; Bellazzini et al. 2003). The most distant GC known in the MW is still AM-1, first discovered by Madore & Arp (1979) at a galactocentric distance of ≈120 kpc. In other galaxies, clusters with large galactocentric radii (≈ 120 kpc) reside in the M_v - r_h parameter space between Palomar-type clusters and ultra-faint dwarfs, and this overlap is now well-established (e.g., Huxor et al. 2005, Gómez et al. 2006 and Belokurov et al. 2007).

Within M31, there are now over 60 known clusters with a projected radius greater than 30 kpc (Huxor et al., 2005; Martin et al., 2006; Mackey et al., 2007; Huxor et al., 2008; Mackey et al., 2010). Some of these distant clusters are rather unlike their MW counterparts as they are found to be both more luminous and have larger sizes (Mackey et al., 2007). Most recently it has been shown that the outer halo clusters appear to follow other substructure (streams of enhanced surface brightness), with the probability of chance alignment less than 1% (Mackey et al., 2010). Mackey et al. conclude that the majority of these clusters are accreted along with their host satellite galaxy, as first proposed by Searle & Zinn (1978).

Observations of the M33 clusters - both young and old - have been collated in the catalogue by Sarajedini & Mancone (2007; SM hereafter). This catalogue includes cluster identifications and data from ground-based observations (Hiltner, 1960; Melnick & D'Odorico, 1978; Christian & Schommer, 1982, 1988; Mochejska et al., 1998), *HST* imaging (Chandar et al., 1999, 2001; Bedin et al., 2005; Park & Lee, 2007; Sarajedini et al., 2007; Stonkutė et al., 2008;

Huxor et al., 2009; San Roman et al., 2009), and further data on identified clusters from Ma et al. (2001, 2002a,b,c, 2004a,b). The SM catalogue contains 595 objects of which 428 are classified as high-confidence clusters (based on *HST* and high-resolution ground-based imaging). The most recent work, currently not within the SM catalogue, includes work based on CFHT/MegaCam imaging by Zloczewski et al. (2008) and San Roman et al. (2010) and *HST* imaging by Zloczewski & Kaluzny (2009), that contain 3554, 599 and 91 new star cluster candidates, respectively. (All of these M33 studies cover only the inner one square degree.) Zloczewski & Kaluzny (2009) claim that ≈20% of the 3554 cluster candidates identified in Zloczewski et al. (2008) are likely to be genuine clusters. Unlike the GCSs of the MW and M31, M33 is host to intermediate-age clusters (Sarajedini et al., 1998; Chandar et al., 2002), suggesting that the evolution of M33 was different from that of both the MW or M31.

Studying the Local Group gives us the best chance to observe the remnants of galaxy formation in detail, but M33 remains to be scrutinized in as much detail as either of its larger neighboring galaxies, or the Magellanic Clouds. The work on the M33 GCS has so far been constrained to the classical disk regions, with the exception of the four outer halo clusters found by Huxor et al. (2009) between projected radii of 9.6 and 28.5 kpc and one cluster by Stonkutė et al. (2008) at a projected radius of 12.5 kpc. The outer halo clusters are important, not least because the most distant clusters may be the last that were accreted (e.g., Mackey & van den Bergh 2005). Mackey et al. (2010) have shown that M31's outer halo is rich with clusters. Huxor et al. (2009) undertook a search for M33 outer halo clusters through 12 sq. degrees of the Isaac Newton Telescope Wide-Field Camera data reaching to V∼24.5

and i∼23.5. The PAndAS data allow this search to be extended to larger radii, deeper depths and better image quality. This is the project that we undertake in this chapter. We define outer halo clusters to be those which are projected beyond the isophotal radius of M33 (∼9 kpc, Cockcroft et al. 2012[1]). Such objects are sufficiently remote that they are unlikely to be associated with the main disk component of the galaxy: McConnachie et al. (2010) find little evidence from direct stellar photometry that the disk extends beyond that point. For comparison, the isophotal radius of NGC 253, an Sc-type galaxy of similar size, is $r \sim 9.8$ kpc (Jarrett et al., 2003). Ultimately however, we will require metallicity and velocity measurements to determine more definitely whether these clusters belong dynamically to the disk or halo.

2.2 Observations, Data Reduction and Calibration

We use 41 images each in g' and i' that are part of the Pan-Andromeda Archaeological Survey (PAndAS; McConnachie et al. 2009) and were taken with the Canada-France-Hawaii Telescope (CFHT)/MegaCam which has a one square degree field-of-view. PAndAS includes over 300 sq. degrees, covering a region of sky that extends to a projected radius of 150 and 50 kpc around the Andromeda (M31) and Triangulum (M33) Galaxies, respectively.

Each of the 82 processed fields, themselves a stack of four or five raw images, is labelled according to the notation shown in Figure 2.2. Fields M72

[1]The original Cockcroft et al. (2011) paper referenced Cockcroft et al. (2011b) here, but this has been updated in this thesis to Cockcroft et al. 2012 because of the later-than-expected publication date.

to M76, the five located along a line towards M31, were taken first (Ibata et al., 2007); we note that for these, CCD chip 4 was only working for M72, but not M73 to M76. The other fields M3301 to M3335 were taken in subsequent runs. The central image (called M33c) was a composite of CADC archived images prepared by Ibata et al. (2007).

All M33 images were taken with sub-arcsecond seeing in both g' and i'. The average seeing on g' frames was 0.75" (standard deviation of 0.11"), and 0.66" on i' (standard deviation of 0.13"). Images have a resolution of 0.187"/pixel, and limiting magnitudes of $g' \approx 25.5$, $i' \approx 24.5$ (AB mags on the SDSS scale) at an S/N = 10. These data were previously presented in McConnachie et al. (2010) who studied the stellar structure of the outer regions of M33 and found a large substructure, shown in Figure 2.2. The data were pre-processed with Elixir[2] by the CFHT team, and then reduced at the Cambridge Astronomical Survey Unit through a pipeline adapted for MegaCam images (Irwin & Lewis, 2001).

2.3 Cluster Search Methods

We used two distinct methods to search for clusters within the M33 images: an automatic search and a separate follow-up visual inspection. In both cases, we started with searching the images that form an annulus in the middle of the frames around M33 (i.e., frames M3306 to M3316, including M74), followed by the images outside this annulus and finally the innermost frames. We chose this order so that we started in regions where the crowding was low but evidence for clusters existed (e.g., Huxor et al. 2009), leaving the innermost

[2]http://www.cfht.hawaii.edu/Instruments/Imaging/MegaPrime/dataprocessing.html

crowded fields until last. We identified and marked all the confirmed clusters in the Sarajedini & Mancone (2007) catalogue on the PAndAS images, to gain experience of their appearance.

2.3.1 Automatic Search

We used Source Extractor (SE; Bertin & Arnouts 1996) to identify all objects in both g' and i' frames. Some values within the configuration files were changed to optimize finding clusters whilst cutting out as much contamination as possible (see Table 2.1). We then converted from a chip-oriented pixel coordinate system to a world coordinate system for each object, using the IRAF/wcsctran routine, before matching the objects across the g' and i' frames using the IRAF/xyxymatch routine. As the latter routine only outputs object coordinates, we then re-assigned all SE parameters to the matched objects, so that we could apply selection criteria using a combination of magnitude, color, half-light radius, and ellipticity as measured by SE to pick out the cluster candidates. After numerous initial tests and iterations, we have adopted the following set of criteria:

$$10.5 \leq g' \leq 14.5, \tag{2.1}$$

$$-1.1 \leq g' - i' \leq -0.175 * g' + 3.4375, \tag{2.2}$$

$$e \leq 0.375, \tag{2.3}$$

$$3.5 \leq r_{flux} \leq 16.0, \tag{2.4}$$

and

$$r_{flux} \leq -2.125 * g' + 41.5, \tag{2.5}$$

where e is the ellipticity (1 - minor/major), g' and i' are the automatic magnitude values returned from SE[3], and r_{flux} is the radius (in pixels) estimated to enclose half the flux. The cluster candidates we select satisfy *all* five of the criteria.

These selection criteria are shown in Figure 2.3. The boundary lines were chosen so that they included almost all of the Sarajedini & Mancone (2007) catalogue confirmed clusters at the edge of the disk (in the MegaCam fields M3301 and M76), while cutting out most of the contaminating objects such as stars and background galaxies. The central field, however, provides a special challenge because of the complex structure of the background light and differential reddening. As can be seen in Figure 2.4, our parameter boundaries do not include every one of the Sarajedini & Mancone high confidence clusters (see Section 2.1) in the central field.

However, our aims here were specifically to isolate candidate clusters in the halo regions. Other types of objects (especially background galaxies) populate all areas of the three parametric diagrams in Figures 2.3 and 2.4, and after many iterations we adopted the boundary lines shown as a compromise between excluding contaminants and including real clusters. Nevertheless, the unavoidable fact is that our survey area is so large (more than 40 square degrees around M33) that even our most careful objective search criteria leave a very large number of field contaminants, which dominate the numbers of objects found in the range of magnitudes, colors, and sizes that we are looking

[3] The following are approximate conversions between true color-corrected magnitudes and SE automatic magnitudes: $g'_{true} = g'_{SE} + 6.2$ and $i'_{true} = i'_{SE} + 6.4$.

for.

We produced a small thumbnail display region to identify each object selected by the above criteria. These regions were then displayed in the g' frame. Each object within these regions was then inspected visually and classified following the description in Section 2.3.2 with 1 (high confidence cluster), 2 (possible cluster), 3 (background galaxy), 4 (unknown object) or 5 (stellar object). Examples of objects in the categories 1, 2 and 3 are shown in Figure 2.5.

2.3.2 Visual Inspection

The next stage in our classification procedure was, following Section 2.3.1, to inspect all objects that had *not* already been selected by the automated criteria, i.e., we looked at all SE detections that did not fall within the selection boxes shown in Figure 2.3. This was similar to the method employed by Huxor et al. (2008, 2009). Only i' frames were inspected this way; red-giant branch stars are brighter in i' than in g' and so clusters, and RGB stars in their halo, would appear more obvious by their resolution into stars (no background galaxies would be resolved into individual stars). By also conducting a visual search in addition to the search via the selection criteria, we ensured that any obvious cluster or candidate cluster would not be overlooked, and also ensured that all g' and i' frames will have been inspected.

The easiest objects to classify were the obvious clusters and background galaxies. Clearly-resolved clusters appeared as having a circular or slightly elliptical core, with uneven contours and resolved stars around the central core. Less obvious were group 1 objects which had slightly uneven contours.

The least obvious candidates, group 2 objects, were the compact objects that could be clusters or galaxies, and as a result the numbers of "possible clusters" were the greatest especially in the central regions. As the contrast and scaling were changed, some objects smoothly grew, some were a faint smear with no sharp edges, and others could be seen to display spiral shape. If the object had smooth contours and if it was in a group of other objects that were clearly galaxies, the object was likely to be a galaxy and not a star cluster. Group 4 objects did not look like a cluster, a cluster-candidate, a galaxy or a star.

As noted above, the influence of background contamination by galaxies on this selection process should not be underestimated. In essence, this is a needles-in-a-haystack process where we are attempting to find a small number of clusters in a huge population of contaminants, and even though our selection and culling is rigorous, there remain a large number of objects whose nature is ambiguous from the current data. Higher resolution imaging, imaging in the near infrared where the cluster red giants would be better resolved (and which also can have better seeing), or ultimately spectroscopy, will be required for more definitive elimination of the last contaminants.

2.4 Results

There was only one definite new outer halo cluster discovered in our study at a projected radius of 87" (or 22 kpc, assuming a distance to M33 of 870 kpc). It was found using the automated search. The new cluster is named M33E following the naming convention begun in Huxor et al. (2009). Four of the five previously-known outer halo clusters (Stonkutė et al., 2008; Huxor et al., 2009) were easily recovered. Cluster D was identified but was too compact to have been recovered without prior knowledge. Clusters A to E and S are shown in Figure 2.6, where S is the cluster found by Stonkutė et al. (2008).

There were 2440 candidates spread throughout the M33 halo; that is, in the region outside of the central MegaCam image. 87 (5) highest-confidence cluster candidates and 2294 (54) possible clusters were found by the automated (visual) search method.

The numbers of all classified objects from both the automated and visual inspection searches are shown in Table 2.2. Results of the above searches were plotted within the original selection criteria, and are shown in Figure 2.7. We wanted to exclude the maximum amount of parameter space so that we could increase the efficiency of the automated search, and it is not obvious from this figure that more space could have been excluded. Radial density plots for the categories 1 (high confidence cluster), 2 (possible cluster), 3 (background galaxy) are also shown in Figure 2.8. We compared these number densities at large radii to control fields, also taken with MegaCam and with very similar image quality, from the M31 outer halo and the field near the Draco dwarf spheroidal. The M31 fields are two square-degree fields selected directly from the PAndAS data, at a similar Galactic latitude to M33 of -31.33 degrees, at the edge of the PAndAS footprint around M31 (i.e., at a projected radius of ∼150 kpc) and did not contain any clusters - either previously-known clusters, or clusters detected in the PAndAS images. The Draco fields are seven square-degree fields at a Galactic latitude of 34.72 degrees (Ségall et al., 2007). Our searches were again applied to the control fields following exactly the same selection criteria, and we obtained an average density of each category of objects in the control fields. The radial distribution plots indicate that few if any of the category 3 objects are genuine clusters since they show little detectable central concentration to the galaxy outside the crowded disk region. For all three categories plotted, the number density settles down to a virtually constant level similar to that of the M31 control fields for $r \gtrsim 1$ degree, consistent with the conclusion that there are few clusters left to be found in the M33 halo down to the PAndAS limiting magnitudes. (The number density of all objects in the Draco fields is much lower than that in either the M33 or M31 fields, highlighting that it was appropriate to compare M33 with the M31 control fields.) If we count the number of candidates for the combined objects of classes 1 and 2 in Figure 2.8 for $r \geq 10$ kpc, and then subtract off the M31 background, we are left with approximately 210±130 candidates (the error is estimated using the error on the M31 background). This number is simply an estimate of the outer halo clusters that possibly remain to be discovered, using the data we have in hand. 210 clusters would be a generous upper limit, given the field contamination issues that we discuss.

We next measured the g' and i' magnitudes, and the colors of the six outer halo clusters. The results are shown in Table 2.3. For clusters A, B, C and S we use an aperture radius of 40 pixels (7.5") and a sky annulus between 60 and 80 pixels (11.2"-15.0"); for the smaller clusters we used 20 pixels (3.7") with a sky annulus between 20 and 40 pixels (3.7"-7.5") for D, and 30 pixels (5.6") with a sky annulus between 50 and 70 pixels (9.4"-13.1") for E. We assume an extinction correction of 0.16 in g', 0.09 in i', 0.14 in V, and 0.08 in I (Schlegel et al., 1998), and a distance of 870 kpc to M33, consistent with SM07 and Huxor et al. (2009), and corresponding to a distance modulus of $(\text{m-M})_0 = 24.69$. We note that there is some disagreement in the literature regarding the distance to M33; see references in McConnachie et al. (2010). For the magnitude and color conversions from (g', i') to (V, I) we used

$$V = g - (0.587 \pm 0.022)(g - r) - (0.011 \pm 0.013) \tag{2.6}$$

and

$$I = i - (0.337 \pm 0.191)(r - i) - (0.370 \pm 0.041) \tag{2.7}$$

from Chonis & Gaskell (2008), and

$$(r - i)_0 = 0.37(g - r)_0 + 0.006 \tag{2.8}$$

from Bilir et al. (2008).

Comparing the magnitudes and colors that we measure in this paper with those in Huxor et al. (2009) for clusters A, B, C and D, we find differences of $V_0 \leq 0.3$mag and $(V - I)_0 \leq 0.1$mag. For cluster S, Stonkutė et al. (2008) measures a V magnitude of 18.5 (at $\sim 2r_h$, which roughly corresponds to our annulus size). As we measure $V_0 \sim 18.5$, the difference between our measurements is the extinction value of 0.14.

Our crude estimate for the cluster magnitude limit is currently $g'_{lim} \approx 20$ ($M_g \approx -4.8$). We will quantify this more accurately in an upcoming paper by inserting fake clusters and testing recovery rates using our search methods. Although our current search limit is comfortably faint, there are small numbers of still less luminous clusters known to exist in the Milky Way, for example (the faintest, sparse Palomar-type objects; see Figure 2.10). We can therefore place no quantitative limits on the numbers of such objects yet to be found in M33. Note that cluster D (Huxor et al., 2009) is a magnitude fainter than our estimated limit, but was found with *HST* imaging. We would not expect to recover such a cluster independently with the MegaCam data.

Finally, we measured the structural parameters of all six outer clusters, including the concentration parameter, and core, half-light and tidal radii. We use the GRIDFIT code described by McLaughlin et al. (2008), which fits various King-type cluster models[4] convolved with the measured PSF to each object. Here we attempt to fit King (1962), King (1966) and Wilson (1975) models to each object. We also use the KFIT2D code of Larsen et al. (2002) with the King (1966) model as an independent measure. The results of all fits are shown in Table 2.4, and examples of the fits are shown in Figures 2.9. We also include an independent measurement of the half-light radii using the curve of growth of the clusters (r_{ap}). For A and D, not all of the three models converged to successful fits, but the other four clusters gave high consistency among themselves for their radii. Fitting models to cluster A was not successful because of its diffuse nature, while cluster D was extremely small. We also note that cluster S has an unusual feature in its surface profile; Stonkutė et al. (2008) also note that this cluster is asymmetrical in its inner regions. Comparing our measured structural parameters for cluster S with those from Stonkutė et al. (2008) we similarly find that this cluster has a very large core radius, although we measure slightly smaller quantities for each radius - even adjusting the value for our assumptions for the distance to M33.

In Figure 2.10, we show the locations of all six M33 halo clusters in luminosity versus r_h, compared with the Milky Way GCs. All clusters have low concentrations, similar to the Palomar outer halo clusters in the Milky Way. Their half-light radii range from 4 to 20 pc, all larger than the typical mean $r_h \sim 3$ pc for the standard Milky Way clusters, but placing them in a

[4]See Section 3.1.1 for a full description of the different fitting models.

similar range as many of the outer halo Milky Way clusters. A full comparison of all M33 clusters will be done in a future paper.

2.5 Discussion and Conclusions

We search more than 40 square degrees of the halo of M33 with CFHT/MegaCam data for outer halo clusters using both an automated search and visual inspection. Unexpectedly, we find only one new cluster, which is smaller, fainter and slightly redder than the three INT clusters found by Huxor et al. (2009) and the cluster found by Stonkutė et al. (2008). However, it does lie within the INT area of Huxor et al. (2009) but the object was not previously recognized due to its small size and faint luminosity. At a projected radius of 22 kpc, the new cluster has $g' \approx 19.9$, $(g' - i') \approx 0.6$, concentration parameter $c \approx 1.0$, a core radius $r_c \approx 3.5$ pc, and a half-light radius $r_h \approx 5.5$ pc. Its projected location is close to the feature observed in the stellar substructure (see Figure 2.2 and McConnachie et al. 2010). Huxor et al. (2009) note that the mean color of the previously-known outer halo clusters is slightly redder ($(V - I)_0 = 0.88 \pm 0.05$ mag) than the inner clusters ($(V - I)_0 = 0.67 \pm 0.30$ mag). Our new cluster is redder still by $\sim$0.2 mag.

M33 has only six definite outer halo clusters between projected radii of 9 kpc $\leq$ r $\leq$ 50 kpc and to $g'_{lim} \approx 20$. We also find 2440 cluster candidates of various degrees of confidence, and although the vast majority are likely to be background contaminants, at least some of the $\sim$ 90 highest-confidence candidate objects beyond the M33 disk may be faint but genuine clusters. We cannot yet assume all the highest-confidence candidate objects are clusters without further confirmation. We will use IR data (now being acquired) and structural parameters in an upcoming paper to determine this more securely.

How many clusters could we expect to find in M33? M31 has 67 outer halo clusters already discovered, 61 of which lie in the PAndAS footprint that has been analyzed so far. These clusters have comparable luminosity to the M33 outer halo clusters and are located at projected radius 30 kpc $\leq r \leq$ 130 kpc (Mackey et al., 2010; Huxor et al., 2011). Huxor et al. (2009) found a GC surface density of $\sim$0.4 deg^{-2} with their 12 deg^2 study, which they note is about half that derived for M31 over the radial range 30kpc $\leq r \leq$ 130 kpc. Here we find an even lower GC surface density of 0.15 deg^{-2}. We note that the search in M31's outer halo is not yet complete so its GC surface density is likely to increase. M33 appears to therefore lack this type of cluster. We briefly mention two scenarios that could have resulted in this observed difference.

M33 could have had a different accretion history compared to M31 - a conclusion that has been drawn before from studies of the inner regions (San Roman et al., 2010), but is now also indicated by the outer halo data. If M33 never interacted with M31 before, M33 would have had a dramatically less active accretion history.

The most compelling evidence for an accretion origin for the outer halo clusters comes from the Sagittarius dwarf in the MW (Ibata et al., 1995), and from the GCs and tidal debris streams in M31 (Mackey et al., 2010), but it is still far from clear how general a result this is.

However, another exciting and more likely prospect, given the tidal distortion of M33, is that perhaps some of M33's outer halo clusters were heavily stripped off in a previous dynamical interaction with M31 (Huxor et al., 2009; San Roman et al., 2010). Some of the GCs originally belonging to M33 may now be closer to M31, but it will be difficult to disentangle the populations.

A more detailed comparison will require spectroscopic studies of these clusters to determine properties that may link the divided populations. Although unlikely, some clusters may be beyond the area that we have imaged so far around M33. These scenarios are not mutually exclusive. Further discussion and comparison with the M33 halo star population will come in subsequent work now in progress.

Acknowledgements

RC and WEH thank the Natural Sciences and Engineering Research Council of Canada for financial support. This research has made use of the NASA/IPAC Extragalactic Database (NED) which is operated by the Jet Propulsion Laboratory, California Institute of Technology, under contract with the National Aeronautics and Space Administration.

Based on observations obtained with MegaPrime/MegaCam, a joint project of CFHT and CEA/DAPNIA, at the Canada-France-Hawaii Telescope (CFHT) which is operated by the National Research Council (NRC) of Canada, the Institute National des Sciences de l'Univers of the Centre National de la Recherche Scientifique of France, and the University of Hawaii. RC would like to thank the CFHT staff for much support.

Thanks to all our collaborators in the PAndAS and to the anonymous referee for providing useful comments that improved this paper. RC would also like to thank the Universities of Edinburgh and Cambridge for funding collaborative visits.

Bibliography

Bedin, L. R., Piotto, G., et al. 2005, A&A, 444, 831

Bellazzini, M., Ferraro, F. R., and Ibata, R. 2003, AJ, 125, 188

Belokurov, V., Evans, N. W., et al. 2007, ApJ, 658, 337

Belokurov, V., Zucker, D. B., et al. 2006, ApJ, 642, L137

Bertin, E. and Arnouts, S. 1996, A&AS, 117, 393

Bilir, S., Ak, S., Karaali, S., Cabrera-Lavers, A., Chonis, T. S., and Gaskell, C. M. 2008, MNRAS, 384, 1178

Chandar, R., Bianchi, L., and Ford, H. C. 1999, ApJS, 122, 431

—. 2001, A&A, 366, 498

Chandar, R., Bianchi, L., Ford, H. C., and Sarajedini, A. 2002, ApJ, 564, 712

Chonis, T. S. and Gaskell, C. M. 2008, AJ, 135, 264

Christian, C. A. and Schommer, R. A. 1982, ApJS, 49, 405

—. 1988, AJ, 95, 704

Cockcroft, R., Harris, W. E., et al. 2011, ApJ, 730, 112

Cockcroft, R., McConnachie, A. W., et al. 2012, submitted to MNRAS

Ferguson, A. M. N., Irwin, M. J., Ibata, R. A., Lewis, G. F., and Tanvir, N. R. 2002, AJ, 124, 1452

Forbes, D. A., Strader, J., and Brodie, J. P. 2004, AJ, 127, 3394

Gómez, M., Geisler, D., Harris, W. E., Richtler, T., Harris, G. L. H., and Woodley, K. A. 2006, A&A, 447, 877

Harris, W. E. 1996, AJ, 112, 1487

Hiltner, W. A. 1960, ApJ, 131, 163

Huxor, A., Ferguson, A. M. N., et al. 2009, ApJ, 698, L77

Huxor, A., Ferguson, A. M. N., and PAndAS collaborators. 2011, in preparation

Huxor, A. P., Tanvir, N. R., et al. 2008, MNRAS, 385, 1989

Huxor, A. P., —. 2005, MNRAS, 360, 1007

Ibata, R., Chapman, S., Ferguson, A. M. N., Lewis, G., Irwin, M., and Tanvir, N. 2005, ApJ, 634, 287

Ibata, R., Martin, N. F., et al. 2007, ApJ, 671, 1591

Ibata, R. A., Gilmore, G., and Irwin, M. J. 1995, MNRAS, 277, 781

Irwin, M. and Lewis, J. 2001, New Astronomy Reviews, 45, 105

Jarrett, T. H., Chester, T., Cutri, R., Schneider, S. E., and Huchra, J. P. 2003, AJ, 125, 525

Kalirai, J. S., Gilbert, K. M., et al. 2006, ApJ, 648, 389

King, I. 1962, AJ, 67, 471

King, I. R. 1966, AJ, 71, 64

Larsen, S. S., Brodie, J. P., Sarajedini, A., and Huchra, J. P. 2002, AJ, 124, 2615

Layden, A. C. and Sarajedini, A. 2000, AJ, 119, 1760

Lynden-Bell, D. and Lynden-Bell, R. M. 1995, MNRAS, 275, 429

Ma, J., Zhou, X., and Chen, J. 2004a, Chinese Journal of Astronomy and Astrophysics, 4, 125

—. 2004b, A&A, 413, 563

Ma, J., Zhou, X., et al. 2002a, Chinese Journal of Astronomy and Astrophysics, 2, 197

Ma, J., —. 2002b, AJ, 123, 3141

Ma, J., —. 2002c, Acta Astronomica, 52, 453

Ma, J., —. 2001, AJ, 122, 1796

Mackey, A. D. and Gilmore, G. F. 2004, MNRAS, 355, 504

Mackey, A. D., Huxor, A., et al. 2007, ApJ, 655, L85

Mackey, A. D., Huxor, A. P., et al. 2010, ApJ, 717, L11

Mackey, A. D. and van den Bergh, S. 2005, MNRAS, 360, 631

Madore, B. F. and Arp, H. C. 1979, ApJ, 227, L103+

Martin, N. F., Ibata, R. A., et al. 2006, MNRAS, 371, 1983

McConnachie, A. W., Ferguson, A. M. N., et al. 2010, ApJ, 723, 1038

McConnachie, A. W., Irwin, M. J., et al. 2009, Nature, 461, 66

McLaughlin, D. E., Barmby, P., Harris, W. E., Forbes, D. A., and Harris, G. L. H. 2008, MNRAS, 384, 563

Melnick, J. and D'Odorico, S. 1978, A&AS, 34, 249

Mochejska, B. J., Kaluzny, J., Krockenberger, M., Sasselov, D. D., and Stanek, K. Z. 1998, Acta Astronomica, 48, 455

Newberg, H. J., Yanny, B., et al. 2003, ApJ, 596, L191

Newberg, H. J., —. 2002, ApJ, 569, 245

Park, W. and Lee, M. G. 2007, AJ, 134, 2168

Richardson, J. C., Ferguson, A. M. N., et al. 2008, AJ, 135, 1998

San Roman, I., Sarajedini, A., and Aparicio, A. 2010, ArXiv e-prints

San Roman, I., Sarajedini, A., Garnett, D. R., and Holtzman, J. A. 2009, ApJ, 699, 839

Sarajedini, A., Barker, M. K., Geisler, D., Harding, P., and Schommer, R. 2007, AJ, 133, 290

Sarajedini, A., Geisler, D., Harding, P., and Schommer, R. 1998, ApJ, 508, L37

Sarajedini, A. and Mancone, C. L. 2007, AJ, 134, 447

Schlegel, D. J., Finkbeiner, D. P., and Davis, M. 1998, ApJ, 500, 525

Searle, L. and Zinn, R. 1978, ApJ, 225, 357

Ségall, M., Ibata, R. A., Irwin, M. J., Martin, N. F., and Chapman, S. 2007, MNRAS, 375, 831

Stonkutė, R., Vansevičius, V., et al. 2008, AJ, 135, 1482

Wilson, C. P. 1975, AJ, 80, 175

Zloczewski, K. and Kaluzny, J. 2009, Acta Astronomica, 59, 47

Zloczewski, K., Kaluzny, J., and Hartman, J. 2008, Acta Astronomica, 58, 23

Table 2.1: Source Extractor values used on the MegaCam images

Parameter	Default Value	New Value
DETECT_MINAREA	5	4
THRESH_TYPE	-	RELATIVE
DETECT_THRESH	1.5	5
DEBLEND_NTHRESH	32	8
CLEAN_PARAM	1.0	1.5
PHOT_APERTURES	5	3
PHOT_AUTOPARAMS	2.5,3.5	2.0,2.5
PHOT_PETROPARAMS	2.0,3.5	2.0,2.5
PHOT_FLUXFRAC	-	0.5
SATUR_LEVEL	50000	60000
MAG_ZEROPOINT	0.0	g'=26.7,i'=25.98
BACKPHOTO_TYPE	GLOBAL	LOCAL

Table 2.2: Categorized objects in M33 PAndAS frames. The column headers are as follows: SM1 are the Sarajedini & Mancone (2007) catalogue's confirmed clusters, OH are the outer halo clusters, 1 are our highest-confidence clusters, 2 are the possible clusters, 3 are the background galaxies, 4 are unknown objects and 5 are stellar objects. The numbers in brackets after the highest-confidence and possible clusters indicate those candidates which matched objects in SM1.

Frame	SM1	OH	1	2	3	4	5
M3301	34	-	7(3)	354(16)	106	114	0
M3302	-	-	1	69	56	8	27

Continued on next page

Table 2.2 – continued from previous page

Frame	SM1	OH	1	2	3	4	5
M3303	1	$1^{c,e}+1$	3	96	43	16	8
M3304	-	$1^{d,e}$	2	69	86	16	7
M3305	-	$1^{b,e}$	2	83	51	19	5
M3306	-	-	2	49	92	20	0
M3307	-	1^{g}	2	31	79	16	0
M3308	-	-	0	45	149	13	0
M3309	-	-	0	77	104	11	0
M3310	-	-	0	64	77	7	0
M3311	-	-	1	27	74	6	0
M3312	-	-	3	38	96	11	0
M3313	-	1^{e}	2	64	60	13	0
M3314	-	-	3	44	55	13	1
M3315	-	-	2	35	87	31	0
M3316	-	-	0	56	81	14	0
M3317	-	-	1	44	114	9	0
M3318	-	-	0	25	121	5	0
M3319	-	-	0	55	96	16	0
M3320	-	-	0	29	86	6	0
M3321	-	-	0	8	74	9	0
M3322	-	-	3	26	66	11	1
M3323	-	-	0	18	69	6	1
M3324	-	-	1	63	61	16	3
M3325	-	-	0	31	61	15	3
M3326	-	-	1	29	104	15	0
M3327	-	-	0	24	81	14	3
M3328	-	-	1	32	115	14	3
M3329	-	-	5	72	81	19	6
M3330	-	-	5	67	117	15	0

Continued on next page

Table 2.2 – continued from previous page

Frame	SM1	OH	1	2	3	4	5
M3331	-	-	2	61	127	25	0
M3332	-	-	1	58	148	22	6
M3333	-	-	3	39	129	16	2
M3334	-	-	2	35	116	15	2
M3335	-	-	2	29	87	25	0
M72	-	-	2	28	71	11	1
M73	-	-	1	45	93	13	2
M74	-	-	0	52	61	12	1
M75	-	-	0	43	95	22	0
M76	19	2[a,e]	32(8)	234(2)	54	86	3
M33c	374[f]	-	259(95)	1521(138)	84	954	19

[a] Also found in M3305

[b] Also found in M76

[c] Also found in M3304

[d] Also found in M3303

[e] Also found by Huxor et al. (2009)

[f] Does not include those on frames M3301, M3303 or M76

[g] New cluster identified in this paper.

Table 2.3: Outer halo cluster positions, luminosities and colors. We assume a distance of 870 kpc to M33, consistent with SM07 and Huxor et al. (2009), and that M33's center is located at ($01^h33^m50.9^s$, $30^d39^m37^s$).

	Degrees		Galactocentric distance					
Cluster	RA	Dec	arcmins	kpc	g'_0	$(g'-i')_0$	V_0	$(V-I)_0$
A	23.92388	28.82086	112	28.4	19.1	0.7	18.8	0.9
B	24.00865	29.96372	48	12.2	17.8	0.7	17.5	0.8
C	24.31026	31.07433	45	11.3	18.4	0.8	18.1	0.8
D	23.75916	31.23925	37	9.4	21.3	0.8	20.9	1.0
E	23.84466	32.07559	87	21.9	19.8	0.5	19.6	1.1
S	23.24374	29.8675	49	12.3	18.9	0.8	18.5	0.8

Table 2.4: Outer halo cluster structural parameters, including concentration, c, core radii, half-light radii, and tidal radii, using both GRIDFIT and KFIT2D. We report the best-fit to the data, whether in g' or in i'. Also shown are half-light radii estimates (r_{ap}) using curves-of-growth, for an independent check on the upper limit of the half-light radii. We assume a distance of 870 kpc to M33, consistent with SM07 and Huxor et al. (2009), and corresponding to a distance modulus of $(m\text{-}M)_0 = 24.69$.

						Radii (pc)		
Cluster	Model	Band	Seeing/FWHM	c	Core	Half	Tidal	r(ap)
	K62	i	3.8	0.5	16.9	20.1	68.0	11.7
A	K66	i	3.8	0.4	17.7	20.3	83.2	
	W	-	-	-	-	-	-	

Continued on next page

Table 2.4 – continued from previous page

					Radii (pc)			
Cluster	Model	Band	Seeing/FWHM	c	Core	Half	Tidal	r(ap)
	kfit2d	i	3.8	0.7	11.7	11.6	59.8	
	K62	g	4.0	0.8	6.1	9.4	44.0	9.0
B	K66	g	4.0	0.9	6.3	9.4	56	
	W	g	4.0	1.0	6.6	9.4	87.3	
	kfit2d	g	4.0	1.1	6.0	10.9	78.5	
	K62	g	4.0	0.8	5.6	8.7	40.7	7.8
C	K66	i	3.3	1.0	4.5	7.3	48.1	7.8
	W	i	3.3	1.0	4.9	7.1	70.8	
	kfit2d	i	3.3	1.3	3.8	8.8	81.9	
	K62	g	4.5	0.3	4.7	4.8	13.6	4.7
D	K66	-	-	-	-	-	-	
	W	-	-	-	-	-	-	
	kfit2d	g	4.5	0.4	4.1	3.7	9.8	
	K62	i	2.6	0.8	3.3	5.2	25.5	5.1
E	K66	i	2.6	0.9	3.5	5.2	31.4	
	W	g	3.1	1.2	3.6	5.6	65.8	5.1
	kfit2d	i	2.6	1.1	2.7	5.0	32.4	
	K62	g	4.6	0.3	15.8	15.7	42.7	18.7
S	K66	i	3.4	0.4	14.8	16.7	67.31	18.7
	W	i	3.4	0.2	15.8	19.2	121.4	
	kfit2d	i	3.4	0.7	17.9	18.7	93.7	

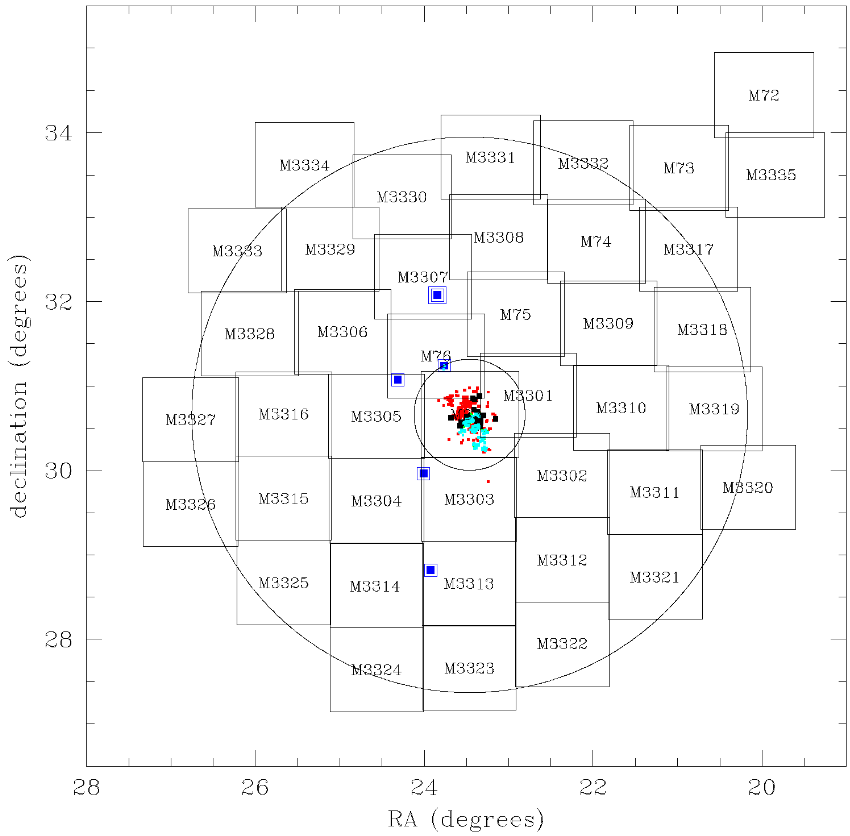

Figure 2.1: The 41 PAndAS frames by CFHT/MegaCam around M33 used in this paper. Each square represents the one square-degree field-of-view of MegaCam. M33c is the central field. The two circles represent projected radii of 10 kpc and 50 kpc centered on M33. Also shown are the locations of the high-confidence clusters in the Sarajedini & Mancone (2007) catalogue (the outer halo cluster found by Stonkutė et al. (2008) being the only catalogue's object outside the 10 kpc radius), the four outer halo clusters in Huxor et al. (2009) enclosed in one box and the newly discovered outer halo cluster enclosed in a double box. The current (October, 2010) online Sarajedini & Mancone catalogue is further subdivided to show the location of the 296 original clusters in red from Sarajedini & Mancone (2007) in addition to the subsequently-discovered 32 clusters in black from Park & Lee (2007), 115 clusters in cyan from Zloczewski & Kaluzny (2009), and 161 (115 new) clusters in green from San Roman et al. (2009). There is much overlap between the clusters found by Zloczewski & Kaluzny (2009) and San Roman et al. (2009).

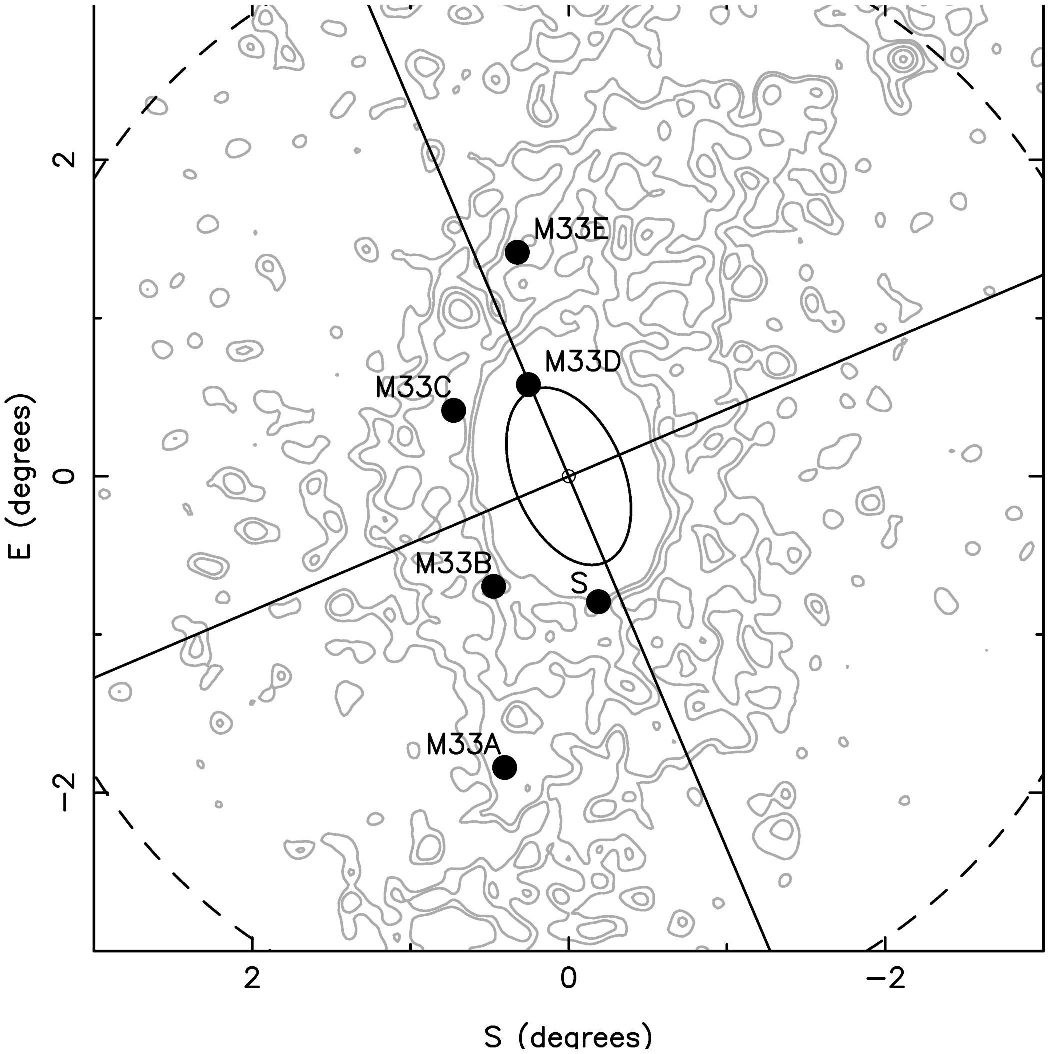

Figure 2.2: The outer halo clusters overlaid on the substructure map from Figure 13 in McConnachie et al. (2010).

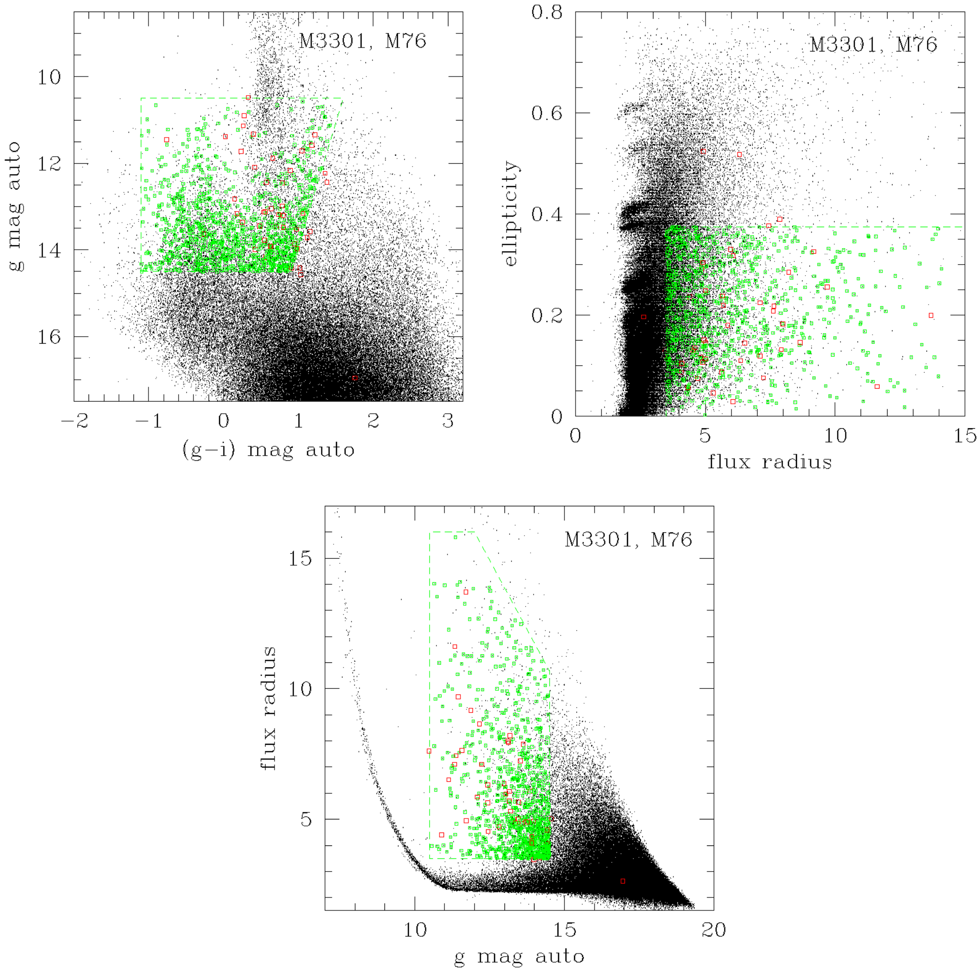

Figure 2.3: Two halo fields and objects on which Section 2.3.1's selection criteria were based. The black dots are the objects of all kinds detected by SE. The green dashed lines show the boundaries of the selection criteria (equations 2.1 to 2.5), and the green squares enclose those points which were picked out by all five of the selection criteria. The red squares show the high-confidence clusters in the Sarajedini & Mancone (2007) catalogue. The following are approximate conversions between true color-corrected magnitudes and SE automatic magnitudes: $g'_{true} = g'_{SE} + 6.2$ and $i'_{true} = i'_{SE} + 6.4$.

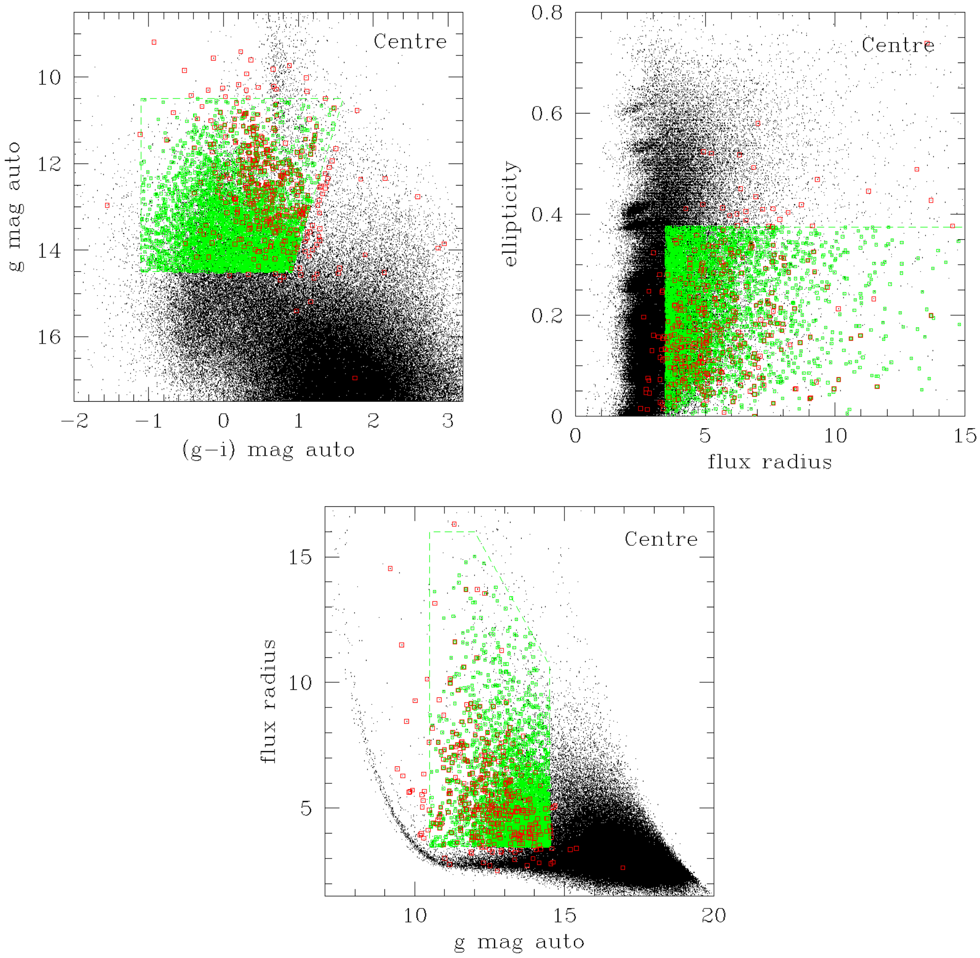

Figure 2.4: Objects within the central field. As with Figure 2.3, the black dots show the SE detections. The green dashed lines show the selection criteria, and the green squares enclose those points which were picked out by all five of the selection criteria. The red squares show the high-confidence clusters in the Sarajedini & Mancone (2007) catalogue. The following are approximate conversions between true color-corrected magnitudes and SE automatic magnitudes: $g'_{true} = g'_{SE} + 6.2$ and $i'_{true} = i'_{SE} + 6.4$.

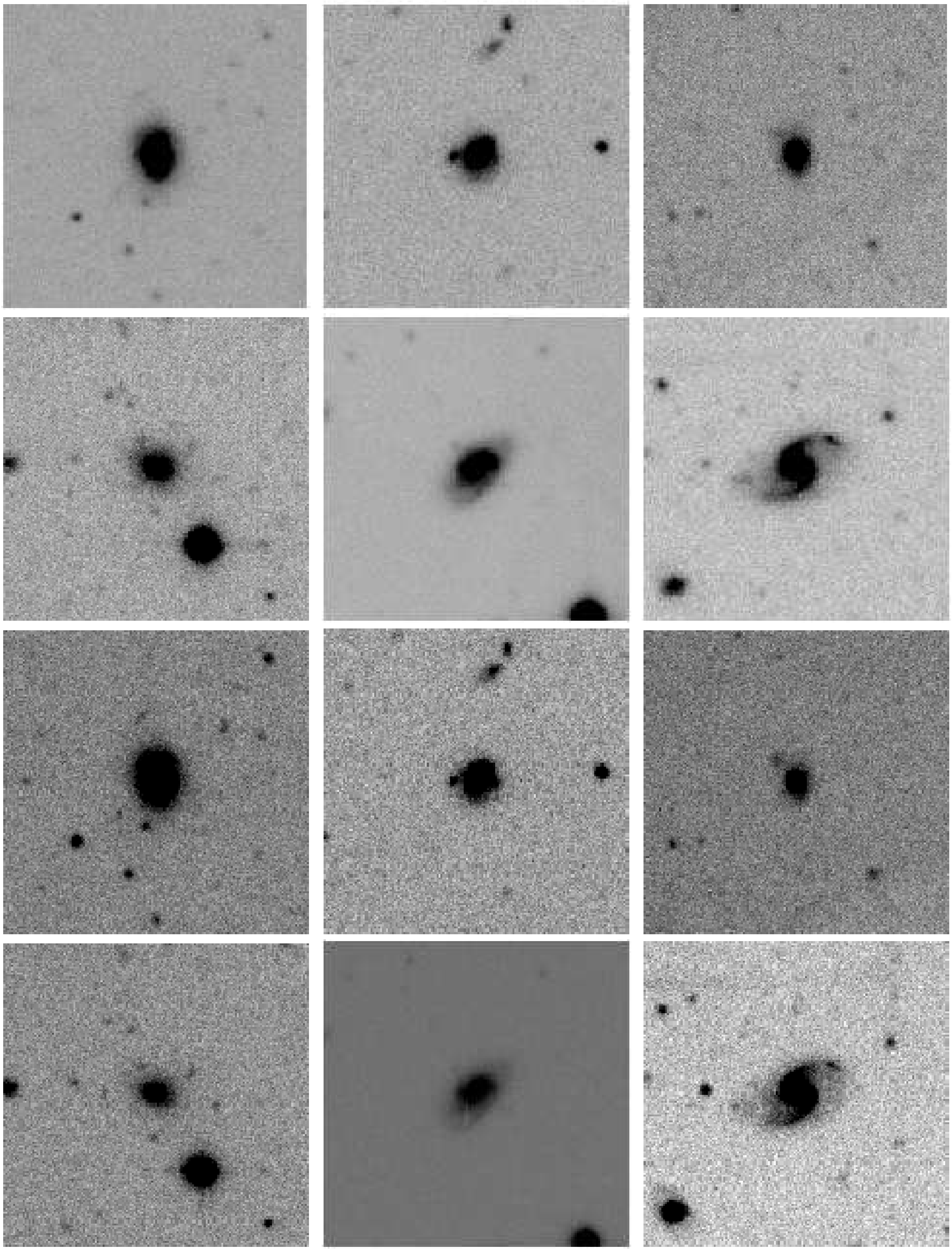

Figure 2.5: Six examples of classified objects in g' (top row) and i' (bottom). From left to right: two examples each of 1 (high-confidence clusters), 2 (possible cluster candidates), and 3 (galaxies). More detail is apparent when changing the scale and contrast in a DS9 window. Each box is 20" square, corresponding to about 84 pc square (at 870 kpc).

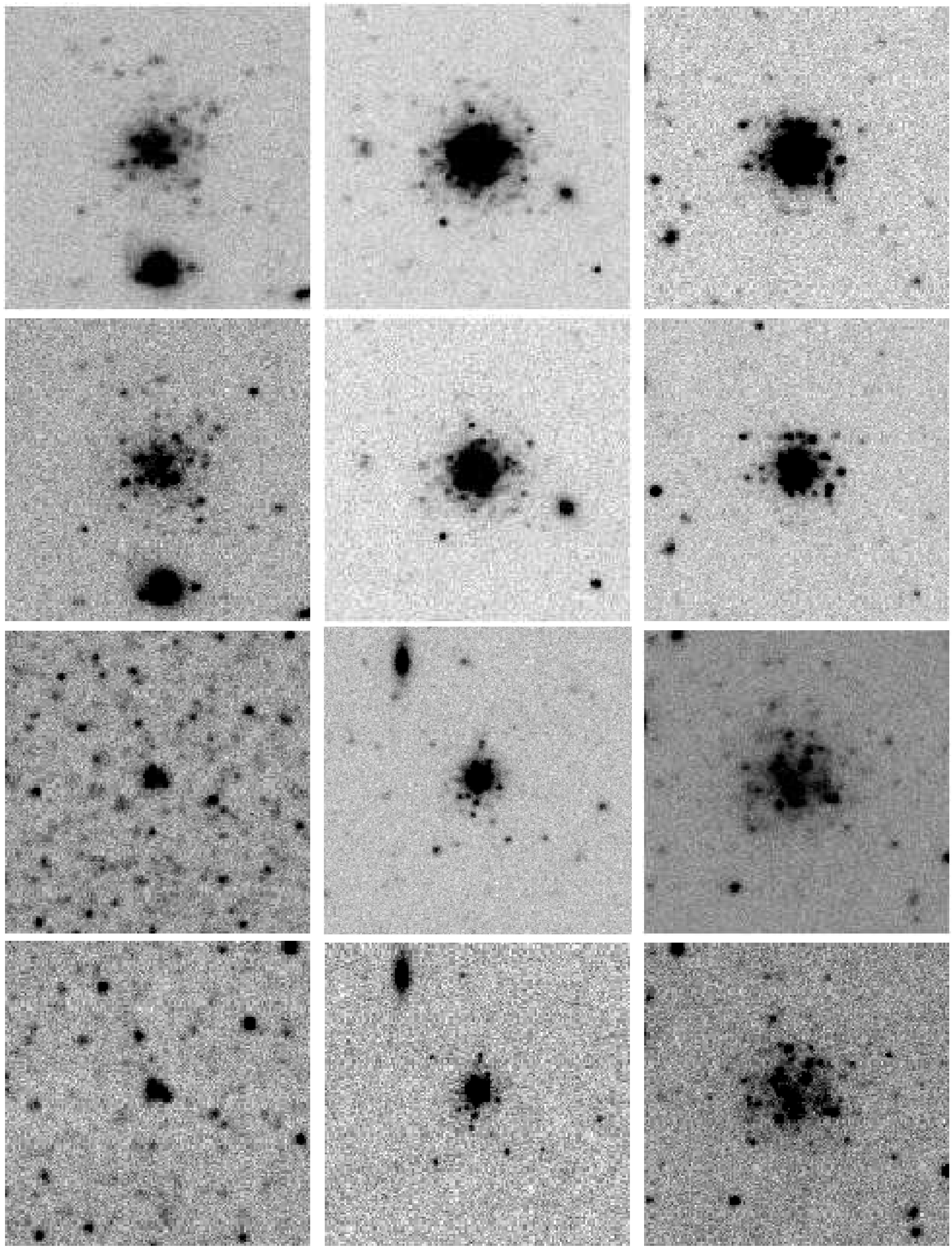

Figure 2.6: M33 A, B, C, D, E and S (left to right) in g' (top) and i' (bottom). Each box is 20" square, corresponding to about 84 pc square (at 870 kpc).

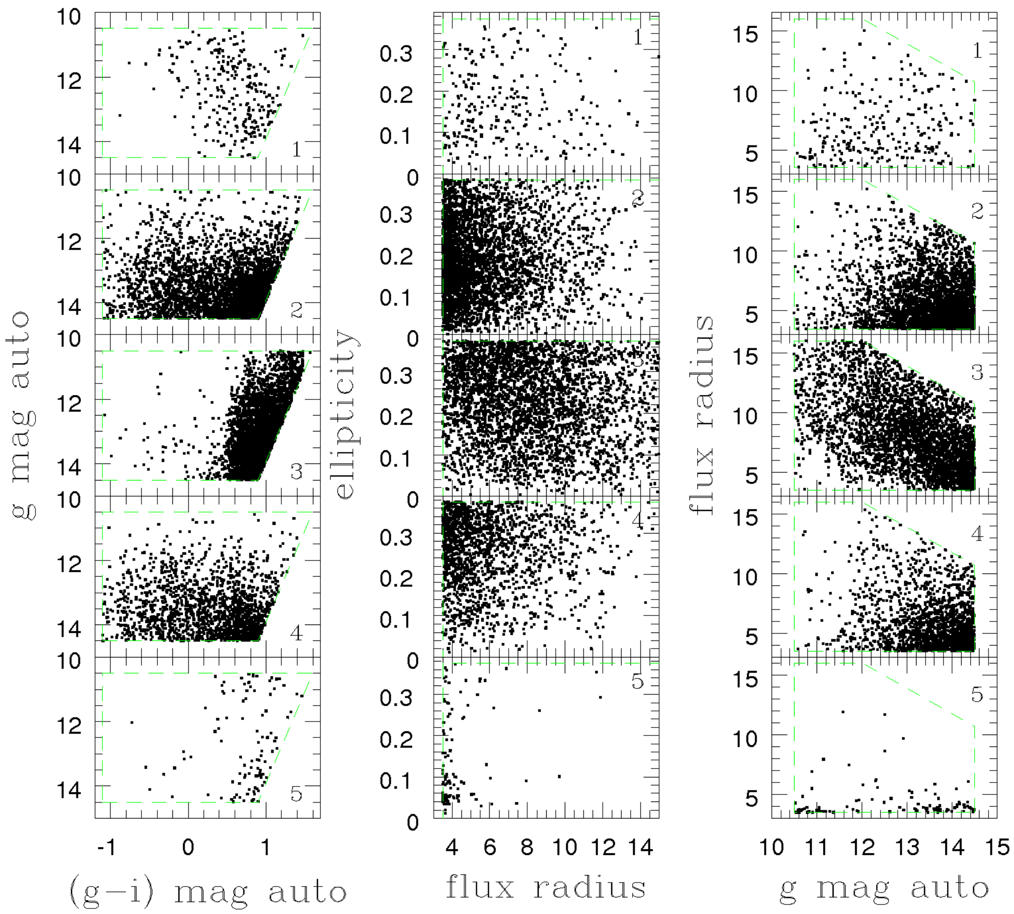

Figure 2.7: The classified objects after visual inspection shown in relation to the automatic selection criteria of Section 2.3.1. Class 1 represents high confidence candidates, class 2 are possible clusters, class 3 are background galaxies, class 4 are unknown objects, and class 5 are stellar objects. To calibrate the "mag auto" values, we added the zeropoint term and corrected for airmass and color.

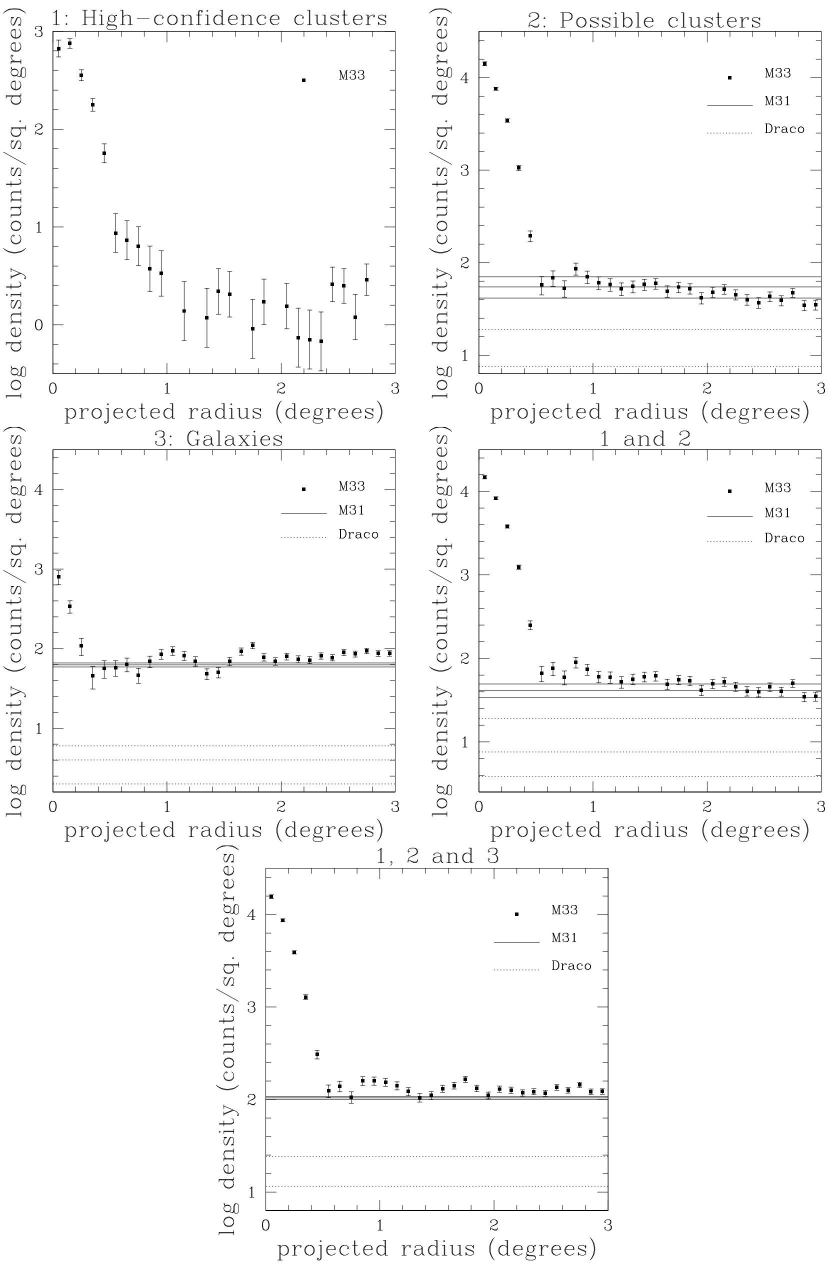

Figure 2.8: Radial densities of objects in circular annuli from categories 1 (high-confidence clusters), 2 (possible clusters) and 3 (background galaxies) along the top, and the sum of 1 and 2, and also 1, 2 and 3 on the bottom. Error bars on the points are simple $n^{1/2}$ uncertainties. Also shown are the mean and 1-sigma errors of the same categories of objects in control fields from the M31 outer halo (solid line) and Draco (dashed line). The Draco number densities are so low, as mentioned in Section 2.4, that in two cases the 1-sigma errors are larger than the mean and so cannot be plotted on a log scale. In these cases, only the mean and upper 1-sigma error are shown.

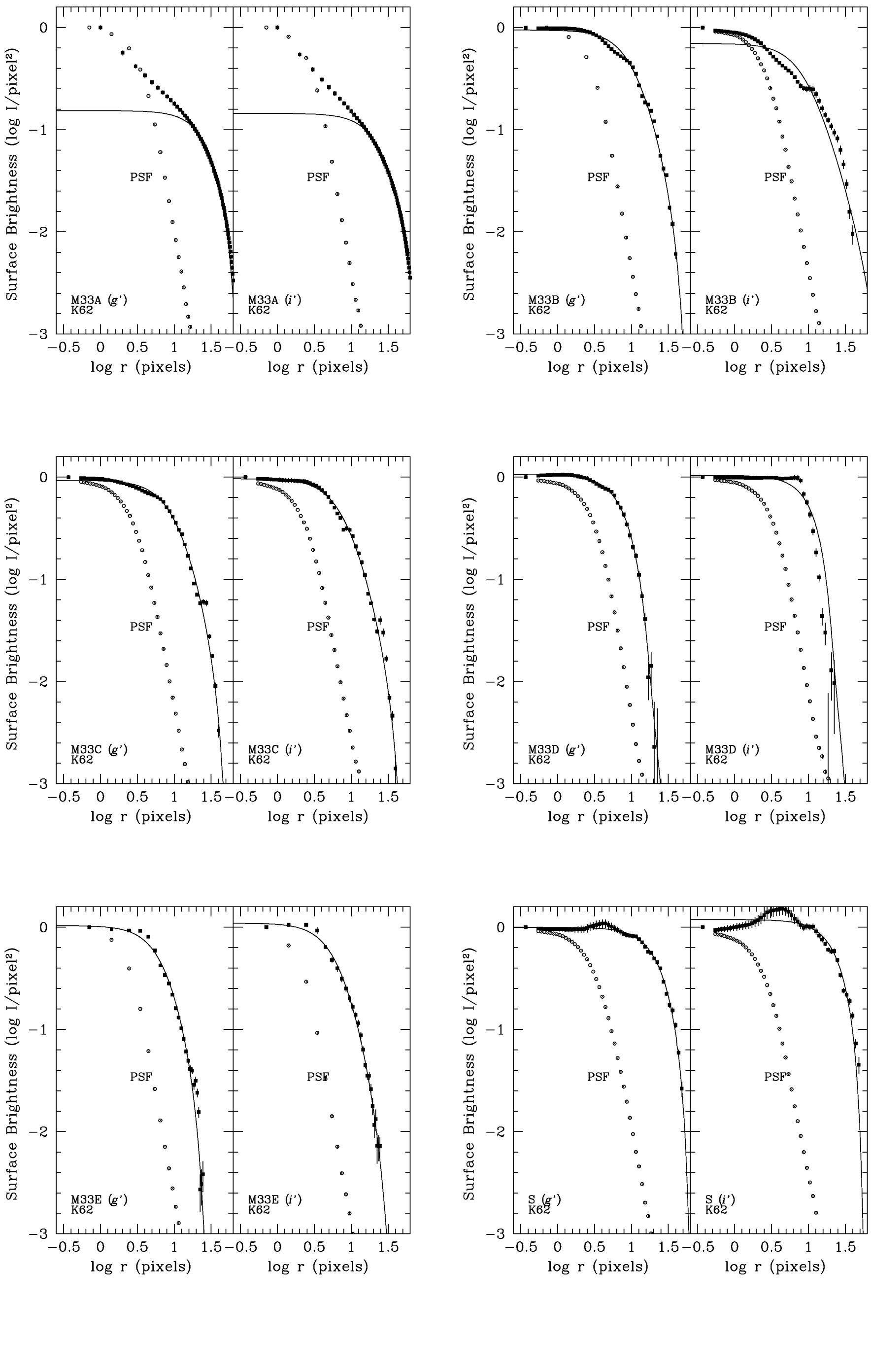

Figure 2.9: Examples of radial profiles for each of the six outer halo clusters. The solid points indicate the data, the line is the best-fit, the open points show the profile for the PSF. Note that for clusters A and D, the fits did not converge to a simple King-type model solution adequately.

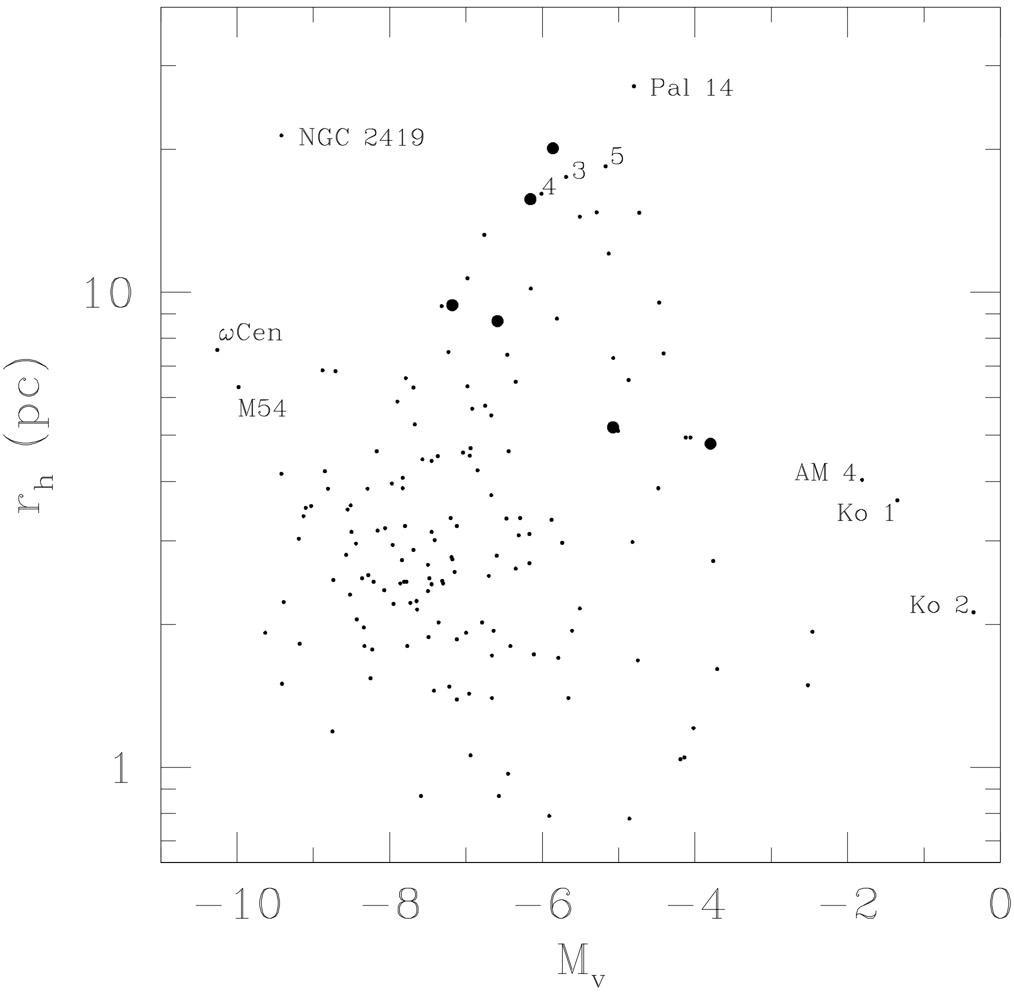

Figure 2.10: Absolute magnitudes versus the half-light radius in parsecs for both the Milky Way clusters (small circles; Harris 1996), and the six M33 outer halo clusters (large circles), from brightest to faintest: B, C, S, A (largest r_h), E and D (smallest r_h). Outliers are labelled, with 3, 4 and 5 indicating the Palomar clusters 3, 4 and 5. (This is a revised version of Figure 9 from Cockcroft et al. 2011.)

Chapter 3

Further Constraining Globular Cluster Candidates

"But I don't have to know an answer. I don't feel frightened by not knowing things, by being lost in the mysterious universe without having any purpose, which is the way it really is, as far as I can tell, possibly. It doesn't frighten me."

Richard Feynman (1918-1988)

3.1 Introduction

In Cockcroft et al. (2011; i.e., Chapter 2), we identified 2440 GC candidates in M33, most of which are likely to be background galaxies but at least a small number that we would expect to be *bona fide* clusters. How do we further explore the parameter space of all these objects, so that we may cull out most of the contamination and provide a list of highest-confidence clusters that we can then follow up with future observations? High-resolution imaging and/or spectroscopic follow-up would be preferable, but completely unfeasible given the large number of candidate objects. To further estimate the robustness of our candidates, we use two methods: 1) we insert simulated clusters and measure our retrieval rate to identify what kinds of clusters we are likely to miss (Section 3.2); and 2) we more accurately measure the structural parameters of real clusters and compare with the objects we identify as cluster candidates and galaxies (Section 3.3).

3.1.1 GC Models

There are a number of models and parameters that we use in this chapter, so we first define and compare their similarities and differences here.

King (1962) described surface brightness profiles of MW GCs, and noted a limit on the spatial extent of the clusters - expected because of Galactic tidal forces. Adding dynamical motivation, King (1966; hereafter "King") developed models of GCs as spherical, modified isothermal spheres, composed of stars with a single mass, and specified by the density profile from the stellar distribution function, $f(E)$:

$$f(E) \propto \begin{cases} exp[-E/\sigma_0^2] - 1, & E < 0 \text{ (King)} \\ 0, & E \gtrsim 0 \end{cases} \tag{3.1}$$

where $E = (1/2)mv^2 + m\phi(r)$ is the stellar energy, $\phi(r)$ is the potential, σ_0 is the central velocity dispersion, $f(E)\mathrm{d}r\mathrm{d}v$ is the mass within $\mathrm{d}r\mathrm{d}v$, and v is the stellar velocity.

We primarily use King models as they are found to fit well for clusters in the MW (e.g., Harris 1996, 2010 version catalogue), M31 clusters (e.g., Galleti et al. 2004, version 4.0 of Revised Bologna Catalogue from 2009), M33 (e.g., Sarajedini & Mancone 2007 catalogue), MCs (e.g., McLaughlin & van der Marel 2005) and NGC 5128 (e.g., Harris et al. 2002, and Martini & Ho 2004). However, we also discuss two other models used to describe GCs in the literature. Wilson (1975; hereafter "Wilson") developed a model for elliptical galaxies:

$$f(E) \propto \begin{cases} exp[-E/\sigma_0^2] - 1 + E/\sigma_0^2, & E < 0 \text{ (Wilson)} \\ 0, & E \gtrsim 0 \end{cases} \tag{3.2}$$

As can be seen above, the Wilson model differs from the King model because of the extra E/σ_0^2 term which spatially extends the King models. A spherical and isotropic version of this model can be applied to clusters (e.g., McLaughlin & van der Marel 2005). Another model used to describe GCs that we briefly mention is by Elson et al. (1987). This model was especially for young clusters, as it uses power-laws to describe extended halos (which are thought will eventually be stripped off the young clusters to leave King-like clusters).

In addition to the above models, there are also a number of important radii to define. The first two radii are used to define the "concentration parameter", c, originally defined by King (1962) as $c = r_t/r_c$, where r_t and r_c are the tidal and core radii, respectively. However, it is now more common to see it defined as follows, with the logarithm:

$$c = \log\left(\frac{r_t}{r_c}\right). \tag{3.3}$$

For example, a "King30" model has a concentration value, c =1.5. The core radius, r_c, is defined as

$$r_c = \sqrt{\frac{9\sigma_0^2}{4\pi G\rho_0}}, \tag{3.4}$$

where ρ_0 is the central density, and σ_0 is the central velocity dispersion, as before. The tidal radius, r_t, is defined observationally by the point at which the sky-subtracted surface density is 0. Theoretically, the tidal radius can be defined as

$$r_t = R\left(\frac{M}{2M_g}\right)^{\frac{1}{3}}, \tag{3.5}$$

where R is the galactocentric distance, M is the mass of the cluster, and M_g is the mass of the galaxy (King, 1962). One further radius is the half-light radius, $r_{1/2}$ or r_h, which contains half the projected integrated light of the cluster, and is also known as the effective radius, r_{eff}. $r_{1/2}$ is always greater than r_c, except for very low c-values.

The above quantities are determined observationally, but there is another set of analogous theoretical quantities used for GC models and simulations. For example, the concentration can also be characterized through a dimensionless energy parameter, $W_0 = -\beta\phi_0$. ϕ_0 is the central potential of the cluster, and $\beta = 2/\sigma_0^2$, where σ_0 is the inverse of the central velocity dispersion (King, 1966; Ashman & Zepf, 1998). A higher value for c or W_0 means that the profile declines more slowly. Similarly, the scale radius can also be described by a parameter, r_0. r_0 is usually (but not always) similar to r_c.

3.2 Simulated Clusters

As mentioned in Section 3.1, we attempt to further constrain the parameter space of the clusters by inserting simulated clusters into the PAndAS images and testing our retrieval rate. This allows us to identify what kind of clusters our previous searches most likely missed. If cluster *candidates* are similar to these simulated clusters it increases the chance that they are genuine clusters rather than background galaxies. We use two types of simulated clusters: one that was created by setting a surface brightness model profile with appropriate parameter space, and the other via Monte Carlo evolved simulations.

3.2.1 Modelled Clusters: First Group

We first use simulated clusters derived to test young massive clusters (YMCs) in M31 (Barmby et al., 2009), and based on a database of structural parameters and dynamical properties for Local Group clusters (McLaughlin & van der Marel, 2005).

The database includes 50 YMCs and 103 old GCs in the MW, the MCs and the Fornax dwarf spheroidal. McLaughlin & van der Marel used King, Wilson and asymptotic power-law models and found that the Wilson models were the best fit for the majority of clusters regardless of age or galaxy that they studied. Therefore, Barmby et al. generated their clusters using a Wilson profile, and used similar ranges as to those found by McLaughlin & van der Marel for the associated parameter space: $2 \lesssim W_0 \lesssim 10$ and $0.5 \lesssim r_0 \lesssim 11$ pc (which covers the parameter space of real clusters). A third parameter was also introduced for each (W_0, r_0) pair: the population size, $N_* = 100$, 300, 1000 and 3000 (also referred to as tiny, small, medium and large). This population size is unrealistically small compared to the real number of stars that globular clusters usually host (10^4 - 10^6), and we will return to discuss this point. In total, there were 284 (W_0, r_0, N_*) combinations. Each of the 284 simulated clusters were produced in both of the two HST/WFPC2 (Planetary Camera chip) filters that Barmby et al. used: F450W and F814W, with central wavelengths of 4520 A and 7940 A (and bandwidths of 958 A and 1531 A), respectively[1].

For this work, we only use the F450W filter simulated clusters, as this filter closely matches the MegaCam g'-filter central wavelength of 487 nm (wavelength range at 50% of 414-559 nm)[2]. Each simulated cluster file that we use comprises a list of stars with (x, y) coordinates in pixels, and F450W apparent magnitudes. We assume that M31 and M33 are at approximately the same distance, and therefore do not adjust the magnitudes. Barmby et al. use the M31 distance estimate of 784±13±17 kpc (statistical plus systematic errors; Stanek & Garnavich 1998).

We randomly select a number of clusters, (1-10; the actual number is not revealed until after completing the tests) from the 284 options and then insert them at random positions onto a real PAndAS g'-filter image. To do this, we use the IRAF/MKOBJECTS package which requires the seeing FWHM radius (in pixels) and the magnitude zero point of the real image. The former is obtained by directly measuring the FWHM of the image using IRAF/IMEXAMINE, and is needed to convolve with the simulated stars in the clusters on the MegaCam images (which have worse seeing and poorer resolution, 0.187"/pixel, compared to that of WFPC2/PC, 0.0455"/pixel). The

[1] http://www.stsci.edu/hst/wfpc2/documents/wfpc2_filters_archive.html
[2] http://cfht.hawaii.edu/Instruments/Imaging/MegaPrime/specsinformation.html

latter is obtained from the relevant information in the image header: $\mathrm{mag}_{zp} = \mathrm{header}_{zp} + \log(\mathrm{t}_{exposure})$, and ensures that the relative brightness of the cluster is correct when compared to the objects and background in the real image.

We then apply our inspection methods - both the visual and automatic methods from Cockcroft et al. (2011) - to see whether or not we could identify the simulated cluster(s). After applying these methods, we then check our retrieval rate by highlighting the positions of the simulated clusters with a display command automatically generated by our procedure.

We run three sets of fifteen trials; in trials 1 and 2 we insert simulated clusters into the chips with real outer halo clusters, while in trial 3 we use 15 different chips on which there are no verified outer halo clusters. The automatic selection method fails to retrieve any simulated clusters, which is due to the unrealistic number of stars in each of these clusters, as mentioned earlier. As a result, the magnitude of each simulated cluster is significantly fainter than the real clusters, and because our automatic selection method uses a magnitude cut these simulated clusters are not selected. The visual inspection methods have varying degrees of success at retrieving the clusters. The results of each set of trials are shown in Tables 3.1-3.3, with the totals combined in Table 3.4. Examples are shown in Figures 3.1-3.4, and are all from Trial 1 (a, b, c, d, and e refer to the real cluster in the frame, and 1, 2 and 3 refer to one of the three different cluster insertions with that particular frame). The parameters of each simulated cluster are given in the caption of each figure. We exclude large simulated clusters in Trial 2 as they clearly did not appear to occupy the same parameter space as the real outer halo clusters.

3.2.2 Simulated Clusters: Second Group

The second set of simulated clusters with which we test our retrieval methods use pure model clusters that follow their internal dynamical and stellar evolution with a Monte Carlo (MC) prescription. The development of these models can be found in Joshi et al. (2000, 2001), Fregeau et al. (2003), Fregeau & Rasio (2007), Chatterjee et al. (2010) and Leigh et al. (2012). The MC method allows the evolutionary code to be completed faster than full N-body simulations, and comparisons show that the MC results are no less robust (Joshi et al., 2000).

We outline various quantities and components that are input to the code in the following paragraph. Single and binary stellar evolution codes are taken from Hurley et al. (2000), and the initial fraction of binary stars is 10%. It is important to include binaries in these dynamical evolutionary codes as binaries are believed to slow core-collapse. Binary stars are combined so that they appear as a single object on the CMD. The clusters are evolved for 12 Gyr, which corresponds to the age of the sample of MW GCs used for comparison in Leigh et al. (2012). The stars within the cluster follow a Kroupa initial mass function (IMF), with a break-mass of 0.5 $M_{\odot}$, and they have a metallicity of Z=0.001.

We use a total of 110 clusters, with various initial values for concentration, Virial radius[3], and total number of stars (see Table 3.5). In a similar manner as to the one in Section 3.2.1, we insert the simulated clusters into real images using the IRAF/MKOBJECTS subroutine. First, however, the output of the MC dynamical evolution codes needs to be converted to a list

[3]The Virial radius here defines the radius of the GC within which Virial equilibrium holds. r_v is within the range of r_0.

of (x,y) coordinates and apparent magnitudes. The code outputs one cluster-centric coordinate for each star, and we use a slightly different technique than detailed in Leigh et al. (2012) to get the cluster's Cartesian coordinates. We randomly generate a polar angle (between -90 and 90 degrees) and an azimuthal angle (between 0 and 360 degrees) for each star, to produce (x,y,z) coordinates in code units. We ignore the z-coordinate as we are only concerned with the projected distance of the stars within the cluster on the sky. The (x,y) coordinates are then multiplied by the cluster's Virial radius, to obtain the (x,y) coordinates in parsecs. If we assume the distance to M33 is 809 kpc (McConnachie et al., 2004), we can calculate the angle that the (x,y) distance subtends on the sky and divide this by the resolution of the PAndAS images (0.187"/pixel). This gives us the location of the stars in the cluster for insertion onto the PAndAS image (i.e., the (x,y) coordinates in pixels). We measure the FWHM of the seeing on the image onto which we insert the clusters, and then MKOBJECTS convolves this with each simulated star to correctly create the whole cluster.

To obtain SDSS ugriz magnitudes for each of the stars within the clusters, we use the subroutine by Dotter et al. (2008). These absolute magnitudes, M, are then converted to apparent magnitudes, m, using

$$m - M = 5logd - 5 + A_\lambda, \tag{3.6}$$

where d is the distance to M33 (809 kpc; McConnachie et al. 2004), and A_λ is the foreground Galactic extinction (A_g=0.16 and A_i=0.08). As mentioned above, we ignore the z-coordinate, which we can do for the magnitudes as this distance is small compared to the distance to M33.

All the clusters are listed in Table 3.6. The first column gives the file name associated with the cluster: c corresponds to the initial concentration, r to the initial Virial radius, and n to the initial total number of stars. The correspondence with the initial parameters is shown in Table 3.5.

Some examples of the simulated CMDs are shown in Figures 3.5-3.6. Examining a well-populated CMD, e.g., c1_r1_n8, we note several obvious features: the main sequence (double-banded because of the singles and binaries), the main-sequence turn-off (MSTO), blue stragglers, the giant branches, the horizontal branch, the double white dwarf (WD) sequence and turnover, and the stellar remnant sequences at the very faintest part of the CMD. We note that these simulated CMDs differ from observed CMDs in the following ways. First, it would not be possible to see the double nature of the main sequence or white dwarfs as they would be blurred together. Also, it would be unlikely to see fainter than the brightest part of the WD sequence even for MW GCs (e.g., the CMD of 47 Tuc in Figure 1, Woodley et al. 2012).

Most of the least-populated clusters (i.e., from n1 to n6) are also unrealistic in that they contain so few stars, if any, above the MSTO. Stars spend progressively less time in each stage in stellar evolution after they leave the MS: e.g., for a solar-mass star, the giant branch phase is $\gtrsim 10\%$ of the MS lifetime (Renzini & Fusi Pecci, 1988). We would therefore expect a well-populated giant branch from the simulations (which would also match observations). We also note that even though the giant and horizontal branches can be seen in most n7 and n8 cases, their ratios of stars above the MSTO to stars below are also too low (the highest fraction is 0.25% for c1_r3_n8).

Examples of simulated clusters inserted onto the real PAndAS images are shown in Figures 3.7 and 3.8. Immediately obvious is that these simulated clusters are more compact than those in Section 3.2.1. Without the red circles to identify them it would be very difficult to determine which were the clusters, and indeed the brightest of them resemble the class 2 objects from our visual inspections of the real images (i.e., possible cluster candidates).

To measure the range of properties these simulated clusters exhibited, we insert all 110 clusters onto the same real background image. As mentioned previously, we do this via the IRAF/MKOBJECTS subroutine. We expect that including very faint stars or stellar remnants included in the simulations will have no effect on the overall magnitude of the cluster. We therefore experiment with a magnitude limit, so that objects fainter than this are excluded from the MKOBJECTS insertion. No change above 0.0001 magnitude is measured with SE when we assume magnitude limits of $g_{absolute}$=10.3 (or $g_{apparent}$=35.0) and $i_{absolute}$=9 (or $i_{apparent}$=33.6), so these are the magnitude limits that we adopt. Each set of clusters n1-n8 is positioned on the image, and we ensure that it is not located near another object on the chip. We then run SE on the image, and identify which clusters have been selected by SE. These clusters are shown in Table 3.7. The clusters in parentheses were only detected by SE in g, whereas all the other clusters were detected in both g and i.

Finally, we compare the clusters that SE is able to detect with the Sarajedini & Mancone (2007) catalogue clusters, and our original selection criteria as shown in Figures 3.9, 3.10 and 3.11. The 17 clusters that fall within all of our selection criteria are emboldened in Table 3.7. Even though these models do not yet include the correct ratio of RGB stars, they appear as clusters that fall within our group 2 (possible cluster candidates). We anticipate that the number of clusters that fall within our selection criteria will increase once the modelling technique is corrected.

3.3 Structural Parameters

We aim to measure the structural parameters (SPs) for all objects that we detect on the PAndAS images, not only to create a homogeneous catalogue for all clusters and cluster candidates - which we hope to also combine with a similar catalogue for the M31 clusters - but also to explore the parameter space of objects and perhaps use it to help accept candidates as high-confidence clusters or reject them as sources of contamination.

Source Extractor, the software that we employ to detect objects within the PAndAS images, also measures their structural parameters (SPs). However, in the literature SE is primarily used only as a source-detection package (or a comparison to other SP measurements), while the two most common software packages used to measure star cluster structural parameters are GRIDFIT (McLaughlin et al., 2008) and ISHAPE (Larsen, 1999).

We previously used GRIDFIT in Chapter 2 to measure the SPs of M33's six outer halo GCs. We also experimented with ISHAPE at that time, but found that it was unsuitable to measure the diffuse and extended clusters. The SPs that ISHAPE returned varied greatly, seeming heavily dependent on the input parameters. GRIDFIT did not vary in that manner, but still had problems fitting two of the outer halo clusters because of their diffuse nature. The effective radius, r_e, is robust, and the code used to measure it makes very little difference to its value. However, the tidal radius, r_t, is very sensitive and its value does depend heavily on which code is used.

In this chapter, the objects that we measure are *not* as spatially extended as the outer halo clusters. Both the Sarajedini & Mancone (2007) catalogue of confirmed GCs (located closer to the disk of M33), and also the cluster candidates for the outer halo are more compact and therefore not as obviously discerned as clusters in the PAndAS images. ISHAPE is used for marginally-resolved GCs such as these, so we use it and further describe it here. Another main reason for using ISHAPE to measure the SPs is that we can also run the procedure in batch mode (courtesy of K. Woodley).

ISHAPE convolves the PSF with the analytic profiles (with different radii) and iteratively determines the best fit. It needs to be supplied with the image file in which the object of interest is located, and the associated subsampled PSF. ISHAPE also requires initial estimates for the object's local coordinates (i.e., the pixel coordinates of the image, and not global coordinates such as equatorial coordinates). ISHAPE has typical errors for fitted parameters of 10% for compact but high S/N ($\gtrsim$40) objects similar to those we find in this study - although these errors become progressively larger for fainter objects (e.g., DeGraaff et al. 2007). ISHAPE is less successful and can fail in crowded regions (e.g., Chandar et al. 2010).

Traditionally, PSFs are produced with DAOPHOT (either in the IRAF/ NOAO/ DIGIPHOT or standalone versions) in a heavily interactive procedure that involves the user selecting genuine isolated stars that will be used to build the PSF. Other objects, such as faint galaxies, cosmic-ray spikes or stars that have nearby neighbours or are in crowded fields, are discarded. However, this approach is not feasible here because of the large number of PSFs we need to produce. Each PSF is different for each MegaCam CCD chip, therefore we need to produce at least 1476 PSFs (41 MegaCam images, with 36 CCD chips on each image). However, the PSF may also be different from one place on a particular chip compared to another place on the same chip, so we prefer to produce one PSF for each object for which we want to get SPs. There are 6 outer halo clusters, 427 confirmed clusters in the central ∼1 degree, 260 high confidence candidates, 2778 possible candidates, and 3588 galaxies - a total of 7059 objects, requiring an equivalent number of PSFs.

To produce all the required PSFs we test, adapt and use S. Fabbro's automated version 0.7.2[4] of DAOPHOT and ALLFRAME (Stetson, 1987). The code auto-creates the option files, and can be chosen in iterative or non-iterative mode. The former is more accurate at selecting genuine stars so we run this on all chips and objects. However, there are 27 chips for which the iterative code does not run. We instead run the non-iterative code, and are able to get an additional 15 PSFs. (This leaves us with 12 chips for which we are not able to create a unique PSF; however, chip-to-chip variations of the PSF are so small, ∼ 10% that we can instead use PSFs from adjacent PSFs.) Having created all the PSFs, we then subsample them. The subsampled PSFs are better for convolving a PSF with an assumed King model. DAOPSF is similar to IRAF/SEEPSF, but will subsample the PSF created by the standalone version of DAOPHOT. This subsampled PSF can then be read into ISHAPE.

ISHAPE has various user-controlled parameters. We use a King30 profile for the reasons mentioned previously. We change the parameters that relate to our images, e.g., we use typical values for read noise (4 electrons), and gain (1.6). Two further parameters that we must also specify are FITRAD, the radius within which we fit the profile, and CENTERRAD, the maximum radius within which we allow ISHAPE to re-estimate the centre of the cluster. We set CENTERRAD at 4 pixels, and we test FITRAD for the most suitable

[4]See http://astrowww.phys.uvic.ca/ seb/allphot/

value. To do this we use 950 M31 GCs from K. Woodley, and 427 M33 GCs from the Sarajedini & Mancone (2007) catalogue. We hold all parameters at the same value except for the fitting radius. Georgiev et al. (2008) tested ISHAPE/FITRAD for the GCs in LG Magellanic-like dIrr galaxies. They varied FITRAD between 4 and 10 pixels ($\sim$ 6 to 15 pc), saw no major differences or trends that were dependent on the different FITRAD values, and adopted a value of 8 pixels (12 pc). The PAndAS images have a resolution of 0.187"/pixel, or 0.66pc/pixel. To test a similar range in parsecs compared to Georgiev et al., we use 10, 15, 20, 25 and 30 pixels. Figures 3.12 and 3.13 show the results, with the axes' ranges chosen to show the majority of GCs. For $\lesssim$7 pixels the results are consistent regardless of the FITRAD value chosen. Above this, the smaller FITRAD values appear to overestimate the FWHM, so that it seems more appropriate to adopt a larger FITRAD value between 20 and 30 pixels. As there seems to be no reason to prefer one value in this range, we adopt 25 pixels.

With these parameters, we run ISHAPE on the Sarajedini & Mancone (2007) clusters, and our class 1 (high-confidence clusters), 2 (possible clusters) and 3 (galaxies) objects. As a consistency check, we compare the values returned from ISHAPE with those measured by SE for the Sarajedini & Mancone (2007) clusters. We compare these values in Figure 3.14. First, we compare the SE magnitude with the ISHAPE flux, and note that the correlation is fairly consistent over 4 magnitudes, with only minor outliers (we are only concerned with outliers, and so do not convert both to either fluxes or magnitudes). Next, we compare the ellipticities measured by the two codes. Ellipticity is generally defined as $e = 1 - b/a$, where b is the semi-minor axis and a is the semi-major axis. We note that the ratio measured by ISHAPE is b/a, so we subtract this value from 1.0 so that we can accurately compare it to the SE ellipticity. Three outliers that have particularly large ellipticities as measured only by ISHAPE are labelled. In general, this plot contains very large scatter because the values of a and b are so small (on the order of a few pixels. Third, we compare the FWHM values - both to show the labelled outliers and then to zoom in on the majority of clusters. As can be seen, the clusters are offset from the $y = x$ line to approximately $y = x - 3.5$. This is due to ISHAPE incorporating and subtracting the PSF from the FWHM measurement. The final comparison is between the effective radii, r_{eff} (or, equivalently, the "half-light" radius, r_h). To convert the FWHM measured by ISHAPE to r_{eff} we use the following two expressions from Larsen (2001):

$$\mathrm{FWHM} = 2\left[\left(\sqrt{0.5} + \frac{1-\sqrt{0.5}}{\sqrt{1+c^2}}\right)^{-2} - 1\right]^{0.5} r_c, \tag{3.7}$$

and

$$\frac{r_{eff}}{r_c} \approx 0.547c^{0.486}. \tag{3.8}$$

where $c = r_t/r_c$ here (and not the logarithm of the ratio), and the approximate sign indicates that the relation between r_{eff} and r_c is only 4% accurate, as there is no simple analytical expression that relates the two (unlike with FWHM and r_c). We use King30, therefore $r_{eff} \equiv r_h = 1.48$ FWHM.

The outliers labelled in Figure 3.14 are shown in Figure 3.15 with annuli of 2 and 20 arcseconds. The majority of the outliers are either in crowded regions, there are two objects very close together, they have bright stars in outer regions, or they are near a chip edge. Cluster 258 genuinely seems to be quite elongated, and cluster 428 is noticeably larger than the other clusters.

We now plot the ISHAPE measurements against one another in Figures 3.16 and 3.17 in order to look for correlations. We also run ISHAPE on the six M33 outer halo clusters, and show the results in Figures 3.16 and 3.17. Unlike our earlier attempts, we now have ISHAPE settings that apply satisfactorily to objects classified as clusters and high-confidence cluster candidates. We apply these same settings to the outer halo clusters. The fits were successful for clusters B, C and E but not for A, D and S. Fitting GRIDFIT models to A, D and S was also a problem, given the diffuse nature of A, the comparatively tiny size of D and the unusual surface feature within S. By increasing the CENTERRAD parameters from 4 to 8 (for cluster D) and to 15 (for clusters A and S) the fits were successful. These steps were necessary because of both the partial resolution of the true cluster profile, and the background contamination.

3.4 Discussion and Conclusions

Using simulated clusters and measurements of structural parameters of clusters and candidates, we attempt to further constrain GC candidates. We discuss the effectiveness of these methods further here.

Using the simulated clusters (first group), we are able to test our visual inspection methods. As expected, the clusters most difficult to recover by this method are the least-populated clusters (i.e., the faintest clusters). Over 50% of the tiny (or N_*=100) clusters were *not* recovered, regardless of their concentration or radius. Recovery was more successful for small (N_*=300) and medium (N_*=1000) clusters, with 19% and 11% not recovered, respectively.

All seven of the medium clusters not recovered had concentrations of $W_0 \lesssim 5.5$, i.e., their profiles declined relatively sharply outside the flat inner core. Only two large (N_*=3000) clusters were not recovered, and they both had the same parameters of W_0=4 and r_V=2.9 pixels.

We keep in mind that we may have errors due to small-number statistics, but we note that of the 237 simulated clusters (first group) that we inserted, we were not able to recover just over one quarter. All of these simulated clusters were inserted onto chips in the halo fields, so it is not only possible that there are undetected clusters in the halo with the above parameters of the unretrieved clusters, but also that there are more clusters hidden in the more crowded central regions. Therefore, we estimate that approximately 25% of real clusters remain to be found in the halo.

With the simulated clusters (second group), we first note that although the current prescription does not correctly account for the number of stars above the MSTO (which is currently having the stellar evolution code rewritten so that it does), the most massive simulated clusters do fall within our selection criteria and therefore provide some measure to compare against real clusters. As with the simulated clusters (first group), only the brightest, most-populated 17 clusters fall within our selection criteria. If we excluded the magnitude limit on our selection criteria, all but 2 of the 110 clusters would be retrieved by our automated method. The ones that do fall within all the selection criteria give more confidence to our cluster candidates, as they are located in similar parameter space (see Figure 2.7).

Two other points that we note about the similarities and differences between the MC evolved clusters and the M33 clusters are the metallicity and [α/Fe] values. As already noted, the MC evolved clusters use MW GC averages for Z = 0.001 and [α/Fe] = +0.3. If we compare these values to the ~150 of 427 clusters in the Sarajedini & Mancone (2007) catalogue that have metallicities, we find that their average value is [Fe/H] = −0.97, ranging between −3.86 and +1.18. These values all come from a collection of papers (Ma et al., 2001, 2002a,b,c, 2004a,b), and are derived from colour estimates. Sharina et al. (2010) make spectroscopic observations of 15 M33 GCs, and find an average [Fe/H] = −0.55 and [α/Fe] = +0.2. The effect that the different value of metallicity would have on the evolution codes is not clear, but the colour transformations can be quite sensitive to these values (Sills, 2012).

Once the next series of simulations is complete, that correctly accounts for the number of stars above the MSTO and the difference in metallicity, it will be interesting to perform another test of our visual search retrieval rate, as we did with the simulated clusters (first group), in addition to the automated search.

In this paragraph, we discuss the results of the structural parameters. Our high-confidence candidate clusters appear to overlap with the parameter space of the Sarajedini & Mancone (2007) clusters, but also do not distinguish themselves from the galaxies. The possible candidate clusters appear to lie in an intermediate stage between the Sarajedini & Mancone (2007) clusters and the galaxies. These measurements are not useful to help distinguish more likely cluster candidates from others, as we hoped that they would, but they will contribute to a future homogeneous catalogue of parameters for all M31 and M33 clusters.

3.5 Summary

The tests in this chapter have given us some insight as to the effectiveness of our retrieval methods. Quantitatively, it is difficult to reduce the estimate of cluster candidates, or to further verify our confidence estimates for any of the candidates beyond methods via our visual inspection. We have been unable to narrow the parameter space (we need higher resolution), which would have allowed us to have a higher degree of confidence that cluster candidates were either genuine clusters or background contaminants. However, our tests have described the parameter space of the clusters we are most likely unable to retrieve. We have discovered through the simulated clusters (first group) that we are likely to miss the clusters with the lowest concentration values with small radii, and also half of the faintest clusters. The tests with the simulated clusters (second group) have shown us that the automated search method should be capable of retrieving all of the clusters brighter than the magnitude cut in our selection criteria. These clusters would then most likely be classified as our class 2 objects (i.e., possible clusters), again suggesting that we should expect a certain number of our cluster candidates and possible candidates to be genuine clusters. The next step will be to determine what fraction of candidates we can expect to be clusters. That will still require follow-up using higher-resolution imaging (feasible for a small subsample), or metallicity and velocity measurements, to confirm the candidates nature. The latter is a more plausible possibility, with multislit spectroscopy allowing several cluster candidates to be observed at once.

In addition to the simulated cluster tests, we also measure the structural parameters of the Sarajedini & Mancone (2007) high-confidence clusters, and our class 1, 2 and 3 objects (high-confidence cluster candidates, possible cluster candidates and galaxies, respectively). This data set will contribute to the first homogeneous catalogue of structural parameters of M31 and M33 clusters.

Acknowledgements

RC is grateful to Pauline Barmby, Nathan Leigh, Stefan Umbreit, Alison Sills and Evert Glebbeek for providing him with both the simulated clusters and the following discussions regarding how to use them. RC would also like to thank Kristin Woodley and Sebastien Fabbro for their help measuring the structural parameters. This research used the facilities of the Canadian Astronomy Data Centre operated by the National Research Council of Canada with the support of the Canadian Space Agency.

Bibliography

Ashman, K. M. and Zepf, S. E. 1998, Globular Cluster Systems

Barmby, P., Perina, S., et al. 2009, AJ, 138, 1667

Chandar, R., Whitmore, B. C., et al. 2010, ApJ, 719, 966

Chatterjee, S., Fregeau, J. M., Umbreit, S., and Rasio, F. A. 2010, ApJ, 719, 915

Cockcroft, R., Harris, W. E., et al. 2011, ApJ, 730, 112

DeGraaff, R. B., Blakeslee, J. P., Meurer, G. R., and Putman, M. E. 2007, ApJ, 671, 1624

Dotter, A., Chaboyer, B., Jevremović, D., Kostov, V., Baron, E., and Ferguson, J. W. 2008, ApJS, 178, 89

Elson, R. A. W., Fall, S. M., and Freeman, K. C. 1987, ApJ, 323, 54

Fregeau, J. M., Gürkan, M. A., Joshi, K. J., and Rasio, F. A. 2003, ApJ, 593, 772

Fregeau, J. M. and Rasio, F. A. 2007, ApJ, 658, 1047

Galleti, S., Federici, L., Bellazzini, M., Fusi Pecci, F., and Macrina, S. 2004, A&A, 416, 917

Georgiev, I. Y., Goudfrooij, P., Puzia, T. H., and Hilker, M. 2008, AJ, 135, 1858

Harris, W. E. 1996, VizieR Online Data Catalog, 7195, 0

Harris, W. E., Harris, G. L. H., Holland, S. T., and McLaughlin, D. E. 2002, AJ, 124, 1435

Hurley, J. R., Pols, O. R., and Tout, C. A. 2000, MNRAS, 315, 543

Joshi, K. J., Nave, C. P., and Rasio, F. A. 2001, ApJ, 550, 691

Joshi, K. J., Rasio, F. A., and Portegies Zwart, S. 2000, ApJ, 540, 969

King, I. 1962, AJ, 67, 471

King, I. R. 1966, AJ, 71, 64

Larsen, S. S. 1999, A&AS, 139, 393

—. 2001, AJ, 122, 1782

Leigh, N., Umbreit, S., et al. 2012, MNRAS, 422, 1592

Ma, J., Zhou, X., and Chen, J. 2004a, Chinese Journal of Astronomy and Astrophysics, 4, 125

—. 2004b, A&A, 413, 563

Ma, J., Zhou, X., et al. 2002a, Chinese Journal of Astronomy and Astrophysics, 2, 197

Ma, J., —. 2002b, AJ, 123, 3141

Ma, J., —. 2002c, Acta Astronomica, 52, 453

Ma, J., —. 2001, AJ, 122, 1796

Martini, P. and Ho, L. C. 2004, ApJ, 610, 233

McConnachie, A. W., Irwin, M. J., Ferguson, A. M. N., Ibata, R. A., Lewis, G. F., and Tanvir, N. 2004, MNRAS, 350, 243

McLaughlin, D. E., Barmby, P., Harris, W. E., Forbes, D. A., and Harris, G. L. H. 2008, MNRAS, 384, 563

McLaughlin, D. E. and van der Marel, R. P. 2005, ApJS, 161, 304

Renzini, A. and Fusi Pecci, F. 1988, ARA&A, 26, 199

Sarajedini, A. and Mancone, C. L. 2007, AJ, 134, 447

Sharina, M. E., Chandar, R., Puzia, T. H., Goudfrooij, P., and Davoust, E. 2010, MNRAS, 405, 839

Sills, A. 2012, in preparation

Stanek, K. Z. and Garnavich, P. M. 1998, ApJ, 503, L131

Stetson, P. B. 1987, PASP, 99, 191

Wilson, C. P. 1975, AJ, 80, 175

Woodley, K. A., Goldsbury, R., et al. 2012, AJ, 143, 50

Table 3.1: Trial 1 results of inserting simulated clusters (first group) onto PAndAS images. Large, medium small and tiny refer to the number of stars within the cluster (100, 300, 1000 and 3000, respectively). The notes refer to properties of the clusters that were not retrieved. r_0 is in pixels (where 1 pc $\approx$ 6 pixels).

Cluster size	Total inserted	Retrieved	Not retrieved	Notes
Large	16	16	0	-
Medium	17	15	2	W_0=5.5,r_0=8.7 and W_0=4,r_0=2.9
Small	21	14	7	Many W_0 values, and all but one have r_0 <11.6
Tiny	24	15	9	Many W_0 and r_0 values
Total	78	60	18	-

Table 3.2: Similar to Table 3.1 but for Trial 2.

Cluster size	Total inserted	Retrieved	Not retrieved	Notes
Large	-	-	-	-
Medium	26	24	2	W_0=4,r_0=5.8 and W_0=2,r_0=2.9
Small	25	22	3	Many W_0 values; two have r_0 <11.6, one has r_0=40.6
Tiny	28	7	21	Many W_0 and r_0 values
Total	79	53	26	-

Table 3.3: Similar to Table 3.1 but for Trial 3.

Cluster size	Total inserted	Retrieved	Not retrieved	Notes
Large	6	4	2	Both W_0=4,r_0=2.9
Medium	23	20	3	All W_0=2,r_0=5.8,8.7,11.6
Small	23	20	3	W_0=2,5,10 and r_0=29,40.6,63.8
Tiny	28	16	12	Many W_0 and r_0 values
Total	80	60	20	-

Table 3.4: Summary totals from Trials 1, 2 and 3.

Cluster size	Total inserted	Retrieved	Not retrieved	% not retrieved
Large	22	20	2	9
Medium	66	59	7	11
Small	69	56	13	19
Tiny	80	38	42	52
Total	237	173	64	27

Table 3.5: Initial parameters of the MC evolved clusters.

Parameter	Initial Values (Code Name)				
Concentration, W_0	5	5.5	6	6.5	7
	c1	c2	c3	c4	c5
Virial radius, r_V (pc)		3	4	5	
		r1	r2	r3	

Continued on next page

Table 3.5 – continued from previous page

Parameter	Initial Values (Code Name)							
Total number of stars, n	10^5	$2x10^5$	$4x10^5$	$6x10^5$	$8x10^5$	10^6	$2x10^6$	$4x10^6$
	n1	n2	n3	n4	n5	n6	n7	n8

Table 3.6: Within each of the MC evolved simulations, the number of stars with absolute magnitudes $g_0 < 3$ and $i_0 < 3$, compared to total number of stars. These numbers can be compared visually to the CMDs shown in Figures 3.5 and 3.6.

File	Number of stars with with g_0 <3	with i_0 <3	Total number of stars within file
c1_r1_n1	1	1	40822
c1_r1_n2	0	4	156649
c1_r1_n3	2	11	367363
c1_r1_n4	5	22	574858
c1_r1_n5	3	26	778369
c1_r1_n6	0	41	979993
c1_r1_n7	194	524	1976986
c1_r1_n8	1940	4139	3961669
c1_r2_n1	0	0	49333
c1_r2_n2	0	7	166839
c1_r2_n3	5	25	378447
c1_r2_n4	35	103	582738
c1_r2_n5	150	348	784163
c1_r2_n6	277	633	984437
c1_r2_n7	1346	2839	1979661

Continued on next page

Table 3.6 – continued from previous page

File	Number of stars with		Total number of
	with g_0 <3	with i_0 <3	stars within file
c1_r2_n8	4147	8485	3963782
c1_r3_n1	0	1	47178
c1_r3_n2	4	13	165838
c1_r3_n3	68	160	378720
c1_r3_n4	263	568	582782
c1_r3_n5	520	1054	784452
c1_r3_n6	699	1439	985213
c1_r3_n7	2215	4322	1980001
c1_r3_n8	5087	10154	3964888
c2_r1_n1	0	2	36929
c2_r1_n2	1	4	154326
c2_r1_n3	2	9	365168
c2_r1_n4	4	21	571273
c2_r1_n5	0	18	776541
c2_r1_n6	0	37	978137
c2_r1_n7	57	195	1976478
c2_r1_n8	1102	2430	3960227
c2_r2_n1	-	2	44611
c2_r2_n2	-	7	163223
c2_r2_n3	-	20	376151
c2_r2_n4	-	32	581100
c2_r2_n5	-	154	782947
c2_r2_n6	-	306	983735
c2_r2_n7	-	2031	1979256
c2_r2_n8	-	7400	3963311
c2_r3_n1	1	2	42169
c2_r3_n2	3	10	162243

Continued on next page

Table 3.6 – continued from previous page

File	Number of stars with with g_0 <3	with i_0 <3	Total number of stars within file
c2_r3_n3	22	65	376007
c2_r3_n4	163	371	581082
c2_r3_n5	361	757	783372
c2_r3_n6	513	1134	983808
c2_r3_n7	1966	3892	1979751
c2_r3_n8	4776	9555	3964421
c3_r1_n1	0	0	36644
c3_r1_n2	0	5	150216
c3_r1_n4	0	18	569524
c3_r1_n6	2	32	975534
c3_r1_n7	5	80	1974814
c3_r1_n8	195	608	3960622
c3_r2_n1	1	1	39174
c3_r2_n2	3	8	158566
c3_r2_n3	2	13	372750
c3_r2_n4	1	23	578811
c3_r2_n5	6	35	781494
c3_r2_n6	18	95	982309
c3_r2_n7	463	1075	1978574
c3_r2_n8	2339	4924	3963582
c3_r3_n1	0	1	35572
c3_r3_n2	1	7	156867
c3_r3_n3	10	31	372158
c3_r3_n4	42	109	578279
c3_r3_n5	126	289	781002

Continued on next page

Table 3.6 – continued from previous page

File	Number of stars with with g_0 <3	with i_0 <3	Total number of stars within file
c3_r3_n6	360	761	982029
c3_r3_n7	1335	2723	1978959
c3_r3_n8	3981	7999	3964361
c4_r1_n1	0	2	31603
c4_r1_n2	0	5	149900
c4_r1_n4	1	16	566229
c4_r1_n5	0	14	768902
c4_r1_n6	1	25	971458
c4_r1_n8	28	149	3959299
c4_r2_n1	0	2	32670
c4_r2_n2	1	6	153369
c4_r2_n3	5	15	367584
c4_r2_n4	2	22	574976
c4_r2_n5	1	19	778461
c4_r2_n6	4	41	980026
c4_r2_n7	45	181	1977221
c4_r2_n8	958	2100	3962817
c4_r3_n1	0	0	25935
c4_r3_n2	1	10	148919
c4_r3_n3	4	12	366034
c4_r3_n4	5	38	574079
c4_r3_n5	10	46	777520
c4_r3_n6	65	195	979519
c4_r3_n7	667	1487	1977695

Continued on next page

Table 3.6 – continued from previous page

File	Number of stars with		Total number of
	with g_0 <3	with i_0 <3	stars within file
c4_r3_n8	2923	5890	3964112
c5_r1_n1	0	0	25255
c5_r1_n2	1	5	142339
c5_r1_n4	1	18	561998
c5_r2_n1	0	0	20392
c5_r2_n2	1	6	146015
c5_r2_n3	1	11	361734
c5_r2_n4	3	22	568812
c5_r2_n5	3	18	773420
c5_r2_n6	3	37	975942
c5_r2_n8	34	227	3961828
c5_r3_n1	1	1	13186
c5_r3_n2	2	7	138322
c5_r3_n3	2	10	357123
c5_r3_n4	2	23	567549
c5_r3_n5	1	19	772753
c5_r3_n6	1	40	975552
c5_r3_n7	62	217	1975529
c5_r3_n8	774	1989	3963165

Table 3.7: MC simulated clusters that fall within the selection criteria. Clusters shown in bold fall within *all* the selection criteria, clusters in parentheses are only detected by SE in g, and all other clusters are detected in g and i.

Cluster c and r	Cluster n				
c1_r1	(n4)	(n5)	n6	n7	**n8**
c1_r2		(n5)	n6	**n7**	**n8**
c1_r3		(n5)	n6	**n7**	**n8**
c2_r1		(n5)	n6	n7	**n8**
c2_r2					
c2_r3		(n5)	n6	**n7**	**n8**
c3_r1			n6	n7	**n8**
c3_r2		(n5)	(n6)	n7	**n8**
c3_r3		(n5)	(n6)	**n7**	**n8**
c4_r1			(n6)	n7	**n8**
c4_r2		(n5)	(n6)	n7	**n8**
c4_r3		(n5)	(n6)	n7	**n8**
c5_r1					
c5_r2			(n6)	(n7)	**n8**
c5_r3			(n6)	n7	**n8**

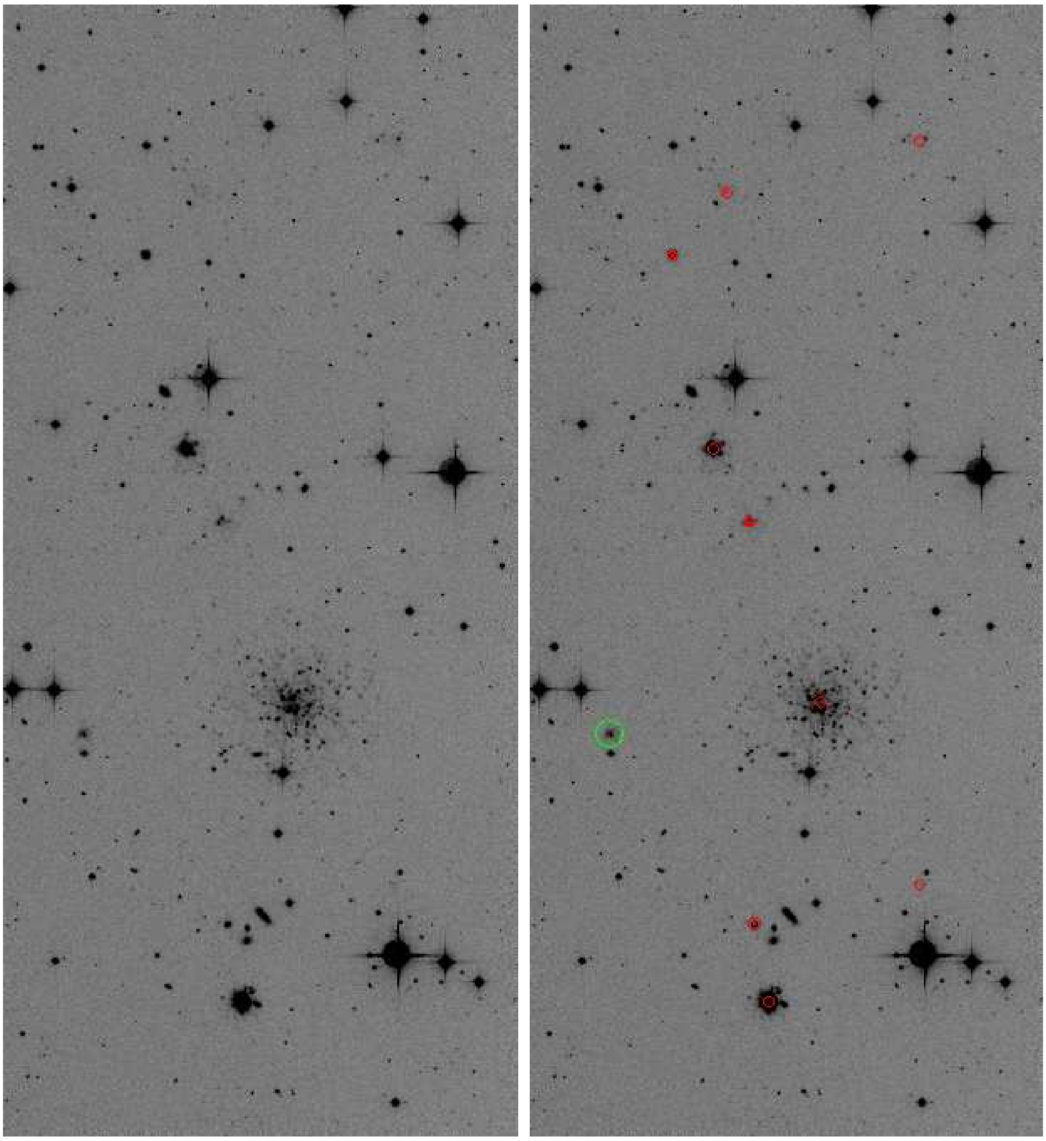

Figure 3.1: Simulated clusters (first group) (Barmby et al., 2009) inserted onto the PAndAS frame on which we see real cluster M33-A. The left- and right-hand panels are exactly the same, except that the real (green circle, radius of 50 pixels) and simulated clusters (red circles, radii of 2 and 20 pixels) are indicated on the right. The parameters of each simulated cluster are, from bottom up, (l,w06.0,r05.8), (t,w06.5,r02.9), (t,w10.0,r02.9), (l,w08.0,r63.8), (s,w06.0,r40.6), (m,w06.5,r08.7), (s,w04.0,r05.8), (t,w05.0,r40.6), (t,w02.0,r63.8).

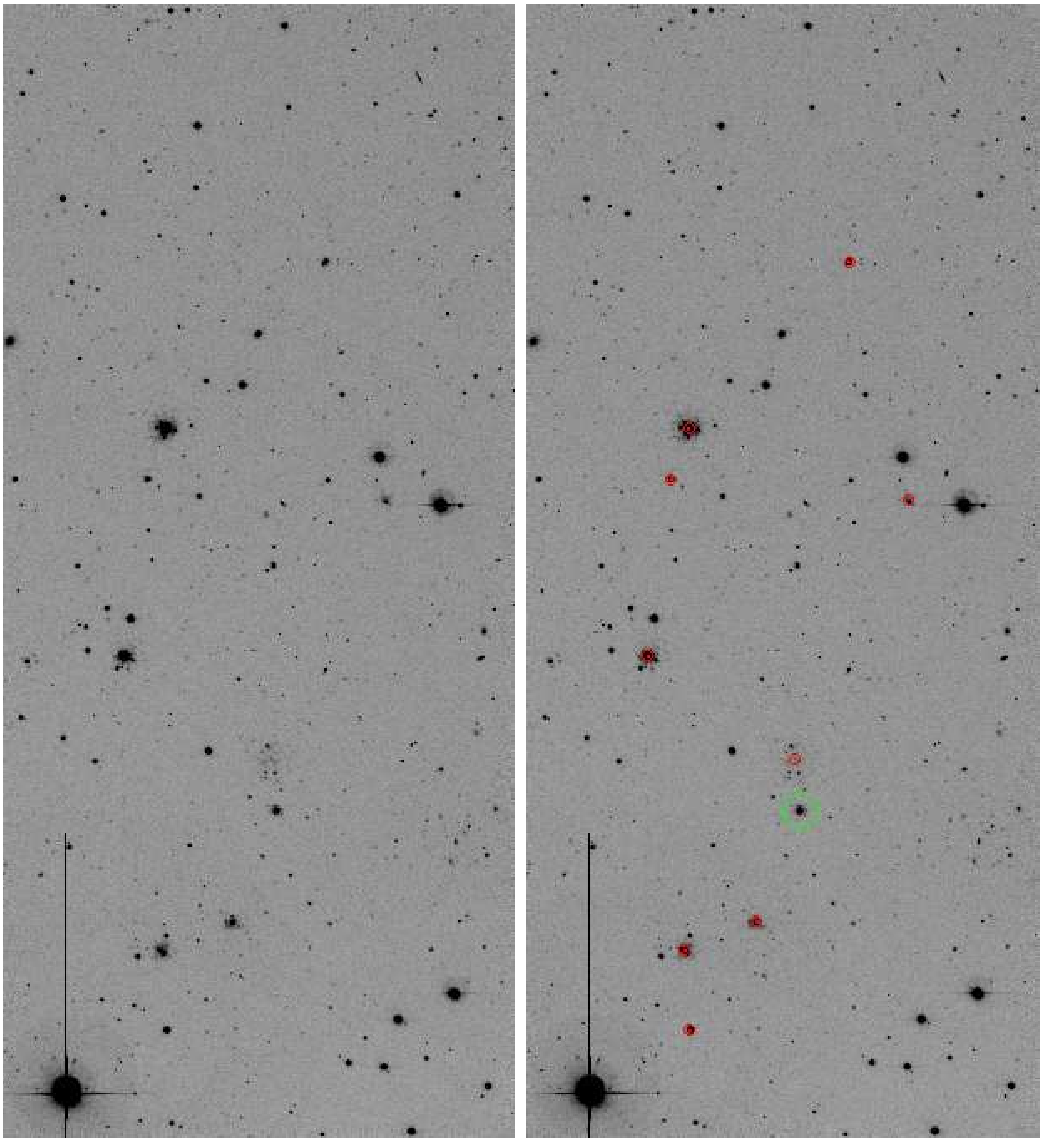

Figure 3.2: Similar to Figure 3.1, but the simulated clusters are inserted on to the frame with real cluster M33-C. The parameters of each simulated cluster are, from bottom up, (s,w02.0,r02.9), (s,w04.0,r17.4), (s,w07.0,r08.7), (s,w05.0,r40.6), (m,w07.0,r02.9), (t,w05.5,r11.6), (t,w07.0,r02.9), (m,w05.5,r17.4), (t,w02.0,r11.6).

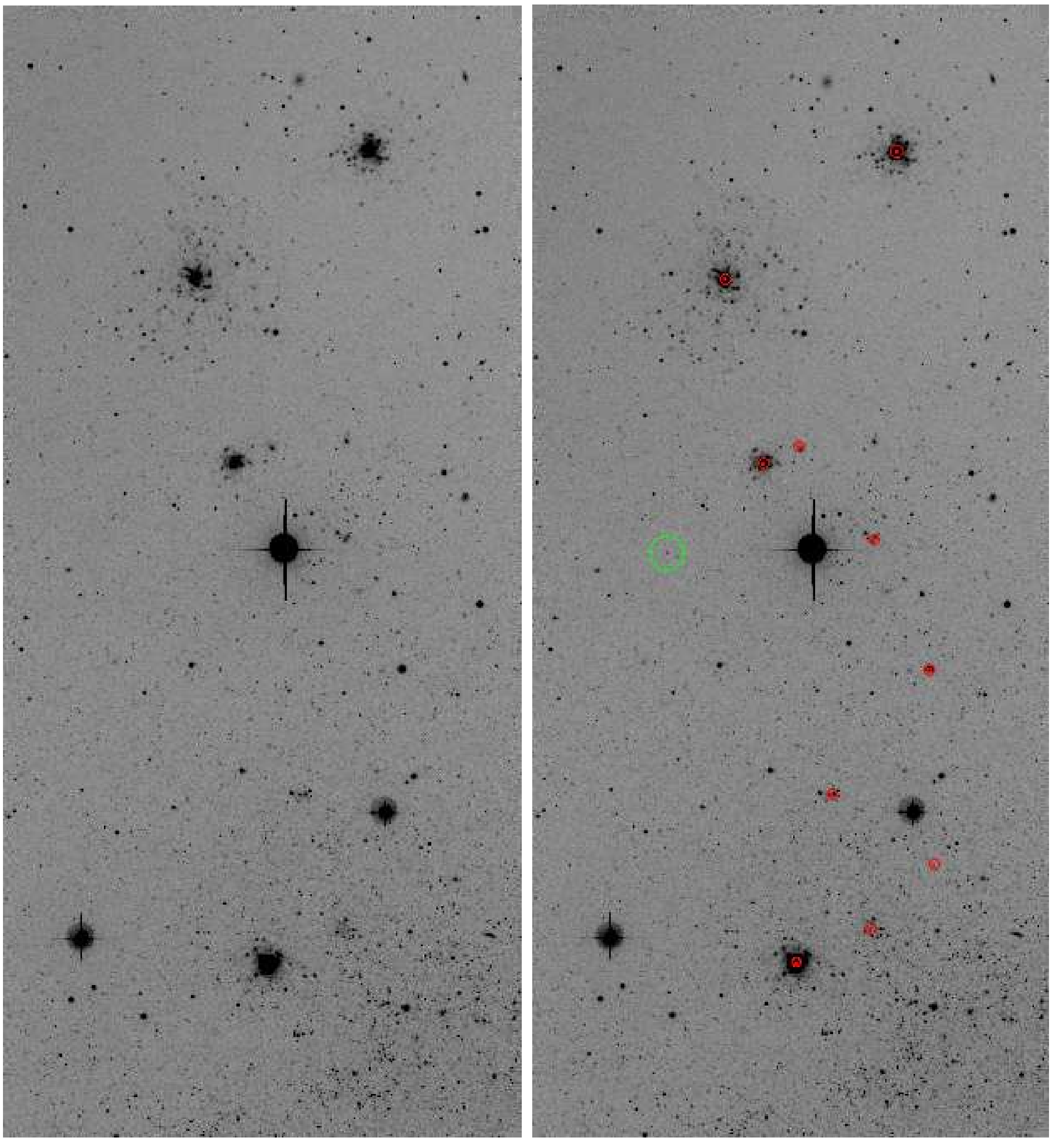

Figure 3.3: Similar to Figure 3.1, but the simulated clusters are inserted on to the frame with real cluster M33-D. The parameters of each simulated cluster are, from bottom up, (l,w06.0,r17.4), (s,w06.0,r29.0), (t,w05.0,r40.6), (s,w10.0,r11.6), (s,w06.0,r02.9), (t,w05.5,r17.4), (m,w05.0,r17.4), (t,w05.5,r11.6), (l,w10.0,r17.4), (l,w08.0,r05.8).

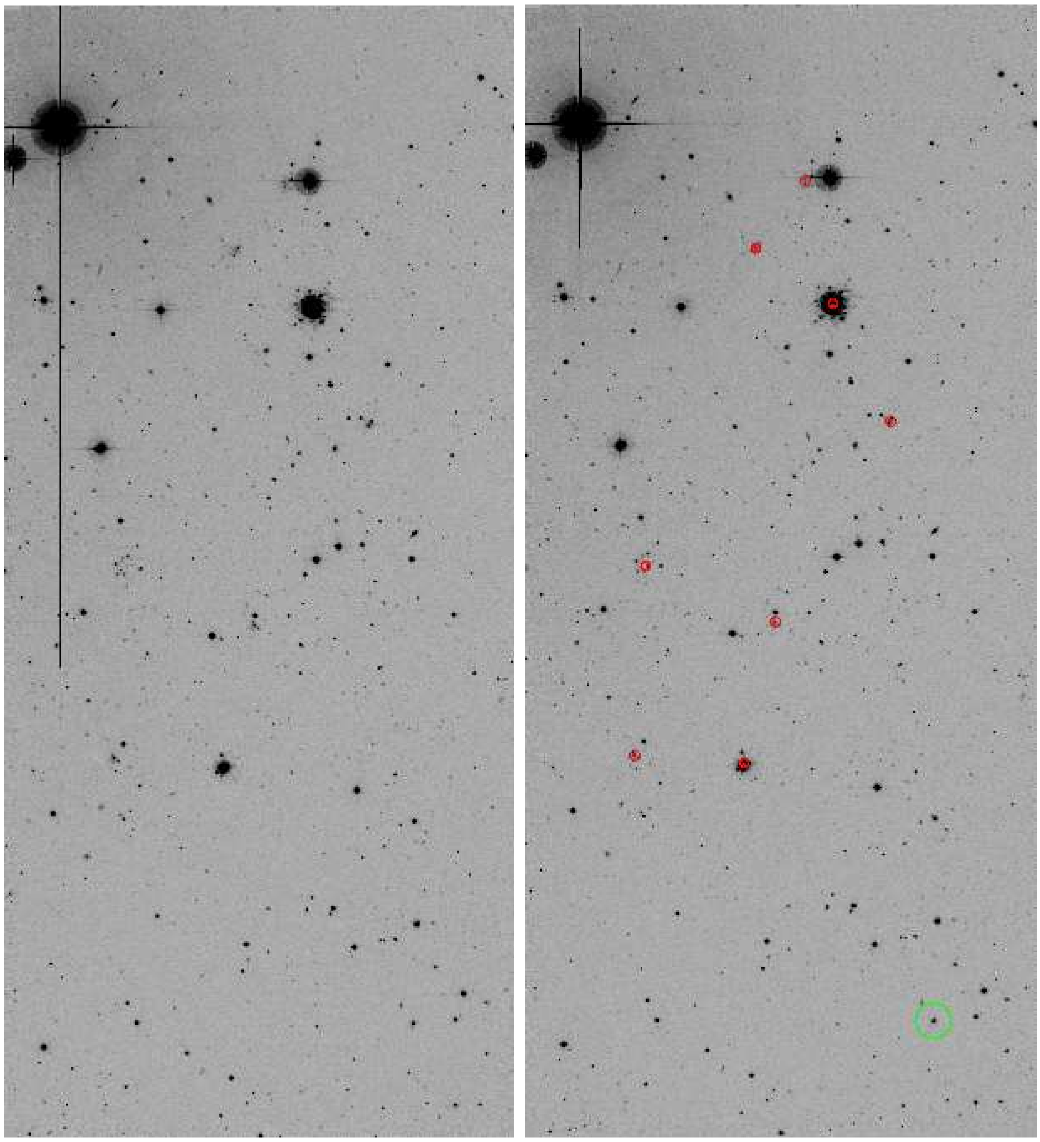

Figure 3.4: Similar to Figure 3.1, but the simulated clusters are inserted on to the frame with real cluster M33-E. The parameters of each simulated cluster are, from bottom up, (m,w06.0,r05.8), (t,w08.0,r05.8), (t,w08.0,r05.8), (s,w10.0,r40.6), (t,w05.5,r17.4), (l,w02.0,r40.6), (t,w07.0,r11.6), (t,w02.0,r29.0).

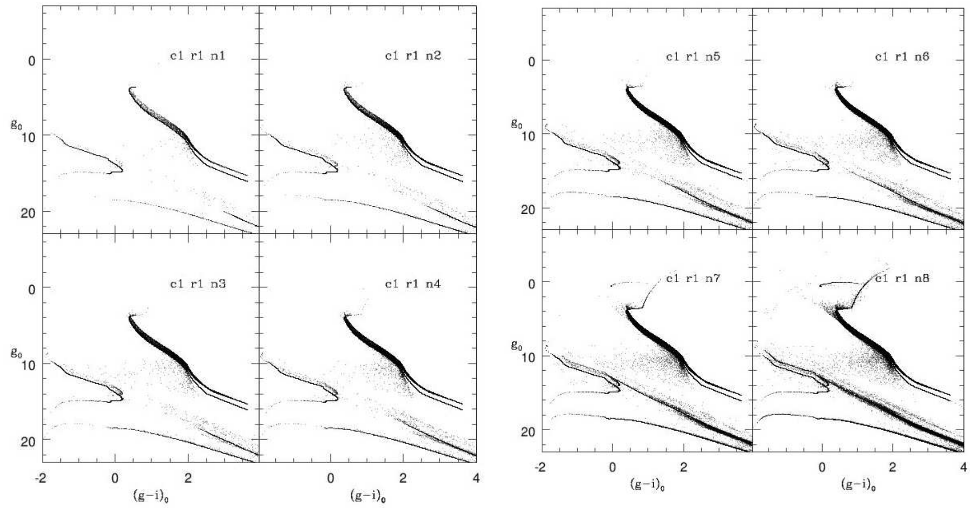

Figure 3.5: CMDs of the simulated clusters (second group) (most recently, Leigh et al. 2012). In particular, we show the CMDs for the simulations c1_r1_n*, which corresponds to concentration, $w_0 = 5$, and Virial radius, $r_V = 3$ pc. The n-value refers to the initial number of stars in the cluster, and ranges from $n1$=10^5 to $n8$=4x10^6. The most obvious feature is the main sequence (MS) at the centre of the plots, with the MS turn-off (TO) at $\sim g_0 = 4$ mag, $(g-i)_0 = 0.5$. Blue-stragglers appear on the blue side of the MSTO, and the subgiant branch (SGB) on the red side. The SGB extends into the red-giant branch (RGB), and from that we also see the horizontal branch (HB). Below the MS, are stellar remnants: white dwarfs (WDs, on the left), neutron stars and black holes. It is clear that the most realistic simulations are $n7$ and $n8$, as they are populated above the MSTO. However, even these simulations appear to be under-populated in this region.

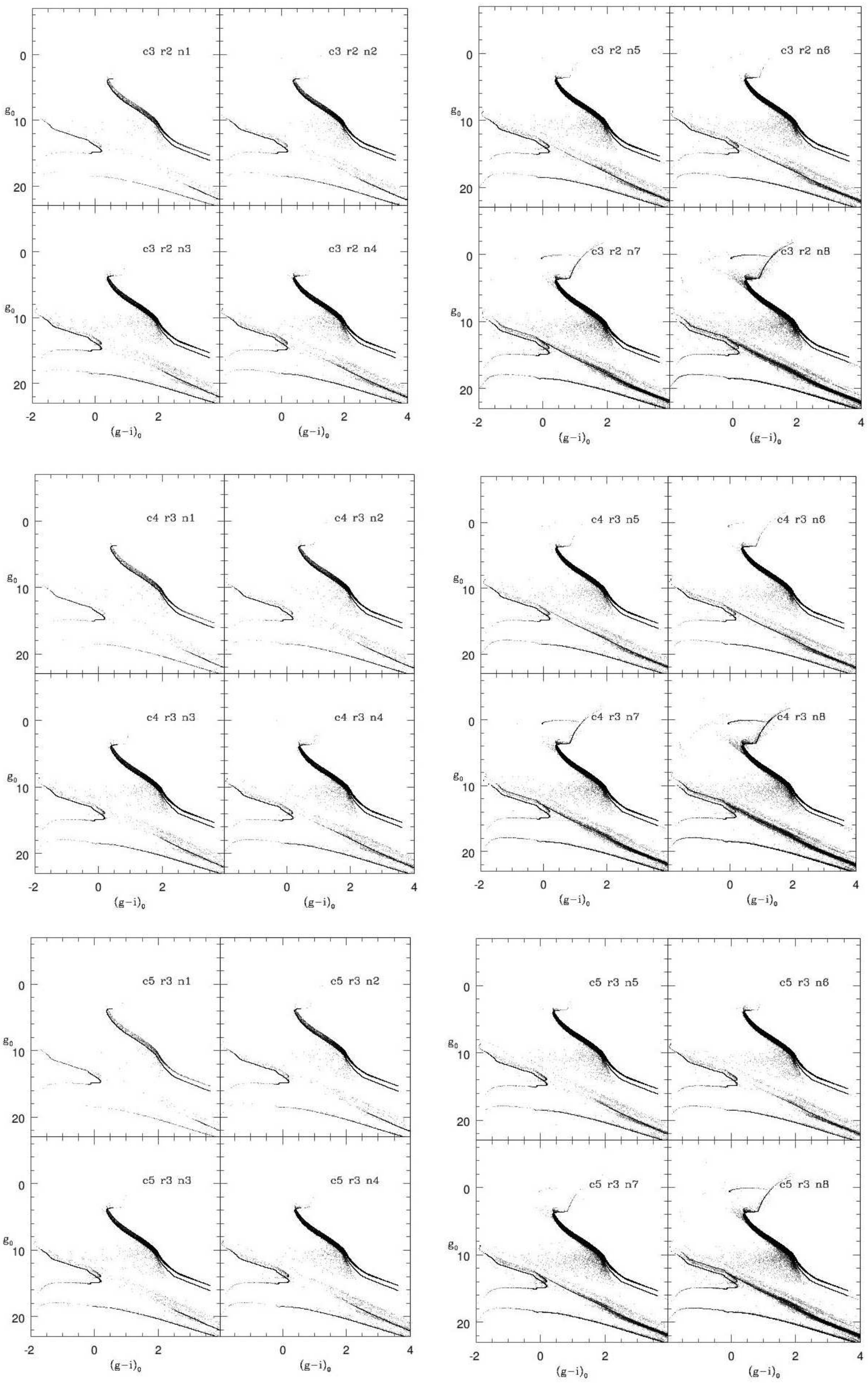

Figure 3.6: Similar to Figure 3.5, but for the c3_r2_n*, c4_r3_n*, and c5_r3_n* simulations.

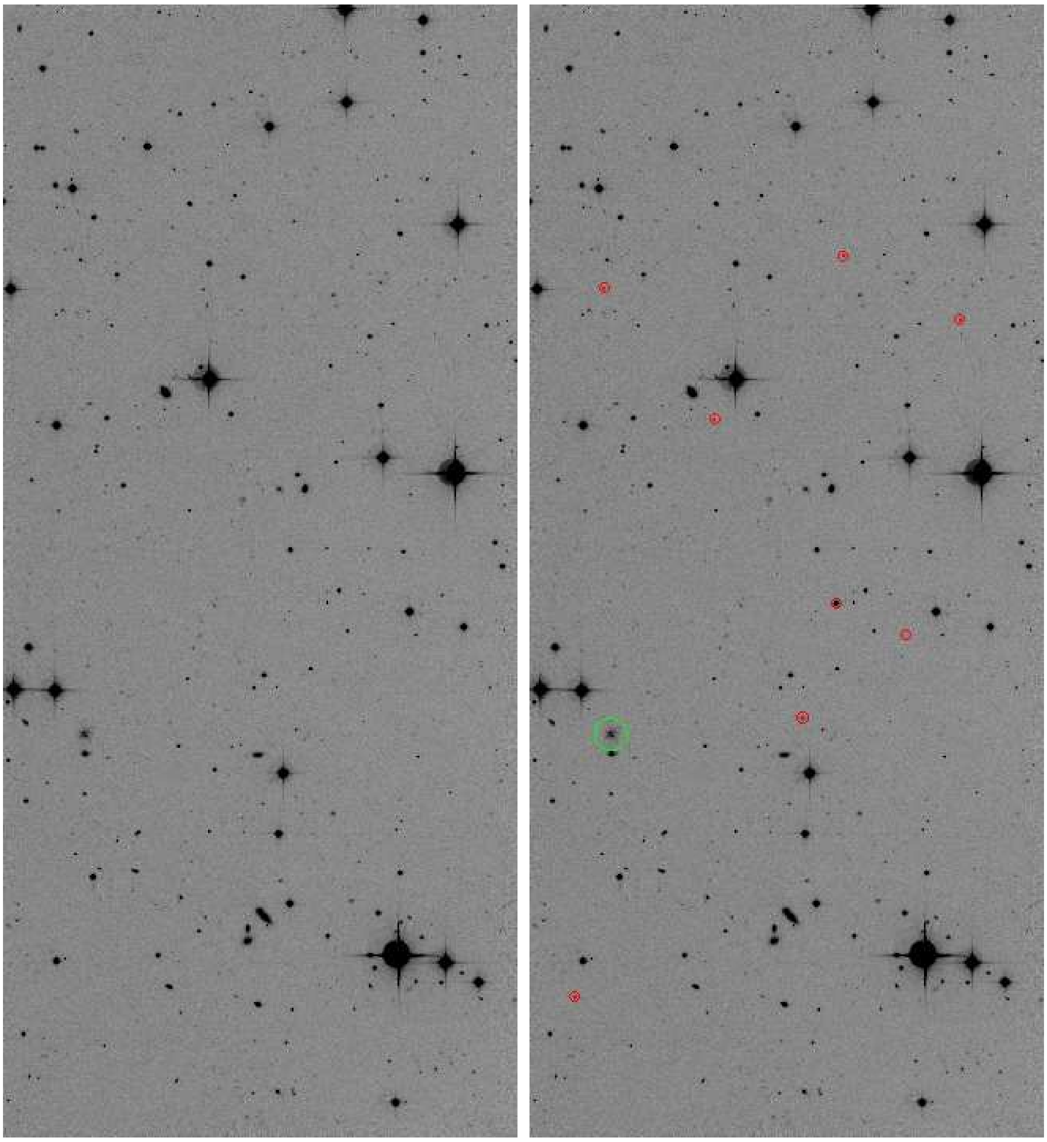

Figure 3.7: Before and after images inserting MC evolved simulated clusters, from the c1_r1_n* set. The right-hand panels indicate the real (green circle, radius of 50 pixels) and simulated clusters (red circles, radii of 2 and 20 pixels). Unlike the simulated clusters (first group), most of these clusters are barely discernible on the images.

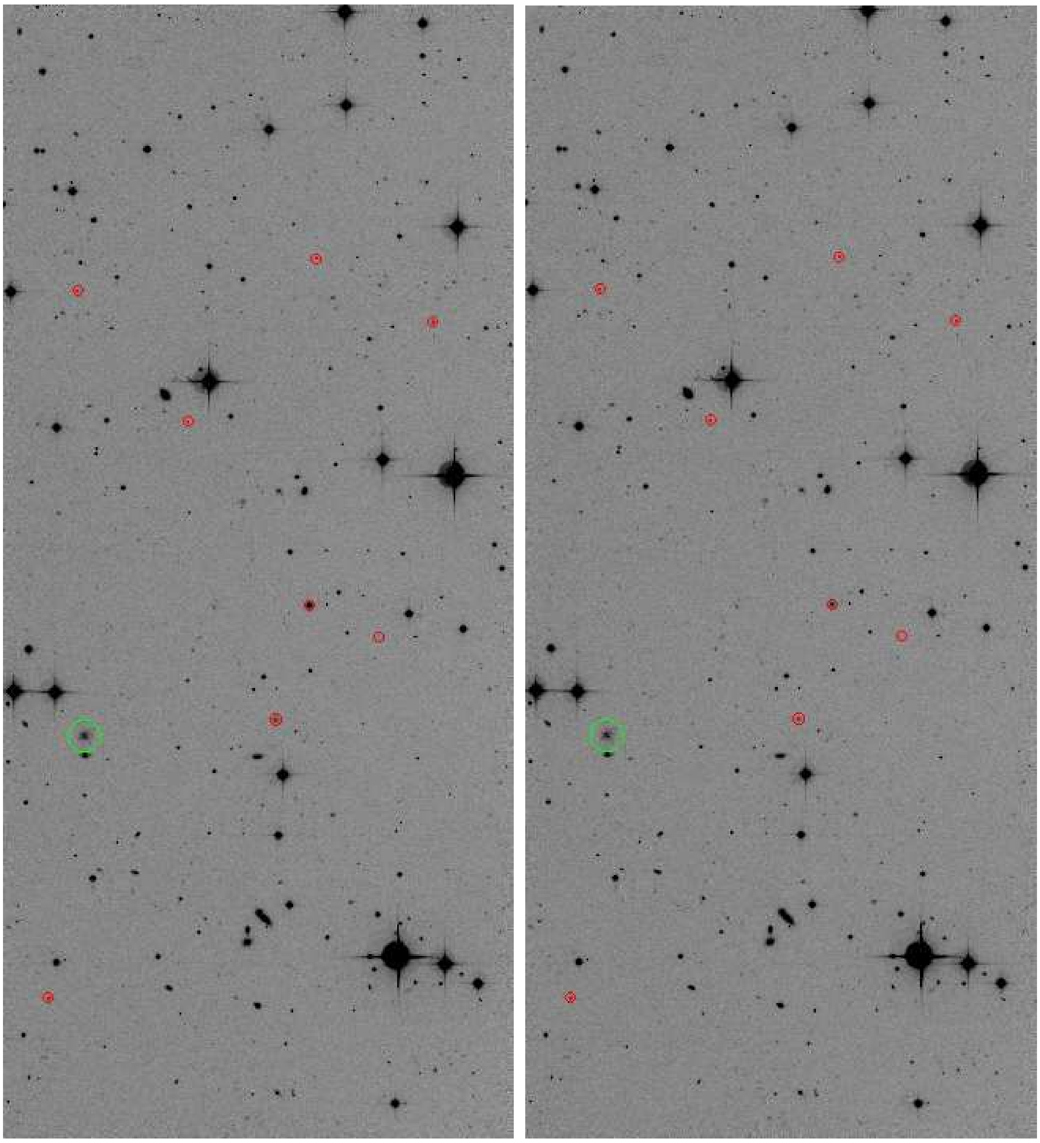

Figure 3.8: Similar to the right-hand panel of Figure 3.7, but for simulations c3_r1_n* and c5_r3_n*.

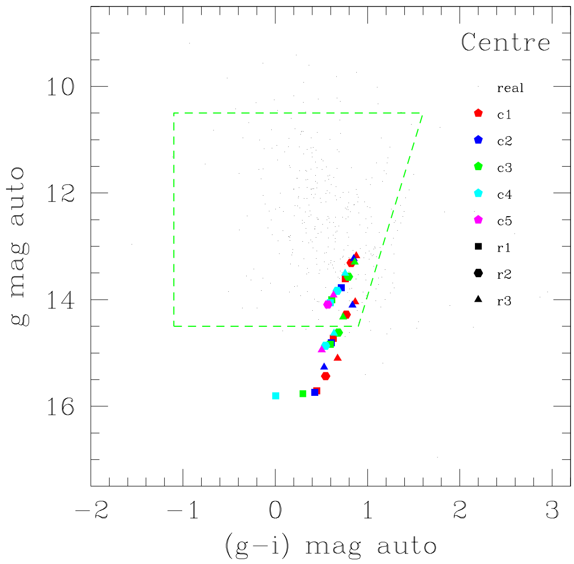

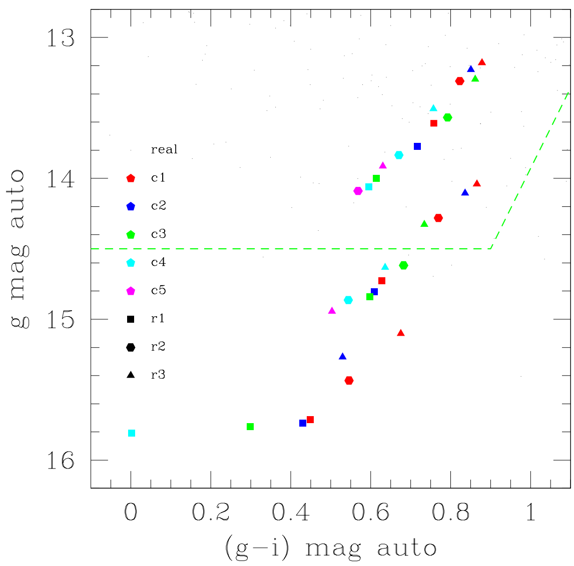

Figure 3.9: CMDs of the Sarajedini & Mancone (2007) clusters, the MC evolved clusters and our original selection criteria from Cockcroft et al. (2011). The lower plot shows a zoom in on the region where the simulated clusters are plotted. The different simulations are subdivided into groups by different concentrations (shown by the coloured symbols in the key), and by initial Virial radii (indicated by the different shapes of the symbols). In any particular concentration-radius set (e.g., the red squares correspond to c1_r1), the brightest point indicates the n8 simulation, the next brightest point n7, and so on.

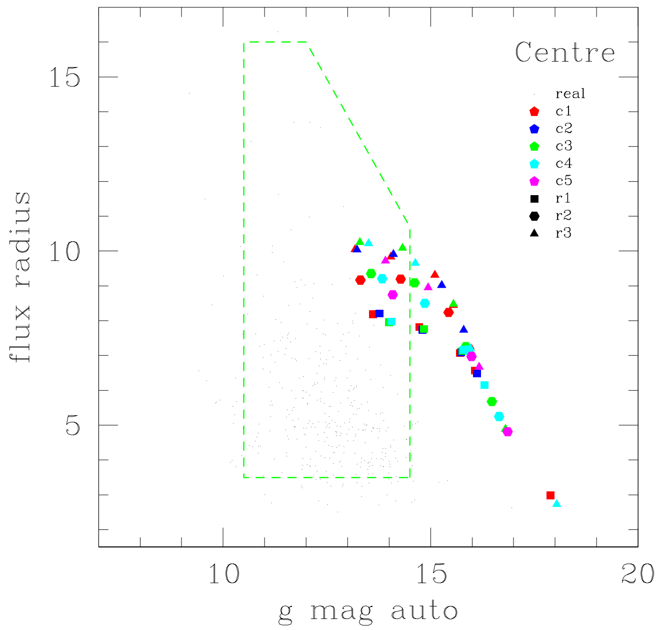

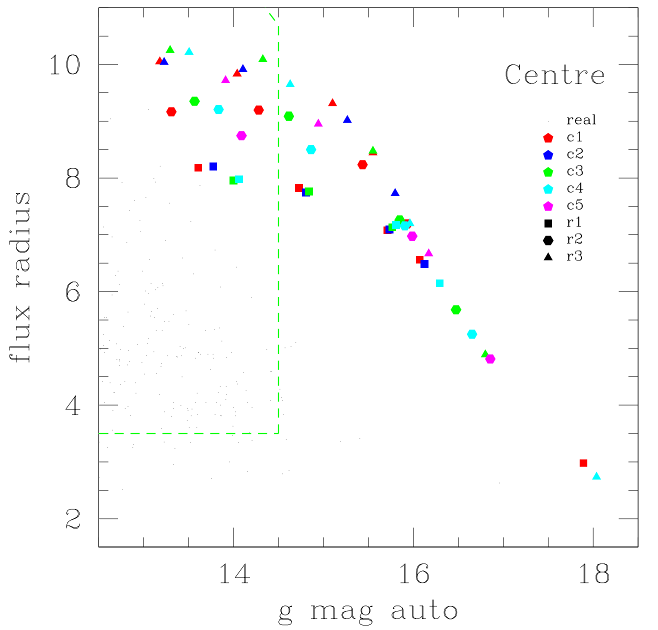

Figure 3.10: Similar to Figure 3.9 but showing the flux radius (equivalent to half-light radius) against the g-magnitude.

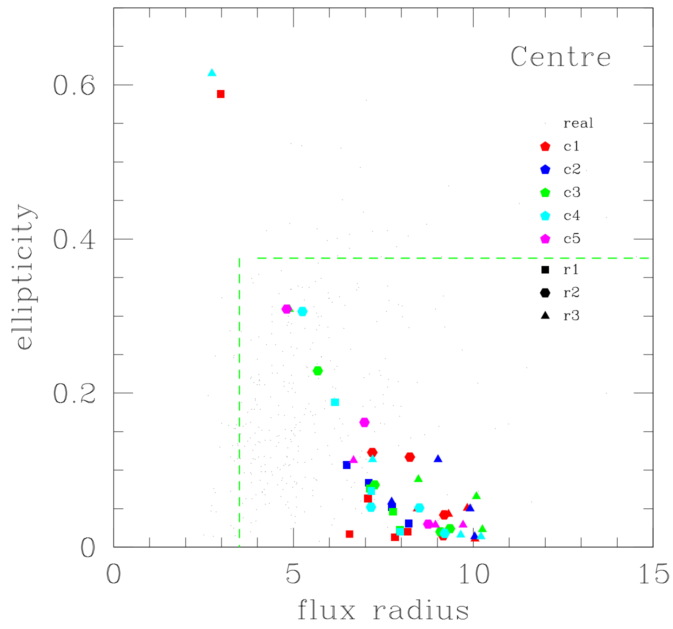

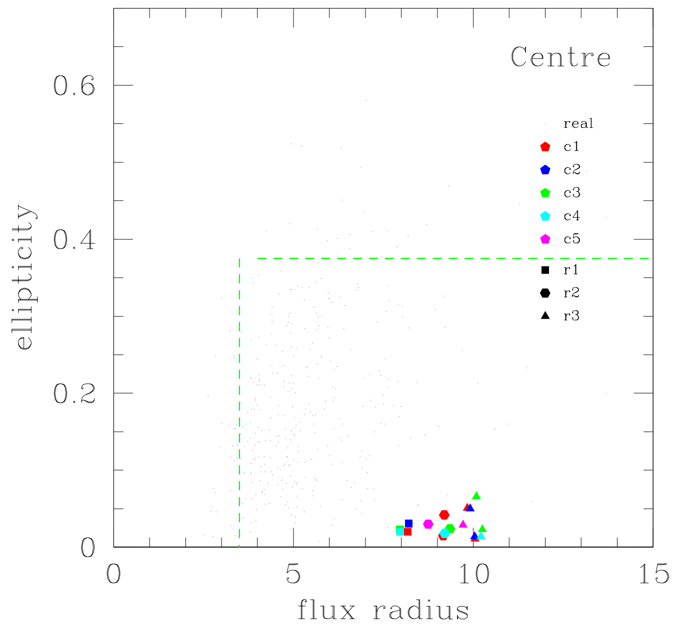

Figure 3.11: Similar to Figure 3.9 but showing the ellipticity against flux radius. The lower panel is not a zoom in, as in the previous figures, but rather it excludes the points that lie outside the selection criteria on the other two figures (i.e., the CMD and the flux radius vs. g mag auto plots).

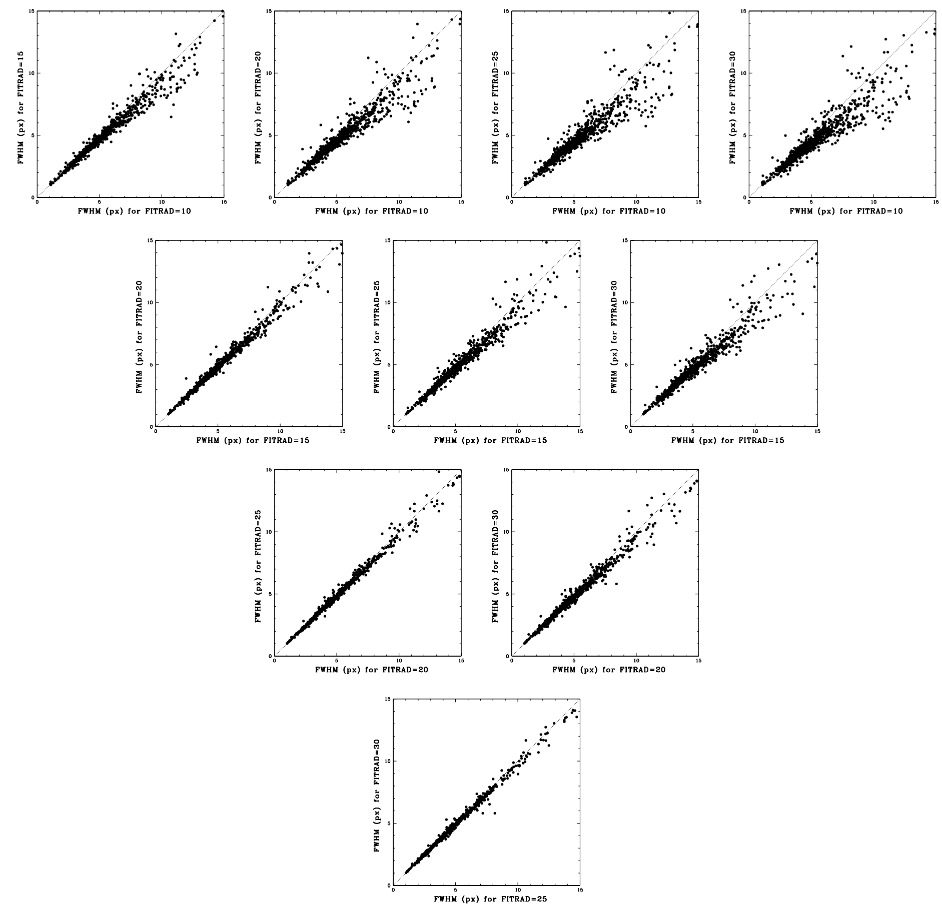

Figure 3.12: The results of testing ISHAPE/FITRAD with 950 M31 GCs for the most suitable value, from K. Woodley. All ISHAPE parameters are held constant, except for FITRAD which we vary between 10 and 30 pixels, in 5 pixel increments. The axes' ranges are chosen to show the majority of GCs. For objects with measured FWHM$\lesssim$7 pixels, the results are consistent regardless of the FITRAD value chose. However, above this value the smaller FITRAD values appear to overestimate the FWHM. It therefore seems more appropriate to adopt a larger FITRAD value in our range of tested values; we adopt 25 pixels.

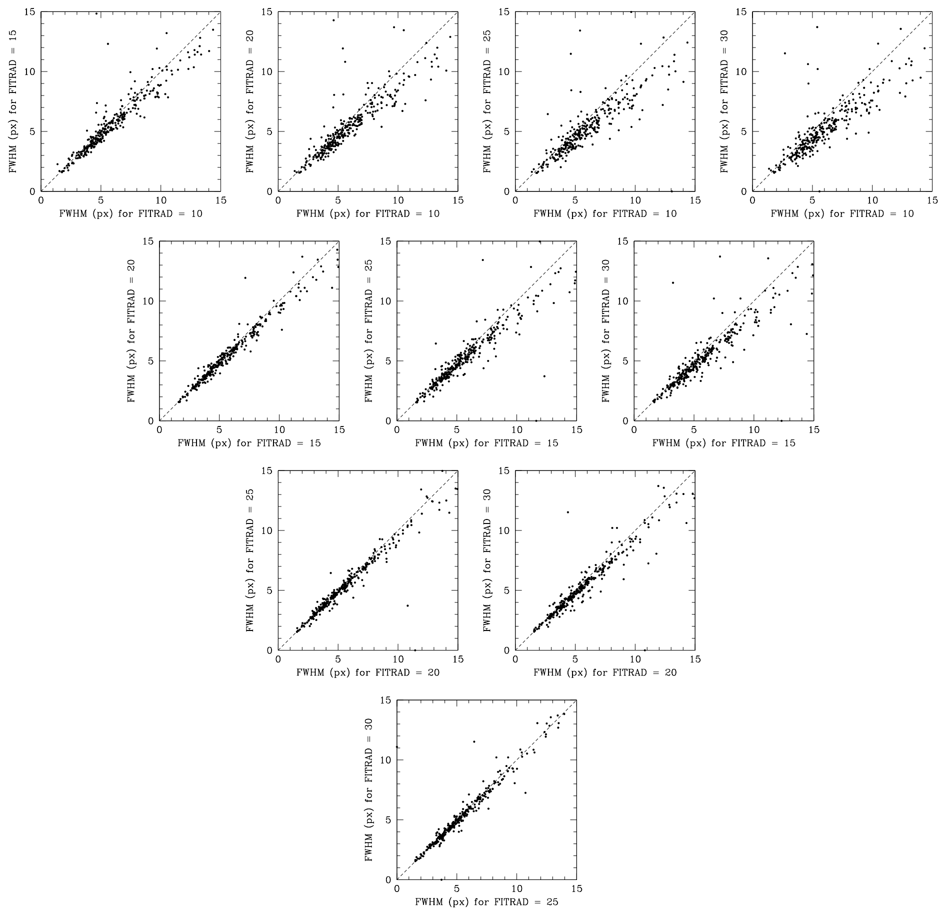

Figure 3.13: Similar to Figure 3.12 but for M33 GCs from the Sarajedini & Mancone (2007) catalogue.

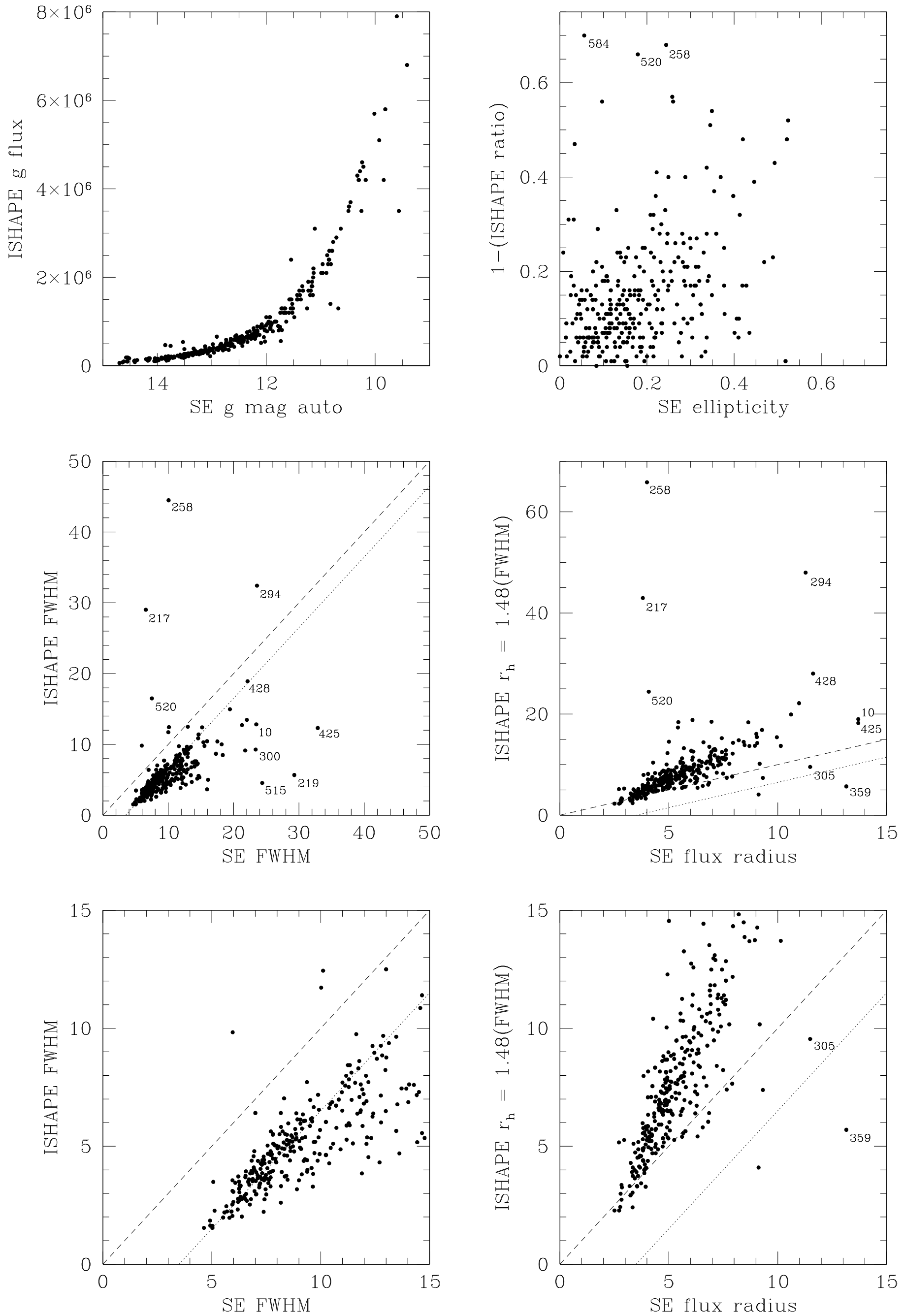

Figure 3.14: Comparing measurements from ISHAPE and Source Extractor. The bottom two panels show zoom ins of the panels immediately above them. Note that for the half-light radii (also called "flux radius" by Source Extractor), ISHAPE and SE agree for smaller objects, but ISHAPE is consistently larger for larger objects. This is because SE cannot model the flux from the outermost regions of the profile, and therefore neglects the objects' wings.

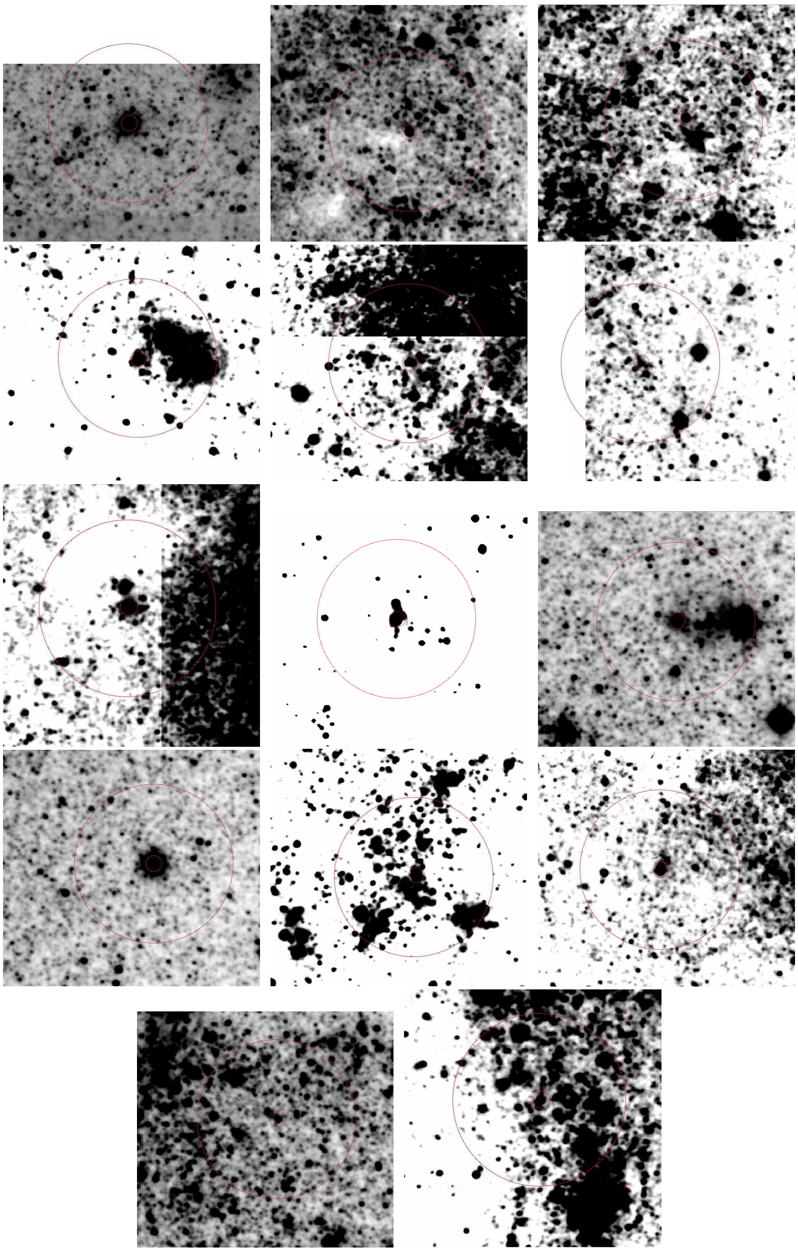

Figure 3.15: Images of outliers labelled in Figure 3.14. From top left, going right and then down to the next row, are clusters 10, 88, 217, 219, 258, 294, 300, 305, 425, 428, 515, 520 and 584 as identified in the Sarajedini & Mancone (2007) catalogue. Most of the outliers appear so because they are either in crowded regions, there are two objects very close together, they have bright stars in outer regions, or they are near a chip edge. However, cluster 258 genuinely seems to be quite elongated, and cluster 428 is noticeably larger than the other clusters.

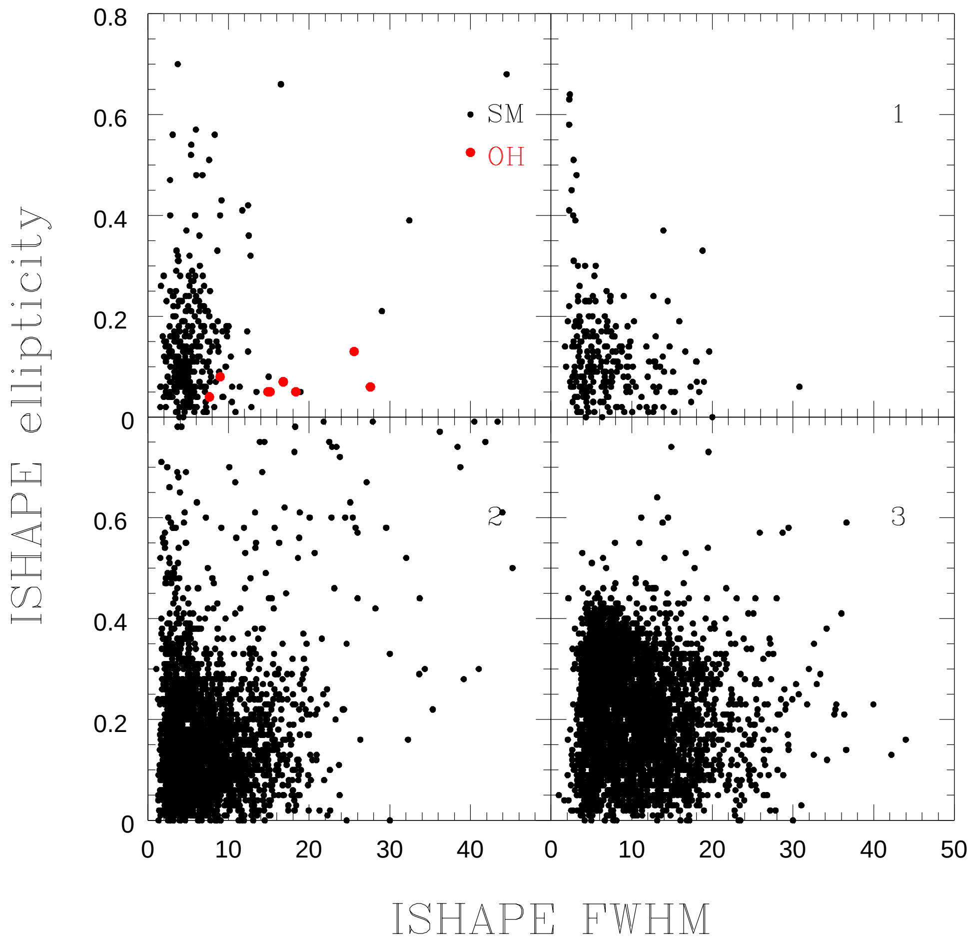

Figure 3.16: Ellipticity against flux radius (i.e., half-light radius) for the Sarajedini & Mancone (2007) clusters, and our class 1 (high-confidence clusters), 2 (possible clusters) and 3 (galaxies) objects. Also overlaid on the top-left panel with the Sarajedini & Mancone (2007) clusters are the six outer halo clusters.

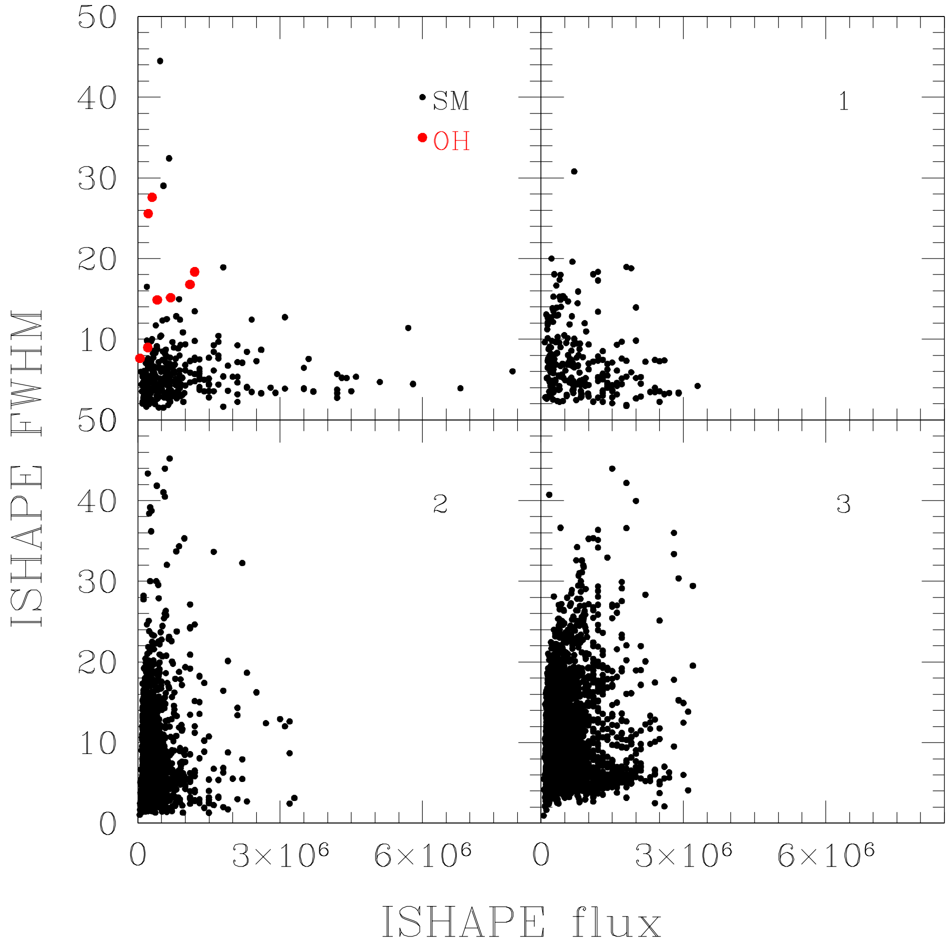

Figure 3.17: Similar to Figure 3.16 but with flux radius against flux.

Chapter 4

Unearthing Foundations of a Cosmic Cathedral: Searching the Stars for M33's Halo

Robert Cockcroft, Alan W. McConnachie, William E. Harris, Rodrigo Ibata, Mike J. Irwin, Annette M. N. Ferguson, Mark A. Fardal, Arif Babul, Scott C. Chapman, Geraint F. Lewis, Nicolas F. Martin and Thomas H. Puzia

Originally submitted to the Monthly Notices of the Royal Astronomical Society on 22nd May 2012. This chapter contains the revised manuscript, submitted in response to the referee's comments on 28th August 2012.

"The most beautiful thing we can experience is the mysterious. It is the source of all true art and science. [S]He to whom this emotion is a stranger, who can no longer pause to wonder and stand rapt in awe, is as good as dead: [her/]his eyes are closed."

Albert Einstein (1879-1955)

4.1 Introduction and Background

Λ Cold Dark Matter (ΛCDM) cosmology predicts that larger galaxies are built through the hierarchical merging of smaller galaxies. Infalling components are disrupted partially or entirely, and part of that material forms the stellar halo of the larger galaxy. Stellar halos therefore contain the remnants of past interactions between galaxies, and their properties can indicate the approximate time, size and frequency of past mergers (e.g., Purcell et al. 2007).

We can directly observe only a few relatively nearby halos in any great detail due to their faint nature, and only a small number of halos are directly observed through their resolved stars outside of the Local Group. Due to their faintness, it is problematic to determine whether or not the halos are smooth and/or symmetric. There is likely a continuum of scenarios that we observe between newly-accreted objects (creating streams, shells, etc.; e.g., Martínez-Delgado et al. 2010) and smooth halos, and our interpretation will depend on the time since the accretion and the spatial resolution and depth of the observations. The long dynamical timescales for structures outside of the disk implies that they are long-lived (Johnston et al., 1996).

Outside of the Local Group, halo detections are extremely challenging as it becomes more difficult with increasing distance to distinguish the halo from other stellar components (e.g., Dalcanton & Bernstein 2002; de Jong et al. 2008) and even more so in the absence of kinematical data (Barker et al., 2009, 2012). Scattered light and non-stellar pollution of counts also interfere with halo detections (e.g., de Jong 2008). (The surface brightness detection limits generally needed are ≥ 7 magnitudes fainter than the sky where the "darkest" skies (20th percentile), at Mauna Kea, are fainter than $\mu_V \gtrsim 21.3$.)[1]

Searches for halos around distant galaxies began with deep observations around single galaxies using surface brightness photometry and, as recent studies continue to do, focussed on late-type edge-on galaxies (e.g., Sackett et al. 1994; Shang et al. 1998; Zibetti & Ferguson 2004; Tikhonov & Galazutdinova 2005; Buehler et al. 2007; de Jong et al. 2007; Seth et al. 2007; Rejkuba et al. 2009; Mouhcine et al. 2007, 2010; Radburn-Smith et al. 2011). Each stellar component is revealed more easily in the cross-section rather than the face-on view. An alternative technique stacks many re-scaled images of galaxies together before looking for a halo signal (Zibetti et al., 2004; de Jong, 2008; Bergvall et al., 2010; Zackrisson et al., 2011; Zackrisson & Micheva, 2011), again highlighting the difficulty of detecting halos because of their extreme faintness.

Halos have also been observed around other types of galaxies, not just late-type edge-on galaxies: for example, the Virgo Cluster's central elliptical galaxy, M87 (Weil et al., 1997), nearby starburst galaxies (Bailin et al., 2011; Ryś et al., 2011; Rich et al., 2012), the Leo elliptical NGC 3379 (Harris et al., 2007), and the giant elliptical NGC 5128 (Centaurus A; see Malin et al. 1983; Peng et al. 2002; Rejkuba et al. 2011).

[1]http://www.gemini.edu/sciops/telescopes-and-sites/observing-condition-constraints

§ 4.2 provides a literature review of stellar halos in the Local Group. Details of the PAndAS observations around M33 are given in § 4.3. We are ultimately concerned with identifying the RGB stars in the M33 halo (if it exists). However, we must exclude the regions associated with the extended optical substructure surrounding the disk identified in McConnachie et al. (2009, 2010), and we must also correctly account for and subtract off the contribution from the foreground Milky Way disk and halo components, and the background galaxies misidentified as stars. § 4.4 describes these corrections and exclusions as part of the analysis. We discuss our results in § 4.5, before summarizing in § 4.6.

4.2 Halos of the Local Group Galaxies

4.2.1 The Milky Way Galaxy

The Local Group provides the closest opportunity to study a stellar halo but even the Milky Way (MW) is problematic to observe because of the restrictions and biases associated with viewing our Galaxy from within - although it has obviously been studied in depth (e.g., see the annual review by Helmi 2008, and references therein). Current seemingly contradictory evidence means it is unclear whether the MW stellar halo is oblate, prolate or triaxial (Newberg & Yanny 2006, Deason et al. 2011), although models of the dark matter (DM) halo seem to favour triaxiality (Law et al. 2009, Law & Majewski 2010). Numerous detections of substructure beyond the stellar bulge and disk are another reason that this ambiguity remains - substructure such as the Sagittarius dwarf galaxy (Ibata et al., 1994) and associated tidal streams (Ibata et al., 2001b, 2002; Majewski et al., 2003), the Monoceros ring (Ibata et al., 2003; Yanny et al., 2003; Crane et al., 2003), overdensities in Canis Major (Martin et al., 2004a,b) and Virgo (Vivas et al., 2001; Newberg et al., 2002; Xu et al., 2006; Jurić et al., 2008), clouds in the Triangulum-Andromeda region (Rocha-Pinto et al., 2004; Martin et al., 2007) and the Hercules-Aquila region (Belokurov et al., 2007a), and finally the Orphan (Grillmair, 2006; Belokurov et al., 2006, 2007b) and Cetus Polar (Newberg et al., 2009) streams.

There is growing evidence to suggest that the MW halo has a dual halo, with the different components a result of their different formation processes (e.g., Chiba & Beers 2000; Carollo et al. 2007; Miceli et al. 2008; de Jong et al. 2010; Beers et al. 2012), such as satellite accretion and in-situ formation (e.g., Bell et al. 2008; Schlaufman et al. 2009, 2012; Zolotov et al. 2009; Oser et al. 2010; McCarthy et al. 2012).

The total (dark plus luminous) mass of the Galaxy within 300 kpc is estimated to be in the range $0.7 \leq M_{MW} \leq 3.4$ x 10^{12} $M_\odot$ (Baiesi Pillastrini, 2009; Watkins et al., 2010). The MW stellar halo luminosity, including all substructure, is estimated to be of order $L_{MW,halo,V} \sim 10^9 L_\odot$ (Carney et al. 1990; Bullock & Johnston 2005, and references therein), compared to the MW host luminosity, $L_{MW,host,V} = 2.1^{+1.0}_{-0.6}$ x $10^{10} L_\odot$ (Sackett, 1997).

4.2.2 The Andromeda Galaxy

Observations of the Andromeda and Triangulum Galaxies (M31 and M33, respectively) are free from the problems inherent with viewing the MW from within, but are still close enough to resolve individual stars (Mould & Kristian, 1986; Crotts, 1986) - and many ground-based studies are now also resolving individual stars beyond the Local Group (e.g., Barker et al. 2009, 2012; Bailin et al. 2011; Tanaka et al. 2011). However, progress on the study of M31's full extended stellar halo has only come relatively recently - and the degree to which it is similar to the MW's halo is still uncertain (Kalirai et al., 2006; Ibata et al., 2007; Koch et al., 2008). M31's total (dark plus luminous) mass is estimated to be in the range 9.0 x $10^{11} M_{\odot} < M_{M31} \lesssim 2$ x $10^{12} M_{\odot}$ (Evans & Wilkinson, 2000; Chapman et al., 2006; Watkins et al., 2010). The lower limit is determined from the kinematics of RGB stars out to 60 kpc with 99% confidence (Chapman et al., 2006). An alternative dynamical mass that uses kinematics of M31's giant stream rather than those of the satellite galaxies, globular clusters, planetary nebulae or RGB stars, gives $M_{M31,R<125kpc} = 7.5^{+2.5}_{-1.3}$ x $10^{11} M_{\odot}$ (Ibata et al., 2004). M31 has a total host luminosity of $L_{M31,host,V} \sim 2.6$ x $10^{10} L_{\odot}$ (van den Bergh, 1999), which is approximately 25% brighter than the MW. Many photometric substructures have been revealed around M31 (Ibata et al., 2001a; Ferguson et al., 2002; Irwin et al., 2005; Ibata et al., 2005, 2007; McConnachie et al., 2009). Irwin et al. (2005) fit minor-axis profiles of a de Vaucouleurs law out to a projected radius of ∼20 kpc, and beyond this a power law (index ∼ -2.3) or exponential (scale length ∼ 14 kpc). Ibata et al. (2007) also find a smooth underlying component to which they fit a Hernquist profile (scale length ∼ 55 kpc), and a power law (index ∼ -1.91 ± 0.11), similar to the MW halo. If symmetric, Ibata et al. estimate that the total luminosity of the smooth halo is $L_{M31,halo,V} \sim 10^9 L_{\odot}$, again similar to the MW halo. More recently, Courteau et al. (2011) combine ground- and space-based data from several sources and decompose the resulting composite luminosity profile to find a halo component described by a power law (index ∼ -2.5 ± 0.2). M31's halo has further similarities to that of the MW's in terms of metallicity and velocity dispersion (Chapman et al., 2006). Using a Keck/DEIMOS sample of ~800 stars, Chapman et al. find a non-rotating metal-poor ([Fe/H] ~ -1.4) smooth halo between 10 - 70 kpc with no metallicity gradient underlying the metal-rich ([Fe/H] ~ -0.9) rotating extended component. Along with a comparable dark matter halo mass, the similar metallicities and dispersions are suggestive that the early formation periods of both were also similar.

4.2.3 The Magellanic Clouds

The Large Magellanic Cloud (LMC) is the fourth most massive Local Group member. It has a total mass of $M_{LMC} \approx 10^{10} M_{\odot}$ (van der Marel et al., 2002; Bekki & Stanimirović, 2009). The total host luminosity is $L_{LMC,host,V} = 3.0$ x $10^9 L_{\odot}$ (Bekki & Stanimirović, 2009). It may also have a stellar halo. A study of RR Lyrae stars, generally associated with old and metal-poor stellar populations, finds that these stars have a large velocity dispersion of 53 $\pm$ 10 km s^{-1} (Minniti et al., 2003; Alves, 2004). A photometric and spectroscopic survey has also revealed individual RGB stars enveloping the LMC out to large distances and consistent with a de Vaucouleurs profile, suggestive of a classical halo (Majewski et al., 2009). If the LMC does have a stellar halo it seems somewhat surprising given that another tracer of old and metal-poor populations - globular clusters - show no evidence for a halo as they lie within a disk region around the LMC (Freeman et al., 1983; Schommer et al., 1992). This inconsistency could be explained if the GCs are accreted in earlier, more gas-rich merger events compared to those that populate the halo with individual stars (Bekki, 2007).

The stellar outskirts of the Small Magellanic Cloud (SMC) have recently been studied through the MAgellanic Periphery Survey (MAPS; Nidever et al. 2011) to reveal a population of nearly azimuthally-symmetric RGB stars out to a radius of ∼11 kpc. The profile of these stars is well fitted with an exponential profile (scale length ∼1 kpc) out to ∼8 kpc, with a shallower profile beyond (scale length ∼7 kpc) - the latter of which the authors suggest could be a stellar halo or a population of extratidal stars.

4.2.4 The Triangulum Galaxy

M33, the Triangulum Galaxy, is the third most massive galaxy in the Local Group, with a mass close to one tenth that of M31 (Corbelli & Salucci 2000 measure M33's rotation curve out to 16 kpc, and find an implied dark halo mass of $M_{M33} \gtrsim 5 \text{ x } 10^{10} M_{\odot}$). M33 has a total host luminosity of $L_{M33,host,V} \sim 10^9 L_{\odot}$ (de Vaucouleurs et al., 1991) and is more face-on ($i = 56° \pm 1°$, Zaritsky et al. 1989) than M31 ($i = 77°$; e.g., Rubin et al. 1973; Athanassoula & Beaton 2006). It is classified as a SA(s)cd II-III galaxy (de Vaucouleurs et al., 1991), has little or no bulge component, a UV- and X-ray bright nuclear cluster (e.g., Long et al. 1981, Dubus et al. 1999 and Foschini et al. 2004), and perhaps a bar (Javadi et al., 2011), so most of the central light is distributed over an exponential disk component (e.g., de Vaucouleurs 1959; Bothun 1992; Minniti et al. 1993; McLean & Liu 1996; Corbelli et al. 2008; Kormendy et al. 2010; Javadi et al. 2011). The distance estimates to M33 cover a wide range from 730 ± 168 kpc (Brunthaler et al., 2005) to 964 ± 54 kpc (Bonanos et al., 2006). This disagreement appears to arise because of the combination of the different techniques used, and also perhaps due to inhomogeneous interstellar extinction in M33. Consistent with McConnachie et al. (2010), we adopt a distance modulus for M33 of $(m - M_0) = 24.54 \pm 0.06$ (809±24 kpc; McConnachie et al. 2004) throughout this paper. This distance is based on the TRGB method, and is consistent with our new findings (820^{+20}_{-19} kpc; Conn et al. 2012). At 809 kpc, 1° corresponds to 14.1 kpc.

Is there an M33 halo akin to those found in the MW, M31 and possibly the LMC? Previous claims of a detection for M33's halo have come from various sources, in studies that resolve individual stars (RGB or RR Lyrae stars), or globular clusters, which we briefly review here.

Mould & Kristian (1986) used the Hale Telescope/PFUEI to observe two fields both 7 kpc from the centre of each M31 and M33, along their south-east minor axes. By comparing the observed giant branches to those for M92 ($< [M/H] >= -0.6$) and 47 Tuc ($< [M/H] >= -2.2$), they inferred the presence of inner halos. However, Tiede et al. (2004) observed a field with WIYN/S2KB that included the region studied by Mould & Kristian and found that the peak of the MDF showed a radial variation with a gradient consistent with that of the inner disk region and *not* of an inner halo. Chandar et al. (2002) obtained WIYN/HYDRA spectra for 107 of M33's star clusters. These clusters, from a sample with known integrated HST/WFPC2 colours, were selected to cover the entire age range of M33's clusters (6 Myr to >13 Gyr; Chandar et al. 2001). Chandar et al. observed a large velocity dispersion that, with Monte Carlo simulations, suggested that old (> 1 Gyr) clusters could be split into two components which they associate with a disk population and the other with a halo. Similarly, Sarajedini et al. (2006) observed 64 RR Lyrae variable stars (type RRab) using HST/ACS to have a double peak in periods, again suggesting two subpopulations: a disk and a halo component. RR Lyrae stars are only observed in populations older than 10 Gyr, and therefore stars in these populations should be at least as old as the RR Lyraes.

Further hints of M33's halo also come from the following sources. Barker et al. (2007a,b) inspected three HST/ACS southeastern fields ~20'-30' (~4.7-7.1 kpc, assuming a distance to M33 of 809 kpc; McConnachie et al. 2004) from M33's nucleus. Mixed stellar populations were revealed in the CMDs, with an age range from $<$ 100 Myr to a few Gyr. The authors compared synthetic populations with the observed CMDs, and found that the mean age increased with radius from $\sim$ 6 to 8 Gyr, and the mean metallicity decreased from ~ -0.7 to -0.9 dex. They concluded that while the fields are dominated by a disk population, a halo component may also be present. Cioni et al. (2008) used UKIRT/WFCAM near-infrared observations of a 1.8 degree^2 region centred on M33 to look at the ratio of C- to M-type AGB stars. They also found metallicity and age gradients such that the outer regions were more metal poor and a few Gyr older than the central regions, in agreement with Barker et al. (2007a,b). Ferguson (2007) reviews results for M31 and M33, and notes that while a halo-like component with a power-law structure was proving elusive, the RGB narrows and becomes more metal poor beyond ~10 kpc. Teig (2008) used RGB and AGB star counts along M33's minor axis, and also observed a break in the surface brightness profile at 11 kpc. The profile at this region appeared to change from an exponential to a power-law. Barker et al. (2011) use HST/ACS to observe two fields 9.1 kpc and 11.6 kpc along M33's north major axis. They find that the outer field is old (7 $\pm$ 2 Gyr), moderately metal poor (mean $[M/H] \sim -0.8\pm$ 0.3), and contained ~30 times less stellar mass than the inner field. One of the interpretations that Barker et al. discuss is that the outer field is a transition zone from the outer disk to another structural component. Grossi et al. (2011) use Subaru/Suprime-Cam data with seven fields $10 \lesssim r < 30$ kpc from the centre of M33 in the NW and SE. An exponential scale length of ∼7 kpc is found for both regions, and these authors favour that this component is an extended disk rather than a halo.

The previous section highlights that unambiguous detections of the various galactic components - even for one of our closest neighbouring galaxies - are still extremely difficult. While studies of star clusters and RR Lyrae stars show evidence for an old halo, studies of individual stars in other subpopulations have only been marginally conclusive. Part of the problem was the limited coverage and/or depth.

McConnachie et al. (2006) undertook a spectroscopic survey of RGB stars using Keck/DEIMOS. Radial velocity distributions of these stars were best-fit by three Gaussian components, which McConnachie et al. interpreted as contributions from a halo, a disk, and a component offset from the disk (which they suggested could have been a stellar stream or another stellar halo component). Ibata et al. (2007) extended the observations of Ferguson et al. (2007) with CFHT/MegaCam along the southeastern corner of M31's halo out to M33's centre. Ibata et al. clearly saw the classical disk of M33, and in addition revealed an extended component. They fit a profile to the data between 1 and 4 degrees (the edge of the disk, and the point just before where the profile starts rising again, respectively) and found the exponential scale length to be 18 ± 1 kpc, or 55 ± 2 kpc using a projected Hernquist model. These scale lengths were surprisingly as big as they found for M31, although Ibata et al. cautioned that without a full panoramic view it was not possible to determine whether or not this feature was a "bona fide" halo.

Direct and unambiguous evidence for a stellar halo around M33 remains elusive but is the aim of this chapter. Any such component must be quite faint. We extend the work begun by McConnachie et al. (2009, 2010) as part of the Pan-Andromeda Archaeological Survey (PAndAS), which itself built on previous surveys with the INT/WFC (Ferguson et al., 2007) and CFHT/MegaCam (Ibata et al., 2007). Optical observations prior to PAndAS suggested M33's disk had an undisturbed appearance - a view that persisted until relatively recently (e.g., Sarajedini 2007; Ferguson et al. 2007). This implied that the disk had not been tidally disrupted by either the MW or M31, and was seemingly discrepant when compared to the radio detection of a warped gaseous disk component (e.g., Rogstad et al. 1976; Putman et al. 2009). We note, however, that the primary problem with the Ferguson et al. data set was depth and that the observations could only rule out the presence of substructure or a halo with surface brightnesses brighter than μ_V ~31 mag arcsec^{-2}.

PAndAS observations covering the area around M33 with unprecedented combination of depth and coverage have revealed a vast low surface brightness stellar substructure. The S-shaped optical warp of this substructure is generally aligned with the HI warp, and therefore resolves the previous discrepancy. It now seems most likely that this warp was the feature that was previously partially detected by McConnachie et al. (2006) (thereby casting doubt on the previous interpretations from this kinematic study) and Ibata et al. (2007). Although the nature of the substructure is still being investigated, the favoured interpretation for its origin is that it is a disruption of the disk that was caused by a tidal interaction with M31 as M33 orbits M31 (McConnachie et al., 2009, 2010; Dubinski et al., 2012). Preliminary models can reproduce the shape of the extended disk substructure, and also satisfy

M33's proper motion constraints (Brunthaler et al., 2005). Spectroscopic observations may provide further clues (see upcoming paper by Trethewey et al. 2012).

The depth of the PAndAS data allows us to test whether or not a genuine halo component is observable in addition to the disk-like warp. Given that the warped extended disk substructure is extremely faint and had eluded detection for so long, it would be reasonable to expect any underlying component of a halo to also be extremely faint. Indeed, a faint extended stellar component is hinted at beyond the extended disk substructure, and one possibility put forward is that this is a halo component (McConnachie et al., 2010).

Since M33 is relatively low mass, would we expect it to have a detectable halo? Purcell et al. (2007) predict that a galaxy with total mass $M \sim 10^{11} M_{\odot}$ will, *on average*, have a halo that contributes $\leq$1% of the total luminosity from the galaxy. Therefore, the expected total halo luminosity of M33 could be as low as $L_{M33,halo} \leq 10^{7} L_{\odot}$. Their halo estimates make no distinction between the smooth component and the substructure. Here, we *define* the "halo" as the component or stellar population in the outer regions of M33 that is not clearly associated with the disk or the extended disk substructure identified by McConnachie et al. (2010). Note that we do not distinguish between smooth or lumpy halos, similarly to Purcell et al. (2007).

4.3 Observations, Data Reduction and Calibration

We use data from the Pan-Andromeda Archaeological Survey (PAndAS; McConnachie et al. 2009) to observe 48 degree^2 around M33 with CFHT/MegaCam out to a projected radius of 50 kpc (cf. $r_{M33,virial}$ = 152 kpc, Martin et al. 2009). The data has limiting magnitudes for point-source detections of $g' \approx 25.5, i' \approx 24.5$ (AB magnitudes on the SDSS scale) at S/N = 10 in subarcsecond seeing. MegaCam is composed of 36 individual CCDs, has a 0.96 x 0.94 degree field of view and a resolution of 0.187" pixel^{-1}.

Figure 4.1 shows each location of the MegaCam ∼square-degree images around M33 in a tangent-plane projection. To be explicit, for our analysis we only consider the data for MegaCam images within the annulus with radius 3.75 degrees centred on M33 as shown in Figure 4.1. The MegaCam subexposures are dithered in order to cover the small gaps, but not the large gaps[2]. In the large gaps there may be fewer detections due to shallower depths. However, the area of the chip gaps is very small compared to the overall MegaCam field and can be neglected for the purposes of this analysis.

The prefixes of the image labels in Figure 4.1 represent the timeline of the observations: The central field, m33c, was observed primarily in the observing semester 2004B and retrieved from the CFHT archive, with some data from 2003B. All other fields with prefix m were observed in 2008B. Fields with prefix nb were observed in 2009B. Due to a failure of CCD 4 in the 2003B observing semester, the data from Ibata et al. (2007) which extended the southeastern section of M31's halo in a line to the centre of M33 was

[2]See http://www.cfht.hawaii.edu/Instruments/Imaging/Megacam/specsinformation.html

replaced with data from 2010B (prefix tb). The ellipse in Figure 4.1 marks the $\mu_B \approx 25$ mag arcsec^{-2} (Nilson, 1973) contour of M33's disk, and the solid-line cross represents the major and minor axes of M33, with the major axis inclined 23 degrees to North (Nilson, 1973). The dashed concentric circles represent radii at r = 1, 2, 3 and 3.75 degrees (14.1, 28.2, 42.4 and 53.0 kpc, respectively) from the centre of M33. The data within the annuli that they delineate will be used in the analysis that follows. M33 is approximately 31 degrees below the central axis of the Milky Way disk, M33$_{(l,b)}$ = (133.61, -31.33) degrees, compared with M31 which is about 21 degrees below, M31$_{(l,b)}$ = (121.18, -21.57) degrees. The three dashed lines in Figure 4.1 are lines of equal Galactic latitude ($b = -35.3$, -31.3 and -27.3 degrees).

Pre-processing and reduction were undertaken with Elixir[3] by the CFHT team, and by the Cambridge Astronomical Survey Unit (CASU) through a pipeline adapted for MegaCam images (Irwin & Lewis, 2001), respectively. The reader is referred to McConnachie et al. (2009, 2010) and Cockcroft et al. (2011) for more details.

4.4 Analysis

Taking advantage of the wide coverage of the PAndAS data, we deliberately seek direct evidence for M33's stellar halo in this data, and expect it to be extremely faint, centrally-concentrated, and detectable via RGB stars. However, this low-luminosity component will be mixed with stars from the M33 disk, M33 extended disk substructure surrounding the disk, and the MW foreground (both its thick disk and halo), in addition to background galaxies misidenti-

[3] http://www.cfht.hawaii.edu/Instruments/Imaging/MegaPrime/dataprocessing.html

fied as stars. Our technique involves statistically removing the MW foreground stars and background galaxies, excluding the regions identified as belonging to M33's extended disk substructure, and seeing what signal remains.

Figure 4.2 shows the colour-magnitude (Hess) diagrams for the data in the annuli in Figure 4.1. We note that Figure 4.2 contains more than 1.4 million objects that were identified as robust stellar candidates in both g_0 and i_0 through the CASU pipeline's object morphological classification. Magnitudes are de-reddened source by source using values of $E(B-V)$ in the range $0.034 \leq E(B-V) \leq 0.130$, with g_0 = g - 3.793 $E(B-V)$ and i_0 = i - 2.086 $E(B-V)$ (Schlegel et al., 1998). The data is binned in 0.025 x 0.025 mag bins and is shown with a logarithmic scale for the number counts of stars. As mentioned previously, we want to identify M33 RGB stars but first we need to estimate the level of contamination. To examine the MW foreground contamination, we look at the two sources of contribution from MW stars easily identifiable in the CMDs. The MW halo turn-off stars are seen as a thin band on the left of the CMDs, and we use a region defined as $0.1 < (g-i)_0 < 0.6$, $19 < i_0 < 22$ to measure their relative numbers in each zone. The red MW disk dwarfs are seen as a broader band on the right, and we identify them in the region $1.5 < (g-i)_0 < 3$, $17 < i_0 < 20$. Both of the regions for the MW disk and halo stars are consistent with McConnachie et al. (2010). Finally, M33 RGB stars are selected by the colour-magnitude locus where we would expect to find RGB stars. This locus is defined using isochrones from the Dartmouth Stellar Evolution Database (Dotter et al., 2007, 2008) which are transformed to the CFHT photometric system (McConnachie et al., 2010). These isochrones are between the 12 Gyr [α/Fe] = 0.0 isochrones, shifted to the M33 distance modulus, with metallicities of -2.5 dex $< [Fe/H] < -1$ dex.

This is a necessarily broad cut to allow for the possible range of metallicities that may be present in M33's halo, which we expect to be predominantly metal poor. Note that metal-rich stars may also be present, but will likely contribute a small amount to the overall halo component, while increasing dramatically the contamination from foreground stars that occupy a similar locus in the CMD. We could expect some α-enhancement in the M33 halo, as we see in the MW halo (e.g., Venn et al. 2004), but since there is no evidence to suggest this we adopt $[\alpha/\mathrm{Fe}] = 0.0$ for simplicity. We also note that the isochrones are being used to help define a locus in the CMD, and an absolute interpretation of the implied metallicities is not intended (for example, there will also be age degeneracies). A magnitude limit of $21.0 < i_0 < 24.0$ is also imposed on the RGB candidate stars, with the lower limit ensuring a high level of completeness while excluding the majority of bright background galaxies mis-identified as stars (which becomes a major source of contamination at faint magnitudes; $i_0 \approx 25$, $0 \lesssim (g-i)_0 \lesssim 1$). We test the effect of raising the faint limit to $i_0 < 23.5$ in Section 4.4.3.

The four panels in Figure 4.2 correspond to annuli with the radii between r = 0-1, 1-2, 2-3 and 3-3.75 degrees. We use the latter annulus to estimate the spatial variation in the MW foreground since any M33 halo component, if present, is likely to be very weak. The number of stars in each annulus, and the number of stars within each of the three selection regions, are shown in Table 4.1.

4.4.1 Extended Disk Substructure

Figure 4.3 is a revised version of Figure 13 in McConnachie et al. (2010), using the new data in images tb62-tb66 (see Figure 4.1). The map was created in an identical way to McConnachie et al. (see their Section 3.2.2 for details). Figure 4.3 shows the density contours of candidate RGB stars, and uses a slightly narrower metallicity cut of -2.0 dex $< [Fe/H] < -1.0$ dex than the cut we impose on the candidate RGB stars in the CMDs. This narrower cut is used simply because this is the metallicity range in which the extended disk substructure component is strongest. There is hardly any contribution to the extended disk substructure from stars with metallicity between -2.5 dex $< [Fe/H] < -2.0$ dex; however, we would not necessarily expect this to be true of M33's halo RGB stars. The single grey contour represents 1σ above background, or an estimated surface brightness limit of $\mu_V = 33.0$ mag arcsec^{-2}. The other (black) contours are 2, 5, 8 and 12σ above the background ($\mu_V = 32.5$, 31.7, 31.2, and 30.6 mag arcsec^{-2}, respectively).

Figure 4.4 shows the contributions to the total radial profile from the regions defined both within and excluding the 1σ contour shown in Figure 4.3. The profiles for the extended disk substructure and non-substructure regions are normalized using the total annulus area. The non-substructure regions are seen to start dominating the profile for $r > 2$ degrees. We exclude data within the 1σ contour when probing for the stellar halo. When we excise the extended disk substructure area denoted by the 1σ contour, note that we cannot probe radii smaller than $r \lesssim 1$ degree.

4.4.2 Foreground and Background Contamination

We have identified candidate stars for the M33 RGB, and MW disk and halo populations, and we have identified the regions associated with the extended disk substructure surrounding the disk. We now test the populations for variations in the spatial distributions. Figure 4.5 shows smoothed non-excised maps of the spatial distribution for the background galaxies and each of the three populations identified in Figure 4.2 (i.e., the MW disk, MW halo and the M33 RGB candidate stars). We identify background galaxies morphologically using the CASU pipeline, and those shown in Figure 4.5 have had broad colour and magnitude cuts applied ($17 < i_0 < 23.5$, $17 < g_0 < 23.5$, and $-2 < (g-i)_0 < 4$).

The data is binned into 18 x 18 arcsecond cells. The galaxy, disk and halo maps are smoothed once, and the RGB map is smoothed three times, all with a boxcar size of 13 x 13 cells (or equivalently 3.9 x 3.9 arcminutes; exactly four times smaller than in McConnachie et al. 2010). The RGB map is smoothed three times to better highlight the faint extended disk substructure surrounding the disk.

The galaxy, MW disk and MW halo maps clearly show no significant global features, although the centre of M33 is apparent due to the crowded nature in this region where the automated object morphological classification is less successful. Apparent holes in the data are caused by bright foreground stars preventing detection of faint objects in their surroundings. The galaxies misidentified as stars in our sample are expected to have a similar distribution to the galaxies shown in the galaxy map. The RGB map shows the extended substructure surrounding M33's disk, and Andromeda II to the north-west.

Now we excise the regions associated with the extended disk substructure surrounding the disk and investigate the variations of the MW disk and MW halo populations in different regions on the CMD within the 3-3.75 degree annulus (in which we expect little contribution from bona-fide M33 stars).

Figure 4.6 shows the variation of these three populations with respect to the azimuthal (left-hand column) and Galactic latitudinal (right-hand column) distributions. All panels show the variation between $3 < r \leq 3.75$ degrees, with extended disk substructure regions excised. Each of the three rows shows the density variation of M33 RGB, MW disk and MW halo candidate stars. The density of disk stars increases towards the disk, as does the density of the stars in the MW-halo selection region but with a smaller amplitude. As we do not expect the halo stars to vary in latitude in this manner, this suggests some cross-contamination with the thick disk stars.

Within the RGB selection shown in Figure 4.6, there is little variation in the annulus at large radii. Indeed, the best fit weighted least-squares fit in both RGB panels is consistent with a slope of zero. As such, we conclude that there is no reason to adopt a spatially-varying foreground for our analysis, and instead use a constant background, Σ_{bg}.

4.4.3 Radial Profile

Having determined the extended disk substructure area to avoid, we produce substructure-excised radial profiles. As previously stated, we expect M33's halo to be extremely faint and centrally-concentrated so we bin the data in annuli centred on M33, where we require a certain signal-to-noise ratio for the bins in each profile.

Figure 4.7 shows radial density profiles of the RGB stars after excising extended disk substructure regions. The small vertical radial density error bars are calculated using $\sqrt{n}$/area as the error on the mean of the star counts in each stellar population. The horizontal error bars indicate the width of the annulus. The size of the annulus was allowed to vary until the signal-to-noise reached the required value (where the "noise" is the radial density uncertainty). Each bin in Figure 4.7 has a signal-to-noise (S/N) cut of 25. We also use different S/N cuts, but later show that the results are statistically the same. The larger error bars shown in Figure 4.7 show the variation due to residual substructure. These latter errors were measured as the standard deviation of number counts between azimuthal bins (36 degrees in width) around a given radial annulus.

In all the radial profiles, we see evidence for a low-luminosity and centrally concentrated profile in M33's RGB stars, which is beyond the extended disk substructure surrounding the disk, and has not previously been seen. For illustrative purpose only, as this component is so faint and the error bars are large, we use a Levenberg-Marquardt least squares method to fit the following exponential model, as shown by the curved lines in Figure 4.7:

$$\Sigma(r) = \Sigma_0 exp\left(-\frac{r}{r_0}\right) + \Sigma_{bg}; \quad (4.1)$$

The data points are overlaid with the best fit, as shown by the curved dashed line. The horizontal dashed lines show the background level estimated by the fit. We also show the background-subtracted fit with the solid curved lines at the bottom of each panel, where the use of a constant background is justified in the previous section. Table 4.2 shows the parameters associated with each of the fits at different S/N cuts, including the S/N = 25 cut shown in Figure

4.7. As previously mentioned, although the parameters vary slightly for each different S/N cut used, they are statistically the same.

We also test the effect of raising the faint limit of the RGB selection criteria to $i_0 = 23.5$ from $i_0 = 24.0$ magnitudes. When we make the brighter magnitude cut we exclude more contamination - as we would expect - but we include proportionally less signal. The form of the radial profile is essentially the same, although less defined. We therefore continue the analysis using the $i_0 = 24.0$ cut.

We approximate an equivalent surface brightness scale by using the conversion between star counts and surface brightness described in McConnachie et al. (2010) (specifically, for $n_{RGB} < 350$ stars degree^{-2} from their Figure 15). For details of this conversion, see McConnachie et al. (2010), but note that *the conversion is only an approximation.* The RGB stars in McConnachie et al. are selected using $-2 <$ [Fe/H] < -1 dex, and $i_0 < 23.5$ magnitudes, whereas here we use $-2.5 <$ [Fe/H] < -1 dex, and $i_0 < 24.0$ magnitudes. There are also large systematic uncertainties inherent in the technique.

We estimate the luminosity of this component by first simply summing the total number of stars contributing to the profile in the radial range for which we have data (i.e., $0.88 \leq r \leq 3.75$ degrees), and using the conversion as above. Assuming Poisson statistics, we obtain 765 $\pm$ 95 stars (assuming a background of 355 stars degree^{-2}, and without propagating the uncertainty in the background), corresponding to a luminosity of $L = 2.4 \pm 0.4$ x $10^6 L_\odot$. Note that this initial estimate is independent of any assumptions we could make about the profile of the component.

To calculate the luminosity extrapolated to the center, however, we assume a spherically symmetric smooth profile that is described by the exponential fit with a scale length of 1.5 degrees (or 21.1 kpc). We calculate the fraction of the integral of the exponential fit between $0.88 \leq r \leq 3.75$ degrees compared to $0 \leq r \leq 0.88$ degrees, allowing us to calculate the luminosity between $0 \leq r \leq 3.75$ degrees. This simple extrapolation yields an estimate of $L = 3.8 \pm 0.5 \text{ x } 10^6 L_\odot$. (If we use a similar technique to extrapolate under the whole exponential curve, i.e., out to infinity, we obtain $L = 4.1 \pm 0.5 \text{ x } 10^6 L_\odot$.) We note that the large uncertainties on the exponential profile fit to our data and the unknown intrinsic profile of this component, make these extrapolated estimates highly uncertain. As noted above, we also do not include the error on the background. The effect of including this is seen in Figure 4.8; as we integrate out to larger radii, the relative luminosity error estimates increase. At larger radii, there are fewer candidate RGB stars but a relatively larger contribution from the background.

4.5 Discussion and Conclusions

It was expected that any stellar halo signal around M33 would be at least as faint as the recently discovered extended optical disk substructure surrounding the disk (McConnachie et al., 2009, 2010). Hints of a radial falloff beyond the extent of the extended disk substructure suggested a tentative halo detection (McConnachie et al., 2010). We followed up this possibility in our present study, using higher spatial resolution maps, excising any contribution from the extended disk substructure, and subtracting off contamination from foreground and background sources, so that we are more able to cleanly resolve and identify any remaining signal.

We detect a radial density drop off that we interpret as an upper limit of the M33 candidate stellar halo. The signal is extremely faint, but seems robust to various signal-to-noise cuts; as previously noted, we observe only 765 $\pm$ 95 excess stars between $0.88 < r < 3.75$ degrees.

Are we justified in claiming this extra component is a halo? We have azimuthally averaged annuli centred on M33 to find a low-luminosity and centrally concentrated profile. The top panel of Figure 4.9 shows the azimuthal distribution of the RGB candidate star density within 3 degrees having excised the extended disk substructure regions. We see contamination of the MW foreground stars does not appear to affect the density variation of these RGB candidate stars (i.e., we do not see a reflection of the density profiles shown in Figure 4.6 for the MW disk candidate stars). If our extra component was actually residual low-level emission from the already known extended disk substructure we would expect to see this reflected in this plot, with overdensities around the regions associated with the tips of the S-shaped warp, indicated by the two arrows in the top panel. The azimuthal distribution is fairly flat, but we note that overdensities are apparent near the warp's tips suggesting some contamination from the extended disk substructure. We further split the data into two annuli, 1-2 and 2-3 degrees, but we do not see evidence that the RGB candidates show any major differences in their azimuthal distribution from one another in either annulus.

Further constraining this newly discovered component, we show in Figure 4.10 the CMD for all objects with $r < 3$ degrees, except for those within the extended disk substructure's 1σ contours in Figure 4.3 (again, this imposes a minimum radius of $\sim$1 degree). We note that the RGB stars that we aim to detect are just visible to the eye on the left-hand plot. Again, we see the extreme relative faintness of this component. On the middle panel we overlay an [Fe/H] = -2 dex isochrone to this feature. As expected if this component is a halo, this crude measurement indicates that it is relatively metal-poor. The extended disk substructure metallicity for comparison is [Fe/H] = -1.6 dex (McConnachie et al., 2010). We show the CMD for the extended disk substructure in the right-hand panel, again overlaying an [Fe/H] = -2 dex isochrone for comparison. We can see that the candidate halo lies on the metal-poor side of the extended disk substructure RGB.

With this component that we identify as M33's candidate halo, it is appropriate to ask - even with such poor signal-to-noise - if we see any azimuthal asymmetry. To test for this, we split the data into the four quadrants split by the major and minor axes, e.g., as shown in Figure 4.3. The resulting radial profiles for each quadrant are shown in Figure 4.11, and the associated CMDs are shown in Figure 4.12. It appears as if the east and south quadrants have the steepest radial declines, whereas the north and west quadrants are flatter. In other words, there may be a variation in the radial profile of the candidate halo when split along the major axis. Further interpretation of this possible asymmetry must wait for higher quality and deeper data.

In summary, we have a weak detection that is not clearly indistinguishable in either azimuthal distribution or metallicity from the extended disk substructure component. If this is a halo, we use the estimates so far obtained to place upper limits on the luminosity. We note that with the data at hand we must leave open that it could be another component, such as a very extended thick disk.

The location of the extended disk substructure was the most important knowledge prior to beginning this study, in a similar way that the spectroscopic knowledge of the metal-rich component led to the discovery of the metal-poor halo in M31 (Chapman et al., 2006; Kalirai et al., 2006). If we directly compare M31's halo with M33's candidate halo we find that apart from the obvious difference in luminosity ($L_{M31,halo,V} \sim 10^9 L_\odot$, Ibata et al. 2007; $L_{M33,halo,V}$ = 4.1 $\pm$ 0.5 x $10^6 L_\odot$.), expected because of the mass difference between the two galaxies, it is unclear if the exponential scale lengths are significantly different; we estimate M33's scale length to be 21 $\pm$ 18 kpc, similar to that found for M31 ($\sim$ 14 kpc; Irwin et al. 2005). In light of the discovery here, the spectroscopic work by McConnachie et al. (2006) needs to be revisited so that a comparison of M31 and M33's halo metallicity can be made (see Trethewey 2011, and a forthcoming paper by Trethewey et al. 2012).

As mentioned in Section 4.2.4, the favoured interpretation to explain M33's extended disk substructure surrounding the disk is a tidal interaction with M31 (McConnachie et al., 2009, 2010). It is extremely likely that this interaction also affected M33's halo: at least altering if not stripping it, with some of M33's halo then being accreted onto M31. The halo could also extend beyond the point to which the PAndAS data set is able to measure it ($\sim$ 3.75 degrees, or $\sim$ 5 degrees to the north-east.) In the supplementary material movie of McConnachie et al. (2009), the end of the modelled interaction also includes the stellar halo. Though a significant amount of halo material is stripped from M33, appearing to extend beyond the virial radius to form a low-luminosity bridge between M33 and M31, most of the halo appears to remain bound to M33. The material stripped from M33's halo also extends well beyond the area observed in PAndAS. More of the remaining bound material appears on the south-east side (away from M31) than in the north-west (closest to M31). Our observations appear to broadly agree with this model, as we see more of a gradient in the radial profile in the south quadrant.

The most probable scenario(s) for how M33's candidate halo was built could be quite different from Milky Way and M31 because it is approximately ten times less massive than either. Unlike M31, M33 has no bulge, a warped extended disk substructure, and is likely interacting with a much more massive neighbour. Studies of the M33 outer halo clusters also suggest that with the low GC surface density ($\Sigma_{GC,M33} \sim 0.14$ deg^{-2}) compared to M31 ($\Sigma_{GC,M31} \sim 0.8$ deg^{-2}), M33 either had a much calmer accretion history than M31 or that some of the outer halo clusters could have been tidally stripped by M31 (Huxor et al., 2009; Cockcroft et al., 2011). The latter idea obviously supports the favoured interpretation that could explain the warped extended disk substructure component.

We now compare our results with a model that predicts the size of M33's stellar halo. Purcell et al. (2007) use an analytic model with empirical constraints from $z \sim 0$ observations to predict the fraction of stellar halo mass compared to the total luminous mass. They define the diffuse stellar mass fraction as $f_{IHL} = M_*^{diff}/M_*^{total}$; note that they use mass rather than luminosities, to avoid uncertainties involved with luminosity evolution. There is no distinction made between the substructure in the halo, or the smooth diffuse halo that might underlie the substructure. Their predictions cover a range of host galaxy's dark matter halo masses, from small late-type galaxies to large galaxy clusters ($\sim 10^{11}$ to $\sim 10^{15}$ $M_\odot$). The stellar material is assumed to be able to become part of the diffuse stellar halo when its dark matter subhalo has become significantly stripped. The dark matter subhalo is considered disrupted when its maximum circular velocity falls below a critical value - which is set by considering the empirical constraints. For DM halos of mass $\sim 10^{11} M_\odot$ ($\sim M_{M33}$; Corbelli & Salucci 2000), the stellar halo luminosity fraction is expected to be $\leq$ 1.0% (thus, $L_{stellarhalo} \leq 10^7 L_\odot$). A galaxy's mass-to-light ratio (over the entire halo out to the virial radius) varies as a function of DM halo mass, and this drives the fraction of stellar halo material; small galaxies are expected to accrete material from dwarf galaxies, which have high mass-to-light ratios and therefore share little luminous material with their host galaxy's stellar halo (Purcell et al., 2007). Even if they share all of their material, the contribution is not large. This picture seems to broadly agree with our upper limit estimate of M33's extremely faint candidate stellar halo, $L_{M33,halo,V} = 4.1 \pm 0.5$ x $10^6 L_\odot$ (0.4% $\lesssim L_{M33,host,V} \lesssim$ 0.5%).

Figure 4.13 plots the fraction of halo luminosity compared to the host galaxy luminosity, against the host galaxy mass for several galaxies including M33. The lines represent equation 7 from Purcell et al. (2007) for the model of the intrahalo light, with different values for the parameters n_{eff} and f_d. Here, n_{eff}, expected to be of order unity, represents the effective number of satellites with mass $M_{sat} = M_{host}/20$; f_d represents the total stellar mass fraction a satellite contributes to its host galaxy halo. We note that if we swap the values for f_d and n_{eff}, the lines would vary in the same way.

The two estimates for M33's candidate halo luminosity fraction are for the directly observed estimate ($0.88 < r < 3.75$ degrees), and the implied, extrapolated estimate ($r < 10.64$ degrees). The values for the MW and M31 are taken from Sections 4.2.1 and 4.2.2, respectively. We also include estimates of NGC 2403's extended component (Barker et al., 2012), as it has a similar total stellar mass to M33 (9.4 ± 0.7 x $10^{10} M_\odot$; Fraternali et al. 2002). It is at a distance of 3.1 Mpc (Freedman et al., 2001), has an inclination of 63 degrees (Fraternali et al., 2002), and is the brightest member of a loose galaxy group and is therefore considered much more isolated than M33 (the closest large galaxy is M81, which is four times further from NGC 2403 than M33 is from M31; Barker et al. 2012). Barker et al. use Subaru/Suprime-Cam to obtain images 39 x 48 kpc around the centre of NGC 2403, and see an extended component which could be disk structure or a halo. Extrapolating out to 50 kpc they find that the halos contain $\sim$ 1-7 % of the total V-band luminosity, or $L_{2403,halo,V} \sim$ 1-7 x $10^8 L_\odot$, depending on whether or not an exponential or Hernquist profile is used (if they extrapolate out to 100 kpc the estimate does not significantly change).

The values of $L_{halo}/L_{hostgalaxy}$ for the MW and M31 are close to those of the models by Purcell et al. (2007). However, for the less massive galaxy NGC 2403 we find the models seem to underestimate the contribution of halo light from these smaller galaxies - and may also do the same for M33, although with such a weak signal as we detect here there are large uncertainties. If we further include M33's extended disk substructure ($L_{substructure} \sim 10^7 L_\odot$) in the "halo" term, we see that M33 lies even further from the model lines. How do we interpret this information? A value of $f_d = 1$ implies that any satellite galaxy has been completely destroyed and contributed all of its material to the halo. The MW and M31 data seem to favour a value of $f_d = 1$, which is of course inconsistent with observations (e.g., M31's latest tally is up to 29; Richardson et al. 2011, Slater et al. 2011, Bell et al. 2011). If the M33 candidate halo fraction is closer to the upper bounds, then it also appears that the models underestimate the halo fraction for lower-luminosity galaxies.

4.6 Summary

We use Pan-Andromeda Archaeological Survey (PAndAS) data to identify RGB candidate stars in the regions unrelated to the disk and extended disk substructure surrounding the disk. Contamination from both Milky Way foreground stars and misidentified background galaxies is subtracted. We reveal a new component centred on M33 that has a low luminosity. With such a weak signal, measurements are not well constrained by our data. However, it appears that this component has an exponential scale length is of order $r_{exp} \sim 20$ kpc, a photometric metallicity of around [Fe/H] ~ -2 dex, a luminosity range of less than one percent of M33's total host luminosity, and is azimuthally asymmetric. More observations and deeper photometry are required to better determine the detailed structure of the stellar populations.

If this feature is truly a halo, it provides support that stellar halos are a ubiquitous component of all galaxies, built through the hierarchical merging predicted in ΛCDM cosmology.

Acknowledgements

We thank the anonymous referee who provided useful comments that helped to improve the paper. RC and WEH thank the Natural Sciences and Engineering Research Council of Canada for financial support. GFL thanks the Australian Research Council for support through his Future Fellowship (FT100100268) and Discovery Project (DP110100678). RI gratefully acknowledges support from the Agence Nationale de la Recherche though the grant POMMME (ANR 09-BLAN-0228). Based on observations obtained with MegaPrime/MegaCam, a joint project of CFHT and CEA/DAPNIA, at the Canada-France-Hawaii Telescope (CFHT) which is operated by the National Research Council (NRC) of Canada, the Institute National des Sciences de l'Univers of the Centre National de la Recherche Scientifique of France, and the University of Hawaii. RC would like to thank the CFHT staff for much support. This research has made use of the NASA/IPAC Extragalactic Database (NED) which is operated by the Jet Propulsion Laboratory, California Institute of Technology, under contract with the National Aeronautics and Space Administration. Thanks to Mike Rich for providing useful comments that improved this paper.

Bibliography

Alves, D. R. 2004, ApJ, 601, L151

Athanassoula, E. and Beaton, R. L. 2006, MNRAS, 370, 1499

Baiesi Pillastrini, G. C. 2009, MNRAS, 397, 1990

Bailin, J., Bell, E. F., Chappell, S. N., Radburn-Smith, D. J., and de Jong, R. S. 2011, ApJ, 736, 24

Barker, M. K., Ferguson, A. M. N., et al. 2011, MNRAS, 410, 504

Barker, M. K., Ferguson, A. M. N., Irwin, M., Arimoto, N., and Jablonka, P. 2009, AJ, 138, 1469

Barker, M. K., Ferguson, A. M. N., Irwin, M. J., Arimoto, N., and Jablonka, P. 2012, MNRAS, 419, 1489

Barker, M. K., Sarajedini, A., Geisler, D., Harding, P., and Schommer, R. 2007a, AJ, 133, 1125

—. 2007b, AJ, 133, 1138

Beers, T. C., Carollo, D., et al. 2012, ApJ, 746, 34

Bekki, K. 2007, MNRAS, 380, 1669

Bekki, K. and Stanimirović, S. 2009, MNRAS, 395, 342

Bell, E. F., Slater, C. T., and Martin, N. F. 2011, ApJ, 742, L15

Bell, E. F., Zucker, D. B., et al. 2008, ApJ, 680, 295

Belokurov, V., Evans, N. W., et al. 2007a, ApJ, 657, L89

Belokurov, V., —. 2007b, ApJ, 658, 337

Belokurov, V., Zucker, D. B., et al. 2006, ApJ, 642, L137

Bergvall, N., Zackrisson, E., and Caldwell, B. 2010, MNRAS, 405, 2697

Bonanos, A. Z., Stanek, K. Z., et al. 2006, ApJ, 652, 313

Bothun, G. D. 1992, AJ, 103, 104

Brunthaler, A., Reid, M. J., Falcke, H., Greenhill, L. J., and Henkel, C. 2005, Science, 307, 1440

Buehler, S., Ferguson, A. M. N., Irwin, M. J., Arimoto, N., and Jablonka, P. 2007, in IAU Symposium, Vol. 241, IAU Symposium, ed. A. Vazdekis & R. F. Peletier, 321–322

Bullock, J. S. and Johnston, K. V. 2005, ApJ, 635, 931

Carney, B. W., Latham, D. W., and Laird, J. B. 1990, AJ, 99, 572

Carollo, D., Beers, T. C., et al. 2007, Nature, 450, 1020

Chandar, R., Bianchi, L., and Ford, H. C. 2001, A&A, 366, 498

Chandar, R., Bianchi, L., Ford, H. C., and Sarajedini, A. 2002, ApJ, 564, 712

Chapman, S. C., Ibata, R., et al. 2006, ApJ, 653, 255

Chiba, M. and Beers, T. C. 2000, AJ, 119, 2843

Cioni, M., Irwin, M., et al. 2008, A&A, 487, 131

Cockcroft, R., Harris, W. E., et al. 2011, ApJ, 730, 112

Conn, A. R., Ibata, R. A., Lewis, G. F., Parker, Q. A., and Zucker, D. B. 2012, ApJ, in prep

Corbelli, E., Magrini, L., and Verley, S. 2008, in Astronomical Society of the Pacific Conference Series, Vol. 396, Formation and Evolution of Galaxy Disks, ed. J. G. Funes & E. M. Corsini, 19

Corbelli, E. and Salucci, P. 2000, MNRAS, 311, 441

Courteau, S., Widrow, L. M., et al. 2011, ApJ, 739, 20

Crane, J. D., Majewski, S. R., Rocha-Pinto, H. J., Frinchaboy, P. M., Skrutskie, M. F., and Law, D. R. 2003, ApJ, 594, L119

Crotts, A. P. S. 1986, AJ, 92, 292

Dalcanton, J. J. and Bernstein, R. A. 2002, AJ, 124, 1328

de Jong, J. T. A., Yanny, B., Rix, H.-W., Dolphin, A. E., Martin, N. F., and Beers, T. C. 2010, ApJ, 714, 663

de Jong, R. S. 2008, MNRAS, 388, 1521

de Jong, R. S., Radburn-Smith, D. J., and Sick, J. N. 2008, in Astronomical Society of the Pacific Conference Series, Vol. 396, Formation and Evolution of Galaxy Disks, ed. J. G. Funes & E. M. Corsini, 187

de Jong, R. S., Seth, A. C., et al. 2007, ApJ, 667, L49

de Vaucouleurs, G. 1959, ApJ, 130, 728

de Vaucouleurs, G., de Vaucouleurs, A., Corwin, Jr., H. G., Buta, R. J., Paturel, G., and Fouque, P. 1991, Third Reference Catalogue of Bright Galaxies (New York: Springer-Verlag)

Deason, A. J., Belokurov, V., and Evans, N. W. 2011, MNRAS, 416, 2903

Dotter, A., Chaboyer, B., et al. 2007, AJ, 134, 376

Dotter, A., Chaboyer, B., Jevremović, D., Kostov, V., Baron, E., and Ferguson, J. W. 2008, ApJS, 178, 89

Dubinski, J., Widrow, L., W., M. A., R., I., and et al., I. M. J. 2012, in preparation

Dubus, G., Long, K. S., and Charles, P. A. 1999, ApJ, 519, L135

Evans, N. W. and Wilkinson, M. I. 2000, MNRAS, 316, 929

Ferguson, A., Irwin, M., Chapman, S., Ibata, R., Lewis, G., and Tanvir, N. 2007, Resolving the Stellar Outskirts of M31 and M33 (Island Universes: Berlin: Springer), 239

Ferguson, A. M. N. 2007, in Astronomical Society of the Pacific Conference Series, Vol. 374, From Stars to Galaxies: Building the Pieces to Build Up the Universe, ed. A. Vallenari, R. Tantalo, L. Portinari, & A. Moretti, 239

Ferguson, A. M. N., Irwin, M. J., Ibata, R. A., Lewis, G. F., and Tanvir, N. R. 2002, AJ, 124, 1452

Foschini, L., Rodriguez, J., et al. 2004, A&A, 416, 529

Fraternali, F., van Moorsel, G., Sancisi, R., and Oosterloo, T. 2002, AJ, 123, 3124

Freedman, W. L., Madore, B. F., et al. 2001, ApJ, 553, 47

Freeman, K. C., Illingworth, G., and Oemler, Jr., A. 1983, ApJ, 272, 488

Grillmair, C. J. 2006, ApJ, 645, L37

Grossi, M., Hwang, N., Corbelli, E., Giovanardi, C., Okamoto, S., and Arimoto, N. 2011, A&A, 533, A91

Harris, W. E., Harris, G. L. H., Layden, A. C., and Wehner, E. M. H. 2007, ApJ, 666, 903

Helmi, A. 2008, A&A Rev., 15, 145

Huxor, A., Ferguson, A. M. N., et al. 2009, ApJ, 698, L77

Ibata, R., Chapman, S., Ferguson, A. M. N., Irwin, M., Lewis, G., and McConnachie, A. 2004, MNRAS, 351, 117

Ibata, R., Chapman, S., Ferguson, A. M. N., Lewis, G., Irwin, M., and Tanvir, N. 2005, ApJ, 634, 287

Ibata, R., Irwin, M., Lewis, G., Ferguson, A. M. N., and Tanvir, N. 2001a, Nature, 412, 49

Ibata, R., Irwin, M., Lewis, G. F., and Stolte, A. 2001b, ApJ, 547, L133

Ibata, R., Martin, N. F., et al. 2007, ApJ, 671, 1591

Ibata, R. A., Gilmore, G., and Irwin, M. J. 1994, Nature, 370, 194

Ibata, R. A., Irwin, M. J., Lewis, G. F., Ferguson, A. M. N., and Tanvir, N. 2003, MNRAS, 340, L21

Ibata, R. A., Lewis, G. F., Irwin, M. J., and Cambrésy, L. 2002, MNRAS, 332, 921

Irwin, M. and Lewis, J. 2001, New Astronomy Reviews, 45, 105

Irwin, M. J., Ferguson, A. M. N., Ibata, R. A., Lewis, G. F., and Tanvir, N. R. 2005, ApJ, 628, L105

Javadi, A., van Loon, J. T., and Mirtorabi, M. T. 2011, MNRAS, 414, 3394

Johnston, K. V., Hernquist, L., and Bolte, M. 1996, ApJ, 465, 278

Jurić, M., Ivezić, Ž., et al. 2008, ApJ, 673, 864

Kalirai, J. S., Gilbert, K. M., et al. 2006, ApJ, 648, 389

Koch, A., Rich, R. M., et al. 2008, ApJ, 689, 958

Kormendy, J., Drory, N., Bender, R., and Cornell, M. E. 2010, ApJ, 723, 54

Law, D. R. and Majewski, S. R. 2010, ApJ, 714, 229

Law, D. R., Majewski, S. R., and Johnston, K. V. 2009, ApJ, 703, L67

Long, K. S., Dodorico, S., Charles, P. A., and Dopita, M. A. 1981, ApJ, 246, L61

Majewski, S. R., Nidever, D. L., Muñoz, R. R., Patterson, R. J., Kunkel, W. E., and Carlin, J. L. 2009, in IAU Symposium, Vol. 256, IAU Symposium, ed. J. T. van Loon & J. M. Oliveira, 51–56

Majewski, S. R., Skrutskie, M. F., Weinberg, M. D., and Ostheimer, J. C. 2003, ApJ, 599, 1082

Malin, D. F., Quinn, P. J., and Graham, J. A. 1983, ApJ, 272, L5

Martin, N. F., Ibata, R. A., Bellazzini, M., Irwin, M. J., Lewis, G. F., and Dehnen, W. 2004a, MNRAS, 348, 12

Martin, N. F., Ibata, R. A., et al. 2004b, MNRAS, 355, L33

Martin, N. F., Ibata, R. A., and Irwin, M. 2007, ApJ, 668, L123

Martin, N. F., McConnachie, A. W., et al. 2009, ApJ, 705, 758

Martínez-Delgado, D., Gabany, R. J., et al. 2010, AJ, 140, 962

McCarthy, I. G., Font, A. S., Crain, R. A., Deason, A. J., Schaye, J., and Theuns, T. 2012, MNRAS, 420, 2245

McConnachie, A. W., Chapman, S. C., et al. 2006, ApJ, 647, L25

McConnachie, A. W., Ferguson, A. M. N., et al. 2010, ApJ, 723, 1038

McConnachie, A. W., Irwin, M. J., Ferguson, A. M. N., Ibata, R. A., Lewis, G. F., and Tanvir, N. 2004, MNRAS, 350, 243

—. 2005, MNRAS, 356, 979

McConnachie, A. W., Irwin, M. J., et al. 2009, Nature, 461, 66

McLean, I. S. and Liu, T. 1996, ApJ, 456, 499

Miceli, A., Rest, A., et al. 2008, ApJ, 678, 865

Minniti, D., Borissova, J., Rejkuba, M., Alves, D. R., Cook, K. H., and Freeman, K. C. 2003, Science, 301, 1508

Minniti, D., Olszewski, E. W., and Rieke, M. 1993, ApJ, 410, L79

Mouhcine, M., Ibata, R., and Rejkuba, M. 2010, ApJ, 714, L12

Mouhcine, M., Rejkuba, M., and Ibata, R. 2007, MNRAS, 381, 873

Mould, J. and Kristian, J. 1986, ApJ, 305, 591

Newberg, H. J. and Yanny, B. 2006, Journal of Physics Conference Series, 47, 195

Newberg, H. J., Yanny, B., et al. 2002, ApJ, 569, 245

Newberg, H. J., Yanny, B., and Willett, B. A. 2009, ApJ, 700, L61

Nidever, D. L., Majewski, S. R., Muñoz, R. R., Beaton, R. L., Patterson, R. J., and Kunkel, W. E. 2011, ApJ, 733, L10

Nilson, P. 1973, Nova Acta Regiae Soc. Sci. Upsaliensis Ser. V, 0

Oser, L., Ostriker, J. P., Naab, T., Johansson, P. H., and Burkert, A. 2010, ApJ, 725, 2312

Peng, E. W., Ford, H. C., Freeman, K. C., and White, R. L. 2002, AJ, 124, 3144

Purcell, C. W., Bullock, J. S., and Zentner, A. R. 2007, ApJ, 666, 20

Putman, M. E., Peek, J. E. G., et al. 2009, ApJ, 703, 1486

Radburn-Smith, D. J., de Jong, R. S., et al. 2011, ApJS, 195, 18

Rejkuba, M., Harris, W. E., Greggio, L., and Harris, G. L. H. 2011, A&A, 526, A123

Rejkuba, M., Mouhcine, M., and Ibata, R. 2009, MNRAS, 396, 1231

Rich, R. M., Collins, M. L. M., et al. 2012, Nature, 482, 192

Richardson, J. C., Irwin, M. J., et al. 2011, ApJ, 732, 76

Rocha-Pinto, H. J., Majewski, S. R., Skrutskie, M. F., Crane, J. D., and Patterson, R. J. 2004, ApJ, 615, 732

Rogstad, D. H., Wright, M. C. H., and Lockhart, I. A. 1976, ApJ, 204, 703

Rubin, V. C., Ford, Jr., W. K., and Krishna Kumar, C. 1973, ApJ, 181, 61

Ryś, A., Grocholski, A. J., van der Marel, R. P., Aloisi, A., and Annibali, F. 2011, A&A, 530, A23

Sackett, P. D. 1997, ApJ, 483, 103

Sackett, P. D., Morrisoni, H. L., Harding, P., and Boroson, T. A. 1994, Nature, 370, 441

Sarajedini, A. 2007, in Revista Mexicana de Astronomia y Astrofisica Conference Series, Vol. 29, Revista Mexicana de Astronomia y Astrofisica Conference Series, ed. R. Guzmán, 48–50

Sarajedini, A., Barker, M. K., Geisler, D., Harding, P., and Schommer, R. 2006, AJ, 132, 1361

Schlaufman, K. C., Rockosi, C. M., et al. 2009, ApJ, 703, 2177

Schlaufman, K. C., —. 2012, ApJ, 749, 77

Schlegel, D. J., Finkbeiner, D. P., and Davis, M. 1998, ApJ, 500, 525

Schommer, R. A., Suntzeff, N. B., Olszewski, E. W., and Harris, H. C. 1992, AJ, 103, 447

Seth, A., de Jong, R., Dalcanton, J., and GHOSTS Team. 2007, in IAU Symposium, Vol. 241, IAU Symposium, ed. A. Vazdekis & R. F. Peletier, 523–524

Shang, Z., Zheng, Z., et al. 1998, ApJ, 504, L23

Slater, C. T., Bell, E. F., and Martin, N. F. 2011, ApJ, 742, L14

Tanaka, M., Chiba, M., Komiyama, Y., Guhathakurta, P., and Kalirai, J. S. 2011, ApJ, 738, 150

Teig, M. 2008, PASP, 120, 474

Tiede, G. P., Sarajedini, A., and Barker, M. K. 2004, AJ, 128, 224

Tikhonov, N. A. and Galazutdinova, O. A. 2005, Astrophysics, 48, 221

Trethewey, D. 2011, University of Cambridge: Masters dissertation

Trethewey, D., Chapman, S. C., et al. 2012, in preparation

van den Bergh, S. 1999, A&A Rev., 9, 273

van der Marel, R. P., Alves, D. R., Hardy, E., and Suntzeff, N. B. 2002, AJ, 124, 2639

Venn, K. A., Irwin, M., Shetrone, M. D., Tout, C. A., Hill, V., and Tolstoy, E. 2004, AJ, 128, 1177

Vivas, A. K., Zinn, R., et al. 2001, ApJ, 554, L33

Watkins, L. L., Evans, N. W., and An, J. H. 2010, MNRAS, 406, 264

Weil, M. L., Bland-Hawthorn, J., and Malin, D. F. 1997, ApJ, 490, 664

Xu, Y., Deng, L. C., and Hu, J. Y. 2006, MNRAS, 368, 1811

Yanny, B., Newberg, H. J., et al. 2003, ApJ, 588, 824

Zackrisson, E., de Jong, R. S., and Micheva, G. 2011, ArXiv e-prints

Zackrisson, E. and Micheva, G. 2011, ArXiv e-prints

Zaritsky, D., Elston, R., and Hill, J. M. 1989, AJ, 97, 97

Zibetti, S. and Ferguson, A. M. N. 2004, MNRAS, 352, L6

Zibetti, S., White, S. D. M., and Brinkmann, J. 2004, MNRAS, 347, 556

Zolotov, A., Willman, B., et al. 2009, ApJ, 702, 1058

Table 4.1: The number of stellar objects located in each annulus shown in Figure 4.1, and in each region shown in Figure 4.2. The sixth column includes all points out to a radius of $r \lesssim 3.75$ degrees.

	Annuli (degrees)				
Region	0-1	1-2	2-3	3-3.75	All
M33 RGB	83394	7597	7235	3472	101698
MW Disk	9064	15431	26326	13716	64537
MW Halo	9894	4309	6784	3479	24466
Total within annulus	595878	163178	243949	148885	1151890

Table 4.2: The fit parameters for the exponential model fits in Section 4.4.3 shown in Figure 4.7. Each column shows the quantity first in measured units, then in physical units in parentheses. Units for each column are shown as footnotes. The uncertainties on each parameter are shown under the columns labelled with Δ.

S/N	Σ_0 [a]	$\Delta\Sigma_0$ [a]	r_0 [b]	Δr_0 [b]	Σ_{bg} [c]	$\Delta\Sigma_{bg}$ [c]	χ^2
15	233 (3.7)	189 (3.0)	1.0 (14)	0.6 (8)	365 (5.7)	14 (0.2)	1.2
20	163 (2.6)	102 (1.6)	1.4 (20)	1.1 (16)	360 (5.6)	23 (0.4)	1.1
25	158 (2.5)	83 (1.3)	1.5 (21)	1.3 (18)	355 (5.6)	28 (0.4)	1.1
30	182 (2.9)	124 (1.9)	1.3 (18)	1.0 (14)	361 (5.7)	23 (0.4)	1.2

[a] Counts degree^{-2} (10^{-9} $L_\odot$ kpc^{-2}).

[b] Degrees (kpc).

[c] Counts degree^{-2}(10^{-9} $L_\odot$ kpc^{-2}).

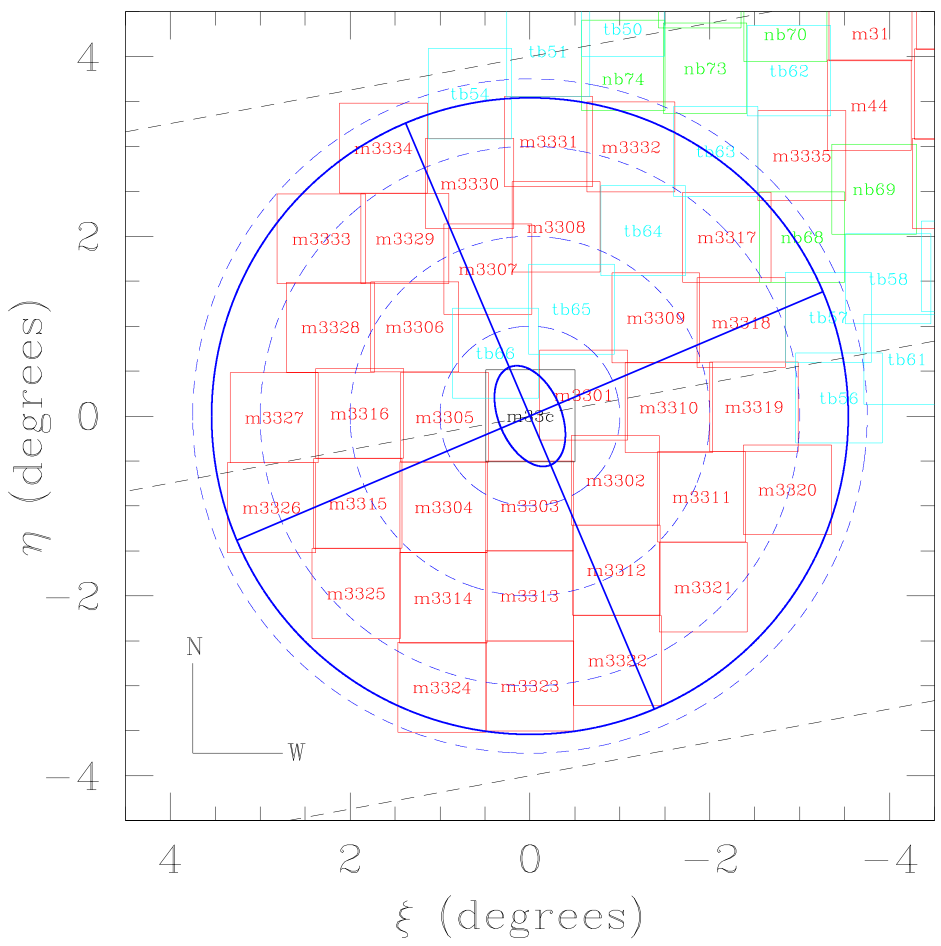

Figure 4.1: A tangent-plane projection of the PAndAS fields around M33. The central field, m33c (black), was observed primarily in 2004B, with some data from 2003B. All other fields with prefix m (red) were observed in 2008B. Fields with prefix nb (green) and tb (light blue) were observed in 2009B and 2010B, respectively. The dark blue solid ellipse marks the diameter (73 x 45 arcminutes) at which $\mu_B \approx 25$ mag arcsec^{-2} (Nilson, 1973). The two perpendicular lines show the major and minor axes (the major axis is inclined 23 degrees from the vertical; Nilson 1973). The solid-line circle represents $r = 50$ kpc ($\approx 0.33\, r_{M33,virial}$). The concentric dashed-line circles mark radii of $r = 1, 2, 3$ and 3.75 degrees (14.1, 28.2, 42.4 and 53.0 kpc, respectively). We assume a distance modulus of $(m - M_0) = 24.54 \pm 0.06$ (809±24 kpc; McConnachie et al. 2004, 2005). The three straight black dashed lines each represent one line of equivalent Galactic latitude ($b = -35.3$, -31.3 and -27.3).

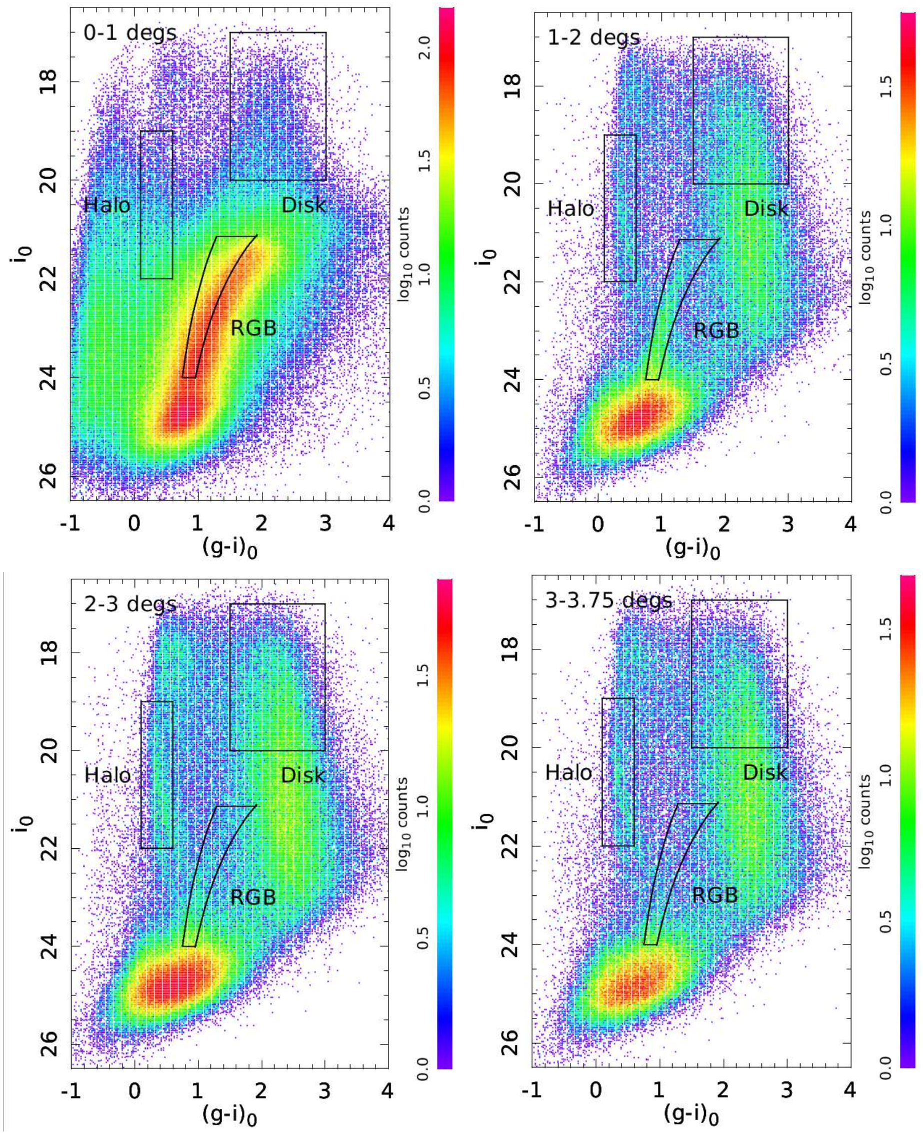

Figure 4.2: Color-magnitude (Hess) diagrams of the different annuli shown in Figure 4.1. Bins are 0.025 x 0.025 mag, and are shown with a logarithmic scaling in number counts of stars. Contamination due to the foreground MW **halo** and **disk** stars is estimated with the regions defined by $0.1 < (g-i)_0 < 0.6$, $19 < i_0 < 22$, and $1.5 < (g-i)_0 < 3$, $17 < i_0 < 20$, respectively (shown as the boxes in each panel). The isochrones correspond to [Fe/H] $= -1.0$ and -2.5 dex for a 12 Gyr, [α/H]=0.0 stellar population at the distance of M33, and have magnitude limits of $21.0 < i_0 < 24.0$. The annulus between $3 < r \leq 3.75$ degrees was used to determine the levels of foreground contamination. The bright clump at $< i_0 \approx < 25$, $0 < i_0 < 1$ is mainly composed of misclassified background galaxies (with a very small number of M33 horizontal-branch/red-clump stars).

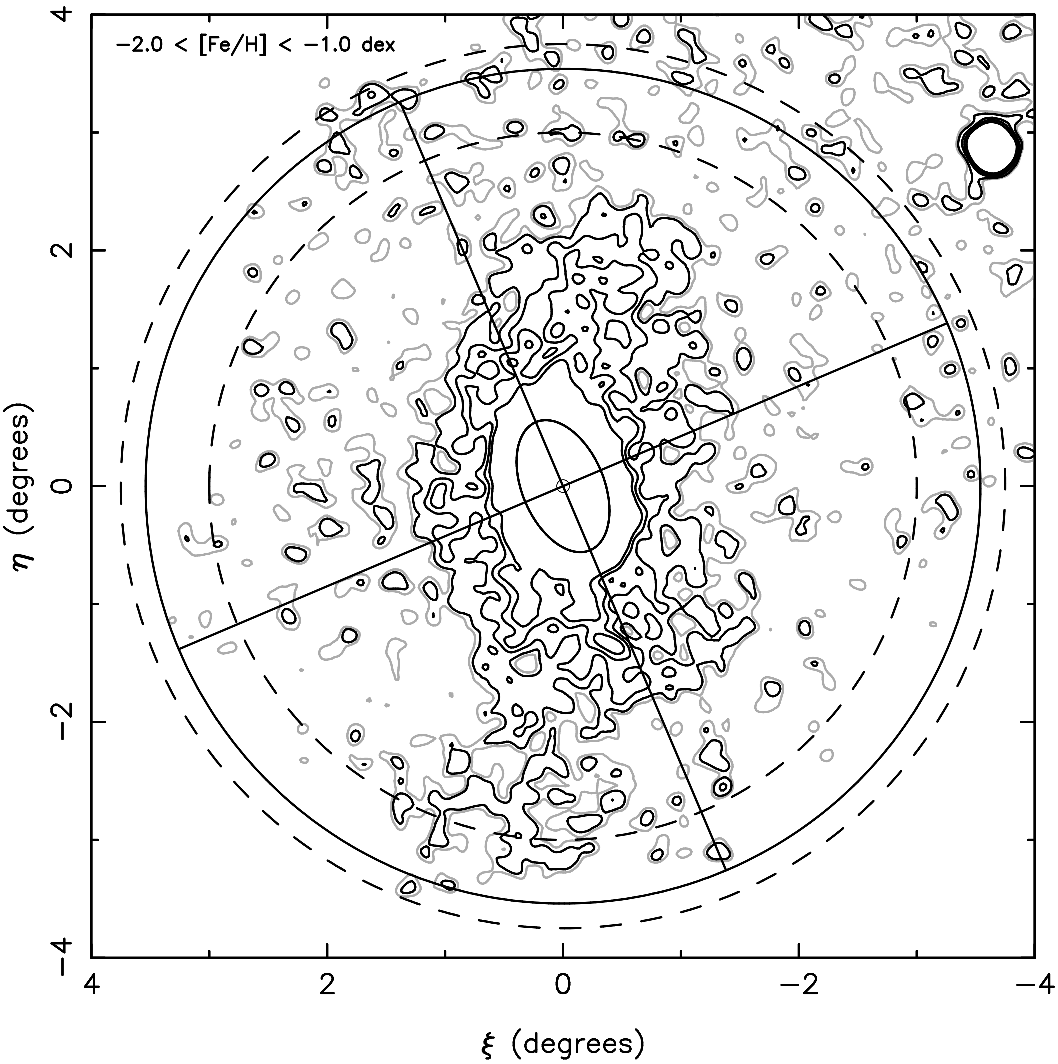

Figure 4.3: Density contours of candidate RGB stars similar to Figure 13 in McConnachie et al. (2010) but updated using data from 2010B for frames tb62-tb66 (see Figure 4.1). The grey contour is 1σ above the background, corresponding to an estimated surface brightness limit of $\mu_V = 33.0$ mag arcsec^{-2}. We exclude any area within this contour for our estimate of the stellar halo. The black contours correspond to 2, 5, 8 and 12σ above the background (μ_V = 32.5, 31.7, 31.2, and 30.6 mag arcsec^{-2}, respectively). The feature at (ξ, η = (−3.5, 3.6) is Andromeda II.

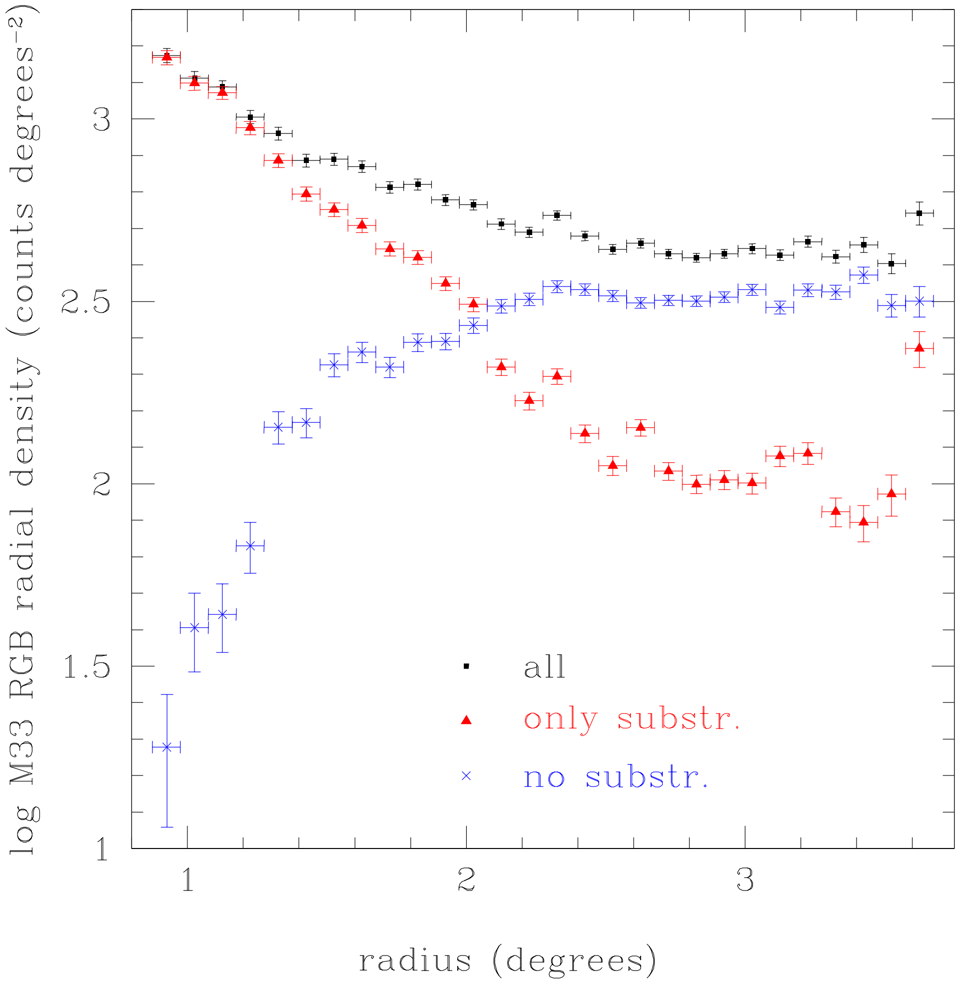

Figure 4.4: The radial profiles of substructure (red triangles) and non-substructure (blue crosses) regions, identified by the grey 1σ contours in Figure 4.3, normalized using the total annulus area. The total radial profile is shown by the black squares. We only show the profiles beginning at ~0.85, within which the substructure completely dominates. Each bin location is fixed for all three components, and all bins have a fixed width of 0.1 degrees (shown by the horizontal error bars). The vertical error bars show $\sqrt{n}$/area.

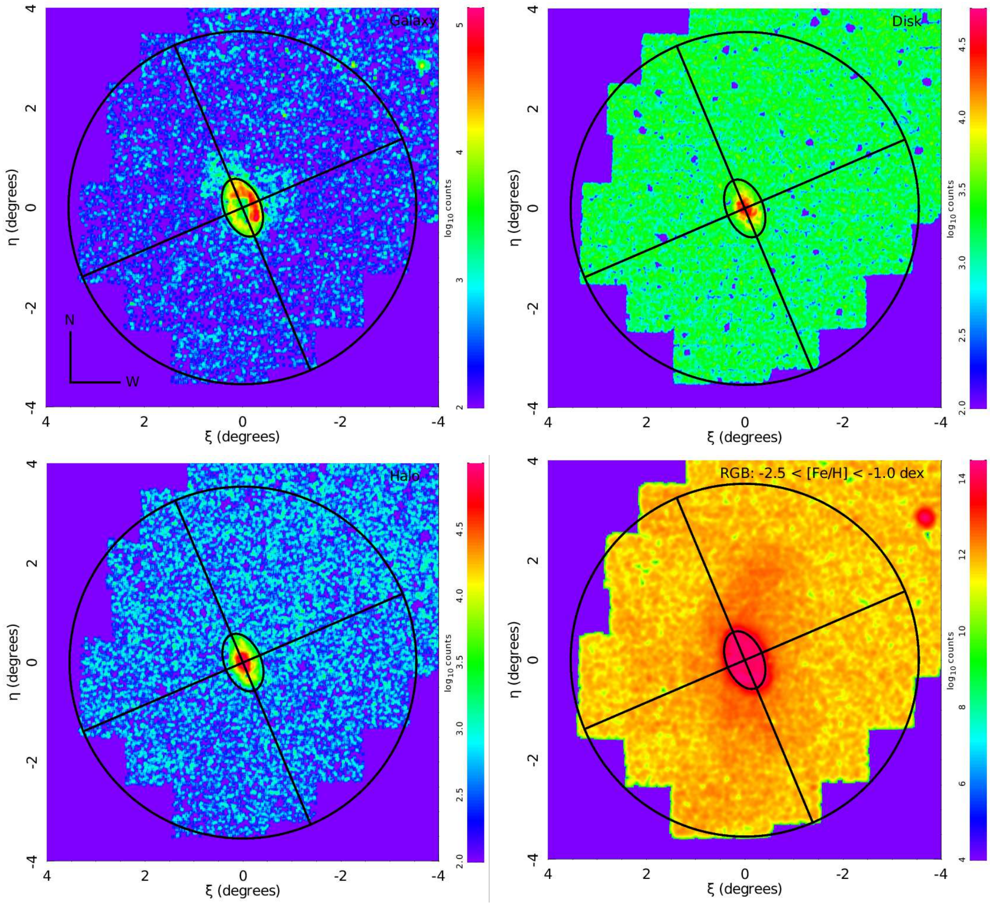

Figure 4.5: Smoothed maps of the spatial distribution maps for the candidate galaxies, disk, halo and RGB stars. See Section 4.4 for details. Clearly visible in the RGB map is the M33 substructure, and Andromeda II in the NW. The ellipse, two perpendicular lines and circle are as in Figure 4.1. To ensure the most effective colour range to show features (or lack thereof), zeropoints were set at log counts = 2 for the galaxy, disk and halo plots, and log counts = 4 for the RGB plot.

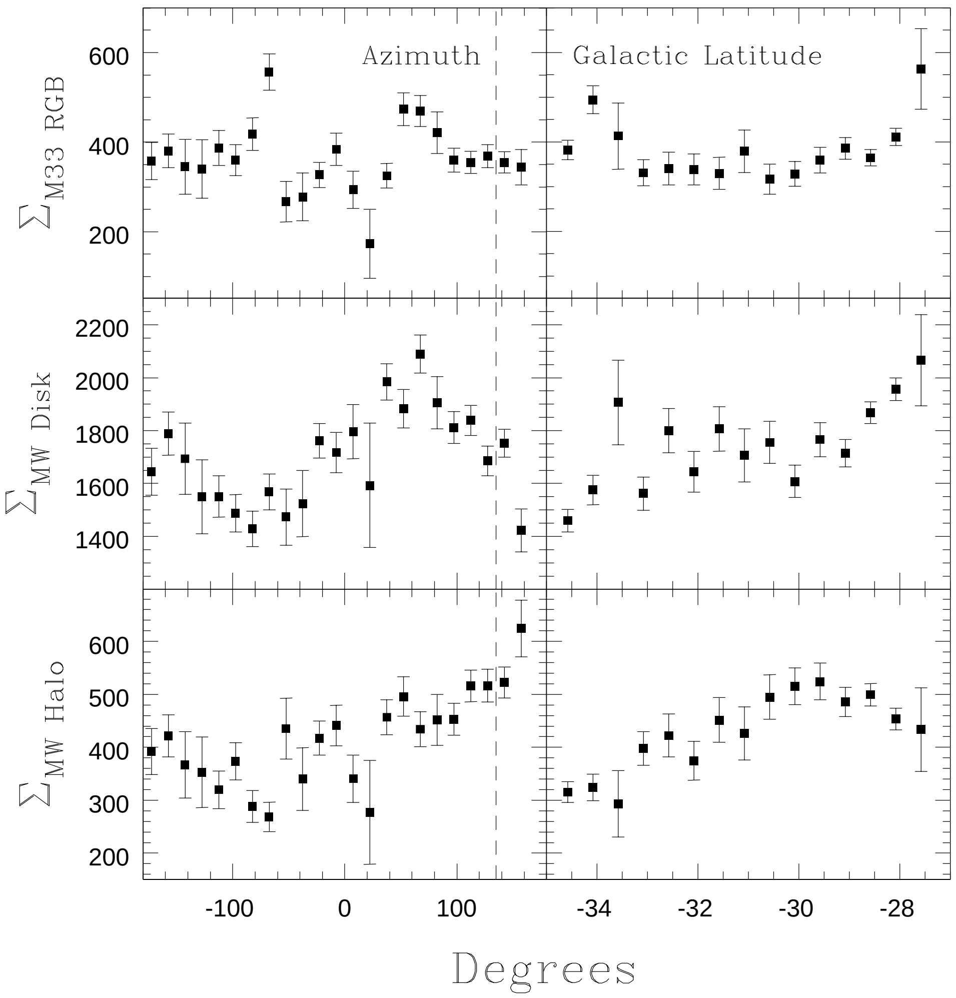

Figure 4.6: The left- and right-hand columns show the azimuthal and Galactic latitudinal distributions, respectively, of the density (counts degree^{-2}) variations for each region in Figure 4.2. The data within the $3 < r \leq 3.75$ degree annulus, having excised the area associated with the extended substructure, is shown. For the azimuthal distributions, 0, 90, ±180, and -90 degrees correspond to east, north, west and south, respectively. M31's centre is at approximately 135 degrees in this orientation (as indicated by the dashed line). The errors in all panels correspond to the values of $\sqrt{n}$/area.

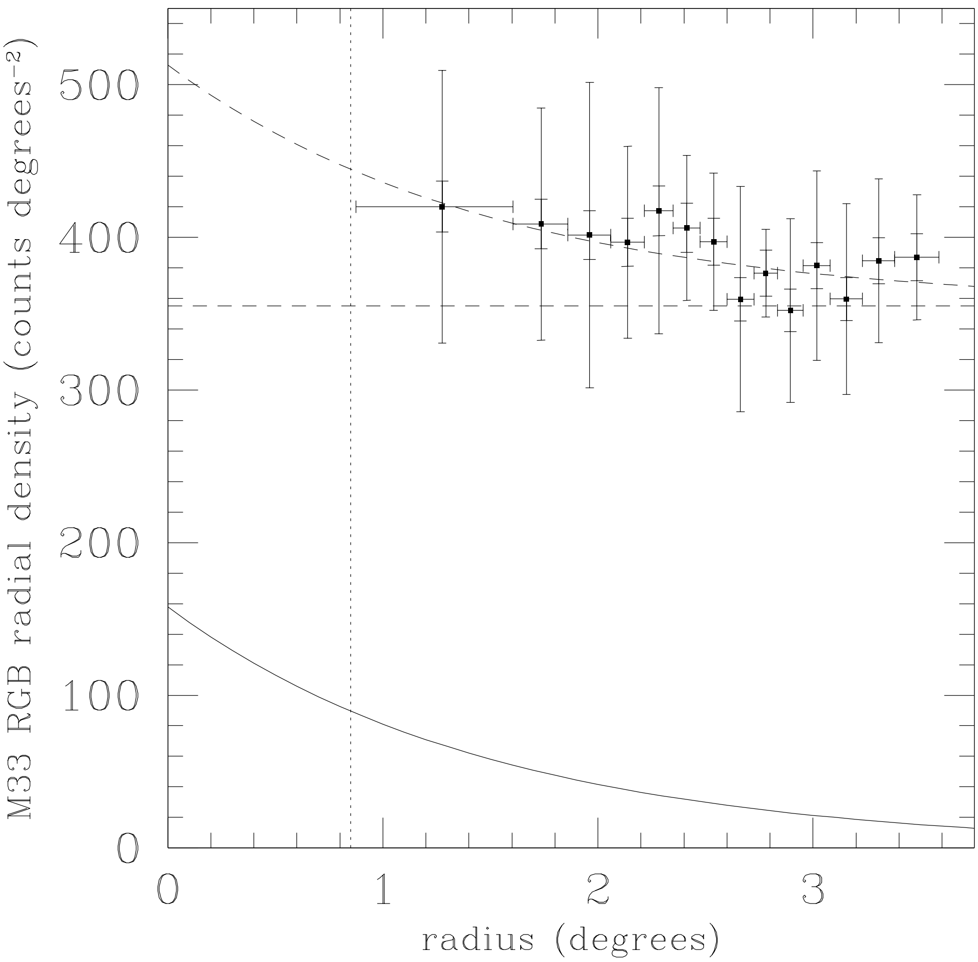

Figure 4.7: The background-uncorrected (upper dashed curved line and points) and the background-corrected (lower solid curved line) radial profiles of RGB candidate stars. The horizontal dashed line indicates the background level, Σ_{bg}. Two radial density (vertical) error bars are shown: the smaller set is calculated using $\sqrt{n}$/area as the error in each bin. The bin size was allowed to vary until the required signal-to-noise ratio of 25 was reached. Horizontal "error" bars show the width of the bin. The vertical dashed regions indicate the radius within which we do not have any data because we excise the area dominated by the disk and extended disk substructure surrounding the disk. The larger vertical error bars show the variation due to residual substructure (see Section 4.4.3 for details).

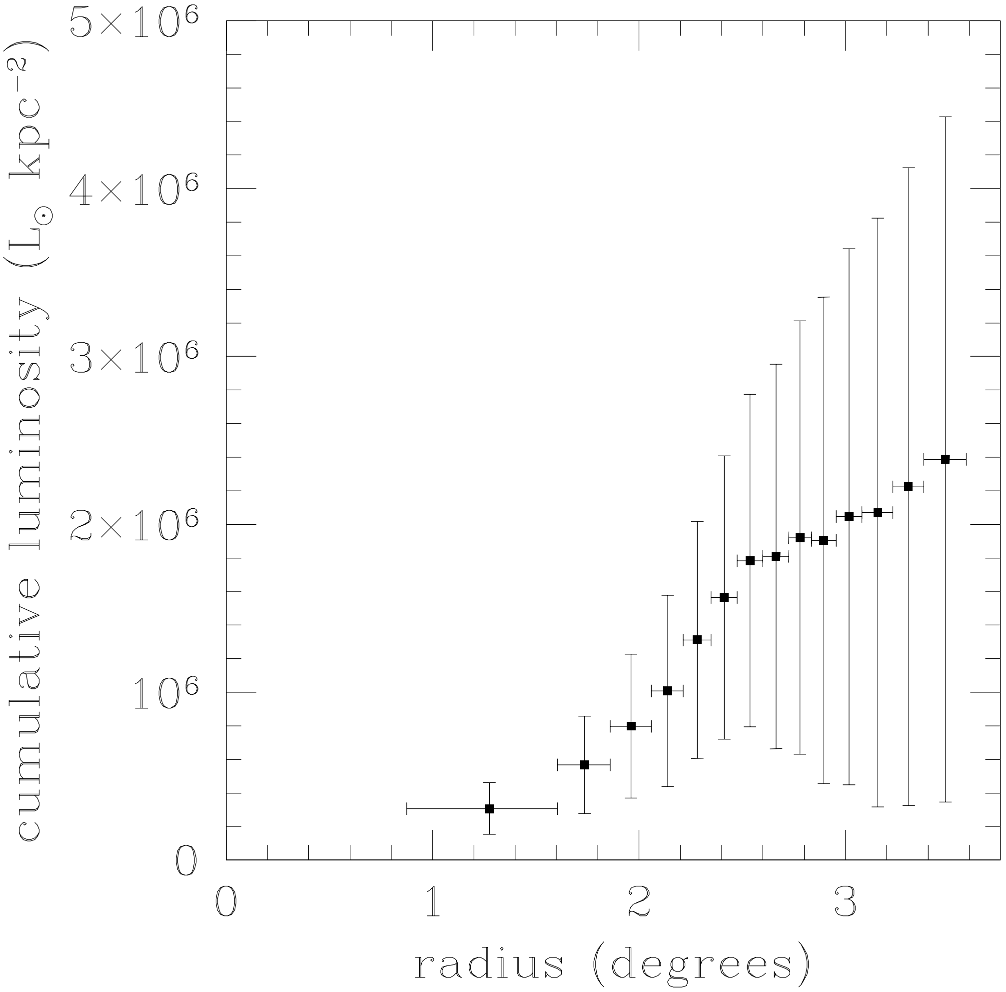

Figure 4.8: The cumulative luminosity as a function of radius. Horizontal "error" bars show the width of the bin, and are the same as those shown in Figure 4.7. The error on the luminosity is calculated by combining the Poisson errors for the RGB candidate star counts with the uncertainty of the background. This figure highlights the increase in our estimate of the luminosity uncertainty as we increase the area we consider.

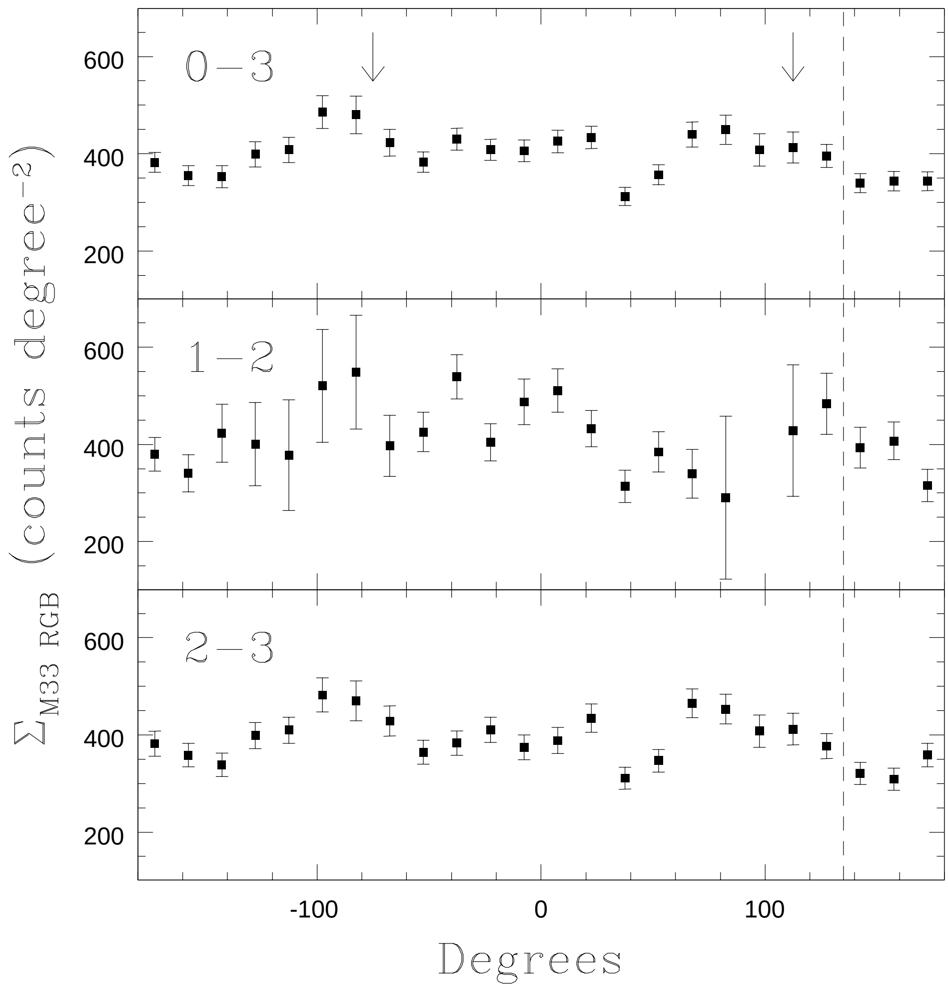

Figure 4.9: The azimuthal distribution of RGB candidate stars for the annuli shown in the top left of each plot. 0, 90, ± 180, and -90 degrees correspond to east, north, west and south, respectively. M31's centre is at approximately 135 degrees in this orientation (as indicated by the dashed line). The top, middle and bottom panels show the data with $r < 3$, $1 < r < 2$, and $2 < r < 3$ degrees, with the regions associated with substructure excised in all panels. The left- and right-hand arrows correspond approximately to the SE and NW tips of the S-shaped warp of the extended substructure.

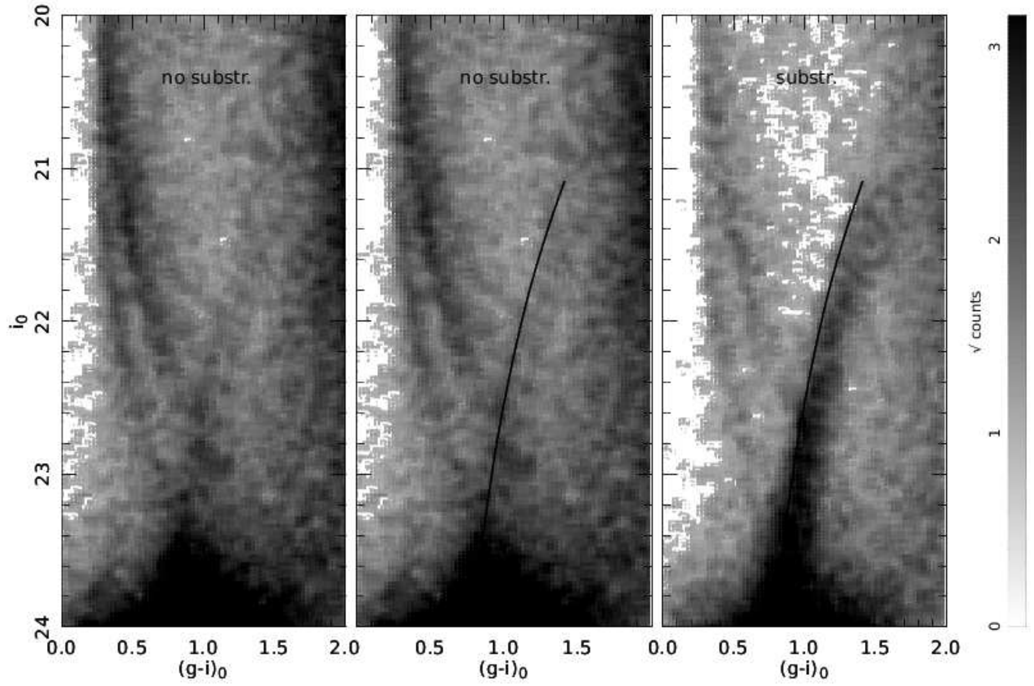

Figure 4.10: Similar to Figure 4.2, but here showing the CMD for the region with $r < 3$ degrees. The left-hand and middle panels show the CMD after excising the substructure areas in Figure 4.3 (which effectively imposes a minimum radius of $r = 0.88$ degrees). The RGB that we aim to detect is so faint that it is barely visible on the left hand plot. We overlay a [Fe/H] $= -2$ dex isochrone on the middle plot. The right-hand plot shows the CMD of the substructure areas for comparison.

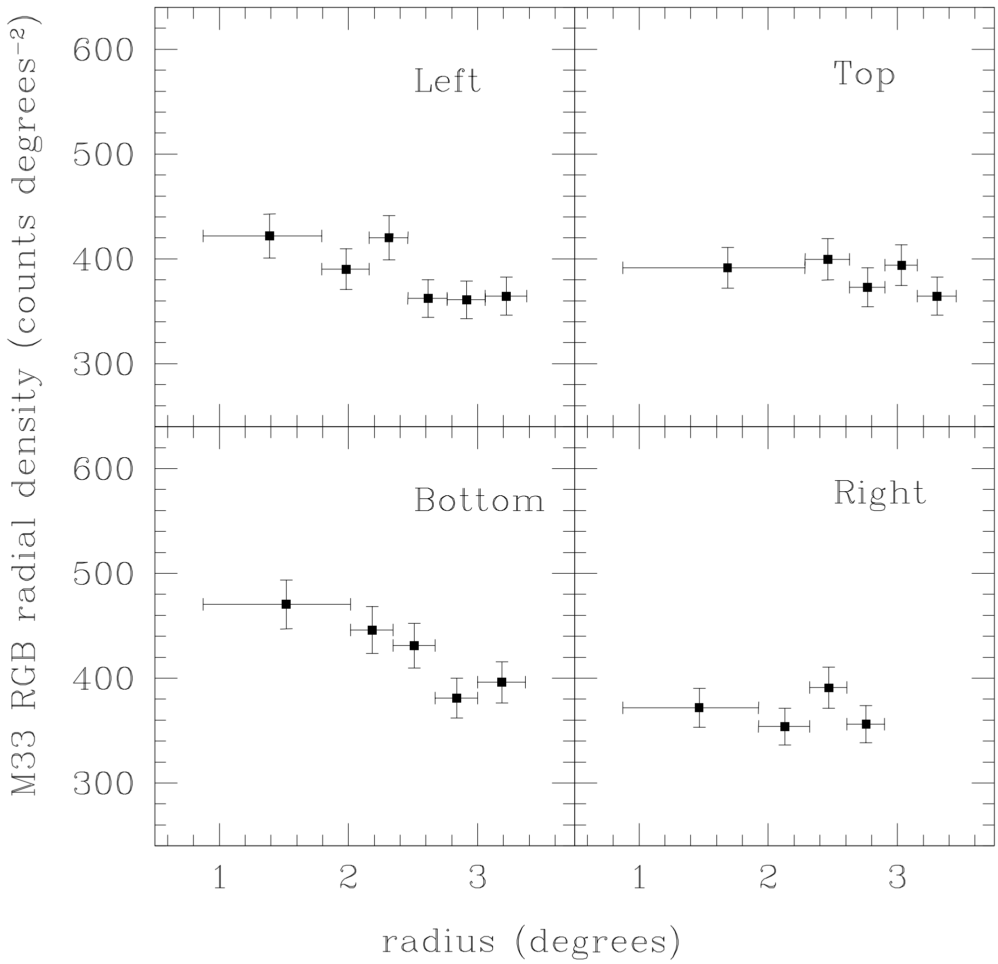

Figure 4.11: Background-uncorrected profiles for the quadrants split by major and minor axes, e.g., as shown in Figure 4.3.

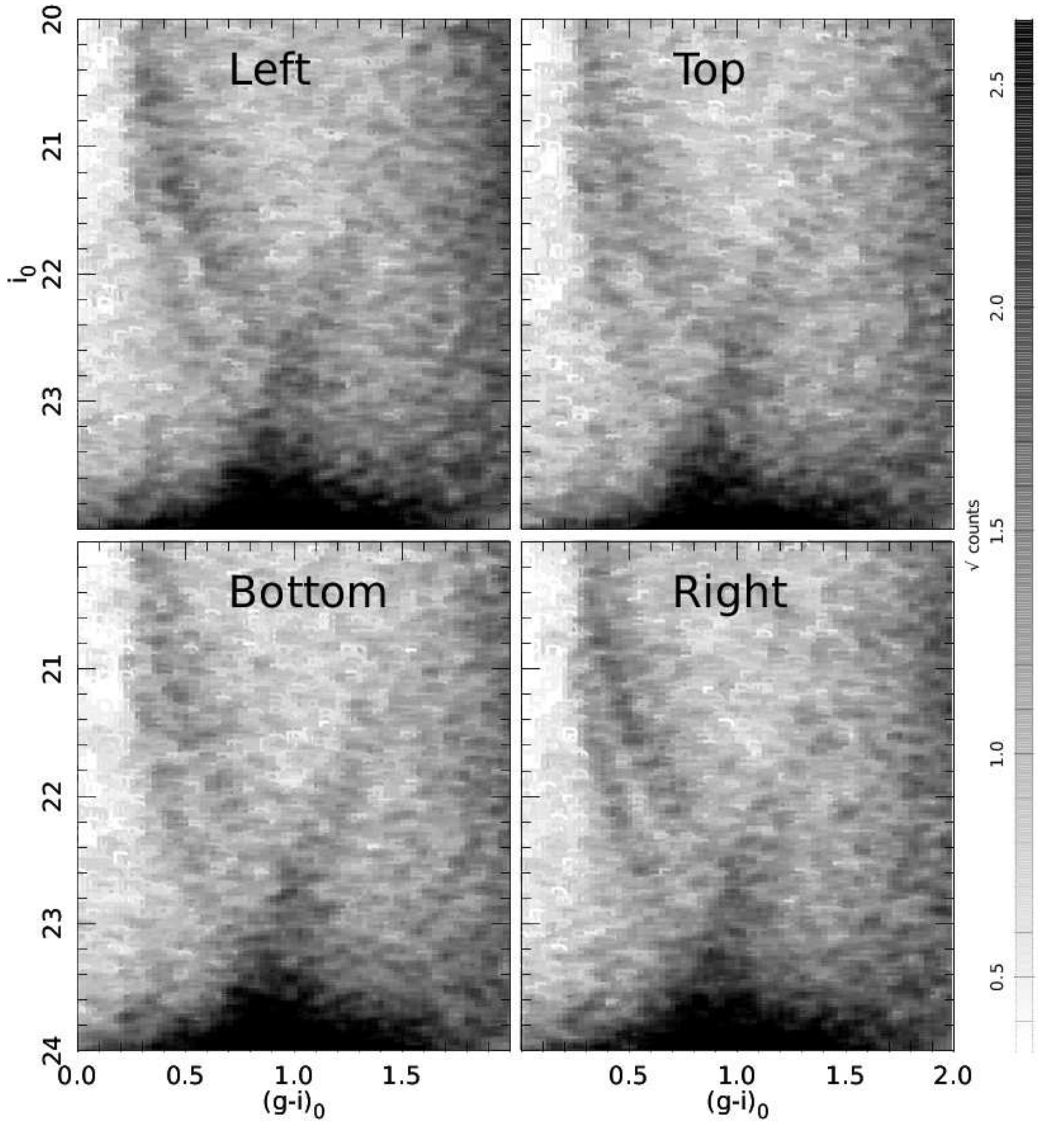

Figure 4.12: The CMDs for the quadrants used in Figure 4.11.

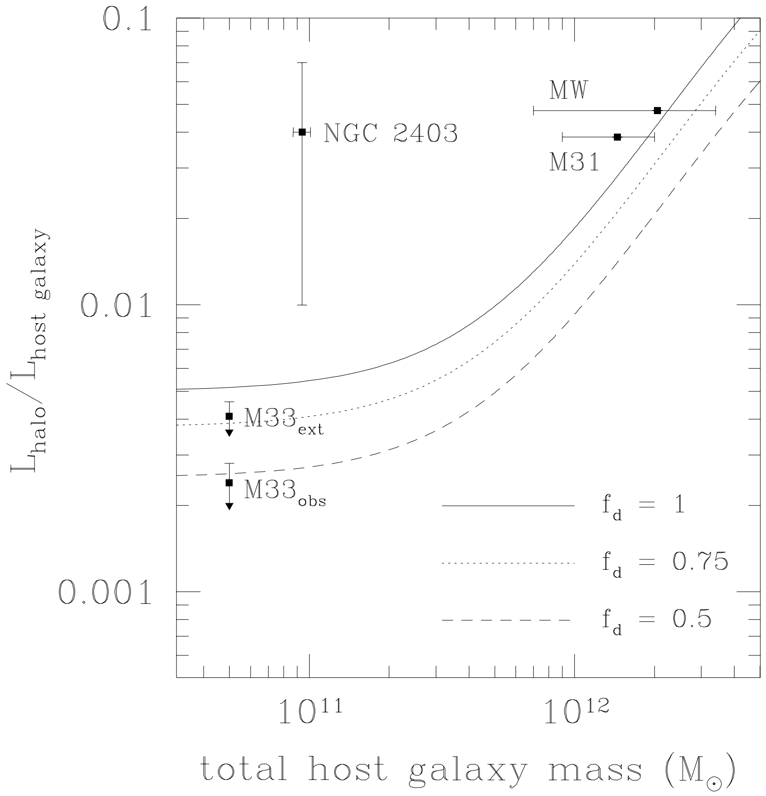

Figure 4.13: The halo luminosity as a fraction of the host galaxy luminosity against the total host galaxy mass (dark plus luminous) for the MW, M31, M33 and NGC 2403. Data for the MW, M31 and NGC 2403 are from the literature (see Sections 4.2.1, 4.2.2 and 4.5, respectively, for details and references). M33's host galaxy mass is from Corbelli & Salucci (2000). The ranges of M33's halo luminosity are our estimates from this paper. The observed range comes from strictly limiting the integration between the range of our actual data, whereas the extrapolated range comes from extrapolating inwardly to the centre of M33 and outwardly to M33's Virial radius. The lines represent the models for the intrahalo light fraction in Purcell et al. (2007). We use $n_{eff} = 1$ in conjunction with the three values for f_d shown in the plot. n_{eff} represents the effective number of satellites with mass $M_{sat} = M_{host}/20$; f_d represents the total stellar mass fraction a satellite contributes to its host galaxy halo. McConnachie et al. (2010) estimate $L_{substructure} \approx 1\% L_{M33}$ so $L_{substructure} \approx 10^7 L_\odot$. No distinction is made between substructure and a smooth halo component for the host luminosity estimates in the literature for the MW, M31, and NGC 2403 - similarly for the Purcell et al. models. M33's extended substructure is in the halo region, and if it was to be included in the estimates shown in this figure it would raise each $L_{halo}/L_{hostgalaxy}$ estimate by 0.01.

Chapter 5

Summary and Future Work

"Behind it all is surely an idea so simple, so beautiful, so compelling that when - in a decade, a century, or a millennium - we grasp it, we will say to each other, how could it have been otherwise? How could we have been so blind for so long?"

John Archibald Wheeler (1911-2008)

The ΛCDM paradigm successfully explains many of the large-scale structures that we can see throughout the Universe, but has difficulty matching observations on the small scale in our Local Universe (e.g., the missing satellite problem, and the cusp-core problem). With new instruments and capabilities, and the discoveries of more stellar systems and different classes of objects (e.g., UFDs and ECs), this has further motivated astro-archaeological projects in our own Local Group. Can we unearth all of the smallest components and assemble a consistent picture of how they may have interacted with one another in our own Galaxy and nearest neighbours?

My thesis uses data collected with the CFHT as part of PAndAS to study M33, the third most massive member of our Local Group. In particular, we look for evidence of this galaxy's old halo component which we do by searching for both GCs in the outer halo region ($\gtrsim$9 kpc from M33's centre), and the individual RGB stars that may constitute the diffuse stellar halo.

In Chapter 2, we search over 40 square degrees surrounding M33 looking for GCs and cluster candidates. We do this by employing two methods: a visual search, and an automated search. With the former, we look for the characteristic structure of GCs where there is a central concentration of unresolved stars (the "globule"), surrounded by a small sprinkling of stars (most likely RGB stars) in their outer halo. With the latter, we use Source Extractor to select objects and then with various parameter space (colour, magnitude, ellipticity and half-light radius) we compare to already-known GCs to select the most appropriate selection criteria to cull out most of the contamination while retaining objects of interest. We then visually examine and classify these objects.

We find one new definite cluster, resulting in a total of six outer halo clusters for M33 beyond the central square degree. The surface density of outer halo clusters is $\Sigma \sim 0.15$ deg^{-2}, which is much less than the more massive neighbouring galaxy, M31, which has an (incomplete) surface density of $\Sigma \sim 0.8$ deg^{-2}. For M33 to have so few readily identifiable outer halo GCs suggests either that M33 had a calmer accretion history than M31, or that M31 tidally stripped some of M33's clusters. The latter is currently the favoured view as it is in line with other observational evidence, such as the warped extended substructure surrounding the disk, and initial modelling of the M31-M33 interaction.

For the six outer halo clusters, we measure the luminosity, colour and all structural parameters. The new cluster is slightly smaller, fainter and redder than all but one of the other outer halo clusters. All M33 outer halo clusters are similar to the MW Palomar clusters in that they have low concentrations, and similar to the MW outer halo clusters in general with M33 outer halo cluster half-light radii in the range from 4 to 20 pc.

Many objects picked out by our selection criteria are identified as contamination (the majority are background galaxies, as expected), but we are left with 2440 objects for which the resolution cannot distinguish between genuine clusters and background galaxies. We split these candidate clusters into two groups: high-confidence candidates (class 1) and possible candidates (class 2).

In Chapter 3, we extend the analysis begun in Chapter 2 and use two methods to help predict which cluster candidates are the most likely genuine clusters. We use two types of simulated clusters: the first and second sets are based on surface brightness models and MC evolved simulations, respectively. The surface brightness simulated clusters were originally created for use on *HST* images on M31, so we adapt them for use on MegaCam images of M33. Our automated search method fails to detect any of these clusters because they contain unrealistic numbers of stars, and therefore fall well below our magnitude cut in the selection criteria. However, we have used them to test our visual search method and find that we are likely to miss the clusters with the lowest concentration values with small radii, and also half of the faintest clusters.

The MC evolved simulated clusters are also adapted for use on MegaCam images as though they were at the distance of M33. Our automated search method *can* retrieve the brightest of these clusters, and upon subsequent visual classification would be placed in our class 2 objects (i.e., possible candidate clusters) if we had no prior knowledge of them being clusters. This again suggests that some of our candidate clusters are genuine clusters - but we are not able to quantify how many.

In this chapter, we also measure the structural parameters of the Sarajedini & Mancone (2007) high-confidence clusters, as well as our own classified objects (high-confidence and possible cluster candidates, and galaxies) on the PAndAS images. Our results do not enable us to narrow our parameter space for real clusters, therefore we are unable to discern further which candidate clusters are most likely to be genuine clusters. However, our measurements of the M33 clusters will contribute to the first homogeneous catalogue of both M31 and M33 clusters.

In Chapter 4, we search for the elusive stellar halo of M33. To do this we simply select M33 RGB candidates from the CMD of all the objects identified in the PAndAS images around M33. We must exclude any region associated with the extended substructure surrounding the disk (identified in detail by McConnachie et al. 2010), and also correctly account for all contamination - both the MW foreground stars and the background galaxies. The latter is done by plotting the decline in the radial density of RGB candidates, and measuring the level at which the density flattens out. This level is then considered to estimate the contamination, and subtracted off the signal.

Our signal-to-noise ratio is not high enough to determine convincingly whether the radial density decline that we see is residual substructure, a thick disk, or a genuine halo component. We see some evidence that the newly-discovered component is metal-poor, as would be expected for a stellar halo. The component may also be asymmetric, but to see this the data has to be split and so further reduce the signal-to-noise. An intriguing possibility is that we observe an asymmetric halo, which could be due to material having been stripped from M33 during its interaction with M31 - and if so, would match the model of that interaction (McConnachie et al., 2009).

The results in this thesis further our understanding of one of our nearest neighbouring galaxies, and thereby add a piece to the seemingly open-ended puzzle of galaxy formation and evolution within our local Universe. Gnedin (2009) comments that "Just as Gothic cathedrals usually stand on layers of archaeological treasures, so do the cathedrals of the cosmos. In their ultra-deep images of Andromeda and its neighbourhood, the PAndAS team discovered a wealth of information about Andromeda's violent past and its relations with its most famous satellite galaxy, the Triangulum galaxy... [T]he beauty of cosmic cathedrals is only perfect to the near-sighted; look deeper and under the veil of perfection you'll find the messy traces of their violent past." The "messy traces" that we have helped unveil here are the new GC, M33E, thousands of cluster candidates, and a new component that we suggest is the stellar halo of M33.

There is obviously more work to be done. As already mentioned, high-resolution imaging (e.g., from *HST*) or spectroscopic follow-up to obtain metallicities and velocities would help distinguish clusters from contamination - but could only be feasibly done for a limited number of our candidates. Subaru's Hyper Suprime-Cam is an anticipated instrument that would more feasibly allow follow-up work on the material in this thesis; it will allow a still deeper panoramic view of M33, and is expected to see first light later this year (2012). Its greater sensitivity and larger field-of-view (1.8 square degrees; almost twice that of MegaCam)[1] will allow a more definitive answer on the tentative halo discovery here, and potentially also some of the cluster candidates.

[1]See specification file at http://oir.asiaa.sinica.edu.tw/hsc.php

Bibliography

Gnedin, N. Y. 2009, Nature, 461, 43

McConnachie, A. W., Ferguson, A. M. N., et al. 2010, ApJ, 723, 1038

McConnachie, A. W., Irwin, M. J., et al. 2009, Nature, 461, 66

Sarajedini, A. and Mancone, C. L. 2007, AJ, 134, 447

Appendix A

Local Group Globular Cluster Systems

The three most massive galaxies in our Local Group have online catalogues of their globular clusters and their properties. We give further details of those catalogues here.

A.1 The Milky Way GCS

Since 1996, W. E. Harris has composed and updated a catalogue of the MW GCs and their properties. The first edition (Harris, 1996) included 147 GCs, and subsequent editions have raised that number to 150 (2003) and 157 (2010). The 2010 version also includes 8 GC candidates, and since its publication a further 3 GC candidates have been suggested (VVV CL001, Minniti et al. 2011; Mercer5, Longmore et al. 2011; VVV CL002 Moni Bidin et al. 2011).

The current catalogue contains the following information about the MW GCs: ID (and alternative names), positions (equatorial and Galactic coordinates), distances (from the Sun and the Galactic centre), metallicities, magnitudes, colours, ellipticities, velocities (heliocentric and relative to the

Solar neighbourhood Local Standard of Rest), velocity dispersions, structural parameters (King model concentrations, core radii, and half-light radii), central surface brightnesses, central luminosity densities, and relaxation times. There is also a complimentary bibliography table that lists the sources for each entry in the data table.

The online catalogue can be found at www.physics.mcmaster.ca/ ~harris/mwgc.dat.

A.2 The Andromeda Galaxy GCS

The Revised Bologna Catalogue (RBC) is a repository for the information on M31 GCs. Since its initial publication (Galleti et al., 2004), there have been a series of updates and revisions. The latest version (4.0) was released in December 2009[1]

The RBC is not as straightforward to interpret as the MW GC catalogue - for two reasons. The first is that it is much more difficult to definitively classify M31 GCs because they are so much further away, therefore there are many more candidates included with the list of *bona fide* GCs. It also contains objects that were previously identified as GCs but were subsequently re-classified as non-cluster objects (to avoid similar mistakes in the future). The RBC contains the names, positions, photometric measurements and radial velocities of all the objects, in addition to metallicities and Lick indices for the confirmed GCs.

Table A.1 summarizes the 2045 objects in the RBC version 4.0. All objects are given an f-value (first classification), that denotes the object as a (1) GC, (2) GC candidate, (3) controversial object, (4) galaxy, (5) HII region, (6) star, (7) asterism or (8) an extended cluster. Within each f-value, the

[1]We note that version 5.0 was released in August 2012.

objects are then categorized again. Objects with f-values of 1 or 3-8 also have a c-value (confirmation flag), whereas objects with an f-value of 2 have a p-value (which is similar to, but not exactly the same that as the -value). The c-value indicates whether or not an object has been confirmed.

Table A.1: Summary of the various classifications within the Revised Bologna Catalogue (Galleti et al. 2004; v4.0, December 2009)

f (first classification)		c (confirmation flag)						
	Total	0	1	4	5	6	7	9
1 = GC	654	268	329	0	0	1	4	52
3 = Controversial	43	19	0	5	0	10	0	9
4 = Galaxy	288	225	0	63	0	0	0	0
5 = HII region	20	15	0	0	5	0	0	0
6 = Star	420	213	3	1	0	203	0	0
7 = Asterism	1	0	0	0	0	0	1	0
8 = EC	13	0	13	0	0	0	0	0

f (first classification)		p (possible classification)				
	Total	2*	1	4	5	6	0*
2 = GC candidate	606	424	41	41	1	97	2

c = 0 indicates "no data"
c = 1 indicates "GC"
c = 4 indicates "galaxy"
c = 5 indicates "HII region"
c = 6 indicates "star"
c = 7 indicates "asterism"
c = 9 indicates "GC with f=1, but also -150< v_r <300"
p = 2* indicates "no classification"
p = 0* indicates "other"

For example, of the 420 objects with f=6 (a star), 203 objects have c=6 (a confirmed star), but 213 objects have c=0 (no additional data available), 3 objects have c=1 (the additional data has confirmed that the object is not a star, but a GC), and 1 object has c=4 (the additional data has confirmed that the object is not a star, but a galaxy).

There are 447 objects that are confirmed clusters in the RBC, if one chooses the following classifications: (f=1,c=1), (f=6,c=1), (f=8,c=1), (f=2,c=1), (f=3,c=9), and (f=1,c=9). There are potentially a further 692 cluster candidates, with classifications (f=1,c=0) and (f=2,c=2), but it is far from uncertain as to their actual nature. The figure quoted in the literature for M31's GCs is usually given as $\sim$3 times as many MW GCs.

The online RBC can be found at http://www.bo.astro.it/M31/.

A.3 The Triangulum Galaxy GCS

Sarajedini & Mancone (2007) published an online, interactive catalogue of the M33 clusters. As we also mention in Section 2.1, they compile information about young and old M33 clusters from ground-based observations (Hiltner, 1960; Melnick & D'Odorico, 1978; Christian & Schommer, 1982, 1988; Mochejska et al., 1998), and *HST* imaging (Chandar et al., 1999, 2001; Bedin et al., 2005; Park & Lee, 2007; Sarajedini et al., 2007; Stonkutė et al., 2008; Huxor et al., 2009; San Roman et al., 2009). They also include further data on these clusters by Ma et al. (2001, 2002a,b,c, 2004a,b).

Table A.2: Age range of the clusters with age estimates from Ma et al. (2001, 2002a,b,c, 2004a,b) and San Roman et al. (2009).

Age range (log years)	Number of clusters		Total
	Ma	San Roman	
$6 \lesssim$ age < 7	43	0	43
$7 \lesssim$ age < 8	31	12	43
$8 \lesssim$ age < 9	59	105	164
$9 \lesssim$ age < 10	34	3	37
$10 \lesssim$ age < 11	12	0	12

There are a total of 595 objects identified in the catalogue, and where the data is available the positions, alternate names, photometric measurements, ages, masses, metallicities, galactocentric distances, velocities, and classifications are given for each. 428 objects are classified as high-confidence clusters (based on *HST* and high-resolution ground-based imaging). Table A.2 shows the number of clusters in various age range intervals, which are all between $2.5\text{x}10^6 <$ age $\lesssim 10^{11}$ years. Only twelve classical GCs have been discovered in M33's centre; the six outer halo clusters are also likely classical GCs based on their photometric colours (which are similar to those of the outer GCs in the MW and M31). This gives a total of 18 classical GCs for M33.

Since the publication of the Sarajedini & Mancone (2007) catalogue, others have undertaken further studies within the central square degree field around M33. These include Zloczewski et al. (2008) and San Roman et al. (2010) who use CFHT/MegaCam imaging to identify 3554 ($\lesssim$ 20% are expected to be real) and 599 star cluster candidates, respectively. Zloczewski & Kaluzny (2009) use *HST* imaging to observe 91 star clusters.

Bibliography

Bedin, L. R., Piotto, G., et al. 2005, A&A, 444, 831

Chandar, R., Bianchi, L., and Ford, H. C. 1999, ApJS, 122, 431

—. 2001, A&A, 366, 498

Christian, C. A. and Schommer, R. A. 1982, ApJS, 49, 405

—. 1988, AJ, 95, 704

Galleti, S., Federici, L., Bellazzini, M., Fusi Pecci, F., and Macrina, S. 2004, A&A, 416, 917

Harris, W. E. 1996, AJ, 112, 1487

Hiltner, W. A. 1960, ApJ, 131, 163

Huxor, A., Ferguson, A. M. N., et al. 2009, ApJ, 698, L77

Longmore, A. J., Kurtev, R., et al. 2011, MNRAS, 416, 465

Ma, J., Zhou, X., and Chen, J. 2004a, Chinese Journal of Astronomy and Astrophysics, 4, 125

—. 2004b, A&A, 413, 563

Ma, J., Zhou, X., et al. 2002a, Chinese Journal of Astronomy and Astrophysics, 2, 197

Ma, J., —. 2002b, AJ, 123, 3141

Ma, J., —. 2002c, Acta Astronomica, 52, 453

Ma, J., —. 2001, AJ, 122, 1796

Melnick, J. and D'Odorico, S. 1978, A&AS, 34, 249

Minniti, D., Hempel, M., et al. 2011, A&A, 527, A81

Mochejska, B. J., Kaluzny, J., Krockenberger, M., Sasselov, D. D., and Stanek, K. Z. 1998, Acta Astronomica, 48, 455

Moni Bidin, C., Mauro, F., et al. 2011, A&A, 535, A33

Park, W. and Lee, M. G. 2007, AJ, 134, 2168

San Roman, I., Sarajedini, A., and Aparicio, A. 2010, ArXiv e-prints

San Roman, I., Sarajedini, A., Garnett, D. R., and Holtzman, J. A. 2009, ApJ, 699, 839

Sarajedini, A., Barker, M. K., Geisler, D., Harding, P., and Schommer, R. 2007, AJ, 133, 290

Sarajedini, A. and Mancone, C. L. 2007, AJ, 134, 447

Stonkutė, R., Vansevičius, V., et al. 2008, AJ, 135, 1482

Zloczewski, K. and Kaluzny, J. 2009, Acta Astronomica, 59, 47

Zloczewski, K., Kaluzny, J., and Hartman, J. 2008, Acta Astronomica, 58, 23

Appendix B

Addenda

This section answers the questions raised by the thesis defence's external examiner on the material in Chapters 2 and 4, which were already published and submitted, respectively, at the time of thesis submission.

B.1 Chapter 2 Addendum

- The isophotal radius used to define M33's optical disk is described by the surface brightness contour, $\mu_B = 25$ mag arcsec^2. This represents the "edge" of the of the disk, and has a diameter of 70.8 x 41.7 arcmins (NASA Extragalactic Database).
- Two pipelines are used to calibrate the CFHT/MegaCam data. First, the CFHT staff use the Elixir pipeline; bias, flat and fringe frames are used, and the photometric zero point is determined. Then the Cambridge Astronomical Survey Unit (CASU) pipeline is used to re-register and stack the observation frames, and ultimately create a catalogue of objects based on morphological classification (McConnachie et al., 2010).
- The photometric calibration is accurate at the $\pm 5\%$ level peak-to-peak (McConnachie et al., 2010).

- In Section 2.3, the Sarajedini & Mancone (2007) catalogue clusters are *not blindly* identified. The locations of the clusters are highlighted on the image, and we then view the clusters.
- Typically, r_{core} is sampled with $\gtrsim 2$ pixels across the FWHM.
- The magnitude and colour conversions in Section 2.4 use conversions from Chonis & Gaskell (2008) and Bilir et al. (2008). The former compare SDSS data release 5 (Abazajian et al., 2005) *ugriz* magnitudes with corresponding Landolt (1992) $UBVRI$ magnitudes, whereas the latter also use SDSS DR5 *ugriz* magnitudes but compare them with the Stetson (2000) catalogue for $BVRI$ magnitudes. The Stetson catalogue is partially based on data with fields in globular clusters, therefore we believe using these particular conversions are appropriate for our work.
- Section 2.4 compares the fitting models of various profiles to our data. Each model fit is performed, and the "best fit" is chosen to be that with the lowest χ^2 value. Where there are several similar χ^2 values returned for the same model, we also examine the profile fit against the data and visually judge which is the most appropriate fit.

B.2 Chapter 4 Addendum

- In addition to the M31 mass estimates in Section 4.2.2, we note here that Evans et al. (2000) use radial velocity measurements of M31's dwarf galaxies to estimate M31's mass as $M_{M31} = (7-10)$ x $10^{11} M_{\odot}$ consistent with the measurement by Ibata et al. (2004).
- Figure 10 in Courteau et al. (2011) also shows a comparison of the halo to total luminosity versus the mass of the host galaxy, similar to our Figure 4.13. Their measured value of the M31's light fraction is similar to the one we use ($\sim 4\%$). However, because we use different sources

for the MW, their light fraction value is slight lower than ours ($\sim 2\%$, compared to $\sim 5\%$, respectively).

- We note that the mass of the LMC that we reference, $M_{LMC} \approx 10^{10} M_{\odot}$ (van der Marel et al., 2002), is estimated with data out to 8.9 kpc.
- The observations by Barker et al. (2011), discussed in Section 4.2.4, are tested for completeness by the insertion of artificial stars. They find a 50% completeness level occurs in the F814W filter at ~27.3 and ~28.0 magnitudes for the two fields located 9.1 and 11.6 kpc along M33's north major axis, respectively.
- The CASU pipeline's morphological classification was completed by M. Irwin, Cambridge University.
- The bin sizes used in Figure 4.5 and described in Section 4.4.2 do not affect the radial profile; they were simply used to show the smoothed density maps.
- In addition to the exponential profile, we also used power-law and Hernquist profiles to fit the data; however, the results are statistically identical in that the data cannot be used to distinguish which model fits best.
- We applied Kolmogorov-Smirnov (KS) nonparametric tests to pairs of each quadrant's radial profile (shown in Figure 4.11) to find the probability that the pairs represent the same distribution. The north and east quadrants are least likely to be the same, followed by the north and south, then the east and south. The three comparisons with the west quadrant failed because of the almost flat distribution of the binned data points located there.

Bibliography

Abazajian, K., Adelman-McCarthy, J. K., et al. 2005, AJ, 129, 1755

Barker, M. K., Ferguson, A. M. N., et al. 2011, MNRAS, 410, 504

Bilir, S., Ak, S., Karaali, S., Cabrera-Lavers, A., Chonis, T. S., and Gaskell, C. M. 2008, MNRAS, 384, 1178

Chonis, T. S. and Gaskell, C. M. 2008, AJ, 135, 264

Courteau, S., Widrow, L. M., et al. 2011, ApJ, 739, 20

Evans, N. W., Wilkinson, M. I., Guhathakurta, P., Grebel, E. K., and Vogt, S. S. 2000, ApJ, 540, L9

Ibata, R., Chapman, S., Ferguson, A. M. N., Irwin, M., Lewis, G., and McConnachie, A. 2004, MNRAS, 351, 117

Landolt, A. U. 1992, AJ, 104, 340

McConnachie, A. W., Ferguson, A. M. N., et al. 2010, ApJ, 723, 1038

Sarajedini, A. and Mancone, C. L. 2007, AJ, 134, 447

Stetson, P. B. 2000, PASP, 112, 925

van der Marel, R. P., Alves, D. R., Hardy, E., and Suntzeff, N. B. 2002, AJ, 124, 2639

"Our ancestry stretches back through the life-forms and into the stars, back to the beginnings of the primeval fireball. This universe is a single, multiform, energetic unfolding of matter, mind intelligence and life. All of this is new. None of the great figures of human history were aware of this. Not Plato, not Aristotle, or the Hebrew prophets, or Confucius, or Leibniz, or Newton, or any other world-maker. We are the first generation to live with an empirical view of the origin of the universe. We are the first humans to look into the night sky and see the birth of stars, the birth of galaxies, the birth of the cosmos as whole. Our future as a species will be forged within this new story of the world."

Brian Swimme (b. 1950)